Stability Systems for Timber High-Rise Structures

Parametric study on the influence of complementary stabilizing elements to hybrid timber–concrete high-rise structures

by

Nils Paardekooper

in partial fulfillment of the requirements for the degree of

Master of Science

in Civil Engineering

at the Delft University of Technology

to be defended on Wednesday August 20th, 2025

Project Duration:	Dec. 18, 2024 – Aug. 20, 2025	
Thesis Committee:	Ir. S. Pasterkamp	TU Delft, Chair
	Dr. Ir. F. Zhang	TU Delft, Supervisor
	Ir. A.J. Robbemont	Movares, Supervisor

An electronic version of this thesis is available at *http://repository.tudelft.nl/*.

TU Delft

movares smart urban engineering

Abstract

The global construction industry is responsible for a significant share of CO_2 emissions, accounting for approximately 37% of global emissions in 2022. In the Netherlands, the sector is expected to reach net-zero emissions by 2050. At the same time, major cities face a severe housing shortage, made more urgent by the limited availability of space in dense urban areas. This increases the demand for high-rise construction. Timber has emerged as a promising alternative to conventional materials due to its CO_2-storing properties. With the development of mass timber technologies, timber is now increasingly viable for use in high-rise structures.

Despite timber's potential as a sustainable building material, its application in high-rise construction remains limited due to structural, dynamic, and connection-related challenges, as well as high material costs. As a result, the realisation of timber high-rise buildings remains financially and technically complex. Hybrid timber–concrete systems offer a promising solution by combining the strengths of both materials, potentially improving feasibility while maintaining significant advantages in terms of CO_2 impact. However, the optimal implementation of such hybrid systems remains unclear. Key uncertainties include the structural performance in terms of achievable height and net floor area, cost-effectiveness, and actual impact in terms of CO_2. Exploring these trade-offs through distinct design alternatives is essential to understand how both materials can be effectively combined in high-rise construction.

This research aims to investigate the CO_2 impact and material cost implications of hybrid timber–concrete design approaches for high-rise buildings of varying heights. Based on this aim, the main research question is formulated: *What is the influence of different complementary timber lateral stability systems on the material costs and CO_2 impact of timber high-rise structures with a concrete core?* To answer this question, the study first explores existing timber high-rise projects and challenges, then develops a representative base model and structural variants.

The base model features a square floor plan and consists of TCC floors, glulam beams and columns, slotted-in steel connections, and a concrete core. Two design variants were developed by adding timber-based lateral stability systems to this base configuration: one with perimeter bracing in two configurations, and one with timber outrigger structures. These additions aim to enhance lateral stiffness, allowing for a reduction in core size and potentially increasing the net floor area for taller building configurations.

The structural variants with varying heights are analysed using a parametric workflow combining Grasshopper, SCIA Engineer, and Excel in an iterative process. Key elements are verified according to Eurocode-based criteria, including overall deflection. Each iteration is assessed by plotting net floor area against material cost and CO_2 sequestration. Net floor area is used as the main performance indicator, as it better captures the functional value of a design and reflects the influence of increasing core size at greater heights.

The results show that the need for larger cores at greater heights leads to a reduction in net floor area, with corresponding increases in material cost and CO_2 sequestration per square metre. These indicators are strongly correlated: greater timber use leads to both higher cost and higher CO_2 storage. A configuration with dense perimeter bracing showed the most consistent performance gains at greater heights by maintaining a smaller core, increasing net floor area, and improving cost-efficiency. In contrast, the use of concrete columns improved space and cost efficiency but resulted in net CO_2 emissions, underlining the sensitivity of outcomes to material choice.

Keywords: High-Rise Structure, Lateral Stability, Timber, Concrete, Parametric Modelling

Acknowledgements

The master thesis that lies before you marks the end of my time as a student at TU Delft. Over the past year, I have put a great deal of time and effort into this project. It was not always easy, but the process has been both challenging and rewarding. I have learned a lot, not only about structural engineering, but also about how to think more critically and how to communicate ideas more clearly. In the end, the value of this thesis lies not just in the outcome itself, but in everything I developed and improved throughout the process.

I would now like to take a moment to thank the people who supported me throughout this journey.

First of all, I want to thank my main supervisor **Sander Pasterkamp** and second supervisor **Fengqiao Zhang**, both from TU Delft, for their help and guidance during the project. I really appreciated their clear feedback, useful suggestions and the time they took to think along with me at each stage of the research.

I'm also very thankful to **Arnold Robbemont**, my supervisor at Movares (formerly Zonneveld Ingenieurs), for all the support and guidance I received from him during my graduation. I've come to really value the way the company invests time in helping students through this phase. On top of that, I'm grateful for the chance to gain relevant experience as a Junior Structural Engineer while working on my thesis. Thank you for the trust and the opportunities I was given.

A big thank you as well to the rest of my colleagues at Movares. I could turn to them countless times with all sorts of questions, whether about the thesis, the software I was using, structural engineering insights in general or just for a bit of fun and distraction during the day. It made a big difference.

I also want to thank my friends and housemates in Delft, who made my student time at the Faculty of Civil Engineering and Delft in general such a great experience. The many long hours we spent at the university, often struggling through projects or deadlines, became much more bearable and even enjoyable thanks to each other's company. We really got through it together.

Finally, I want to thank my parents, sister and girlfriend for always being there for me. They gave me so much support, read through my thesis more times than I can count, and took care of me during the most hectic times. I truly couldn't have done it without them.

Thank you all.

Contents

List of Figures

List of Tables

Chapter 1

Introduction

In the first section, the research context will be described, outlining the background and relevance of the study in the field of timber–concrete hybrid structures. This is followed by a discussion of the research problem and existing knowledge gaps. Based on this, the aim and objectives of the research are defined. The research questions are then introduced. Finally, the scope of the research is outlined, clarifying its boundaries and limitations.

1.1 Research Context

The current level of CO_2 emissions poses a global challenge, with the building industry being a significant contributor to this problem. The current global construction industry is accountable for 3.6 Gt CO_2 emissions in 2022. This translates to approximately 37% of the global CO_2 emission [63]. To achieve climate goals, the Paris Climate Agreement has been implemented in 2016, to reduce CO_2 emissions. For the Netherlands, this means that 3.4 Mt CO_2 emission needs to be reduced in 2030. This is equal to 49% of total CO_2 emissions [43]. By 2050, the construction industry in the Netherlands is aimed to have net-zero emissions.

Simultaneously, the Netherlands is experiencing a housing crisis, particularly in major cities where a severe shortage of housing exists. This issue is amplified by the general scarcity of available space in major city areas [14]. These issues increase the demand for high-rise constructions.

In addressing the CO_2 problem in the construction industry, the use of timber has emerged as one of the most logical and viable solutions. Unlike concrete and steel, timber is a naturally occurring material. While the production of concrete and steel emits significant amounts of CO_2, timber, on the other hand, will store carbon in its elements. In this way, gloabal CO_2 emissions by the construction industry can be significantly reduced and could potentially reach complete neutrality or even net-negative carbon emissions [13].

Since the initialization and development of laminated timber and other technologies for creating mass timber elements, it has become possible to expand timber's applicability within the construction industry. This advancement should allow the use of timber in the design and construction of high-rise buildings.

1.2 Research Problem

Several challenges remain in the use of timber for high-rise structures. Timber is notably weak in its perpendicular-to-grain direction [22]. Also connections between timber elements can create bottlenecks in capacity [24] [35]. Its low mass compared to concrete and steel complicates lateral stability and increases issues related to dynamic vibrations [51] [24] [1]. Additionally, limited industry experience

with timber projects has created a negative feedback loop, where fewer projects are undertaken, further limiting the sector's growth [27].

In addition to the technical challenges associated with the use of timber compared to conventional construction materials, the high cost of mass timber products may represent an even greater concern. As a result, clients and developers continuously seek ways to build more sustainably while maintaining cost-effectiveness. This presents a complex issue, primarily because the cost difference between timber and concrete buildings is currently driven by the higher material costs [4] [28] [7].

Therefore, the adaptation of timber-based high-rise projects is therefore still a significant step to make. To make this step more feasible, hybrid solutions could be employed. These solutions would make use of the strength properties of timber while combining them with concrete or steel where necessary. This approach should allow for the development of taller buildings than the current tallest timber-focused structures, while using accessible construction techniques and elements. Next to that, because of the lower cost of concrete compared to timber, and the potential elimination for complex load-bearing steel connections, a hybrid approach could definitely help in the adapting of timber in high-rise constructions while maintaining feasibility.

Although these hybrid structures would involve materials like concrete and steel, which emit CO_2, the overall emissions could still be significantly reduced through the integration of timber elements. While main load bearing and stability elements could be made in concrete, timber could constitute a substantial percentage of the total material usage [70], contributing to a meaningful reduction in CO_2 emissions.

The lack of practical experience, along with the fact that this development approach is still in its infancy, means it remains unclear how hybrid solutions can be optimally applied. Questions such as where concrete should be used, what heights or net floor areas can be achieved, how much CO_2 emissions can actually be reduced, and to what extent timber can still be applied in a cost-effective manner to maintain the overall feasibility of the structure are still highly relevant issues. Furthermore, developing distinct design alternatives based on established principles is essential to explore how timber and concrete can be effectively combined in high-rise construction.

1.3 Aim

As outlined in the preceding research problem definition, combining timber and concrete in high-rise construction involves complex trade-offs between structural performance, material cost, and CO_2 impact. The interaction between these factors leaves significant room for further understanding and investigation. On the basis of the research context and problems discussed Section 1.2, the aim of this research can be stated.

This research aims to investigate the CO_2 impact and material cost implications of hybrid timber–concrete design approaches for high-rise buildings of varying heights.

1.4 Objectives

One promising hybrid concept, supported by findings in the literature study (see Section 2.5), is a timber structure with columns and beams of Glued Laminated Timber (GLT) combined with a concrete core. This configuration will serve as the base model in this study. In order to explore how timber can take on a greater structural role within this setup, two complementary variants are developed by introducing additional timber-based lateral stability systems. The goal is to assess whether these additions can improve structural performance while reducing material cost and CO_2 impact. In order to address this goal, the following objectives need to be accomplished.

1. To identify opportunities and challenges in timber high-rise construction based on existing projects and relevant literature.
2. To design a base model and two complementary alternatives composed of additional stability systems, whose features and design choices are based on insights gained from Objective 1.
3. To parametrically develop a generic method for efficient structural analysis and dimensioning of all design alternatives across varying building heights.
4. To define suitable evaluation criteria, apply them to analyse the material cost and CO_2 impact of each design variant in comparison to the base model, and provide a clear visual representation of the results.

1.5 Research Questions

The aim and objectives of this research will lead to the following main research question.

What is the influence of different complementary timber lateral stability systems on the material costs and CO_2 impact of timber high-rise structures with a concrete core?

In order to address the main question, several sub-questions can be formulated. The order of the sub-questions will be given in the same chronological order as the research process. The sub-questions labeled by their governing chapter.

- What are the current construction approaches, effective techniques, and key challenges in timber high-rise building design?
- In what way can a representative base model be designed for variable building heights, and how can meaningful structural variants be derived from it?
- How can the design variants with varying storey numbers be efficiently and parametrically modelled, analysed, and dimensioned?
- How are the model iterations evaluated, structured, and visualised based on defined criteria, and how do the variants perform relative to the base model with respect to these criteria?
- How can the results of the design variants be interpreted and compared, and what are the limitations of the model?
- What are the key findings of the research, and what recommendations can be made for use-cases within the model framework, general structural design, and future studies?

1.6 Research Scope

This section will focus on what exactly lies within the scope of this research. To rephrase the aim of this research once more: This research aims to investigate the CO_2 impact and material cost implications of hybrid timber–concrete design approaches for high-rise buildings of varying heights. This aim will be achieved through iterative calculations and a parametric process. It is therefore essential to clearly define which aspects of the design are included in the analysis and which are deliberately left out. A comprehensive outline of the elements considered and excluded from the research is presented in this section.

This research will include

- The design and development Base model consisting of TCC floors, GLT beams and columns and a concrete core (see Section 3.2)
- The design and development of two complementary design alternatives focused on providing increased lateral stability, based on relevant literature (see Section 3.2).
- Verifications based on strength and stiffness of individual elements, and lateral deflection and acceleration at the top floor, in accordance with building codes and additional relevant guidelines (see Section 3.7).
- Designs based on typical constraints regarding wind loading governing in the Netherlands (see Section 2.4).
- Determination of the connection stiffness and capacity based on a generic relation formed by the cross-sectional dimensions of the timber element and the embedment depth of the steel plates (see Section 3.4).

This research will not include

- The development, investigation, or recommendation of not yet existing elements or connection types.
- Optimization using algorithms or AI techniques.
- Dynamic response due to seismic loading
- Architectural aspects such as building physics and space allocation. While these topics are discussed, no extensive calculations will be performed, as the focus is on the structural properties and potential of the material. The façade will occur as a line load on the outer beams, and will therefore not be detailed.
- Calculations for foundation capacity and settlements. For this research, the foundation is assumed to be rigid and the horizontal deflection of the top floor will be doubled to simulate asymmetrical foundation settlements.
- Extensive CO_2 emission calculations regarding construction, building energy usage and demolition, CO_2 emission comparisons are made based solely on material production emissions or storage.

Chapter 2

Literature Review

This Chapter will provide research in order to answer the sub-question:

What are the current construction approaches, effective techniques, and key challenges in timberhigh-rise building design?

To be able to answer this sub-question and thereby to identify the research gap as accurately as possible, the following chapter will be structured as the follows. Firstly, the current State-of-the-Art of timber high-rise construction will be analyzed in section 2.1. This section reviews several timber high-rise buildings that have contributed significantly to the current understanding of timber behavior in structural applications, including Treet, Brock Commons Tallwood House, HoHo Wien, Mjøstårnet, HAUT, and Ascent MKE. Each structure is evaluated based on its specific characteristics and associated structural challenges. Insights will be derived regarding which structural aspects are effective and which are less effective for timber high-rise construction.

Section 2.2 will address timber as a construction material, with particular focus on its application in hybrid timber-concrete high-rise buildings. It will examine the orthotropic nature of timber, which causes the material to behave differently depending on the direction of loading. Additionally, it will discuss the dimensional limitations of timber elements. The relatively low weight of timber, in comparison to concrete or steel, also introduces new challenges in wind engineering and dynamic behaviour.

Section 2.3 focuses on the connections between timber elements. Large timber components can be connected using slotted-in steel plates and dowels. As the size of the element increases, more dowels can be placed, which increases both the load-bearing capacity and the rotational stiffness of the connection. From this, a relation can be derived that can be implemented in the model in the form of rotational springs.

Section 2.4 addresses wind loads and wind-induced accelerations. In high-rise construction, wind plays a crucial role in the structural design process. The section describes how calculations should be performed in accordance with the Eurocode [45] to determine horizontal wind loads and dynamic accelerations at various heights.

Section 2.5 addresses the lateral stability of high-rise structures. This aspect is essential because wind loading plays a dominant role in the overall structural behaviour. A dedicated system must be designed to ensure that horizontal deflections and accelerations at the top floor remain limited. In this section, two systems are compared: a diagonal bracing system and an outrigger system.

Section 2.6 describes the time-dependent differential deformations that occur in timber-concrete hybrid structures. Shrinkage, creep, and elastic deformations develop differently in timber elements compared to concrete. As a result, combined with the accumulation effect of multiple stacked floors, this can lead to significant differences in vertical shortening. These differences can be compensated by using steel shims.

Due to the combustible nature of timber, fire safety becomes an especially important consideration in the design of high-rise timber structures. This aspect is addressed in Section 2.7. In buildings higher than eight storeys [50], it is no longer possible for fire services to evacuate occupants from the outside. As a result, fire-resistant compartments or protected escape routes must be provided. In addition to the conventional design situation, a separate fire design situation must be considered. This is done in accordance with NEN-EN-1995-1-2 [48], which applies different safety factors than those used in the normal design situation. By protecting timber elements with fire-resistant gypsum boards, the fire safety can be significantly increased.

2.1 State-Of-The-Art

This section examines some of the tallest timber buildings in the world; Treet, Mjøstårnet, Brock Commons Tallwood House, HAUT, Ascent and HoHo, focusing on their design and construction methods. Next to existing high-rise structures, also some conceptual designs for super tall timber buildings are reviewed on their specific characteristics. The analysis covers how timber was applied in each project and the reasons behind specific structural decisions. Special attention is given to the combination of timber with other materials, such as concrete, in areas where timber alone was not sufficient. By identifying where and why concrete was used, this section provides insights into the structural limitations of timber when dealing with load-bearing and stability requirements in high-rise buildings. This exploration highlights the technical challenges that influence the use of timber at great heights and the engineering solutions developed to address them.

2.1.1 Treet - 2015

General Information
In 2014, the construction of 'Treet' started. Treet is a 14-storey timber framed building. With 49 meters, it was the worlds tallest timber structure at that time. The building is engineered by SWECO Norway. The building is located in Bergen in Norway. The building has a residential function, consists of 62 apartments and has a net-area of 5830 m^2 [2].

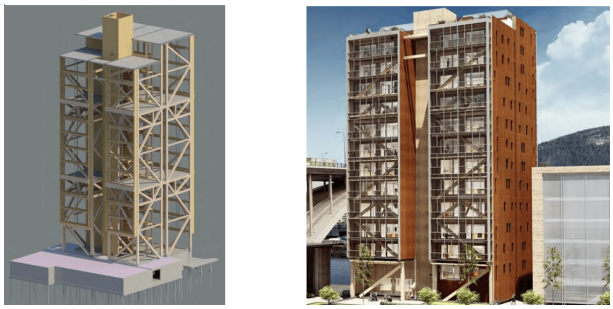

Figure 2.1: Images of Treet, GLT stability system (left) and 3D-render (right) [37]

Structural System Overview
The main element of the structure is timber. The main rooms consist of prefabricated modules assembled out of CLT (Cross Laminated Timber) panels. These CLT panels are stacked upon each other. Around the perimeter of the building, there is a GLT truss frame. An analogy has been made that it is to be compared to a cabinet filled with drawers. On level 5 and level 10, there is a so-called 'power-storey'. This is a GLT truss framed storey that is connected to the GLT frame that envelopes the whole building. On top op this storey is a concrete slab on which the next 4 floors are supported. The connections of the GLT frame are all slotted-in steel plates and dowels[2].

Additional Remarks
Treet has an interesting and innovative design. Several remarks can be made about the structure. The building is located in Norway, a country not highly prone to earthquakes but subject to strong winds, making wind loading the governing factor. As discussed in section 2.4 and 2.5, wind loading affects the serviceability limit state (SLS), ultimate limit state (ULS), and dynamic acceleration. The GLT truss frame is designed to manage all lateral deflections of the building, while the CLT panels within

the prefabricated modules do not contribute to global stiffness. Consequently, the CLT panels are not required to handle horizontal stresses and rely solely on contact stresses between them, facilitating easier stacking [37].

Due to the governing wind loading, the lightweight nature of the structure may lead to issues with horizontal acceleration. To mitigate this, concrete slabs are added on levels 5 and 10, increasing the structure's weight and thereby improving the stiffness-to-mass ratio. These levels are directly connected to the GLT frame, directing gravitational forces from the upper levels into the frame. This distribution enhances the structure's resilience against significant moments at the foundation, as the increased downward force at the perimeter provides a larger lever arm, positively affecting the ULS. Additionally, tolerance gaps are incorporated between the GLT frame and the CLT modules to accommodate horizontal deflections [37].

2.1.2 Brock Commons Tallwood House - 2017

General Information

Brock Commons Tallwood House, completed in 2017 at the University of British Columbia in Vancouver, Canada, stands as an 18-storey student residence, reaching 54 meters in height. It was the tallest mass timber hybrid building in the world at the time of its completion. Brock Commons houses 404 student beds and spans a total gross area of 15,120 m^2[3].

Figure 2.2: Arial view of Brock Commons Tallwood House [3]

Structural System Overview

The main structural system of Brock Commons Tallwood House is a hybrid design that utilizes both timber and concrete elements. The superstructure is composed CLT floor panels supported by GLT and PSL columns. The CLT panels span between columns without the need for beams, creating a flat, point-supported surface. The building has two full-height concrete cores that provide lateral stability, particularly crucial in the seismic zone of Vancouver. A reinforced concrete slab at the second floor serves as a transfer level between the ground floor's concrete structure and the timber superstructure above. Steel connectors are used throughout to link the timber elements[23].

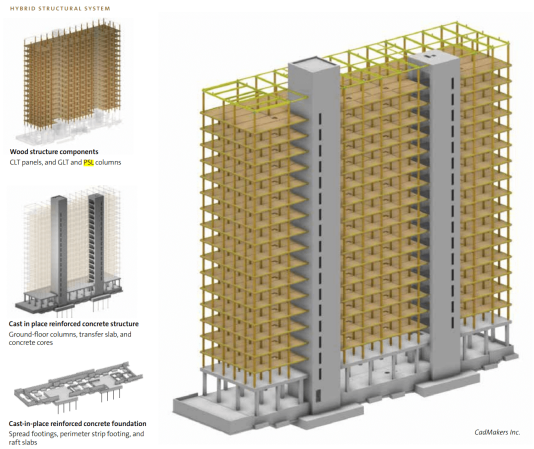

Figure 2.3: Structural system of Brock Commons Tallwood House [3]

Additional Remarks

There are a number of notable aspects in this design worth mentioning. First, the engineers have chosen for a hybrid design, with two separate full-height concrete cores for lateral stability. The reason for this option was because of time and budget limitation. It is said that a timber-based lateral force-resisting system would have been possible as well for this project [23]. Second, PSL columns were used in areas with high loads on floors 2 through 5. PSL columns provide extra compressive capacity. Third, all lateral stability must be absorbed by the concrete cores. This requires sufficient stiffness in the CLT panels, which will function as diaphragms. It is important that the CLT floors do not yield before the concrete cores start yielding. The CLT floors span in two directions, which enhances the diaphragm action[23].

Another point that was carefully studied for this project is time-dependent differential movements, particularly axial column shortening and shrinkage. This structural aspect is reviewed further in section 2.6. When properly accounted for, these factors should not negatively affect the structure. The following aspects affect GLT column shortening:

- Dead and live load elastic shortening
- Shrinkage parallel to grain
- Joint settlement
- Column length tolerances
- Wood creep

The main concern is the impact of these deformations on the vertical services and the elevation tolerances between the wooden and concrete elements. After a detailed analysis, it was found that without any mitigation, the estimated axial shortening would amount to around 50mm. To solve this, metal shim packages were added to certain floor levels. These shims have variable thicknesses but were designed to account for 50% of the calculated deformations, to avoid overcompensation[23].

2.1.3 HoHo Wien - 2019

General Information

HoHo Wien is an 84-meter, 24 storey tall timber high-rise located in Vienna, completed in 2019. The

engineering firm responsible for the project is RWT Plus. The contractor involved is Hinteregger & Söhne. The building has a net floor area of approximately 25,000 m^2 [69] and serves mixed functions, including offices, apartments, a hotel, and wellness spaces [32].

Figure 2.4: HoHo Wien tower upon completion [32]

Structural System Overview

The main structural system of HoHo Wien is a hybrid system. It consist of three buttressed towers. The towers all have in-situ 3 wide concrete cores, one for each tower. They are all rigidly connected to each other. On the sides of the cores, the timber elements are placed. The wall panels are of CLT, the columns are of GLT and the floors are TCC floordecks.The structure also consists of edge beams. These are of prefabricated concrete.

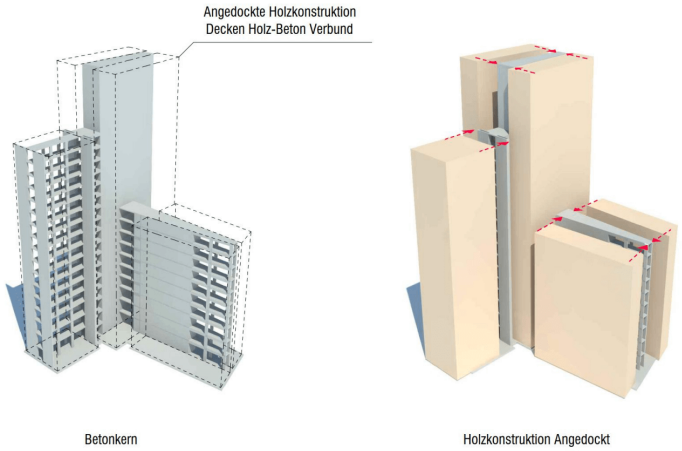

Figure 2.5: Structural overview of the concrete core and timber addition[70]

Additional remarks

There are some additional remarks to be made about the design choices of this structure. The first one is the choice of the concrete cores geometry. Although the dimensions of the concrete cores are rather large, the structure still consists of 76% timber [32]. The large dimensions of the concrete cores will make sure that it provides enough lateral stability. Because of the geometry of the building, and rigid connection between the cores of every tower, enough lateral stability can be provided for in both directions.

Another reason for these particular design choices is that it is designed for efficiency during the construction phase. ”The objective of the system design was to create a flexible, simple, and repeatable module that would make converting programs and making changes relatively easy” [68]. The timber elements are ’horizontally docked’ to the concrete core. This could happen at the same time as the concrete was poured, increasing construction efficiency [70]. In the building, TCC panels were used. These are used to increase the mass and therefore reduce the possibility of wind-induced vibrations. Also, the design opted for construction efficiency, and the prefabricated nature of the elements contributed to this. The TCC panels were supported by concrete side beams. In this figuration, the TCC panels are able to transfer horizontal forces to the building core, without yielding earlier than the core.

2.1.4 Mjøstårnet - 2019

General Information

In 2017, the construction of Mjøstårnet started, and was completed in 2019. Mjøstårnet means Mjøsa tower in Norse, referring to Norways’s largest lake. It consists of 18-storeys. Its architectural height is 85.4 meters and upon constructing, it was the largerst timber tower in the world [61]. The building serves a mixed functionality for offices, residential and a hotel. There effective floor area is approximately 15000 m^2 . The tower is engineered by Sweco Norway and Moelven Limtre, and is build by contractor HENT[65].

Figure 2.6: Image of Mjøstårnet after completion [65]

Structural system overview

The Mjøstårnets main element is timber. It has a rectangular shaped floor section, with a beam-column principle. The floor decks are of Trä8 classification. These are prefabricated timber elements with insulation. They provide enough stiffness, are fire safe, and can handle acoustic requirements. The floors on the upper levels, level 12-18 are made of 300mm thick concrete. The floor decks are supported by GLT beams and these beams are supported by GLT columns. These elements are of class GL30. The four edge beams have a larger higher dimensions. Diagonal timber truss elements are added to the perimeter of the building. The walls are made of prefabricated CLT elements of class C24. These CLT elements are also used for the lift shaft and staircase. The GLT elements are connected by slotted-in steel plates and dowels.

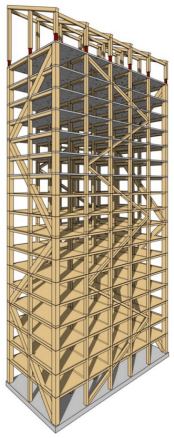

Figure 2.7: Overview of the structural system of Mjøstårnet[1]

Additional remarks
The Mjøstårnet is said to be an all-timber building. This means that the building consists of timber for more than 85% [26]. This fact, along with the building's height, makes the structural system principles applied in its design particularly intriguing for in-depth analysis. The design of the structural system is comparable to the building Treet, also in Norway. The main differences are that this building is some 30 meters heigher, and instead of building modules, Mjøstårnet has columns and beams. This is done to remain a versatile floor plan [1].

Same as in other buildings, the structural stability system is divided in a vertical and horizontal load bearing system. Where the vertical forces are conducted through the timber walls and columns, the lateral forces are handled by the GLT truss around the perimeter of the building. As discussed in section 2.5, horizontal wind-forces acting on the building will result tension in one side at the perimeter of the building. In concrete and steel structures, this poses less of a problem. Compression forces as a result of the weight of the materials will most often compensate for the tension forces generated by the wind-loading. For timber structures, this remains an issue. In Mjøstårnet, this issue is solved by enabling the foundation piles to handle tension. This means that the lightweight nature of the structure creates less of a problem.

However, the lightweight nature of timber also imposes problems in terms of wind-induced vibrations. Norway is not susceptible for earthquakes, but wind-induced vibrations remain an important design factor. The low weight of timber but high stiffness imposes a high stiffness-to-mass ratio. This can become a problem for its modal frequencies, and thereby increase its dynamic accelerations. In other to address this issue, more mass can be added to the lateral stability system. This should increase its stiffness-to-mass ratio and lower its accelerations [2]. In Mjøstårnet, this problem is addressed by adding concrete floors on levels 12 to 18. This concrete is also able to act as a diaphragm to aid in its lateral stability system.

As previously remarked, the diagonal bracings, together with the four corner columns, handle the lateral stability of the structure. These elements are completely out of timber. The truss principle of these element impose that the elements are loading in their in-grain direction as much as possible. In this way, the timber elements have a higher capacity. Also, because the elements are round the perimeter of the building, the 'lever arm' to resist moments caused by the wind-loading is increased. It does mean, that with a building of this height, the cross sections of the GLT elements are rather large. The corner column

dimensions are 1485 x 625 mm^2 [1]. If taller timber building are to be created, the current technologies to create large cross-sections could potentially reach its limit.

2.1.5 HAUT - 2021

General Information

HAUT is a 21-storey timber residential tower located in Amsterdam, the Netherlands. Construction commenced in 2019, with a projected completion date of 2021. The building will reach a height of 73 meters, making it the tallest timber structure in the country. Arup is the engineering firm responsible for the project. The building offers a total net floor area of 14,500 m^2. It is designed to provide high-quality residential space [64]. During the design phase of the project, architectural elegance. This can be traced back to its open façade and irregular shapes.

Figure 2.8: Image of HAUT upon completion [59]

Structural System Overview

In the design of HAUT, the main focus lied in the implementation of timber elements. Next to this, architectural appealing was also an important factor. This can be traced back into certain design choices, for instance the implementation of concrete for several elements. This makes the design a concrete-timber hybrid structure. For the floors, TCC elements are used. This stands for Timber-Concrete-Composite. The building also has a concrete core, in which the elevator shaft and staircases are located. Next to the core, the vertical load bearing elements consist of both CLT walls and GLT beams. The TCC floor panels are supported by these elements [64].

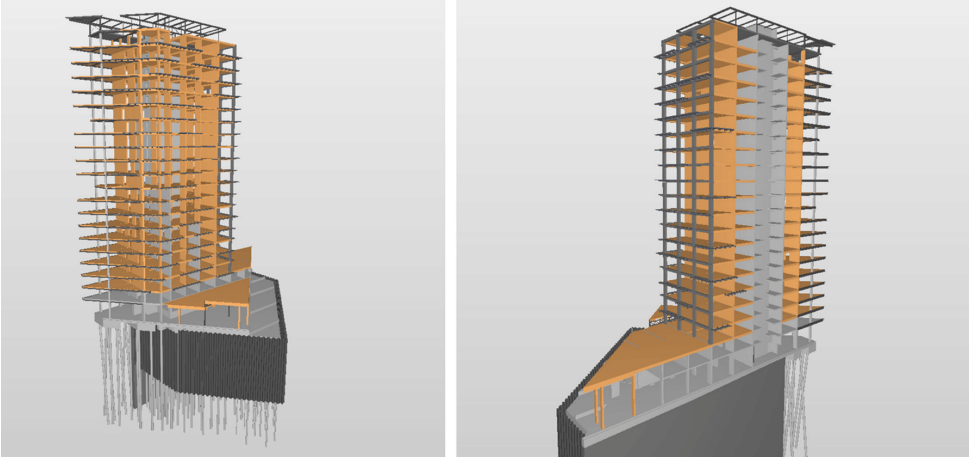

Figure 2.9: Image of HAUT upon completion [64]

Additional Remarks

From an early design phase, the architectural aspirations were given high priority. The architectural design opted for an open façade design. For this matter, both a load bearing façade and a diagonal bracing system along the perimeter were ruled out rather quickly. This is why it was chosen to move towards a hybrid solution. Although the openness of the façade in the field of timber high-rise is quite an inefficient solution. When designing the building, the engineers investigated the possibility CLT core system with steel bracings, but this was ruled out partially due to the fact that very stiff connections had to be created, demanding a large amount of steel. The bad environmental impact of the steel usage would negatively counteract the positive influences of using structural timber, which is in essence the goal of the initiative. Therefore, the engineers decided to opt a concrete core, which was ultimately the more sustainable option [64]. The concrete core, together with two adjacent CLT walls take up all the horizontal forces and consequently form the lateral stability system. The CLT walls have openings in them and because connected CLT walls generally not have sufficient diaphragm action, the CLT walls were coupled as displayed in figure 2.10. For this matter, the openings in certain floors had to be alternated. Because of limited knowledge about the actual stiffness of this CLT wall, the engineers decided to not include the CLT stability wall in the ULS calculations of the lateral excitation. However, it is included in the calculations for SLS [64].

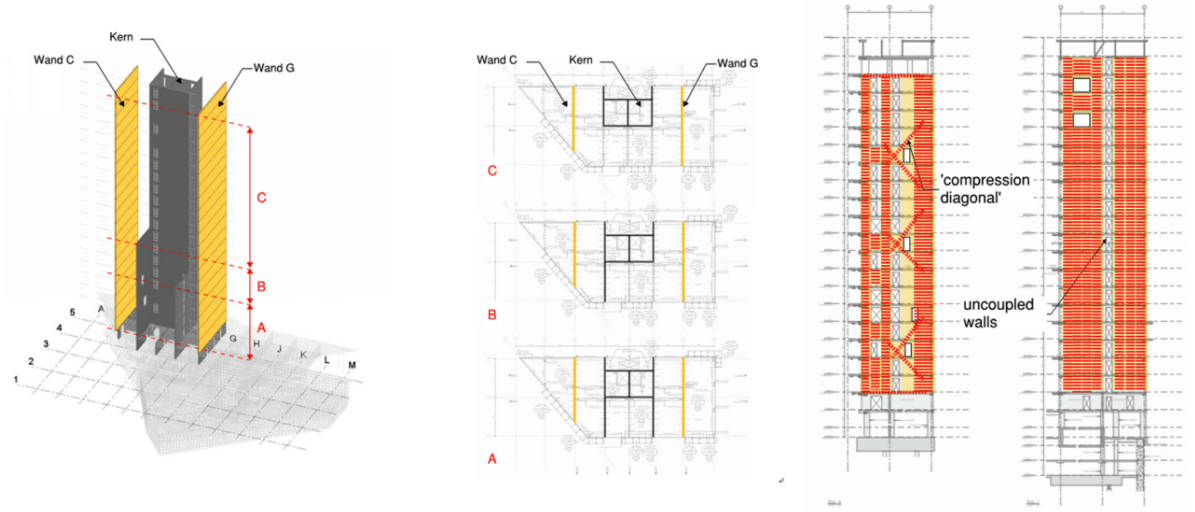

Figure 2.10: Concrete core and CLT stability walls of HAUT[64]

The concrete core and CLT walls also contribute to the load bearing system. Next to this, more CLT walls are placed in the structure. Furthermore, there are also GLT columns that transfer vertical forces. The floors will find their support on these elements. On places were there was no CLT wall, the floor deck was supported by GLT beams. Besides providing support for the floor decks, these GLT beams also acted as a tension ring around the perimeter of the building. This has a positive influence on the transfer of diaphragm forces from the façade of the building to the core, acting as a structural tie [64].

The floors of the building were also of TCC. This system has concrete in the upper part to take on compression forces, and timber in the lower part to take on tension forces. In this floor system, the mass of the floors is higher compared to CLT floors. Because of this, it also aided in meeting the acoustical requirements. Next to that, the floor system also has a positive effect on footfall vibrations [57]. Lastly, the increased mass of the floor system also influences the stiffness-to-mass ratio positively, which is better against wind-induced vibrations.

The concrete height of the floor is extended to full height. Using this principe, a 'platform' type floor-to-wall connection could be made. This favors the construction sequence. In this way, no cross-grain forces would flow through the timber, which is also a structural advantage. It also allowed for easier in-plane connection between the floor decks. This in-plane connection is essential for diaphragm action between the floor decks which is needed to transfer horizontal forces to the core. A construction detail is provided in 2.11. However, the in-plane connection between the floor decks does have a negative effect on the acoustical requirements. For this reason, an innovative solution has been imposed. The total floor consists of four 'sub-diaphragms'. Each of these sub-diaphragms has been connected to the concrete core, but remain decoupled from each other. The GLT tension ring beam discussed earlier still allows for the sub-diaphragms to act as one to favor lateral stability [64].

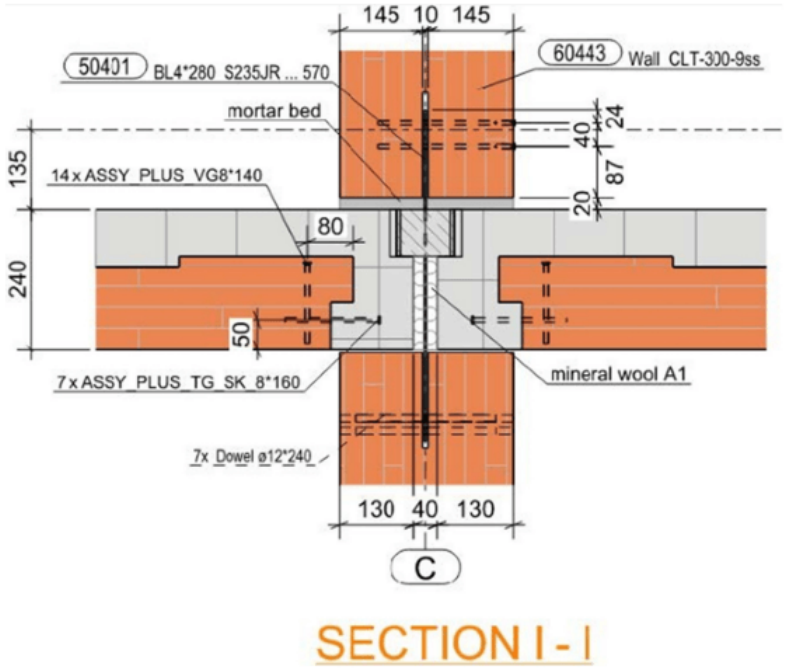

Figure 2.11: Detailing of a typical wall-to-floor connection [57]

2.1.6 Ascent MKE - 2022

General Information

Ascent MKE is an 86.6 meter tall, 25-storey timber-concrete hybrid structure, located in Milwaukee, USA. Upon its completion in 2022, it is current world's tallest timber structure to date. Construction started in 2020. The structural engineering firm responsible was Thornton Tomasetti and the main contractor was C.D. Smith Construction Inc [60]. The net floor area of the building is 45,800 m^2 [62]. The goal of the structure was to 'show of the intrinsic beauty of the material and structure' [25]. This meant that the architects wanted lots of exposed timber. This design choice accounted for much problems later on.

Figure 2.12: Image of Ascent MKE upon completion [60]

Structural System Overview
Although the structure mainly consist as timber as a building material, the 2 building cores and lower 7 parking levels of the building are made of concrete. The upper 18 levels are of timber. The structure has a column-beam typology. The floors consist on one-way spanning CLT slabs, supported by GLT beams. These beams are supported by GLT columns. The timber columns on the 7th level are supported by large concrete beams [25].

Additional remarks
The design of the Ascent MKE tower follows a straightforward approach to timber hybrid high-rise construction. The grid size was selected for economical timber dimensioning, but this grid proved inefficient for parking layouts, necessitating a larger grid for the concrete podium. Due to the low self-weight of timber, it was possible to transfer the load of the timber grid onto larger concrete beams. Despite the introduction of significant eccentric forces on these beams, the post-tensioned concrete design remained structurally sufficient to handle them [25].

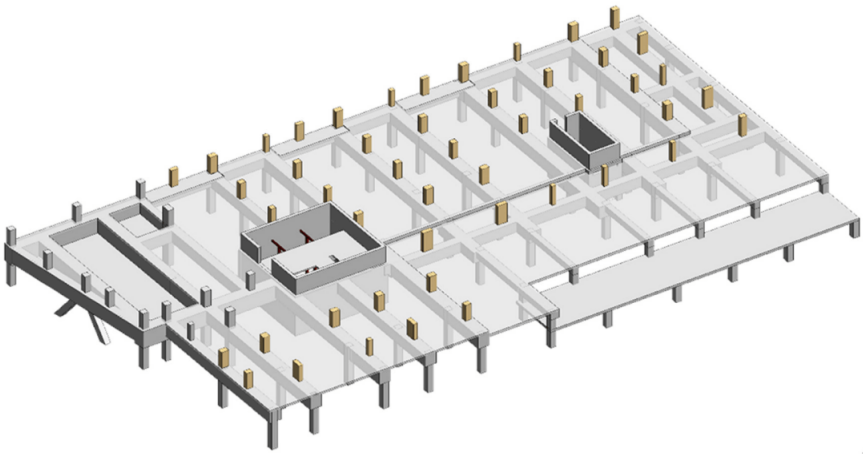

Figure 2.13: Transfer beams at level 7 [25]

The architectural intent emphasized exposed timber to highlight its intrinsic aesthetic qualities, increasing the material's vulnerability to fire. Extensive research was conducted to develop a fire-safe design, particularly for the exposed timber elements. Specially engineered connections were required to meet stringent fire safety standards. Ultimately, all beam penetrations were concealed to ensure compliance with these fire regulations [25].

2.1.7 State-Of-The-Art Overview

To provide a clear overview of the state-of-the-art in timber high-rise construction, all buildings described are presented in a summary table, shown in Table 2.1.

Table 2.1: Overview of selected tall timber buildings and their structural characteristics

Building	**Year**	**Location**	**Height [m]**	**Storeys**	**Area [m^2]**
Treet	2014	Bergen, Norway	49	14	5830
Brock Commons	2017	Vancouver, Canada	54	18	15120
HoHo Wien	2019	Vienna, Austria	84	24	25000
Mjøstårnet	2019	Brumunddal, Norway	85	18	15000
Haut	2021	Amsterdam, Netherlands	73	21	14500
Ascent	2022	Milwaukee, USA	87	25	45800

Building	**Structural System**
Treet	Full timber, GLT truss with diagonal bracings, CLT modules, CLT modules
Brock Commons	2 concrete cores, GLT and PSL columns, CLT floor panels
HoHo Wien	3 wide buttressed concrete cores, GLT columns, edge beams prefab concrete, TCC floor panels
Mjøstårnet	Full timber, GLT diagonal bracings, GLT columns and beams, CLT floors, Upper Floors concrete
Haut	Concrete Core, CLT walls, TCC floor panels
Ascent	2 concrete cores, concrete lower 7 parking levels, GLT beams, CLT floors

2.2 Timber as a construction material

When utilizing timber as a construction material, several important factors must be considered. The construction industry has extensive experience with conventional materials such as concrete and steel, with designs typically centered around the strengths of these materials. Timber, however, behaves differently in key aspects, and structures built from timber must be designed to maximize the material's unique strengths.

2.2.1 Orthotropic Nature of Timber

Timber is a natural material, resulting in construction elements that are inherently inhomogeneous. This inhomogeneity gives timber orthotropic properties, meaning it exhibits different strength characteristics in different directions. As displayed in Figure 2.14, timber is significantly stronger in its grain direction, which, in beams and columns, typically aligns with the longitudinal axis. This property must be strategically implemented in structural designs to maximize efficiency. The varying properties of different raw timber elements are categorized into different strength classes, allowing for more precise strength classification. Unlike concrete, timber can handle tension forces nearly as well as compression forces, with slightly stronger performance in compression. This makes timber highly suitable for truss type designs, where individual members are generally only loaded in longitudinal direction, with both tension and compression occurrence. This could eliminate the need for additional steel in the design.

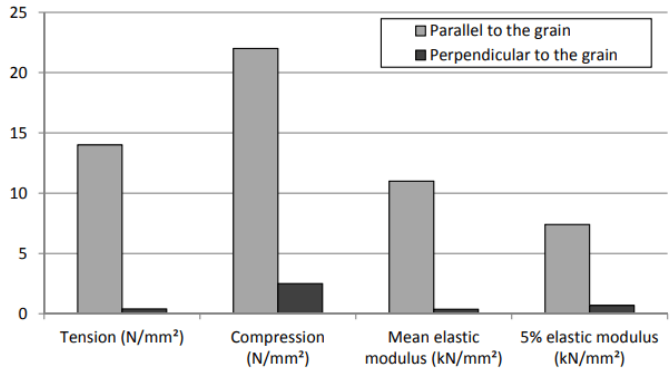

Figure 2.14: Compression and tension strengths of C24 [11]

2.2.2 Dimensioning Limitations

One limitation in using pure timber elements is their dependency on tree sizes. This issue is resolved through the production of mass timber elements such as CLT, GLT, LVL, and PSL. These engineered timber products remove theoretical size limitations, allowing for larger elements. The lamination process involved in creating mass timber products also contributes to the homogenization of the material. Interestingly, increased variability in the individual laminated components improves the overall homogenization effect, leading to more uniform strength properties in various directions, and enhancing the accuracy of design assumptions [9].

2.2.3 Lightweight Material

Timber's volumetric weight is considerably lower than that of concrete or steel, yet its specific strength is comparable to steel [51]. This means, achieving the same load-bearing capacity requires larger cross-sectional areas for timber elements. This may reduce the available net effective floor space and introduces certain limitations, as discussed in the paragraph above, where cross-sectional dimensionality is not unrestricted.

2.3 Timber Connections

Timber, as a construction material, has limitations due to the lengths of available elements. As a result, the use of connections is unavoidable. Connections in timber elements lead to small rotations, caused by the elastic rotational stiffness of the connections (i.e., the fact that they are not infinitely stiff) and by initial slip in either translational or rotational direction.

2.3.1 Rotational Stiff Connections

While it is possible to create rotationally stiff connections, achieving greater stiffness requires the use of more steel. The addition of steel in the connection offsets the environmental benefits of using timber, as the negative environmental impact of the steel becomes significant. At that point, the environmental advantage is lost, rendering the effort counterproductive. This principle is elaborated on in [64].

Additionally, stiff connections may introduce shear forces in the timber elements. These shear forces act perpendicular to the grain, which, as discussed in Section 2.2, is the weaker axis of the material. Therefore, stability should not be achieved by stiff connections, but rather by designing a form-stable structure. In this approach, the overall stiffness of the structure is derived from its form, making the rigidity of individual connections less critical to the building's stability [24]. In this way, perpendicular-to-grain forces are also limited.

2.3.2 Post-Tensioning

Research by T. Znabei has shown that post-tensioning a CLT core can improve performance by eliminating the sliding and rocking failure mechanisms of a building's core [71], this can be seen in Figure 2.15. However, while this method achieved a 60% improvement in building height, resulting in an increase to eight storeys, it still does not provide sufficient stability for high-rise structures.

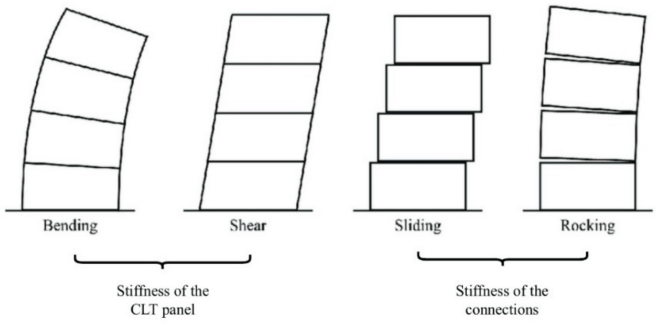

Figure 2.15: Failure modes of a CLT core [71]

2.3.3 Translational Capacity

It can be concluded that rotationally stiff connections between timber members are inefficient both in terms of sustainability due to the steel usage, and they do not provide sufficient lateral stability for the entire building. Besides adopting a form-stable construction, redirecting lateral forces to a concrete core may also offer a solution, as will be discussed in 2.5.

However, in addition to moments, forces will also establish at the location of the connections. To transfer these connection forces effectively, the joints must possess sufficient stiffness. In timber structures composed of large elements and potentially long spans, connections are often realized using slotted-in steel plates [16]. In this technique, grooves are cut into the timber members, into which steel plates are inserted. These plates are then fastened using steel bolts, as illustrated in 2.16.

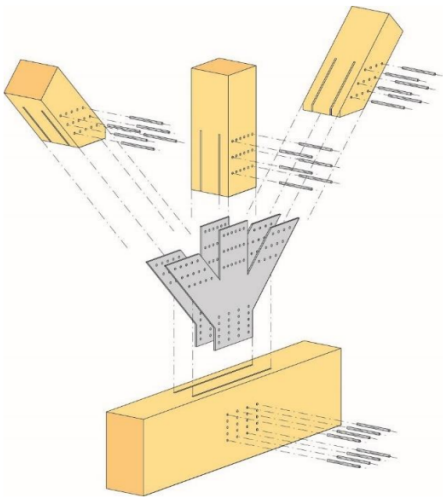

Figure 2.16: Example of a Slotted-in Steel timber connection [16]

As previously mentioned in this section, it is desirable to reduce the rotational stiffness of the connections. However, the minimum strength requirements result in a certain degree of rotational stiffness in the design. Additionally, the use of large connections is not preferred, as this leads to an increased use of steel. The use of more steel not only affects sustainability performance, but also results in additional point loads at the connection locations due to the higher weight of steel compared to timber. However, in order to maintain simplicity for the model, and since these values will not be in the same scale as wind loading and gravitational forces, the additional point loads will be disregarded.

The use of slotted-in steel plates allows for a certain degree of flexibility in the connection design. By varying the length and height of the steel plate, the rotational stiffness of the connection can be influenced. Figure 2.17 shows two connections with different plate dimensions. Both connections have the same number of bolts and approximately the same plate surface area. Nevertheless, the connection on the left has a higher rotational stiffness than the connection on the right [47].

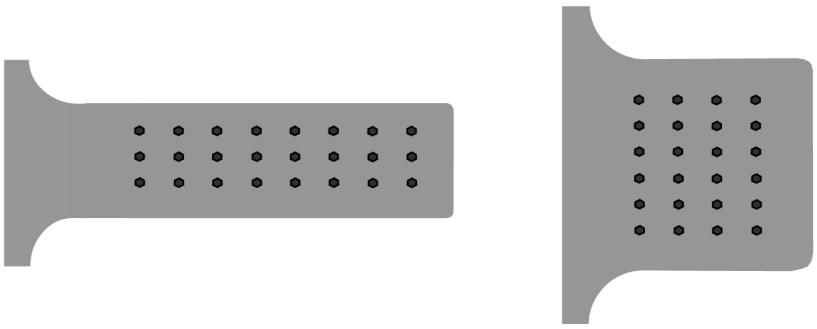

Figure 2.17: Two connections with different rotational stiffnessess

In addition to the dimensions of the steel plate, the size of the timber element itself has an even greater influence on the connection properties. Larger timber elements allow for larger connections and provide more space for bolts. As a result, a relation can be established between the element dimensions on one hand, and the strength capacity and rotational stiffness of the connection on the other. This relation is required to determine the rotational capacity of the connections that will be used in the different designs.

Furthermore, the diameter of the bolts also has a large influence on the total capacity of the connection. This is related to the minimum bolt spacing requirements established in the Eurocode [47]. Smaller spacing allows for a greater number of bolts to be placed side by side, which increases the overall capacity of the connection. However, using more and smaller bolts results in a more complex connection, which introduces challenges in terms of design and manufacturability. The method by which slotted-in steel plate connections for timber elements must be calculated is described in Section B.1 of Appendix B.

2.4 Wind Loads and Wind-Induced Accelerations

For high-rise structures, wind load is a critical factor that must be considered in the structural design. Wind loading significantly affects both the strength and serviceability requirements of a building. In the case of high-rise buildings, it is especially important to analyse the dynamic behaviour induced by wind action. This consideration is even more relevant for timber buildings, as the lower mass of timber elements increases the sensitivity of the structure's dynamic response to wind-induced vibrations [36]. Wind load ultimately manifests as a horizontal surface load applied to one side of the structure at a time. Because of the single degree of symmetry in the structure of research, wind from two principal directions must be considered in the design process. The resulting horizontal wind loads influence the strength capacity verification of columns, the core, and other stabilising elements. Additionally, wind loading leads to critical horizontal displacements at the level of the top floor, as well as to accelerations. Horizontal displacement is relevant for the SLS verification, which must comply with the requirement $u_{total} \leq \frac{1}{500} \cdot h_{total}$ [42]. Acceleration is evaluated against comfort criteria defined in ISO-10137 [33]. These criteria are displayed in Figure 2.18 The determination of wind load, deformation, and acceleration depends on numerous factors. In this section, the methods from NEN-EN-1991-1-4 [45] used to calculate these values will be explained.

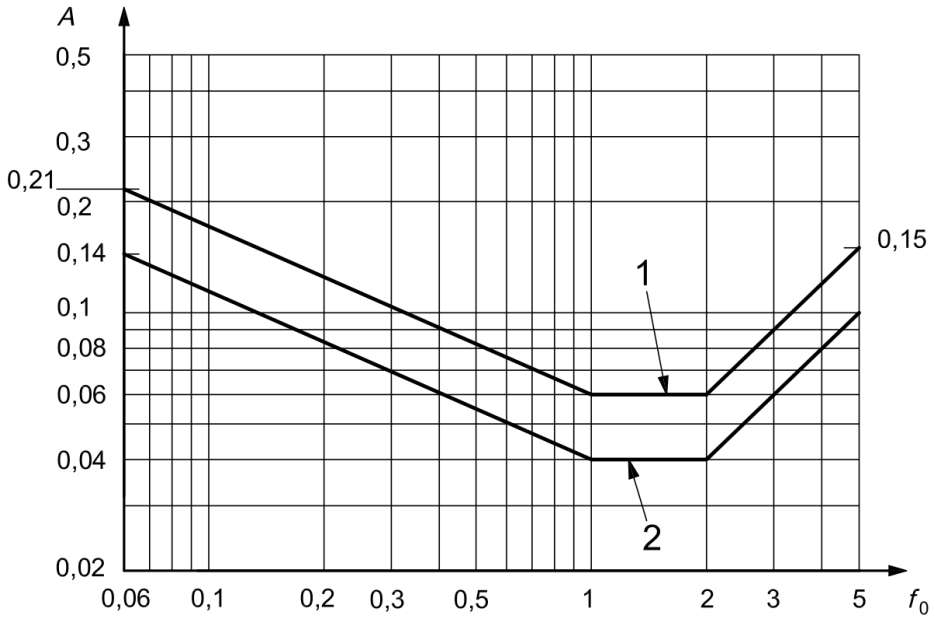

Figure 2.18: Comfort criteria as stated in ISO-10137 (curve 1 is for offices and curve 2 is for residences) [33]

2.4.1 Peak Wind Velocity and Extreme Wind Pressure

The extreme wind load acting on the building depends on the characteristic wind speed at the specific height at which it is evaluated. This characteristic wind speed is, in turn, a function of the basic wind speed v_b, which is defined by Equation 2.1.

$$v_b = c_{\text{dir}} \cdot c_{\text{season}} \cdot v_{b,0} \tag{2.1}$$

Where:

- c_{dir} is the wind direction factor (= 1.0 in the Netherlands)
- c_{season} is the seasonal wind factor (= 1.0 in the Netherlands)
- $v_{b,0}$ is the fundamental value of the basic wind speed, found in Table 2.2

Table 2.2: Reference wind speed $v_{b,0}$ for application in the Netherlands [49]

Wind zone	**I**	**II**	**III**
$\mathbf{v_{b,0}}$ **[m/s]**	29.5	27.0	24.5

Since high rise structures would likely be placed in urban areas, wind zone **II** is applicable as it spans the Randstad. Subsequently, the wind speed at each height can be determined using Equation 2.2.

$$v_m(z) = c_r(z) \cdot c_0(z) \cdot v_b \tag{2.2}$$

Where:

- $c_r(z)$ is the roughness factor, as found in Equation 2.3.
- $c_0(z)$ is the factor for terrain orography (= 1.0 in the Netherlands).

$$c_r(z) = \begin{cases} k_r \cdot \ln\left(\dfrac{z}{z_0}\right) & \text{for} \quad z_{\min} \leq z \leq z_{\max} \\ c_r(z_{\min}) & \text{for} \quad z \leq z_{\min} \end{cases} \tag{2.3}$$

Where:

- z_0 is the roughness length, found in Equation 2.3.
- k_r is the terrain factor dependent on the roughness length, found in Equation 2.4.
- $z_{\min}$ is the minimum height, found in Equation 2.3.
- $z_{\max}$ is the maximum height (= 200 m).

$$k_r = 0,19 \times \left(\frac{z_0}{0,05}\right)^{0,07} \tag{2.4}$$

Table 2.3: Terrain categories and terrain parameters [49]

Terrain Category	**Description**	$\mathbf{z_0}$ **[m]**	$\mathbf{z_{min}}$ **[m]**
0	Sea or coastal area	0.005	1
II	Non-built area	0.2	4
III	Built-up area	0.5	7

For this study, it is assumed that such a building will be located in a built-up area, which means that terrain category **II** applies. The next factor that can be calculated is the turbulence intensity $I_v(z)$ at height z. This is defined as the standard deviation of the turbulence divided by the mean wind speed and is given in Equation 2.5.

$$I_\nu(z) = \frac{k_l}{c_0(z) \cdot \ln\left(\frac{z}{z_0}\right)} \tag{2.5}$$

Where:

- k_l is the turbulence factor (= 1.0 in the Netherlands)

Now, the extreme wind pressure $q_p(z)$ can be determined, as seen in Equation 2.6. In Appendix A, a table can be found with values for $q_p(z)$ per height level for the relevant wind zone 2 of the Netherlands.

$$q_p(z) = (1 + 7 \cdot I_v(z)) \cdot \tfrac{1}{2} \cdot \rho \cdot v_m^2(z) \tag{2.6}$$

Where:

- ρ is the air density (= $1.25\ kg/m^3$ in the Netherlands)

The extreme wind pressure on high-rise structures is not uniform along the height of the building. Therefore, the extreme wind pressure on the lower parts of the structure can be reduced. This principle is illustrated in Figure 2.19.

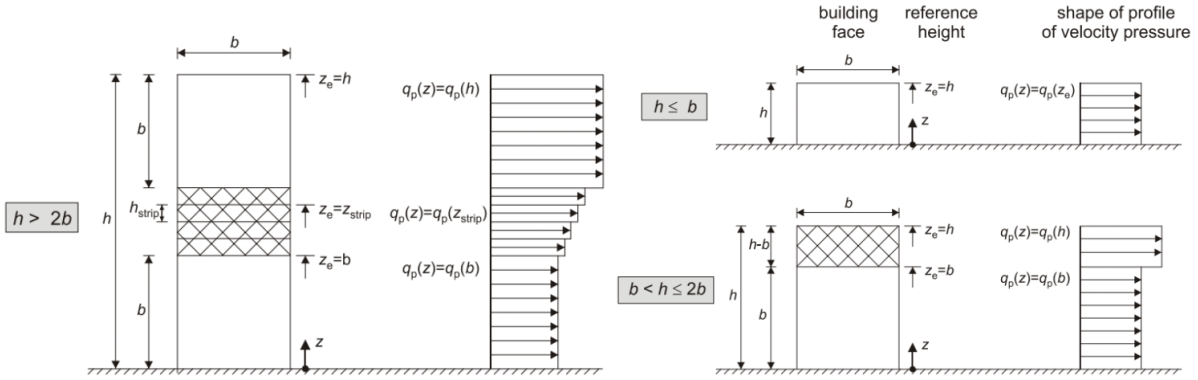

Figure 2.19: Extreme wind pressure distribution over height [45]

2.4.2 Wind Forces

The value of the extreme wind pressure is then used to determine the forces that are actually exerted on the building. This force is denoted as F_w and is given in Equation 2.7. In this Equation, a summation is included to account for the fact that different values of extreme wind pressure can occur at different heights.

$$F_w = c_s c_d \cdot \sum_{\text{elementen}} c_f \cdot q_p(z_e) \cdot A_{\text{ref}} \tag{2.7}$$

Where:

- A_{ref} is the reference area of the construction or construction element
- c_f is the force coefficient of the construction or construction element, as found in Equation 2.8
- $c_s c_d$ is the structural factor, as found in Equation A.1

The force coefficient c_f is a dimensionless factor that accounts for the interaction between the dynamic effects of wind and the geometry of the building. It is stated in Equation 2.8.

$$c_f = c_{f,0} \cdot \psi_r \cdot \psi_\lambda \tag{2.8}$$

Where:

- $c_{f,0}$ is the force coefficient of rectangular cross-sections with sharp corners and without correction for end effects, as given in Figure 2.20.
- ψ_r is the reduction factor for square cross-sections with rounded corners (= 1.0 for this research purpose)
- ψ_λ is the end-effect factor for elements where end effects play a role (= 1.0 for this research purpose)

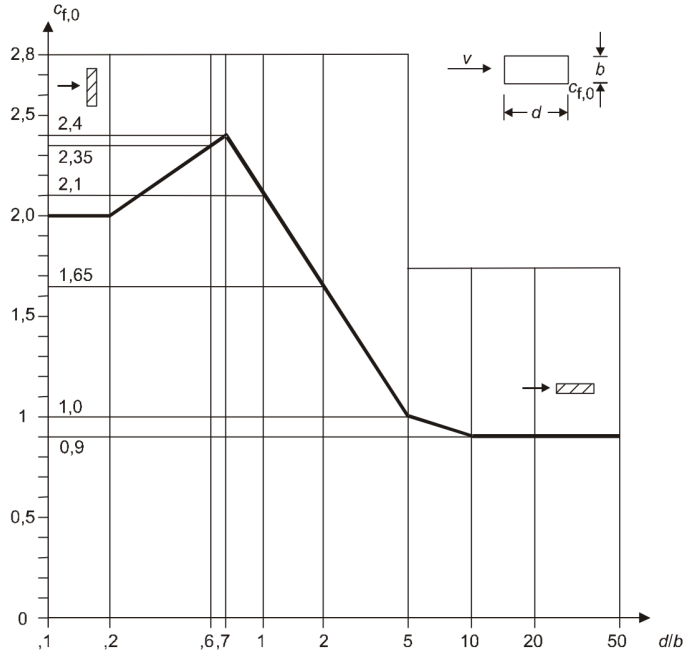

Figure 2.20: Determination of $c_{f,0}$ as function of the depth/width ratio of a building with sharp corners withound end-effects [45]

Given the squared cross-sectional geometry of the structure, $c_{f,0}$ can be taken as 2.1. For the determination of the wind force at this stage, the parameter $c_s c_d$ left to be determined.This parameter, known as the structural factor, consists of two components. First, c_s is the size factor, which acts as a reduction factor that accounts for the fact that extreme wind pressure does not occur simultaneously across the entire surface or height of the building. Second, c_d is the dynamic factor, which is an amplification factor that considers wind-induced vibrations that may resonate with the structure. The combination of these two factors is displayed in section 6.3.1 of NEN-EN-1991-1-4 [45], as stated in Equation A.1. In low-rise buildings, $c_s c_d$ can be taken as 1.0. However, for high-rise structures, the exact value of $c_s c_d$ could have a significant impact, that could result in a value that is either below or above 1.0. The procedure for determining the structural factor can be found in Appendix A.2.

In the equation found in Appendix A.2 and section 2.4.3, $n_{1,x}$ represents the natural frequency of the building. According to the Eurocode, for buildings exceeding a height of 50 metres, this value can be estimated as $\frac{46}{h}$. However, this is merely an approximation and is based on buildings that are not constructed from timber. In various studies, the natural frequency is determined more accurately [24], and in theory, this value can also be computed using finite element method (FEM) software such as SCIA or Abaqus. Nevertheless, to maintain the simplicity of the model and to limit the scope of this research, combined with the fact that the Eurocode does not explicitly state that the estimation is inapplicable to timber structures, the value of $\frac{46}{h}$ will be used in this study.

2.4.3 Characteristic Peak Accelerations

In addition to the characteristic displacement at the top floor, acceleration is also an important factor that must be considered in the design. The characteristic along-wind acceleration at height z of the structure can be determined using Equation 2.9. It is based on the standard deviation ($\sigma_{a,x}$) of the characteristic

acceleration, which is stated in Equation 2.10. This acceleration can be compared against the comfort criteria displayed in Figure 2.18.

$$a_{max} = \sigma_{a,x} \cdot k_p \tag{2.9}$$

$$\sigma_{a,x}(y,z) = c_f \cdot \rho \cdot I_v(z_s) \cdot v_m^2(z_s) \cdot R \cdot \frac{K_y \cdot K_z \cdot \Phi(y,z)}{\mu_{\text{ref}} \cdot \Phi_{\max}} \tag{2.10}$$

Where:

- c_f is the force coefficient (2.8).
- ρ is the air density ($= 1.25\ kg/m^3$).
- $I_v(z_s)$ is the turbulence intensity at height z_s above ground level (2.5).
- $v_m(z_s)$ is the characteristic mean wind speed at height z_s above ground level (2.2).
- R is the square root of the resonant response factor (A.5).
- K_y, K_z are the constants based on the mode shape ($= 1.0$ and $3/2$ respectively for a uniform horizontal and a linear vertical mode shape).
- μ_{ref} is the reference mass per unit area.
- $\Phi(y,z)$ is the mode shape at height z.
- $\Phi_{\max}$ is the value of the mode shape at the point of maximum amplitude.
- k_p is the peak factor defined as the ratio of the maximum value of the fluctuating part of the response to its standard deviation (A.2).

Since the acceleration at the top floor will govern the design, Equation 2.11 can be assumed.

$$\frac{\Phi(y,z)}{\Phi_{\max}} = 1 \tag{2.11}$$

2.5 Lateral Stability

In high-rise structures, the primary challenge lies not in the vertical load capacity but in ensuring lateral stability. Tall buildings are subject to large horizontal forces arising from wind and seismic excitation. These lateral forces induce various effects throughout the structure. If a building is sufficiently stiff, it can be modeled as a cantilevered beam that possesses both bending and shear stiffness. This results in horizontal deflection, with the largest displacement occurring at the top level of the structure.

The foundation itself also has a degree of elasticity, which contributes additional horizontal deflection to the overall movement of the building. A conservative assumption is that the horizontal deflection at the top due to foundation rotation is approximately equal to the deflection resulting from the building's bending and shear stiffness. These values can be summed together to calculate the total horizontal deflection.

Furthermore, the lateral forces due to wind excitation will take the form of a uniform distributed load. Because the building is schematized as a cantilevered beam, this load will exert a large moment at ground level. This will cause compression in the vertical elements on one side of the building, and tension in the other side. In the Netherlands, the aim to allow tension forces in the foundation is very complicated. Therefore, the general preliminary constraint is adapted that no tension forces in the columns are allowed. This means that the tension forces caused by the wind-induced moment in the foundation have to be compensated by the compression force caused by the self weight of the structure.

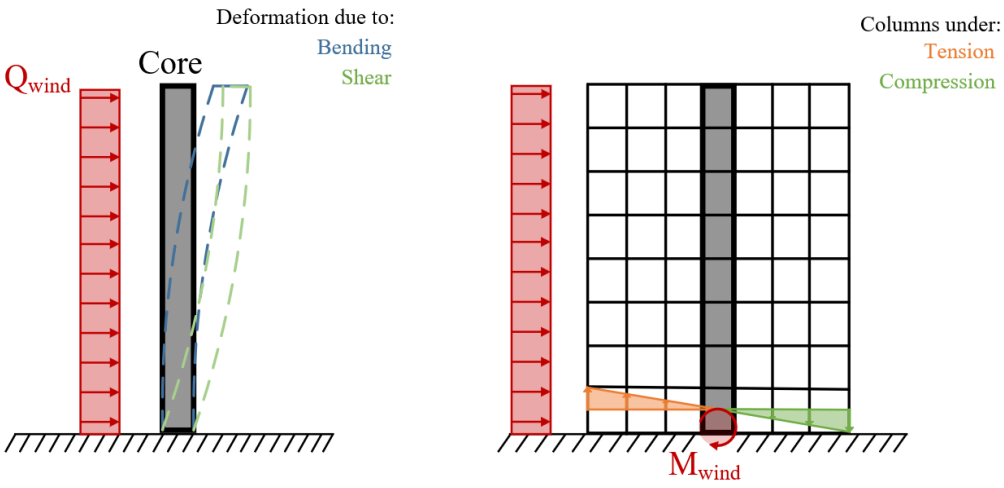

Figure 2.21: Effect of lateral forces on a building

There are specific limits to deflections that are documented in the Eurocode. Therefore, it is essential for the building to have sufficient capacity to resist the imposed lateral forces. To achieve this required capacity, various systems can be incorporated into the building's structural design to enhance stability. Generally speaking, the taller the building, the more sophisticated the lateral stability system needs to be.

2.5.1 Diagonal Bracing System

In steel construction, once certain building heights are reached, a lateral stability system is often achieved by introducing diagonal beams. This is typically implemented through the creation of a diagonal grid system, allowing the building to function as a massive truss. That will provide sufficient lateral stability. Since timber elements tend to have similar characteristics to steel in terms of strength-to-weight ratio and available element lengths, it is logical to explore timber solutions that have similar shapes to steel lateral stability systems.

The effectiveness of a diagonal bracing system for timber structures has been demonstrated in numerous studies and actual building projects. M. Felicita investigated the influence of different preliminary design parameters on timber high-rise structures, finding that the design choice of a braced system had the most positive and effective impact on the design, reaching a height of 200 meters in her case study [24]. A. van Rhijn also investigatied the possibilities for high-rise timber structures in the Netherlands, concluding that a diagrid system positively affects the lateral stability of the structure [52]. J.F. de Gooij developed a multidisciplinary optimization tool for timber high-rise buildings, basing the entire model on a diagonal braced system [27].

Similarly, C. Eckholm, in Side Walk Talk, explored the future of timber mass buildings and found that for a 35-storey tall timber case study, the only viable pure-timber structural system was a timber exoskeleton [19]. This system allowed for complete floor plate flexibility. The engineers behind the River Beech Tower visionary project proposed two adjacent towers, each featuring triangular pattern structural elements, connected by large diagonal elements to provide adequate lateral stability for the 228-meter-high structure [55]. The Oakwood Tower, another ambitious timber high-rise concept at 300 meters, incorporated large diagonal elements alongside multiple buttressed towers for lateral stability [51].

Diagonal timber frames have been used in existing timber high-rise structures as well; Mjøstårnet (2.1.4) and Treet (2.1.1), two of the tallest completed all-timber buildings [54], employ glulam diagonal beams for lateral stabilization.

2.5.2 Outrigger System

Another common approach for providing lateral stability in buildings is the use of a concrete core. This core is effective because it is cast on-site, which eliminates the need for internal connections and results in stiffness comparable to the bending and shear stiffness of a cantilevered beam. The effectiveness of the concrete core can be further enhanced by incorporating outriggers. These consist of steel trusses placed at certain levels throughout the building's height. The rigid nature of these trusses allows them to transform lateral loads caused by wind excitation into vertical loads directed into the perimeter columns. This effectively extends the lever arm over which the lateral forces are applied, thereby reducing the internal moment at the base of the core [12].

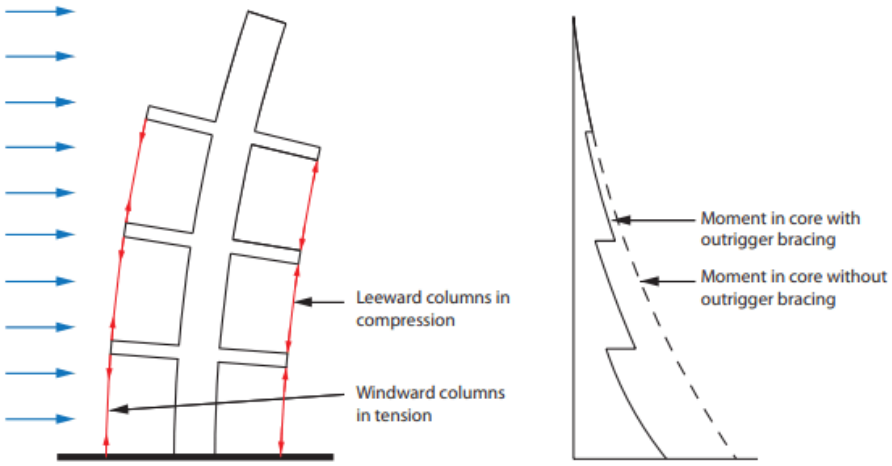

Figure 2.22: Schematization of the mechanical principle of an outrigger system [12]

Outrigger systems have been shown to provide substantial lateral stability and are widely used in existing high-rise structures. Although high-rise timber structures with outriggers have not yet been realized, theoretical studies suggest that timber outrigger systems could also be effective.

F.F. Janssens conducted research on the impact of adding a timber outrigger to a CLT core. The study aimed to evaluate its effectiveness in reducing maximum lateral deflection and peak horizontal acceleration [35]. Although the research focused on a CLT core with a maximum height of 40 meters, it demonstrated that the addition of a timber outrigger positively influences lateral stability. This principle would still be valid for high-rise structures. The reduction in maximum lateral deflection observed in the study reached up to 35% compared to a structure that only used a CLT core.

E.C. Slooten explored the feasibility of a 300-meter tall timber-concrete hybrid tower [56]. The design incorporated a timber outrigger system in combination with a concrete core. Slooten also compared different configurations of timber outriggers to optimize the system. He found that adding a single outrigger significantly decreased maximum lateral deflection by 37%. After adding more outriggers, the additional influence stagnated. The implementation of 2 more outriggers resulted in a total reduction of maximum lateral deflection of 54%. Despite this, Slooten's final design included three timber outriggers. The configuration was able to meet the structural integrity requirements according to the building codes.

2.6 Time-dependent Differential Deformations

During the design of any type of structural system, strains of construction materials must be considered. These strains include both instantaneous of time-dependent deformations. and they introduce additional displacements within the structure. Differences in column loading, or column utilization, lead to varying strains in different columns. Such differences can cause structural problems. Examples include column misalignment or tilt of floors as well as the development of unintended stresses within the structure. In high-rise construction, this effect is further amplified, as small accumulated differences across many floors can result in a significant and non-negligible impact [38]. The use of different material types also results in varying degrees of displacements. Consequently, designing a hybrid structure with a concrete core, together with timber columns, presents an additional challenge for which appropriate solutions must be developed [39].

For concrete and timber, time-dependent displacements are calculated differently according to the Eurocode. The following two sections address these methodologies. A deeper analysis of the exact mechanisms and physical principles behind time-dependent deformations is beyond the scope of this research.

In Eurocodes 2 and 5, corresponding to concrete and timber respectively, methods are provided to calculate the time-dependent strains of these materials. Different calculation approaches must be followed for concrete and timber due to their distinct material behaviors. The method used to compute the time-dependent deformations of both concrete and timber is described in Appendix C.

2.6.1 Inter-material Differential Shortening and Proposed Solutions

When calculating time-dependent deformations for both concrete and timber, as well as from practical examples, it has been observed that timber undergoes greater deformations than concrete [23]. As seen in section 2.1.2, in an 18-storey building, this will result in a differential vertical shortening between timber columns and a concrete core of approximately 50 mm at roof level. This difference is the result of an accumulation of individual shortenings occurring on each floor. By adding steel plates to the column-to-column connections at various levels, this differential can be compensated. The required thickness of these steel plates largely depends on the calculated dead and live loads acting on the column. Due to uncertainties regarding the magnitude of the live loads and the final shrinkage and creep over the building's lifespan, Brock Commons opted to make the total plate thickness 50% of the total predicted shortening, in order to avoid overcompensation.

O. Willebrands conducted research on measures to mitigate differential vertical shortening [66]. He found that the most effective strategy is to place thicker steel shims in the connections of the lower floors, where elastic strain is highest due to greater loading. In addition, he performed a sensitivity analysis considering building height, column utilisation and construction duration. The analysis showed that DVS increases linearly with building height. A reduction in column utilisation, meaning an increase in the cross-sectional dimensions of columns, results in a decaying negative exponential relation with DVS. This implies that increasing column size in small increments has a significant effect, but its influence becomes progressively smaller. Similarly, extending the construction duration also leads to a decaying negative exponential relation with DVS. Consequently, delaying the loading of newly installed columns can be effective, although it has a significant influence on the construction process.

The case study of Brock Commons and the research by O. Willebrands have shown that the effects of differential vertical shortening can in theory be sufficiently mitigated by adding steel plates to the column-to-column connections. This is only possible if the time-dependent deformations are accurately calculated and appropriate steel plate thicknesses are carefully selected based on those calculations. The exact thickness and dimensions of these steel plates have a minimal impact on the outcome of this study, and it is therefore assumed that the implementation of this measure will prevent differential vertical shortening from becoming a governing factor for the designs.

2.7 Fire Safety

Fire safety is a crucial aspect to consider when designing any type of structure. Strict regulations are in place to ensure that buildings meet the required fire safety standards. This research specifically focuses on the minimum fire resistance of structural elements. According to the Dutch Building Decree (Bouwbesluit), a compartment in a building exceeding thirteen meters in height must have a minimum fire resistance of 120 minutes [6].

For timber constructions, fire safety is an especially important point of attention. This is primarily due to the fact that timber is a combustible material. As a result, the main load-bearing structural components can provide additional energy or fuel to the fire. This increases the difficulty of achieving the required fire resistance of 120 minutes.

During the design of a building, it must be verified against the design load under fire conditions. Fire conditions utilize different load factors to be used compared to the normal design situation. The method by which this verification must be performed is described in NEN-EN-1995-1-2 [48] and elaborated in Appendix D.

2.7.1 Refuge Floors and Self-Extinguishment of Timber

The fact that this research focuses on high-rise constructions adds further complications. For floors higher than the 8th, it becomes impossible for the fire department to rescue people using ladders [50]. If a safe route to the ground is no longer available, people will remain trapped in the building until the fire is extinguished. In current high-rise constructions, this challenge is addressed through the use of *refuge floors*. Refuge floors are designated levels, located approximately every 25 stories, where people can seek shelter. These floors are made extra fire safe to allow occupants to remain there until the fire is extinguished or brought under control [40]. Refuge floors are equipped with natural ventilation systems to ensure smoke can be expelled effectively, maintaining breathable air. Additionally, pressurized smoke control systems are installed in the vestibules to prevent smoke infiltration into safe zones. The walls and doors on these floors are constructed using fire-resistant materials to limit heat transfer and maintain structural stability under high-temperature conditions. If this principle is applied, it becomes critically important that these floors do not collapse. Even if the fire resistance requirement of 120 minutes is met, this could still pose a significant problem.

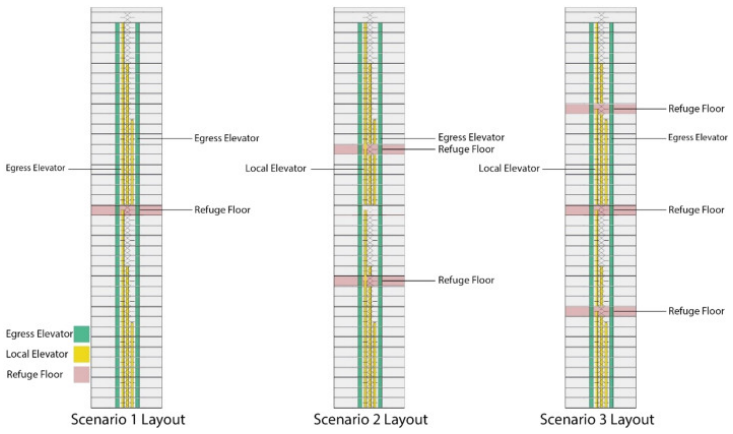

Figure 2.23: Refuge Floors in a high-rise building [41]

This initially points to a focus on achieving complete *burnout* of the building without compromising its structural integrity. Burnout refers to the scenario where all combustible material within a burning compartment is consumed, allowing the structure to survive without failure. However, complete burnout remains a challenge for timber constructions. A study on the self-extinguishment of CLT panels have shown that laminated timber can exhibit this behavior. Nevertheless, this depends on specific conditions and cannot be assumed in all situations. A study indicated that self-extinguishment only occurs when the applied heat flux is below 5–6 MJ/m^2 and the airflow speed is less than 0.5 m/s [15]. In practice, designing to meet these specific requirements remains rather optimistic.

2.7.2 Fire Safety in Existing Timber Structures

Extensive fire safety research was conducted for the design of the Mjøstårnet in Norway (see section 2.1.4). A new method was developed for this project to calculate whether complete burnout would occur. The calculation begins by determining the final charring depth of the material, based on Annex A of Eurocode 5 [48]. This charring depth accounts for additional timber that serves as fuel for the fire, resulting in an increased fire load. The fire load is then incorporated into a revised calculation of the final charring depth, which will be higher than the initial value. This new charring depth will again result in additional fire load, and through an iterative process, the final charring depth can be determined. If these calculations converge, it indicates a complete burnout, which is considered a positive outcome. Furthermore, based on the total charring depth, it is then assessed whether structural requirements are met. If not, additional encapsulation can be applied, and the calculations repeated until compliance is achieved. These calculations allow for determining how much exposed timber can be used without leading to structural failure during complete burnout [34]. This approach enabled the use of exposed timber in the Mjøstårnet's design, offering significant architectural benefits.

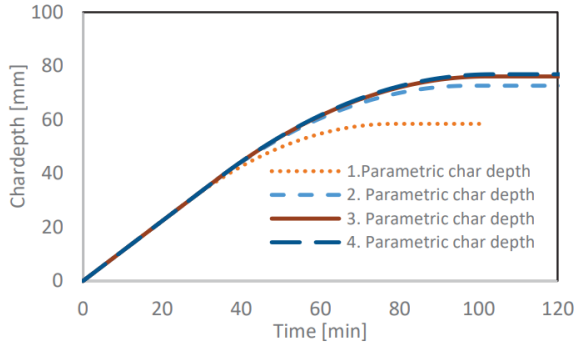

Figure 2.24: Iterative charring depth calculation for the Mjøstårnet building [34]

.

In the Brock Commons building in Canada, the fire resistance requirements were achieved through full encapsulation [29]. This was done by applying multiple layers of Type X gypsum boards (commonly used gypsum board type in North-America, in the Eurocode, type F is more widely used), which protect the timber elements and provide fire resistance. A second principle implemented in this building is the use of a small compartmentalization structure. This makes it highly likely that a fire will remain contained within a single compartment.

2.7.3 Design for Encapsulation and Active Measures

The Brock Commons building is an example of the focus on *encapsulation*. Currently, the fire safety requirements for timber buildings are best achieved by applying encapsulation. Encapsulation is a crucial concept in fire safety design. This also ties back to the fact that occupants on higher floors cannot evacuate a building if a lower floor is fire affected. Table 2.4 provides guidelines for the potential level of specified performance and the corresponding design strategy for timber elements based on the height of a building.

Table 2.4: Possible hierarchy of requirements related to building height [10]

Building Type	**Possible Level of Specified Performance**	**Possible Design Strategy for Timber Elements**
Low-rise buildings	Escape of occupants with no assistance No property protection	No encapsulation
Mid-rise buildings	Escape of occupants with no assistance	No encapsulation
Taller buildings	Some property protection Escape with firefighter assistance Burnout with some firefighting intervention	Limited encapsulation
Very tall buildings	Protect occupants in place Complete burnout with no intervention	Complete encapsulation

The question remains: how can timber elements be best encapsulated? In practice, this is often achieved using gypsum boards. With the addition of a relatively thin gypsum board, a significant protection for timber elements against fire for a considerable amount of time can be achieved. This delays the onset of charring. After a certain period, the gypsum board will fall off, and the charring process will begin. A disadvantage, however, is that the timber elements may have already been heated while the gypsum board was still in place. This results in a higher charring rate compared to the unprotected scenario. Studies have explored new types of gypsum boards that can provide longer protection against charring and keep the temperature of the timber behind the board low simultaneously, thereby preventing accelerated charring once the board falls off [30]. The gypsum board known as 'SFRM' has shown promising results. Nevertheless, more conventional types of gypsum boards, such as Type F, can already provide extended protection against the charring of timber elements.

In addition to focusing on encapsulation, the possibility exists to install a sprinkler system in the various compartments of a building. The use of a sprinkler system significantly reduces the likelihood of flash-over. In the Netherlands, it is generally accepted that the installation of a sprinkler system allows for a 30-minute reduction in the required fire resistance. This means the fire resistance requirement can be lowered from 120 to 90 minutes [31]. This principle was also implemented in the design of HAUT in Amsterdam [67].

At the end of this section, the required thickness of the gypsum board will be calculated to ensure that a standard fire can burn for at least 120 minutes without compromising the structural timber elements. The method for determining the thickness of these boards is specified in the Eurocode and is provided by equation (2.12) [48].

$$t_{ch} = 2.8\, h_p - 14 \tag{2.12}$$

Where:

- h_p is the thickness of the gypsum board, or, in the case of multiple layers, the total thickness of the layers;
- t_{ch} is the time at which charring begins.

The minimum duration to be achieved depends on the fire load present in a compartment, which essentially represents the amount of combustible material available, but is also dependent on the ventilation conditions and other factors. For this study, the conservative assumption has been made that the fire load results in a fire duration of 180 minutes until burnout occurs. Using this information, the minimum required gypsum board thickness can be calculated as $h_p = \frac{180+14}{2.8} \approx 70\,\text{mm}$.

By applying this thickness of gypsum boards to the columns, the timber will be adequately protected against charring. Consequently, structural failure will be prevented. However, this will increase the surface area occupied by each column, which will impact the available net area per floor.

Chapter 3

Methodology

In this chapter, the following sub-questions will be answered:

1. *In what way can a representative base model be designed for variable building heights, and how can meaningful structural variants be derived from it?*

   This question is first addressed by analysing the parameters and variables relevant to the research. This is done in Section 3.1. The base model and the design variants are then developed and described in Section 3.2.

2. *How can the design variants with varying storey numbers be efficiently and parametrically modelled, analysed, and dimensioned?*

   To answer this question, the occurring load cases and load combinations are first examined, as described in Section 3.3. The implementation of the rotational stiffnesses of the connections is then described in Section 3.4. To complete this subquestion in its entirety, Section 3.6 explains how the actual parametric model is created, how a structural analysis can be performed on it, and how the elements can be dimensioned based on this analysis.

3. *How are the model iterations evaluated, structured, and visualised based on defined criteria, and how do the variants perform relative to the base model with respect to these criteria?*

   This chapter addresses the first part of this sub-question. Once the dimensioning of the base model and all variants for different building heights has been completed, it becomes possible to determine how these iterations are evaluated and on the basis of which assessment criteria. This is done in Section 3.7, which concludes the Methodology chapter.

3.1 Variable Study

In this study, numerous types of variables are considered, each influencing the structural performance and sustainability of the design. It is important to eliminate as many variables as possible early in the process by making initial design decisions. Next to this, the approach follows a process in which a variable is first optimized and then fixed as a parameter to facilitate the optimization of other remaining variables.

Since numerous variables influence the design of a structure, it is practical to categorize the remaining variables into different groups. Each variable can then be analyzed to determine whether it should be retained as a variable or assigned a fixed value or configuration earlier in the process.

3.1.1 Geometry Parameters

The following variables significantly affect the geometry of a building:

- **Column Distance**: Defines the span of the floors and beams, directly impacting structural efficiency.
- **Number of Grid Points**: Determines the number of columns along both the x- and y-axes, shaping the overall structural layout, which a squared shape in this study.
- **Storey Height**: Sets the vertical spacing between floors, influencing the overall building height and floor clearance.
- **Number of Storeys**: Establishes the total building height and total usable floor area.
- **Variant Selection**: Discrete selection parameter dat determines the geometry whether and in which arrangement diagonal stabilizing elements will be placed.

The column distance, together with the number of grid points, determines the overall width of the building. However, to ensure consistency across design variants, the building width is intended to remain constant. As a result, these two variables will be constrained to a predefined set of combinations. These combinations will make up the different floor plans described in Section 3.2. Additionally, the storey height is modelled as a variable, but fixed at 3.5 meters, but in practice, it is dependent on the height of the beam element, as this number is dependent on architectural considerations, with a minimum floor height is prescribed by the Eurocode. Finally, a distinction is made between two variants for the selection parameter: a diagonal bracing system and an outrigger system. Within the diagonal bracing system, two options are defined: a light configuration and a heavy configuration. These aspects are further described in 3.2.

3.1.2 Element Properties Parameters

Besides variables that influence the geometry, there are also variables that determine the structural properties of the construction. These variables are listed below:

- **Choice of material type**: Influences the mechanical properties, weight, and environmental impact of the structure.
- **Cross-section dimensions**: Defines the load-bearing capacity of beams and columns, impacting structural performance and material efficiency.

- **Core thickness**: Affects the lateral stability of the building, with thicker cores generally improving stiffness but increasing material usage.
- **Connection size of elements**: Determines capacity and the rotational stiffness of the connections, which on its turn influences the degree of moment transfer between structural elements, affecting the overall stability and load distribution.

The choice of material type depends on the specific variant being analyzed. As a result, it will not remain a free variable. The material types of the concrete and timber are described in section 3.2. Subsequently, an iterative process is used to determine the most slender cross-section dimensions for every element type in each variant. There will be no variation in the same element type at different height within the building. Next to this, the core thickness influences the overall stability against wind loading. However, it will also introducte more CO_2 uses which will negatively influence its performance. The rotation stiffness of the connections is a crucial factor in the building's performance, as greater stiffness enhances overall stability by allowing the structure to act as a unified system. However, as an hypothesis, increased stiffness also raises the risk of larger tensile forces in the outer columns due to horizontal wind loads. Furthermore, stiffer connections generate higher stresses in the elements, and requiring more steel, which negatively impacts both sustainability and the loads on the structure. The connections are introduced in the model as rotational springs and way the corresponding rotational stiffness is determined is described in seciton 3.4.

3.2 Variant Study

In this section, the different design variants used in the study are described. First, a base model is developed, for which the structural behaviour is assessed as the building height increases. This allows the establishment of a baseline for structural behaviour. To this base model, stabilizing elements are added in two different methods. These two approaches will form the variants that will be compared and analyzed. For both variants, the influence on structural behaviour is examined. Within each variant, multiple configurations are possible regarding how the stabilizing elements are integrated into the structure. Since the stabilizing elements are added to a base model with known structural behaviour, the effect of these elements can be, if existing, directly derived from any observed performance increase.

3.2.1 Base Model

In this section, all elements that remain identical across each variant are described. These will include the different Floor Plans that are being used, the core, floor panels, the beams, and the columns.

Floor Plans
At some point as the building height increases, it becomes necessary to increase the dimensions of the core with it. To maintain a perimeter of 30 by 30 meters and ensure simplicity in the floor plans and model, three grid configurations have been selected. These are shown in Figure 3.1.

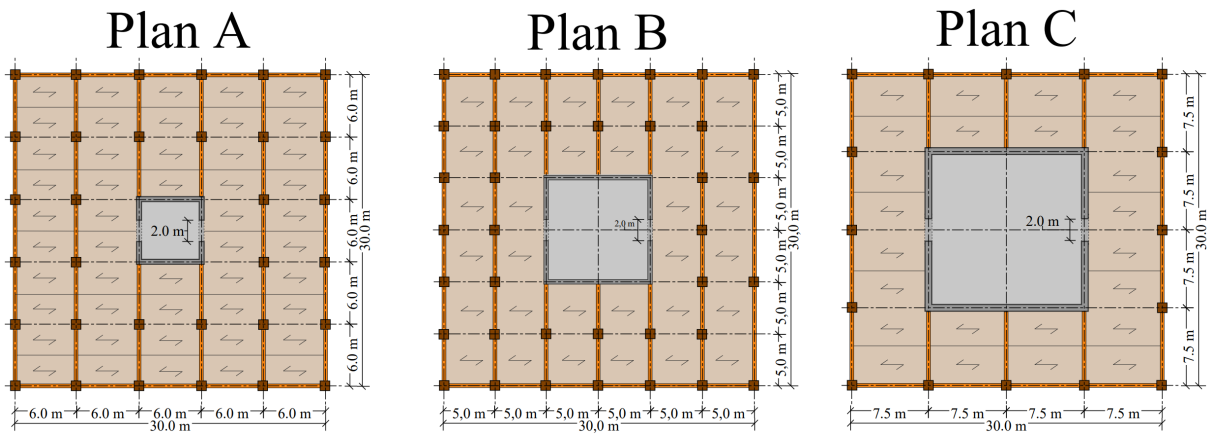

Figure 3.1: Floor Plans A, B & C emphasizing different core sizes

Floor plan A has the smallest core size, which means it provides the highest net floor area. Therefore, this floor plan is initially selected. As the height of the building increases, the core size of floor plan A will eventually no longer provide sufficient stability. At that point, floor plan A will be replaced by floor plan B, and later by floor plan C. When this transition occurs, two effects take place. First, the net floor area is significantly reduced. In addition, the CO_2 emissions resulting from material use will show a significant jump due to the stepwise increase in core dimensions.

To maintain simplicity in the model, changes in core dimensions affect the chosen grid layout, which in turn influences the column spacing. As a result, the required dimensions of the columns and beams will also change. This is an unavoidable negative side effect of the model. However, the impact of this effect on the outcome of this research remains limited, as it occurs in all variants. Therefore, the effects of the different variants can still be analyzed reliably.

Figure 3.2 shows how the base model is configured for the different floor plans. These example side views are presented with 21 storeys.

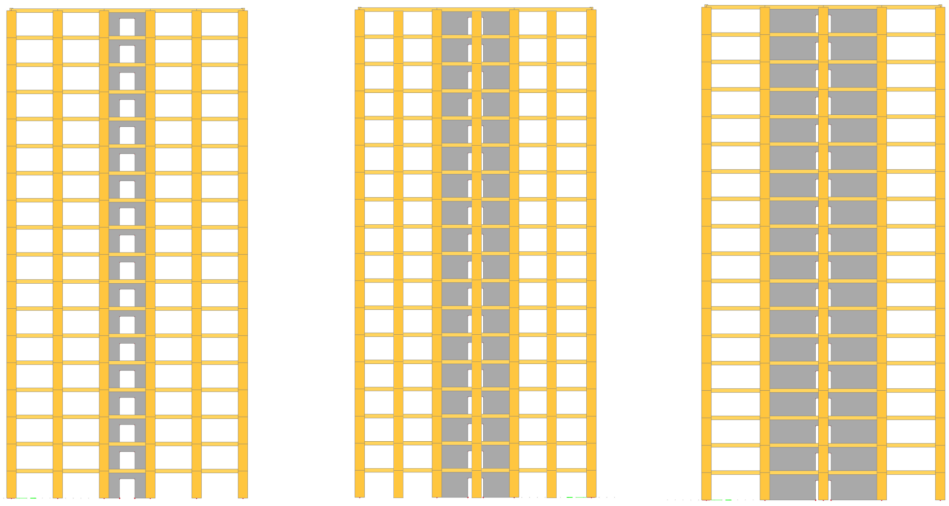

Figure 3.2: Side Views of base model for floor plan A, B & C, from left to right

Concrete Core

As shown in Figure 3.1, each floor plan includes a concrete core. For the sake of simplicity, concrete strength class **C30/37** is used throughout the whole research. The core thickness, as described in section 3.1, is a varied over the iterations of the process, and will range between 100 and 400 mm. If the core fails for the highest possibility, a new Floor Plan must be introduced. In each floor plan, an opening of 2 meters in width is applied on two opposite sides of the core. Figure 3.3 shows a side view and a 3D view of the core.

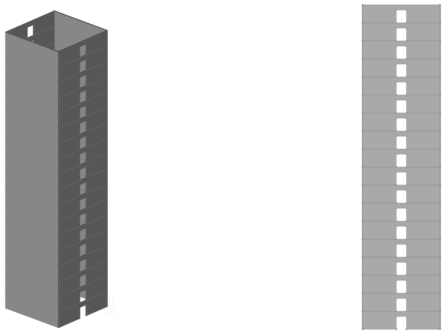

Figure 3.3: 3D- and Side View of the concrete core (example with 21 storeys and floor plan C)

Floor Panels

For the floor structures, it is desirable to use as much timber as possible in the designs. However, the implementation of floors made entirely from CLT introduces several challenges.

- Negative acoustic effects [8],
- Unfavourable dynamic effects regarding acceleration at the top storey due to the lower weight compared to concrete floors [1],
- Reduced performance with respect to footfall-induced vibrations [57],
- Potential risks related to punching shear in a CLT floor caused by high column loads perpendicular to the grain direction, as countered in the floor system displayed in Figure 3.4.

To (partially) compensate for these effects, TCC floors can be used. These floors are discussed in Sections 2.1.5 and 2.1.3. The advantage of such floors is that the timber on the lower is under tension, while the concrete on the upper side is under compression. In addition, the concrete layer improves sound insulation between storeys. At beam supports, the floor can be made entirely of concrete, eliminating the risk of punching shear due to high forces perpendicular to the grain direction. This happens only when the compressive strength of the concrete is higher that that of the timber. Therefore, the concrete type in the floor panels should be of type C30/37 or higher. Figure 3.4 shows a cross-section of such a floor system and illustrates the principles mentioned above.

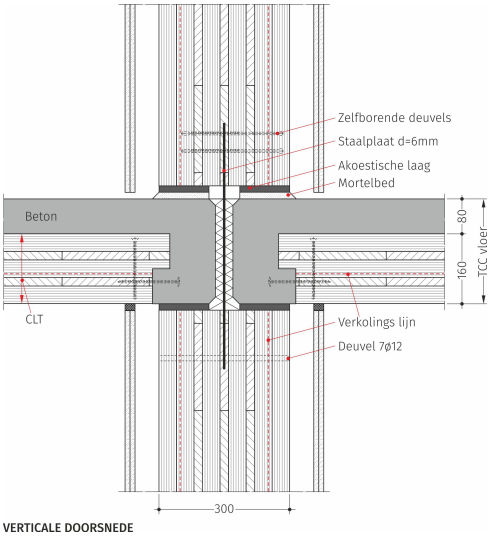

Figure 3.4: Cross Section of a TCC floor panel [8]

As shown in Figure 3.1, the floors span in one direction over the GLT beams. The floor systems will be identical in both the base model and all design variants. Therefore, the floor system shown in Figure 3.4 is applied throughout, and it is assumed that this system will suffice in each case. In reality, this may be an overly optimistic assumption. However, since it is applied consistently across all variants, it does not introduce differences between them and the results are still relevant.

In addition, this specific floor system cannot be implemented as a default material using the Grasshopper KOALA plugin that will be used (see Section 3.6.2). Nevertheless, it is important that the floors are included in the model. This relates to the diaphragmatic function of the floors, which, together with the beams along the building perimeter, contribute to global stiffness of the building and transfer horizontal wind-induced forces to the core. To enable this diaphragmatic action, the floors must be modelled *in-*

plane. Therefore, the floors will be modelled as concrete floors with the same weight as the TCC floors, which equals $108\ kg/m^2$. In the CO_2 calculations, however, the floors are treated as TCC floors.

GLT Beams & Columns
In all Floor Plans, both in the Base Model and in the variants, GLT columns with a square cross-section of type GL 28h are used. Additionally, GLT elements of type Gl 28h are applied for the beams in both the X and Y directions, but with a height-to-width ratio of 1.5 (i.e., $h = 1.5b$). Depending on the forces acting on the elements and the Unity Check of the iteration, an appropriate dimension is selected. GLT beams can be manufactured in any shape and size. To limit the number of cross-sections to choose from and to define minimum and maximum element sizes, the cross-sections are selected from a predefined catalogue, which is presented in Table G.1 of Appendix G. Although this catalogue has been established arbitrarily, it employs realistic material dimensions ranging from 300 mm to 1500 mm. In this table, also entries of concrete dimensions are found. These will be relevant for variant 2 (see Subsection 3.2.3).

3.2.2 Variant 1: Braced System

The first variant added to the base model is a diagonally braced system. This system will include diagonal truss-like GLT beams. The function and demonstrated effectiveness of similar systems are described in Section 2.5.1 of this study. However, no existing buildings currently combine this system with a concrete core. The analysis of this variant will determine whether applying a diagonally braced system in addition to a concrete core can provide increased stability compared to using a concrete core alone. The implementation of this system introduces additional connections and requires the use of extra steel. The use of steel is associated with higher CO_2 emissions than concrete, as discussed in Section 3.7. For this reason, it can be examined whether this system performs better in terms of CO_2 emissions compared to the base model, since a floor plan with a smaller core can potentially be maintained for a larger amount of storeys.

The analysis will also determine whether the application of the diagonally braced system has any significant structural effect at all. A well-known structural principle is that stiffer elements attract the majority of the forces. In general, a concrete core is significantly stiffer than timber diagonals. An alternative hypothesis is therefore that the interaction between the two stabilizing systems is limited, and that the contribution of the diagonally braced system remains minimal. This could especially be the case for the floor plans with larger cores sizes.

For the different floor plans, the diagonally braced system will take on slightly different forms. This is due to the shift in the locations of the nodes between which the diagonal beams can be placed. For each floor plan, two sub-variants are created: one light bracing configuration (Variant 1L) and one heavy bracing configuration (Variant 1H). This allows the difference between these two configurations to be examined as well.

Figure 3.5 shows the configurations of the diagonally braced systems for the different floor plans. This figure also indicates the locations where the slotted-in steel connections will be positioned. In designing the various configurations, the aim was to keep the angles of the diagonals as close as possible to 45 degrees. Due to logistical and constructability considerations, the maximum length of the diagonal beams is limited to below 16 meters.

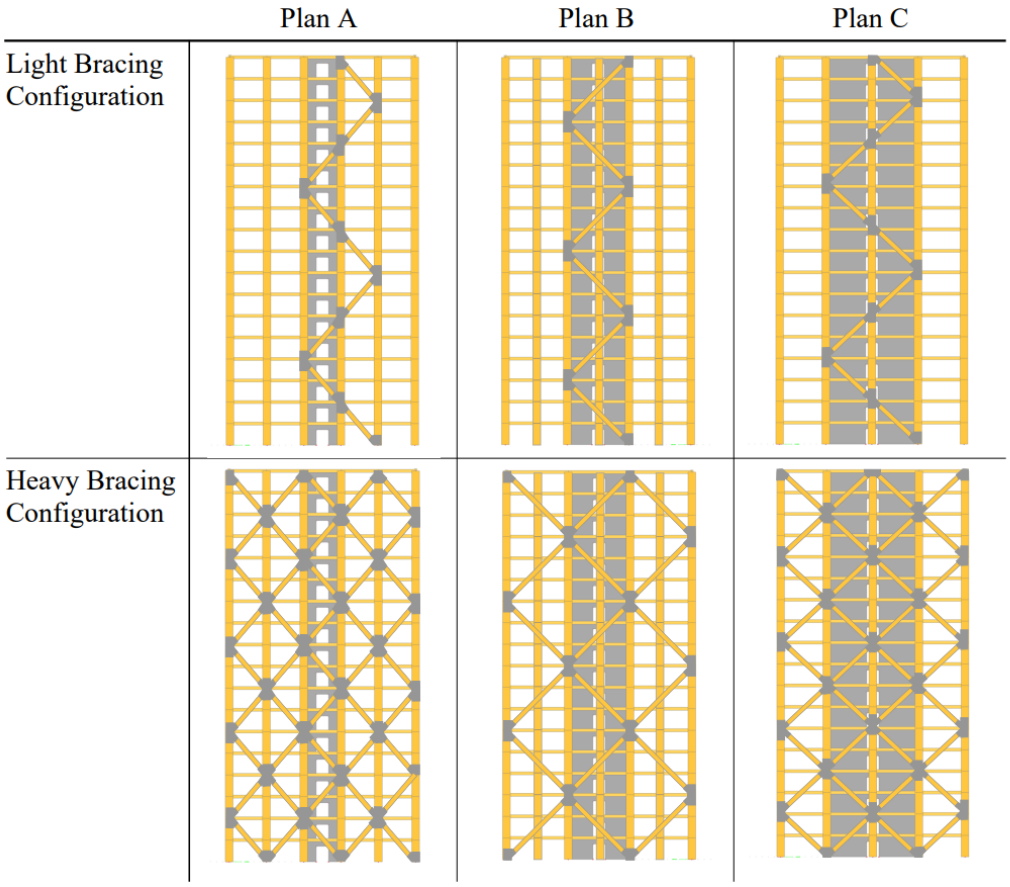

Figure 3.5: Side views of variant 1 for all floor plans with two bracing configurations each

3.2.3 Variant 2: Outrigger System

The second variant that is developed is an outrigger system. Outrigger systems are widely applied in practice and have proven to be effective, as described in Section 2.5.2. As in Variant 1, the base model is supplemented with diagonal GLT beams. These beams are now present in higher density but only on the storeys where an outrigger is implemented. Each outrigger spans two storeys. In order to maintain simplicity of the model, no variations will exist in exact shape of the outrigger, and the number of outriggers. Each height variant will consist of two outriggers, one at a third and one at two thirds of the total height. All diagonals also move two floors up, and one grid space to the side.

Unlike in Variant 1, the diagonal beams are directly connected to the core, which theoretically allows for better interaction between the two stabilizing systems. However, compared to Variant 1, there are significantly fewer diagonal beams, which may lead to less stabilization but also results in fewer steel connections, thus lowering CO_2 emissions.

The analysis will determine whether the GLT beams possess sufficient stiffness to significantly transfer horizontal loads away from the concrete core and towards the perimeter columns. If this is the case, these columns will consequently need to resist substantially higher forces. As a result, a new sub-variant is created in which the timber columns (Variant 2T) are replaced with concrete columns. For this sub-variant, Variant 2C, the assumption is made that the concrete will have C30/37 as a strength type with 0.26% as the reinforcement ratio.

For the different floor plans, the outrigger system will remain constant. Therefore, it is shown only for floor plan B in Figure 3.6. This figure illustrates that the timber columns can be replaced with concrete columns once the forces acting on them become too high. This replacement has a significant impact on the CO_2 emission performance indicator.

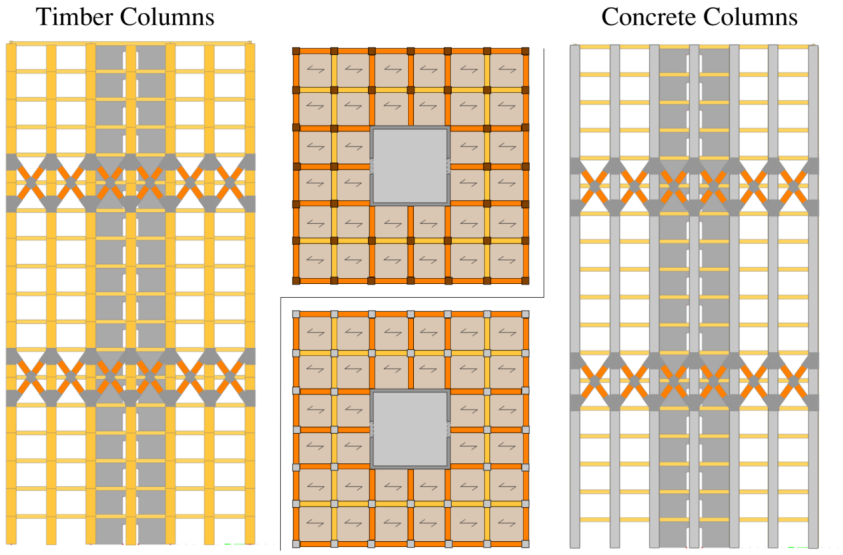

Figure 3.6: Side views of variant 2 for floor plan B with both timber and concrete columns

3.3 Loads

A building is subjected to various types of loads. This section presents the relevant loads. These are divided into load cases, which are subsequently factored using different load combinations. The building will have a residential function.

3.3.1 Load Cases

The model distinguishes between the following load cases. The lists below indicate the various permanent and variable load cases along with their corresponding applied names. Realistic estimations have been made for the weight of the façade, and floor finishes or installations, however, these are not directly calculated or based on literature.

Permanent Loads

- **LC_SW**: Self weight of main load bearing elements (floors, beams, columns, diagonals) to be directly accounted for in the model
- **LC_PERM**: Self weight of facade as a line load on perimeter beams ($= 1.0\,kN/m^2 \cdot$ storey height)
- **LC_PERM**: Self weight of inner walls with residential seperation function as surface loads ($= 1.25\ kN/m^2$ [44])
- **LC_PERM**: Floor finishes and installations as surface loads ($= 0.75\ kN/m^2$)

For the load combination in which wind is the governing action, it could be relevant to split the self-weight into two parts: one located before and one after the building's central axis of rotation. If the part before the axis were considered favourable and the part after unfavourable (see Section 3.3.2), this would result in a governing combination. However, the Dutch National Annex states that such an approach is unnecessary, as it would lead to overly conservative results. For this reason, all permanent loads are merged into a single load case denoted as 'LC_PERM'.

Variable Loads

- **LC_IMPOSED**: Imposed floor loads as surface loads ($= 1.75\ kN/m^2$ [44])
- **LC_WIND**: Wind loads as a horizontal surface load as a function of height (see section 2.4)

To simplify the model, snow load is not included under the assumption that it will not be governing in any load combination, and a standard variable floor load is applied to the top floor. Therefore, this can be regarded as a conservative simplification.

3.3.2 Load Combinations

The fundamental load combinations applied in this study are based on Equations 6.10a and 6.10b of EN 1990, as specified in the Dutch National Annex [42] [21]. In Equation 6.10a, the permanent load is governing, and all variable loads are combined using their accompanying combination factors. In Equation 6.10b, a specific variable load is considered governing, while the remaining variable loads are multiplied by combination factors. The Eurocode formulations also include factors for concentrated loads P, which are not relevant for this study and are therefore omitted from Equations 3.1.

$$
\begin{aligned}
&K_{FI}\left(\sum_{j\geq 1}\gamma_{G,j}G_{k,j}+\gamma_P P+\gamma_{Q,1}\psi_{0,1}Q_{k,1}+\sum_{i>1}\gamma_{Q,i}\psi_{0,i}Q_{k,i}\right) && \text{(6.10a)}\\
&K_{FI}\left(\sum_{j\geq 1}\xi_j\gamma_{G,j}G_{k,j}+\gamma_P P+\gamma_{Q,1}Q_{k,1}+\sum_{i>1}\gamma_{Q,i}\psi_{0,i}Q_{k,i}\right) && \text{(6.10b)}
\end{aligned}
\tag{3.1}
$$

In Equation 3.1, numerical values can be assigned based on the Dutch National Annex [42]. For consequence class CC3, a reliability factor of $K_{FI} = 1.1$ is prescribed. Since this study focuses on high-rise structures with varying heights, the applicable consequence class may vary between CC2 and CC3. However, for simplicity and as a conservative assumption, CC3 has been applied throughout. The specific values are adopted in accordance with Table 3.1.

Table 3.1: Load factors for consequence class CC3 according of NB.5 of Dutch National Annex [42]

Design situation	**Permanent loads** Unfavourable / Favourable	**Dominant variable load**	**Variable loads**	
			simultaneous with dominant	
			Most relevant	Others
(Eq. 6.10a)	$1.5\,G$ / $0.9\,G$		$1.65\,\psi_{0,1}\,Q_{k,1}$	$1.65\,\psi_{0,i}\,Q_{k,i}$
(Eq. 6.10b)	$1.3\,G$ / $0.9\,G$	$1.65\,Q_{k,1}$		$1.65\,\psi_{0,i}\,Q_{k,i}$

Furthermore, the Dutch National Annex allows the use of a reduction factor for imposed floor loads when multiple floors are considered. The two most unfavourable floors must be taken in full, while the accompanying combination factor ψ_0 is to be applied to the imposed loads on all other floors. The relevant combination factors are presented in Table 3.2.

Table 3.2: Combination factors for selected variable actions according to the Dutch National Annex

Load type	ψ_0	ψ_1	ψ_2
Category A: residential areas	0.4	0.5	0.3
Snow load	0	0.2	0
Wind load	0	0.2	0

Various load combinations will ultimately be used in the calculations. These are listed below along with their applied names and descriptions. The following load combinations are governing for the ULS calculations.

- **SELF_WEIGHT**: The first case considers self-weight as governing, according to Equation 6.10a.
- **FLOOR_VAR**: The second case considers variable floor load as governing, based on Equation 6.10b.
- **WIND_VAR_COMP**: The third case considers wind load as governing in combination with unfavourable self-weight, according to Equation 6.10b, to test the compressive force in a critical column on the ground floor, and in the core.
- **WIND_VAR_TENS**: The fourth case considers wind load as governing with favourable self-weight, to test whether a tensile force occurs in a critical column on the windward side. If this is the case, the connection must be verified for its tensile capacity. The tensile forces in the core will determine the needed reinforcement.

The following load combinations are applicable for the SLS calculations.

- **HOR_DEFLECT1/2**: The first and and second load combinations determine the global horizontal deflection at the top floor. One of the two combinations includes variable floor load, while the other does not.
- The first load combination determines the vertical displacement of the beams in both directions.

Table H.1 of Appendix H presents all the different load cases and load combinations that have been applied in the model.

3.4 Capacity and Stiffness of the Connections

As indicated by the equations in the Eurocode, described in section 2.3, the relevant values for capacity and rotational stiffness are highly dependent on several parameters. As the dimension of the timber element increases, more dowels can be placed inside it, which in turn increases the capacity and stiffness of the element. The aim of this part of the research is to parametrically determine a relation between the size of the element and its corresponding capacity and rotational stiffness. In the end, the relation needs to be tweakable by a single parameter, describing the rigidity of the connection, that can be implemented in the main model.

To determine this relation, a separate Grasshopper model is created. In this model, the capacity and stiffness of a slotted-in steel plate timber connection are calculated. The model utilizes the following parameters:

1. Optimizable Parameters
    - Glulam Type
    - Dowel Diameter
    - Height/Width Ratio
2. Free Variables
    - Connection Size (This parameter refers to the length of the steel plates that are inserted into the timber)
    - Element Size (this parameter scales both the height and width of the timber element)

Using these parameters and the minimum dowel distances described in the Eurocode, a geometry can be formed. This geometry allows for the determination of the strength and stiffness of an element with given parameters. However, the relevant relation with the size of the element cannot yet be directly determined. To achieve this, the Grasshopper plugin called Anemone is utilized. Anemone is a plugin that enables looped calculations to be performed within Grasshopper. This means that a range of calculations can be made directly. In this way, the influence of various parameters can be determined. A loop is then used to calculate all outcomes for a certain variable.

The results are stored in an array, which can then be exported to a Python file, from which relevant scatter plots can be generated. At this point, the actual relation can be determined. From the scatter plot, a proper curve can be found using Polynomial Fitting. For this research, the polynomial degree is set to 4, providing sufficient flexibility without significantly increasing the risk of overfitting or unnecessarily complicating the model. Figure 3.7 presents a plot in which the variation in connection capacity (translational strength and rotational stiffness) is shown on the y-axis as a function of the element size on the x-axis. In this figure, all other parameters are held constant at fixed values to isolate the influence of the element size. It is to be noted that all values obtained from the plots in this section are *characteristic values*. This means that these values are still to be adjusted for relevant safety factors in order to achieve the design strength.

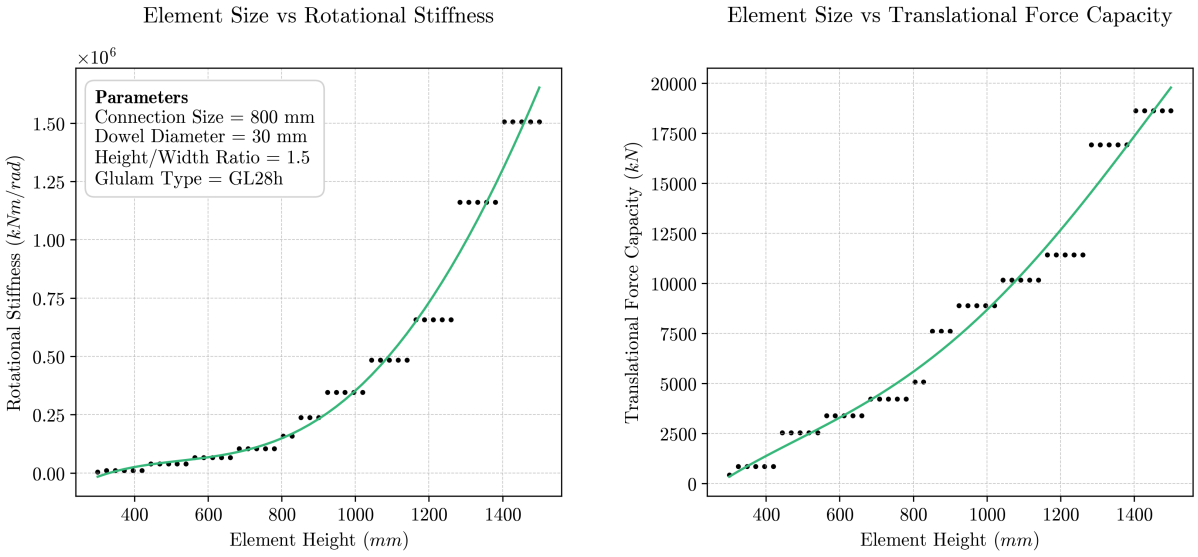

Figure 3.7: The effect of the size of the timber element on Translational Force Capacity and on Rotational Stiffness

From the figure, it can be observed that the rotational stiffness shows an exponential relation with the element size. Additionally, the translational force capacity also shows an exponential trend, although with a clearly smaller exponent, resulting in a tendance towards linear behaviour.

However, this relation remains dependent on too many variables to allow for direct generalization. In order to reduce the amount of variables and to make prior design choices, the influence of different variables on the structural performance of these timber connections are investigated. All different parameters, as seen in Figure 3.7, that are beneficial for the determination of the mentioned relation, are investigated and optimized in Section B.2 of Appendix B.

3.4.1 Connection Size

After the other parameters have been optimized, the influence of the connection size can be determined. The connection size refers to the length of the steel plates. This parameter directly affects the number of bolts that can be fitted into the plates, thereby influencing the strength and stiffness of the connection. This parameter will be a variable in the main model for all different timber elements.

In figure 3.8, the element size (in the x-axis) vs the rotational stiffness and the translational capacity (in the y-axis). Subsequently, for all 50 different element sizes, five connection sizes per element size (a total of 250) were calculated and displayed in the form of a scatter plot. For these data points, a curve was obtained for each connection size using fourth-degree polynomial fitting. The next step is that, based on these five curves, a multivariate polynomial regression, or 2D polynomial fitting, is applied. By applying this process to the data, a heatmap is obtained, which is also associated with a two-dimensional equation. After this is done, the characteristic values that are obtained are transformed into design values, according to B.1.4. This is the final result of this section and is given in equations B.15 and B.16 of Appendix B.

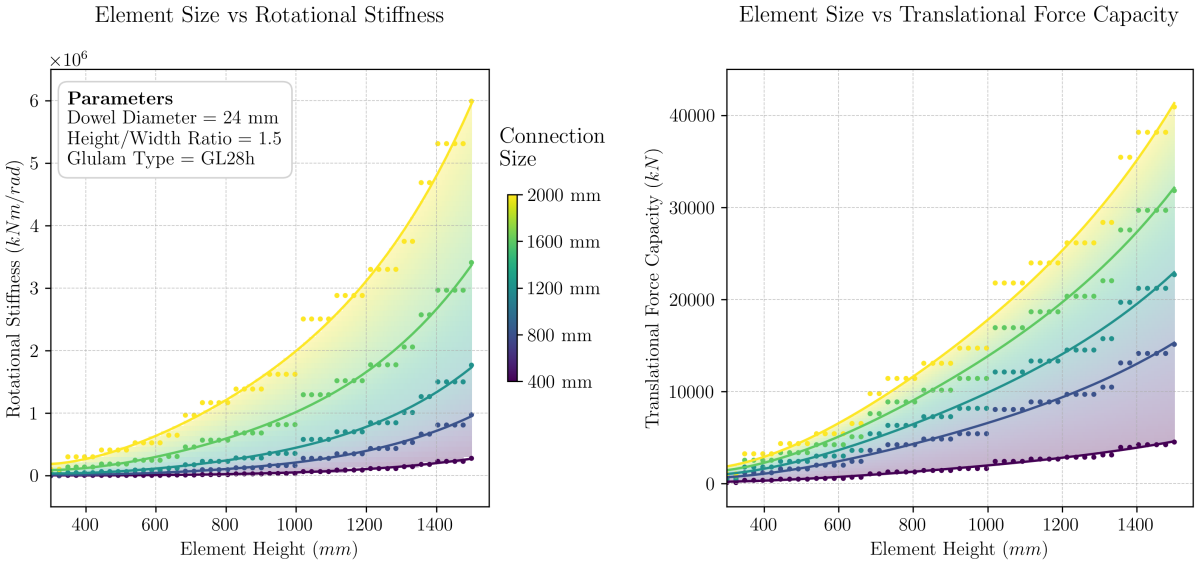

Figure 3.8: The influence of the connection size on the capacity of a timber connection with set parameters

The equations represented by the heatmaps in Figure 3.8 are therefore dependent on both the element size and the connection size. Equation B.15 of Appendix B can then be directly added as a rotational spring for the connections in the main model, which is then exported to SCIA. The connection forces obtained as a result of the calculation in SCIA can then be compared with the values obtained from equation B.16.

3.4.2 Steel Volume of Connection

In addition to the rotational stiffness and translational capacity, the amount of steel used in a connection is also relevant for the total CO_2 emissions of the building. The performance of the design variants will partly depend on this indicator, which is defined and calculated as described in 3.7. The production of steel connections involves significant CO_2 emissions, which negatively affects specific variants that include a high proportion of timber elements. Based on the element height and size, a calculation can be made to determine the volume of steel applied in a single connection. This calculation includes both the steel plates and dowels. In a similar manner as described in section 3.4.1, a plot and equation can be developed to evaluate and compare the required steel volume (in m^3). These are shown in Figure 3.9. The corresponding polynomial is described in Equation B.17.

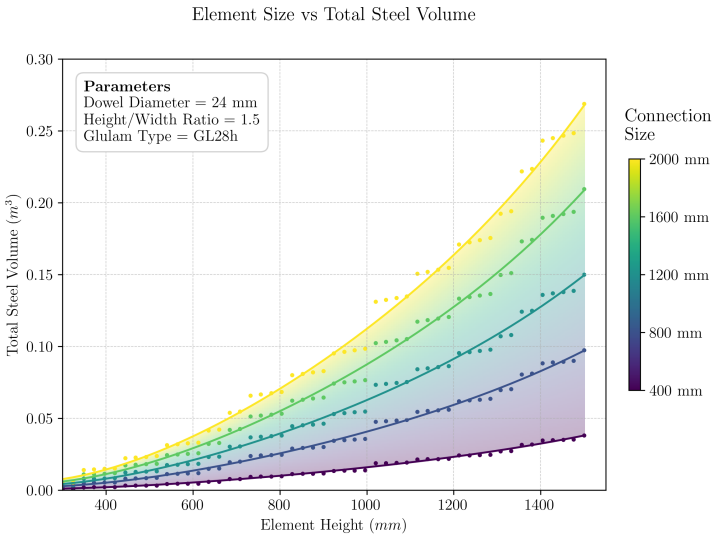

Figure 3.9: The influence of the connection size on the applied steel volume of the connection

3.4.3 Validity and Limitations

In practical applications of slotted-in steel connections, particular attention must be given to the detailing. It may occur that no individual detail is identical to another. Moreover, significant differences may arise in the detailing of various elements; for example, a column-to-column connection requires entirely different detailing than a beam-to-core connection. For the sake of simplicity of the model and for the generisability of this study, the details of the connections are not further developed.

In Section 2.3, specific failure mechanisms are described. The use of multiple steel plates within a GLT beam introduces the possibility of additional failure modes beyond the three outlined in the Eurocode. In practice, the connection may fail through a combination of the different failure modes. This has direct implications for the overall capacity of the connection. As the number of steel plates increases, the number of possible combinations of failure mechanisms grows exponentially. Determining which combinations apply in which situations can provide for a study of its own. For this reason, and for this research, the conservative assumption is made that the failure mode with the lowest capacity will occur in all plates. In this way, the lowest found value of the failure modes is to be multiplied by the number of shear planes.

The steel used for plates and dowels has, in practice, a higher density than timber. The self-weight of the connections would therefore introduce additional point loads acting vertically downward. This could affect the sizing of the columns, as they would be subjected to higher loads. However, since these point loads would occur in every variant, and in order to maintain the simplicity of the model, these additional point loads are not considered further in this study.

Finally, the introduction of rotational stiffness results in the actual transfer of moments. These effects are generally considered unfavourable, as they can lead to unintended stresses within the material. In addition to axial force, the elements are also subjected to shear force, and as mentioned earlier, moments are present in the connections as well. For this reason, connections should ideally be evaluated under the combined action of axial force, shear force, and moment. However, if the results demonstrate that the beams are always governed by either axial force, shear force, or moment individually, and never by a combination of these, it is justified to assess only one force or moment at a time. In that case, the moment

capacity of the connection is not considered in this study. This choice is based on the observation that the connections have a large translational capacity relative to the applied forces, as shown in Unity Checks of the X- and Y- beams in Appendix J. Since the Unity Checks for the connections remain very low within the model, the connection size can also remain small. As a consequence, the associated rotational stiffness remains low and closely approximates pinned behavior. Moreover, the combination of shear and axial force is more favourable for the connections in comparison to only axial force, as the dowels are then loaded at an angle relative to the grain. This condition results in a higher capacity compared to forces acting parallel to the grain, occuring with axial forces.

3.5 Design Verifications

The various element types (beams, columns, diagonals, and core) are assigned to separate layers in the SCIA model. For each layer, the maximum internal forces and moments can be calculated.

These maximum stresses and moments, as described in Section 3.6, are directly re-imported into the Grasshopper file from the generated Excel file. Using these values, the relevant Unity Checks are calculated to enable the structural elements to be dimensioned accordingly.

The verification procedures are carried out in accordance with Eurocode 2 for concrete [46] and Eurocode 5 for timber [47]. The verifications relevant to this research are summarized in Section E.1 of Appendix E, then in this section, this is followed by a justification of which verifications apply to which structural elements. For this study, it is assumed that the longitudinal direction of the elements is parallel to the grain.

3.5.1 Beams in X and Y direction

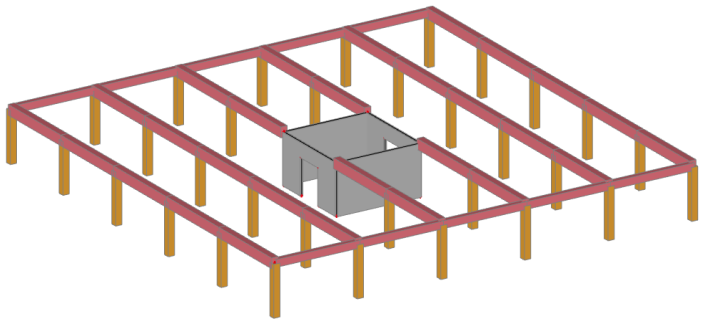

Figure 3.10: Beams in X and Y direction of an arbitrary representative storey displayed in red

Figure 3.10 shows the relevant beams of a specific floor level. The beams in the y-direction support both the floor panels and the façade, while the beams in the x-direction also serve to support the façade. Additionally, they contribute to the in-plane stability of the floor levell. For this reason, the beams in both the x- and y-directions are verified for combined axial and bending stress (equations E.5 and E.6 for tension and compression, respectively) and for shear (equation E.4). In this study, it is assumed that the beams in both directions are sufficiently connected to the floor panels and the façade. As a result, the effect of lateral torsional buckling is neglected.

3.5.2 Columns

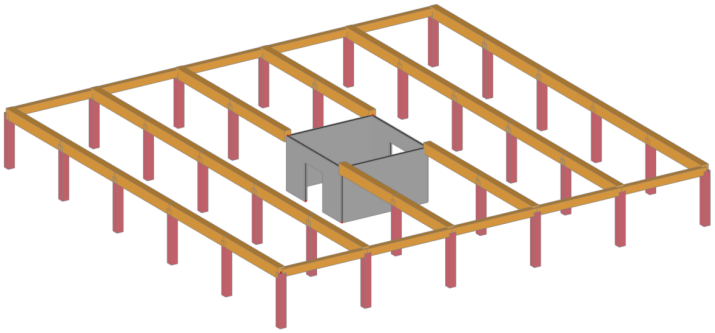

Figure 3.11: Columns of an arbitrary representative storey displayed in red

In Figure 3.11, the columns for a specific floor level are highlighted. For visualization purposes, only one storey is shown, while in reality the columns span across four storeys. This is based on the assumption that longer columns require fewer connections, while the maximum element length is limited to 16 meters. The columns are verified for buckling resistance according to equation E.10.

3.5.3 Core

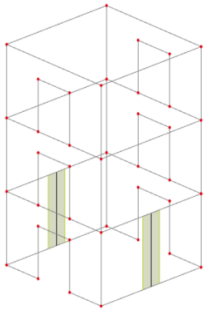

Figure 3.12: Bottom part of core with two integration strips visible

As shown in Figure 3.12, two integration strips are applied at the bottom of the core. As a result of wind loading, these strips will be subjected to either tension or compression. It is assumed that one of the two strips will carry the critical compressive force, while the other will carry the critical tensile force. The corresponding stresses can be determined using equations E.1 and E.2 for compression and tension, respectively. The compressive stress is relevant for determining the concrete thickness of the core, while the tensile stress is taken up by the reinforcement in the core, which thereby defines the required reinforcement ratio and thus the steel usage. The type of reinforcement steel applied is **B500B**.

3.5.4 Diagonals

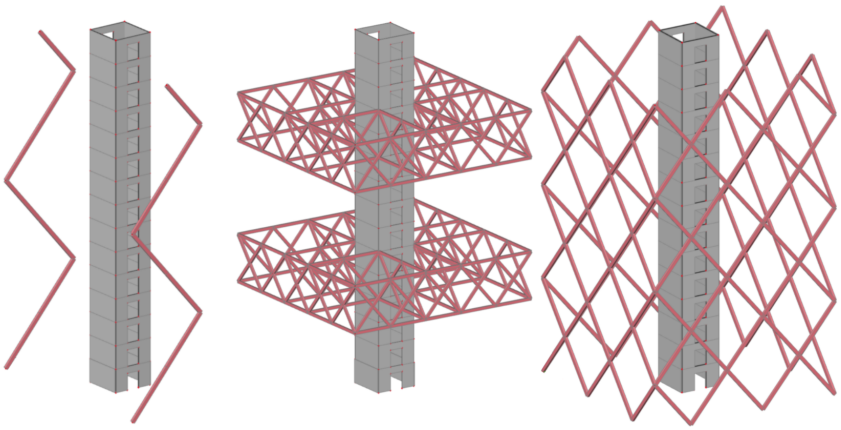

Figure 3.13: Diagonal Beams displayed in red for all different variants

Figure 3.13 shows the diagonals for the different variants, which are not present in the base model. These diagonals can be subjected to both tension and compression. Additionally, due to the rotational stiffness of the connections, they may also experience bending moments and shear forces. For this reason, the diagonals are verified for combined axial and bending stress (equations E.5 and E.6 for tension and compression, respectively) and for shear (equation E.4). In the case of compressive forces, the diagonals are also verified for buckling resistance according to equation E.10.

3.5.5 Slotted-in Steel Connections

The connections must also be verified with respect to their capacity. In Section 3.4, a relation is established between the height of the element and the length of the connection, and the translational capacity. This capacity is based on a tensile force acting parallel to the direction of the element. To simplify the model, it is assumed that this capacity is also valid for shear forces at the location of the connection. Since a reduction factor applies to multiple dowels aligned parallel to the grain direction (see Section B.1), this confirms that the assumption is conservative.

The elements are not intended to be modelled as moment-resisting connections. The rotational stiffness is solely an unavoidable consequence of using multiple dowels and plates. For this reason, the rotational stiffness will be minimized, and no significant moments are expected to occur at the location of the connections. Therefore, and in favour of model simplicity, the calculation of moment capacity is omitted. In practice, however, this effect has to be taken into account.

For the columns and diagonals, the connection capacity is verified only for tensile forces. In the case of compressive forces, the element can directly transfer the load through the timber to the adjacent element, and the connection serves only a stabilizing function. To justify this assumption, the timber elements must be directly connected to each other. In practice, this is a reasonable assumption for columns, but not necessarily for diagonals. However, since the tensile forces in the diagonals are approximately equal to the compressive forces under symmetric conditions, the assumption remains reasonable.

The maximum occurring shear force or axial tensile force is verified against the determined value for the translational capacity. This verification is, in any case, conservative.

3.5.6 Global Horizontal Deflection

On a global scale, the maximum deflection in the top column is determined and assessed against the limit of $1/500 \cdot h$. The calculated maximum deflection is doubled to conservatively account for foundation flexibility.

3.6 Implementation of Parametrized Model

When choosing software for parametric design, it is essential to select a tool that supports efficient manipulation of geometric relations and seamless iteration of design variations. Grasshopper is a suitable option for parametric design due to its capacity to manage complex geometric relations and automate design iterations effectively. Its visual programming interface provides flexibility in adjusting parameters, which makes it possible to rapidly explore multiple design variations without the need for any manual remodeling.

The entire modeling process can be divided into three main stages. The first stage focuses on generating the building geometry to be modeled. The second stage converts this geometry into a structural model by assigning relevant structural properties. The third stage links the Grasshopper model to SCIA for structural analysis, extracting key unity checks that are fed back into the Grasshopper model through an iterative loop for optimization. The following three subsections provide a more detailed explanation of this process.

3.6.1 Geometric Definition in Grasshopper

The first step in the modeling process involves defining the geometry using Grasshopper. This is done by establishing a structured grid of points, between which lines and surfaces are generated to represent future structural elements. The key geometric parameters, such as column spacing, column height, and the number of floors, are set in this step, forming the basis for the overall building configuration.

At this stage, the generated lines and surfaces do not yet function as structural elements but serve as a geometric framework. These entities are stored in lists within Grasshopper, allowing them to be further processed in the next step.

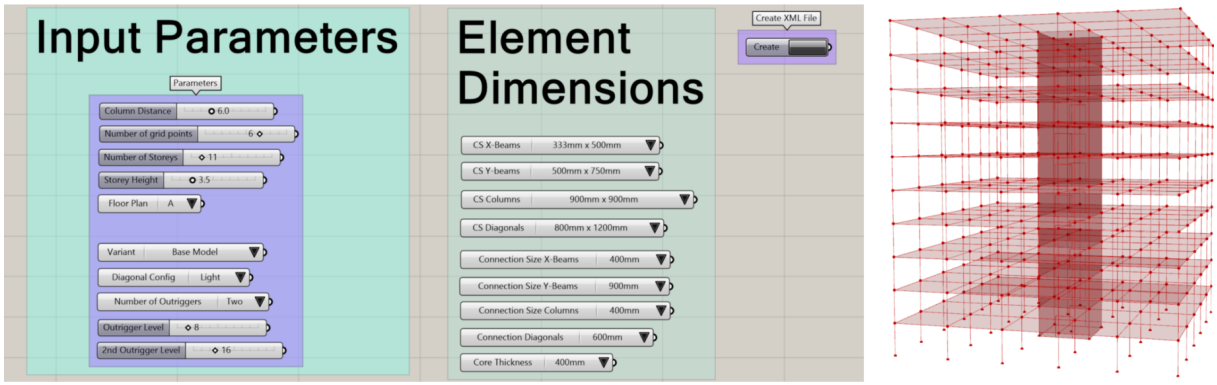

Figure 3.14: Creating a parametrized geometry in Grasshopper

3.6.2 Converting Geometry into a Structural Model using KOALA plugin for Grasshopper

The second step involves translating the geometric representation into a structural model by assigning appropriate structural properties to each element. This is achieved by exporting the geometric data from Grasshopper and processing it through KOALA to generate an XML file suitable for SCIA. Lines created in the first step are now classified as beams or columns, while surfaces are assigned as floors or as the concrete core, depending on their position within the grid.

A critical aspect of this step is the definition of connection behavior. By default, SCIA automatically considers all intersecting elements as rigidly connected. To introduce flexible or pinned connections, additional hinge definitions (node hinges and line hinges) must be specified. In this step, rotation stiffness of the connections is introduced as an important variable for the designs. Furthermore, hinged node supports are assigned at the base of the columns at ground level, and line supports are applied to the core elements at this level. This step also includes the application of external loads, namely variable floor loads and wind loads, which are determined according to Eurocode regulations (see Section 3.3.1). Finally, load cases and load combinations are established, and each element is assigned a material type and cross-section. Once all properties are correctly defined, the structural data is compiled into an XML file that can be directly imported into SCIA. The material properties that are used in SCIA can be found in Table F.4 and F.5 of Appendix F for GL 28h and C30/37 respectively.

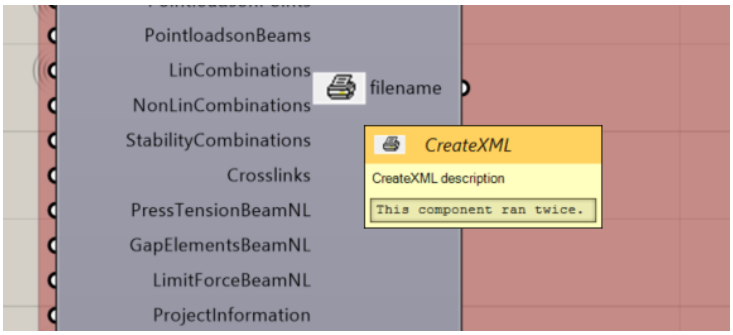

Figure 3.15: XML file component that can be exported to SCIA

3.6.3 Exporting to SCIA, Running Structural Analysis, and Optimization

In the final step, the generated XML file is imported into SCIA, where structural calculations are performed to determine internal forces, deformations, and other critical performance metrics. Additionally, the XML file can be integrated into a pre-configured SCIA template that automatically performs all relevant unity checks and exports the results to an Excel file. As an example, this Excel export for an iteration of the base model for plan A and 15 storeys is found in Appendix K.

The exported data can then be imported back into the same Grasshopper script used to generate the model, enabling to make adjustments to cross-section dimensions with the goal of optimization. If any elements exceed allowable limits in the unity checks or can be made more economic, their dimensions are iteratively modified, and the new model can be exported back to SCIA, until the most economic configuration that still ensures structural integrity is reached.

3.7 Performance Assessment Framework

Once the optimal dimensions for a variant with a specific height are determined, this iteration can be assessed for structural performance and sustainability. Structural performance can be defined in numerous ways. For this research, a number of indicators will be examined to evaluate how a particular iteration or variant performs in this regard. These indicators are described within the sector, and the methods for quantifying them are explained.

3.7.1 Height and Net Floor Area

This research assumes a constant length and width, specifically a 30 by 30 meter floor plan. As the number of floors increases, the required dimensions will also increase. Additionally, beyond a certain number of floors, the floor plan must be adjusted to increase the core size and accommodate greater wind loads. This results in a decrease in net floor area. For this research, the net floor area is defined as the total floor area minus the combined area of the core and columns. In section 4.1, the available floor area is plotted against the number of storeys both for the base model as for all different variants. Non-load-bearing walls, technical rooms, and any space occupied by the facade are excluded from this analysis for the sake of simplicity.

Raising the number of floors, at a certain point, could lead to the column dimensions and core size correspondingly increasing to such an extent that this causes the net floor area to decrease. At this point, the desired effect is no longer achieved and there are no incentives to further increase the building's height. The results will reveal the exact influence of column dimensions and core size on the total net floor area. It will also indicate whether the variants can achieve a higher net floor area compared to the base model. Finally, the increase in net floor area resulting from the application of complementary stabilizing elements can be compared to the additional material usage, cost, and CO_2 emissions or sequestration.

3.7.2 Material Price

The increase in the number of floors and the implementation of new variants are, of course, associated with varying quantities of materials that will be required. The goal of this indicator is to provide insight into these material quantities. It also allows for the determination of the timber-to-concrete-and-steel usage ratios. The amount of material used in a construction is a quantity that strongly influences the cost of the building.

In practice, the price of a construction is one of the most significant factors in the building process. The cost of the building depends on numerous factors that have implications beyond the scope of this research. Significant variations are also possible here. Examples of this include the extent to which specific construction components need to be custom-made for the project, as well as the time and costs associated with research, design and development. Labor costs, transport costs, and costs related to construction time can also vary greatly depending on material and variant choices. However, to provide a general implication of the price of an iteration or variant, the focus is placed on material prices. This is done because the proportional increases or decreases of the price in comparison to the base model are ultimately more important than the total price. Thus, only the material costs are considered in the calculations. Estimated values for material costs per cubic meter are provided in Table 3.3. Note that these values are highly dependent on multiple factors and very project specific.

Table 3.3: Material Prices per m^3

Material	Price per m^3
Concrete	€150 [7]
Steel	€11,000 [7]
Timber	€1,350 [28]

By including the material price in the results, an improvement in net floor area or sustainability indicator can be directly plotted against the corresponding price increase compared to the base model for the different variants. From these plots, conclusions can partly be drawn regarding the efficiency and cost-effectiveness of the variant.

3.7.3 CO_2 Emissions and Sequestration

The sustainability of a building depends on multiple factors. To quantify sustainability, a Life Cycle Assessment (LCA) is often applied [5]. An LCA can be conducted for different life cycles of a specific product or process. A commonly used design philosophy is the cradle-to-grave approach, which for buildings includes all processes from raw material extraction (cradle) to demolition (grave). An alternative philosophy is the cradle-to-gate approach, which considers the life cycle of materials only up to the point they leave the manufacturing facility (gate).

In an LCA, various indicators are considered, each reflecting a specific impact on ecosystems and human health. One of the most important indicators is the Global Warming Potential (GWP), which represents the CO_2 emissions associated with the extraction of required materials and the entire construction process. In Section 1.1, it was stated that the Netherlands must reduce total CO_2 emissions by 49% by the year 2030. Next to this, the CO_2 emissions during the lifespan of a building strongly depend on the nature of its use and on architectural design choices related to building physics. Therefore, this study focuses on the GWP indicator and adopts the cradle-to-gate design philosophy.

Different construction materials vary in the extent to which they contribute to CO_2 emissions. While concrete and steel are associated with CO_2 emissions, timber can act as a carbon sink by sequestring CO_2 (see section 1.1). As a result, structures that incorporate a larger amount of timber elements, or use higher element dimensions, tend to perform better on the GWP indicator due to the increased use of timber. For this reason, it is important to evaluate the trade-off between reductions in CO_2 emissions and the associated increase in construction costs.

The IDEMAT database, originating from TU Delft, is a reliable Excel sheet containing cradle-to-gate CO_2 emissions for a wide range of materials [17]. From this dataset, the relevant values for concrete and steel were selected. Due to the absence of GLT in this list, the Environmental Product Declaration from Studiengemeinschaft Holzleimbau e.V. was consulted to obtain the CO_2 emissions associated with GLT [58]. The applied values are presented in Table 3.4.

Table 3.4: CO_2 Emissions per m^3

Material	**kg CO_2 per m^3**
Concrete	309
Steel	19625
Timber	-614.7

Chapter 4

Results & Discussion

In this chapter, the following sub-questions will be answered:

1. *How are the model iterations evaluated, structured, and visualised based on defined criteria, and how do the variants perform relative to the base model with respect to these criteria?*

   While the first part of the sub-question was addressed in the final section of Chapter 3, the second part: ”how do the variants perform relative to the base model with respect to these criteria?” , is covered in this chapter in Section 4.1. The performance of the base model is first described in Section 4.1.1, after which the variants are compared to the base model one by one in Sections 4.1.2, 4.1.3, and 4.1.4, in that order. Finally, the results of the dynamic acceleration calculations are discussed in Section 4.1.5.

2. *How can the results of the design variants be interpreted and compared, and what are the limitations of the model?*

   Once the results have been visualised and described, it is now possible to answer this sub-question. First, a comparative analysis is conducted in Section 4.2.1, in which the variants are evaluated against one another. Next, the so-called Black Box problem is addressed, along with the underlying mechanical principles, in Section 4.2.2. After that, further implications of the wind induced dynamic behaviour are discussed in Section 4.2.3. Finally, remaining practical and technical considerations are discussed in Section 4.2.4.

4.1 Results

In this study, various building heights are systematically analyzed. This is achieved by incrementally increasing the number of storeys in the structural model with 5 storeys per iteration. It starts at 10 storeys and continues until the structurally best-performing variant no longer satisfies the relevant design criteria. The building heights corresponding to each specific number of storeys are presented in Table 4.1. From this table, it can be observed that the total height ranges between 38.5 and 196 meters.

Table 4.1: Height per Storey Number

Storeys	10	15	20	25	30	35	40	45	50	55
Height [m]	38.5	56.0	73.5	91.0	108.5	126.0	143.5	161.0	178.5	196.0

First, the results of the base model are described. Subsequently, the results of the different variants are projected on top of the base model outcomes in such a way that the effects of each variant can be directly observed. The results of the variants follow the same structure as those of the base model. For this matter, further explanation about how the visualizations are constructed and how relevant observations can be made from them is present in Section 4.1.1.

4.1.1 Base Model

Section 3.6 describes the method by which different iterations or Model Runs are created. Initially, Floor Plan A is used due to its smallest core dimension, which results in the steepest increase in net floor area. Once Floor Plan A no longer meets the requirements at the maximum core thickness, Plan A is swapped for Plan B and eventually Plan C. Table 4.2 presents the different Model Runs along with their corresponding number of storeys and Floor Plan. This table also includes a reference to the a table in Appendix J. In the tables in Appendix J, the dimensions and corresponding Unity Checks for each load combination are listed per Model Run.

Table 4.2: Overview of model runs Base Model

Model Run	**Number of Storeys**	**Floor Plan**	**Dimensions & UCs (Table)**
1	10	A	J.1
2	15	A	J.2
3	20	A	J.3
4	20	B	J.4
5	25	B	J.5
6	31	B	J.6
7	35	B	J.7
8	35	C	J.8
9	40	C	J.9

In the following graphs, the data points are displayed with a number and are equal to the Model Run numbers listed in Table 4.2. This applies to all variants and the data points are numbered in the graphs the same way as in their table. As a result, it is possible to directly trace each data point across the graphs when examining a new indicator. Data points with different Floor Plans are represented in the graphs using distinct markers (circle, cross, or plus). To clarify the trends among data points with similar Floor Plans, a corresponding regression curve is plotted.

Section 3.7 described the indicators by which a variant or iteration is evaluated. Increasing the height of a structure is primarily associated with the goal of achieving a larger net floor area. For this reason, the first visualization produced shows the net floor area plotted against the number of storeys. This visualization is displayed in Figure 4.1.

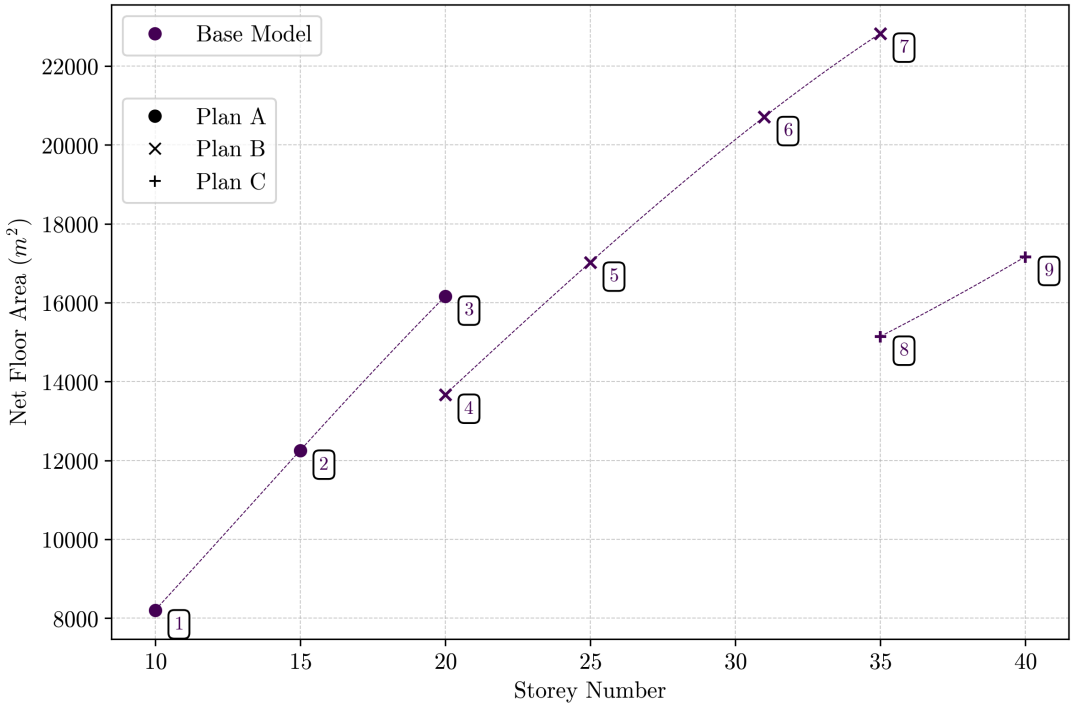

Figure 4.1: Base Model for Storey Number vs Net Floor Area

From Figure 4.1, the following observations can be made.

1. As initially assumed, there is a general increase in net floor area as the number of storeys increases.
2. When a specific Floor Plan no longer satisfies the requirements, a transition to a new Floor Plan occurs. This is visible in the graph between point 3 and 4, and between point 7 and 8, and, as expected, this transition is accompanied by a decrease in net floor area.
3. The curve formed by the data points for each Floor Plan shows a strong tendency towards a linear relation. This result differs from the initial assumption, as it implies that the effect of increasing column dimensions is negligible compared to the impact of switching Floor Plans and increasing number of floors. However, a very slight curvature is visible in the regression curve for Floor Plan B. This curvature becomes more pronounced when plotting the heavy configuration of Variant 1 (see Figure 4.7). The reason that this curvature is visible in the trend line is that Floor Plan B contains 40 columns, compared to only 32 columns in Floor Plan A. The increasing dimensions

of the columns therefore have a stronger effect on the downward curvature of this trend line. Additionally, the slope of the trend line for the data points with Plan B is smaller than that of the data points with Plan A. This is due to the fact that, because of the increased core size, each new storey provides less additional net floor area compared to Plan A.

4. The decrease in net floor area when switching from Plan B to Plan C is significant. This reduction is so substantial that further increasing the number of storeys does not result in a higher net floor area than the highest one found for Plan B. This means, the implementation of Floor Plan C does not provide any more benefit. Therefore, it has been decided to not take Floor Plan C into consideration when displaying the following graphs.
5. The maximum height that can be achieved based on the base model design is 143.5 meters. However, the highest net floor area is already reached at 126.0 meters. This result appears to be plausible.

When the net floor area per model run is known, it can be moved to the x-axis of the subsequent graphs. This is done because this parameter is more relevant than simply the number of storeys, as shown in the fourth point of the above summary. Then, the material price, as described in Section 3.7.2, can be plotted against the net floor area, as presented in Figure 4.2. Next to the total material price, a similar plot has been made for the material price per m^2 of Net Floor Area on the y-axis versus the Net Floor Area on the x-axis. Due to the comparable behaviour of this plot with the plot shown in Figure 4.2, it is displayed in Figure I.1 of Appendix I.

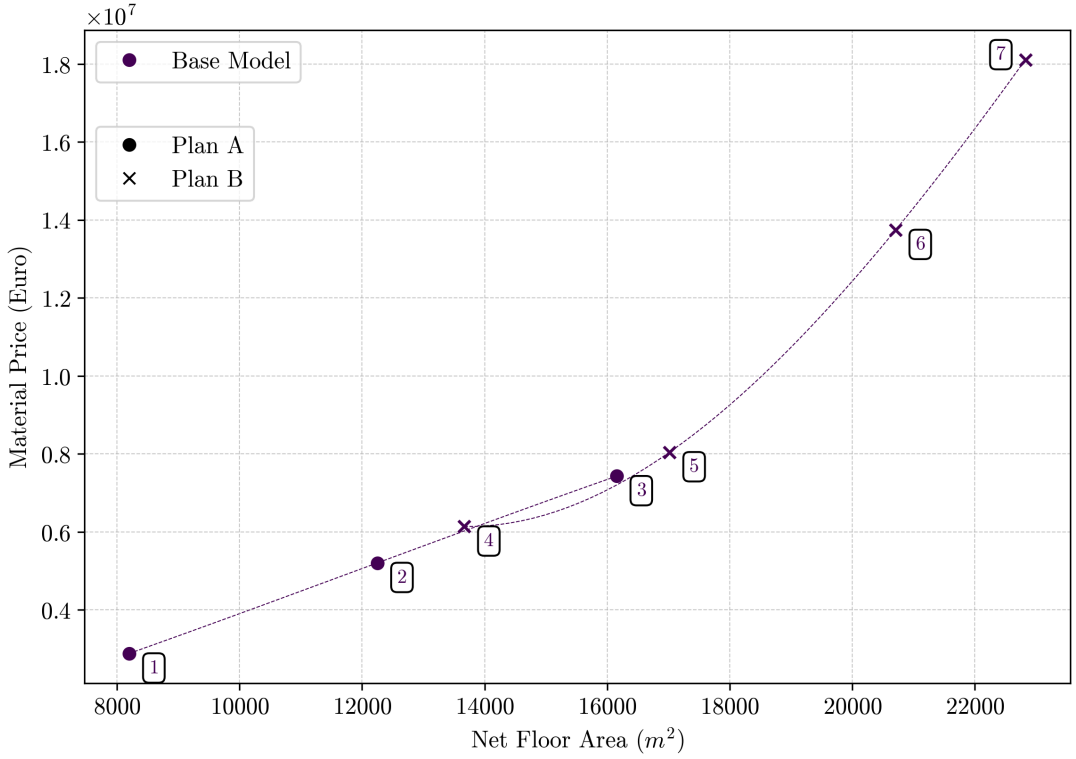

Figure 4.2: Base Model for Net Floor Area vs Material Price

From Figure 4.2, the following observations can be made.

1. The regression curve for Plan B shows a significantly steeper increase than that of Plan A. This is due to the fact that the net floor area in Plan B increases less rapidly with the number of storeys. Consequently, more storeys must be added in Plan B to achieve the same proportional increase in net floor area.
2. Plan A also displays a predominantly linear trend, whereas Plan B demonstrates a more exponential relation. A possible explanation for this is that the required dimensions of the columns increase exponentially. This is related to the fact that, next to the increasing vertical loads, the moment at foundation due to wind loads increases exponentially, putting more force on the columns. Combined with this, is there also the fact that Plan B consists of 40 columns per floor, whereas Plan A only consists of 32 columns per floor. This, together with the increasing dimensions of them, provide a justification for the occuring trend line behaviour.
3. Although Model Run 3 and 4 have the same number of storeys, the material price of Run 4 is lower than that of Run 3. This is due to the assumption in this study that no material is present inside the core. A larger core therefore results in less floor material. In practice, this is more detailed, as material is still required for intermediate floors, staircases, and elevator shafts. For this reason, Plan B will appear slightly more favourable in the material price graphs.
4. Model Run 7 has the highest observed material cost, amounting to €18 million. Although this value is a very rough estimate, it appears to be a plausible order of magnitude.

In addition to the material price, a graph of net floor area versus CO_2 Sequestration can also be generated. This allows for an evaluation of the influence of the timber elements relative to the concrete and steel components on the CO_2. The method used to determine the CO_2 balance is described in Section 3.7.3, and subsequently visualised in Figure 4.3.

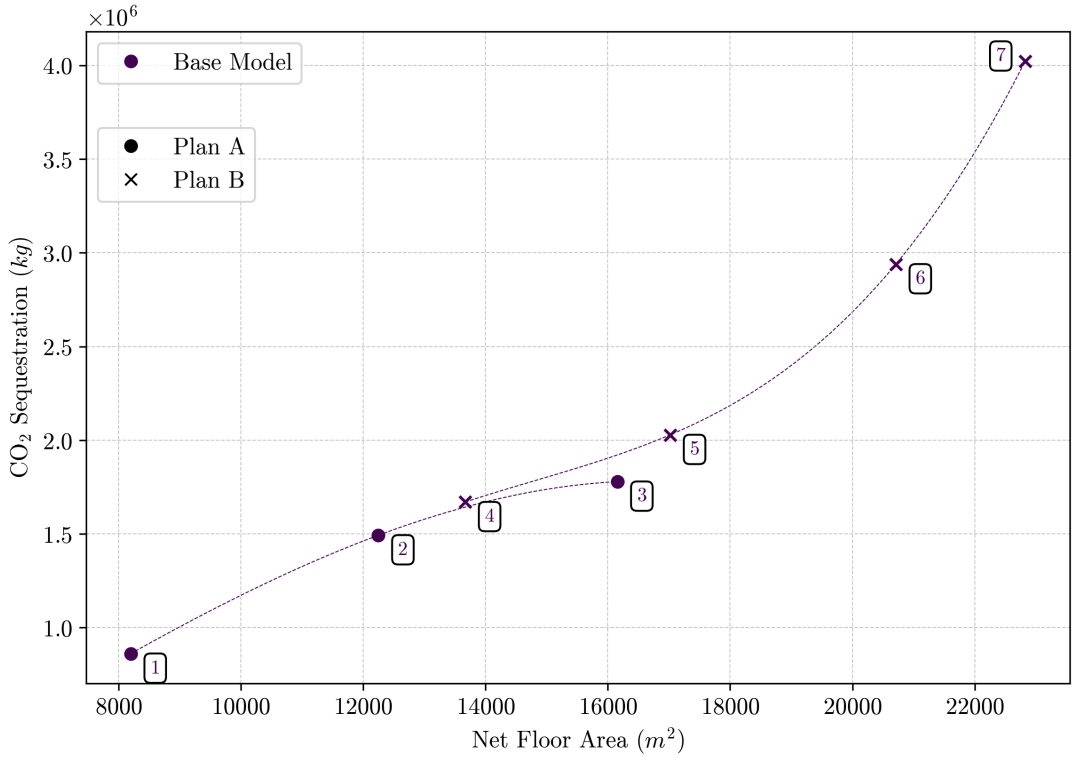

Figure 4.3: Base Model for Net Floor Area vs CO_2 Sequestration

From Figure 4.3, the following observations can be made.

1. The obtained values suggest that the constructions, despite the use of hybrid materials, sequester more CO_2 than they emit. This indicates that the dominant presence of timber offsets the CO_2 emissions from the other materials.
2. The trend of the graph closely corresponds with the development of the material price shown in Figure 4.2. This again points to the dominant role of timber in the constructions.
3. The decreasing trend in the curve for Plan A can be explained by the increasing concrete thickness of the core. As this core in Plan A approaches its structural limit, its thickness increases rapidly, leading to higher CO_2 emissions. Since the column dimensions in Model Run 6 and 7 increase significantly due to the added height, this effect is compensated in Plan B.

4.1.2 Variant 1: Braced System (Light Configuration)

Now that the results of the base model are known, the effects of the different variants can be presented. The results of the various variants can be laid directly on top of those of the base model, and thereby being able to directly observe the effects.

The first variant to be analysed is the light configuration of Variant 1: Braced System. A description of this variant and the mechanical principles applied can be found in Section 3.2.2 and in Section 2.5.1. Table 4.3 lists the different Model Runs along with their corresponding number of storeys, Floor Plan, and the Appendix table in which the dimensions and Unity Checks of each iteration can be found.

Table 4.3: Overview of model runs Variant 1 (Light Configuration)

Model Run	Number of Storeys	Floor Plan	Dimensions & UCs (Table)
1	10	A	J.10
2	15	A	J.11
3	20	A	J.12
4	25	A	J.13
5	31	B	J.14
6	35	B	J.15
7	40	C	J.16

Figure 4.4 presents the net floor area plotted against the number of storeys. This figure also includes the values obtained from the base model, alongside the newly obtained values for this variant shown in a different colour. The numbers indicated in the graph correspond to the Model Runs listed in Table 4.3. For the numbers of the base model can be referred back to Table 4.2. It should be noted that only one Model Run was retained that, based on its dimensions and Floor Plan, appeared to offer a direct improvement compared to the base model. Model Runs that did not demonstrate any improvement were excluded from further analysis. In some of the graphs, two data points may occupy the same location, making one of them occasionally invisible. It is important to note that in such cases, two distinct values are indicated at that position. In the following plots, differences in trend line formatting are also present. Trend lines are only plotted for data points that share the same Floor Plan. However, trend lines based solely on data points within a single variant are shown in the corresponding colour of that variant. trend

lines connecting points across multiple variants are displayed in black, with a wider spacing between the dashes.

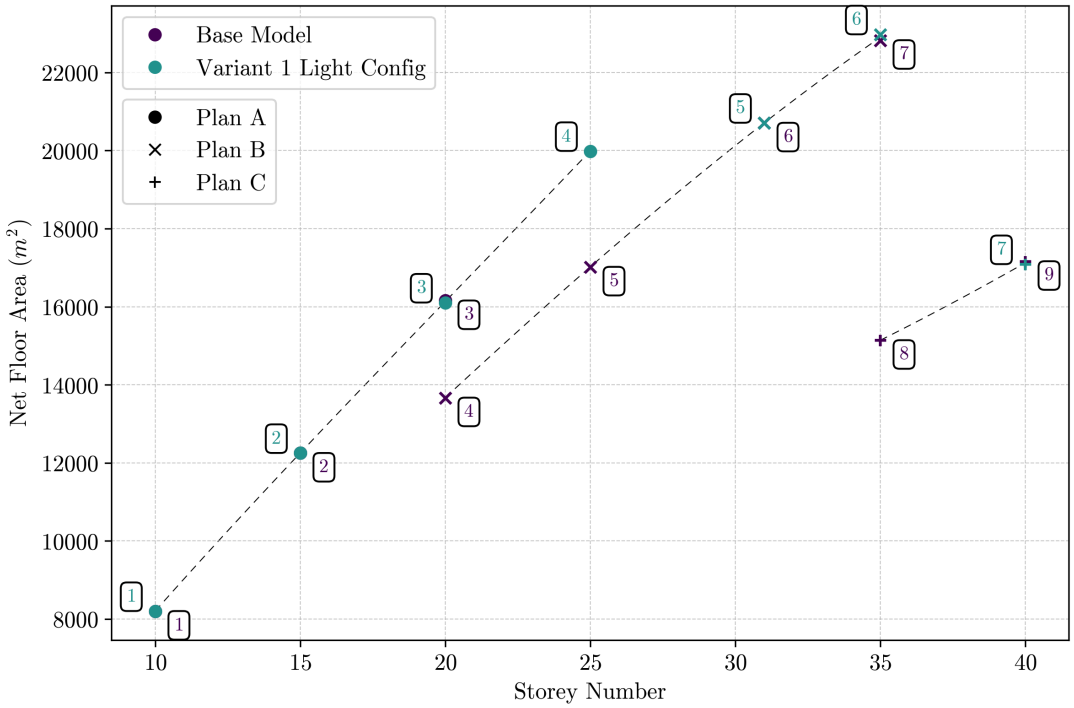

Figure 4.4: Variant 1: Light Configuration for Storey Number vs Net Floor Area

From Figure 4.4, the following observations can be made.

1. Iterations of the variant that fall under the same Floor Plan follow the same trend as the data points of the base model. In fact, data points of the variant with both the same number of storeys and the same Floor Plan either coincide with or nearly overlap the data points of the base model. This is visible in all instances where two numbers appear at approximately the same position in the graph. Similar to the linearity of the trend lines, this suggests that the effect of changing column and core dimensions has a negligible impact on the Free Floor Area of the iteration. Although minimal differences can be observed at points 3 and 3, 6 and 7, and 7 and 9, these deviations are negligible in the comparison to the overall results.
2. Thelight configuration of Variant 1 does not result in an iteration that can provide an overall higher net floor area based on the outcomes of this model.
3. As in the base model, Floor Plan C also does not lead to a higher net floor area in this case.
4. However, one important improvement remains between the Variant and the base model: at 25 storeys, the Variant still meets the requirements with Floor Plan A, whereas the base model must already switch to Floor Plan B. As shown in the graph, this has a significant effect on the net floor area, namely a difference of 36%. This is likely to influence the outcome in terms of both cost and CO_2 emissions.

Applying diagonal beams to improve the lateral stability of a building can result in a decrease in dimension of other structural elements. Although it was previously shown that changes in dimensions have a negligible effect on the net floor area, such changes may still have a greater impact on material cost

and CO_2 sequestration. As a result of increased structural efficiency, it could possibly lead to a decrease in material price per net floor area. To assess this, the material price is plotted again against the net floor area, this time including both the Variant and the base model. These results are shown in Figure 4.5. Again, a similar plot has been made for the material price per m^2 of Net Floor Area on the y-axis versus the Net Floor Area on the x-axis. It is displayed in Figure I.2 of Appendix I.

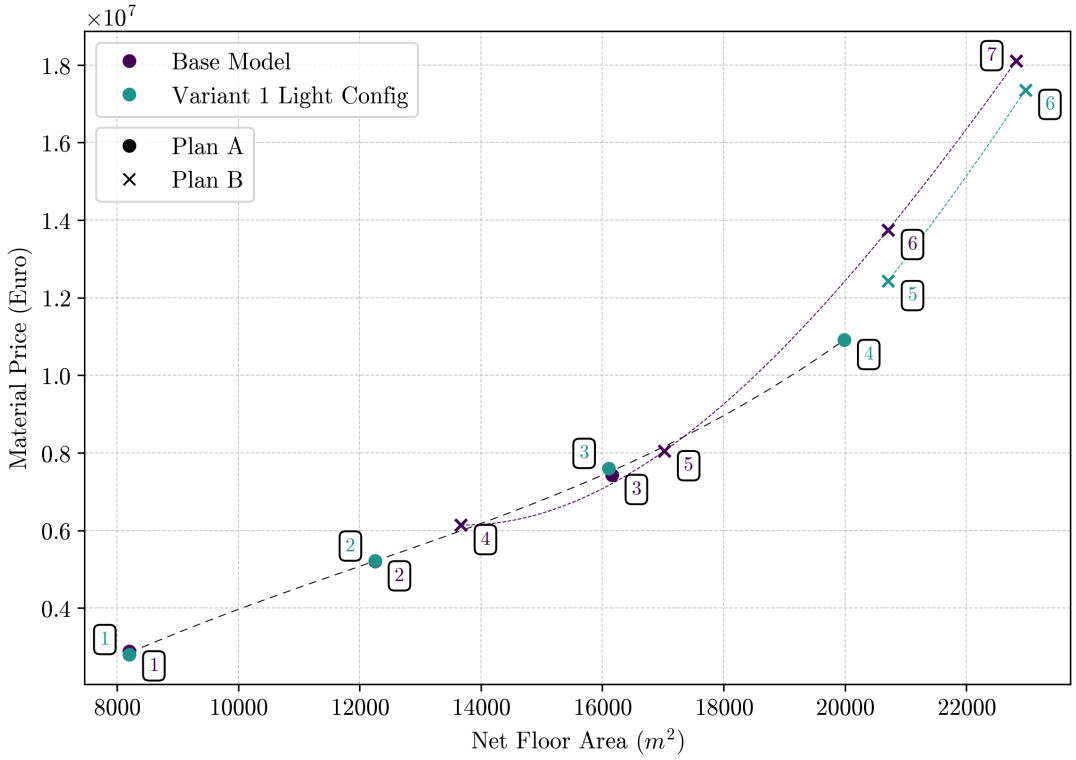

Figure 4.5: Variant 1: Light Configuration for Net Floor Area vs Material Price

From Figure 4.5, the following observations can be made.

1. As in the base model, the Variant also shows a steeper increase in cost under Plan B compared to Plan A. This is consistent with expectations and is based on the same underlying reasoning as described for the base model.
2. For the data points following the curve of Plan A, those of the Variant and the base model are highly overlapping. The application of the variant requires additional diagonals together with their corresponding steel connections, leading to extra material use. This difference is slightly visible in the graph, though its overall impact remains very limited.
3. Data point 4 of the Variant represents the case where Plan A could still be maintained, while in the base model a switch to Plan B was necessary. Although data point 4 is significantly more expensive than data point 5 of the base model (both corresponding to 25 storeys), the substantial increase in net floor area leads to the conclusion that point 4 still falls well below the material price trend line of the base model: approximately 14% lower that what it would cost to provide for the same amount of net floor area with the base model.
4. Data points 5 and 6 of the variant also show a lower cost than the corresponding data point of the base model. This is related to the fact that the variant allowed the use of a smaller dimension for the Y-beams, a principle described in Section 4.2.

Now, the CO_2 sequestration per net floor area for thelight configuration of Variant 1 can be determined. This value is again plotted on top of the existing graph of the base model (Figure 4.3). The resulting graph is shown in Figure 4.6.

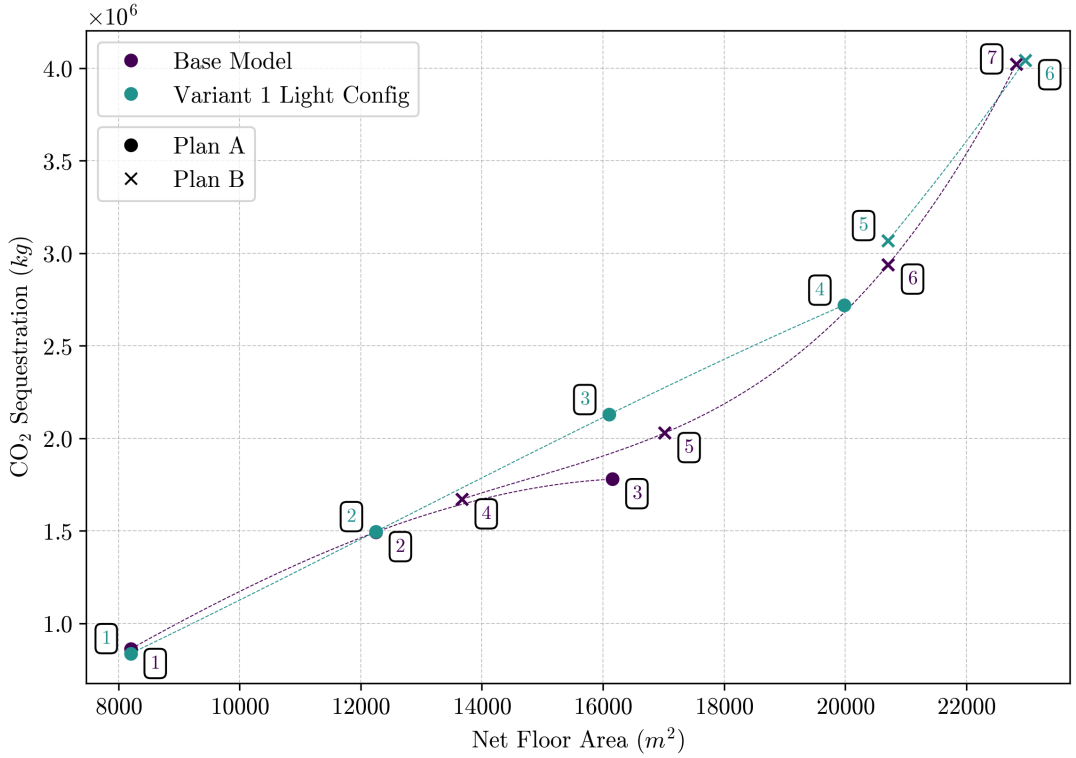

Figure 4.6: Variant 1: Light Configuration for Net Floor Area vs CO_2 Sequestration

From Figure 4.6, the following observations can be made.

1. The obtained values of Variant 1 correspond moderately well with those of the base model. Data point 4 follows the overall curve despite having a different Floor Plan than data point 5 of the base model (with similar height). Likewise, no notable differences are observed for data points 5 and 6 of the Variant when compared to the base model.
2. Contrary to the trend line formed by the Plan A data points of the base model, the trend line of the Variant for points 1 through 4 follows a more linear pattern, whereas the curve in the base model is decreasing. A possible explanation is that the inclusion of additional diagonal elements in the Variant results in increased timber usage compared to the base model. This additional timber leads to higher CO_2 sequestration, which causes the trend line to rise more steeply. The difference is clearly visible at the two data points number 3.

4.1.3 Variant 1: Braced system (Heavy Configuration)

The after thelight configuration, the heavy configuration of Variant 1: Braced System can be analysed. Again, a description of this variant and the mechanical principles applied can be found in Section 3.2.2 and in Section 2.5.1. Table 4.4 lists the different Model Runs along with their corresponding number of

storeys, Floor Plan, and the Appendix table in which the dimensions and Unity Checks of each iteration can be found.

Table 4.4: Overview of model runs Variant 1 (Heavy Configuration)

Model Run	Number of Storeys	Floor Plan	Dimensions & UCs (Table)
1	15	A	J.17
2	20	A	J.18
3	25	A	J.19
4	31	A	J.20
5	45	B	J.21
6	50	B	J.22
7	50	B	J.23

Based on the different Model Runs listed in Table 4.2, the net floor area can again be plotted against the number of storeys, this time for the heavy configuration. This plot is shown in Figure 4.7.

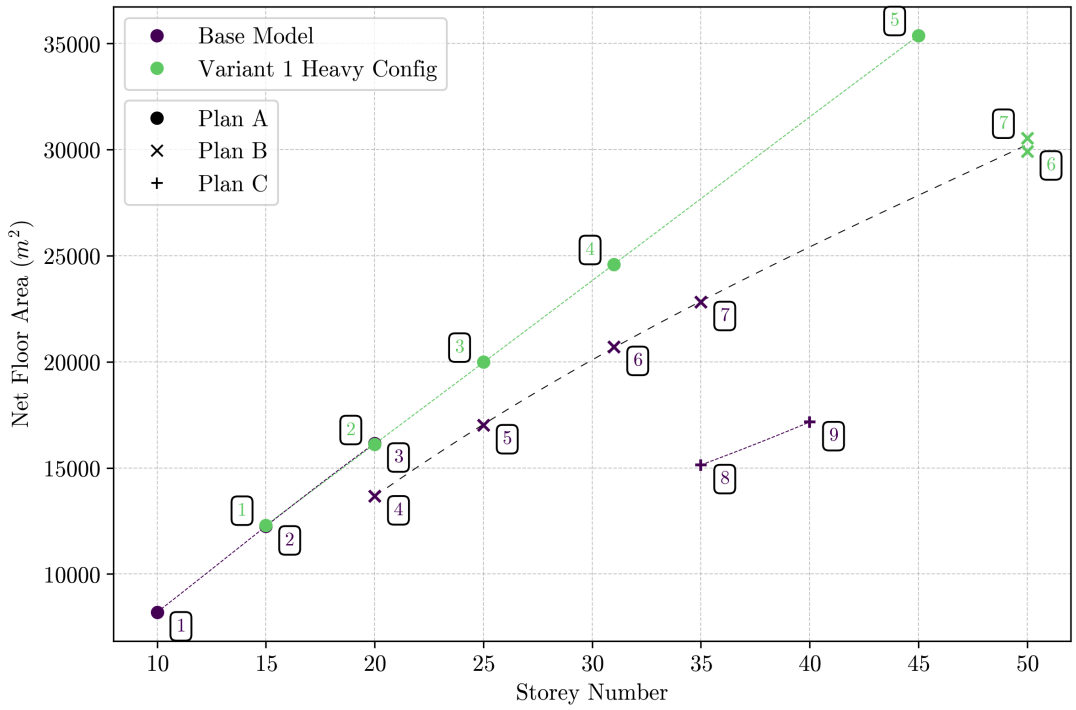

Figure 4.7: Variant 1: Heavy Configuration for Storey Number vs Net Floor Area

From Figure 4.7, the following observations can be made.

1. The first observation that can be made from the graph is that the newly added data points continue to follow the existing trend lines. For Plan A, the linear trend already present in the base model has been maintained with the same slope. The trend line for Plan B, which has now been rendered in

black due to the combination of data points, also shows no deviation after adding the new values. For Plan B, the curvature that was previously identified in Section 4.1.1 is now more clearly visible.

2. Two data points with 50 storeys have been added for Plan B. The reason for this is that two different configurations were possible using alternative combinations of column dimensions and core thickness. The results indicate that the effect of these differences is relatively insignificant.
3. As is immediately visible in the figure, the structure still satisfies the requirements for high storey numbers when using Plan A. This means that the increase in storeys continues to result in a significant gain in net floor area per storey. This has significant implications for the structure, as it can be seen that with 45 storeys, approximately 17% more net floor area can be achieved compared to the Model Runs of the Variant with Plan B, while having 5 storeys less. As a result, similar to what was previously observed for Plan C, no advantages remain associated with the application of Floor Plan B.

Applying a substantial number of diagonal elements in this variant will influence the material price per unit of net floor area. On the one hand, the structure becomes more expensive due to the additional material use, but on the other hand, the increase in net floor area resulting from the reduced core size may lead to a financial advantage in terms of material cost. The significant extension of the range of storey numbers that can be realized using Plan A, as shown in Figure 4.7, will likely be seen back in the material cost. Figure 4.8 illustrates the effect of applying this variant on the material price plotted against the net floor area. Also here, a similar plot has been made for the material price per m^2 of Net Floor Area on the y-axis versus the Net Floor Area on the x-axis. It is displayed in Figure I.3 of Appendix I.

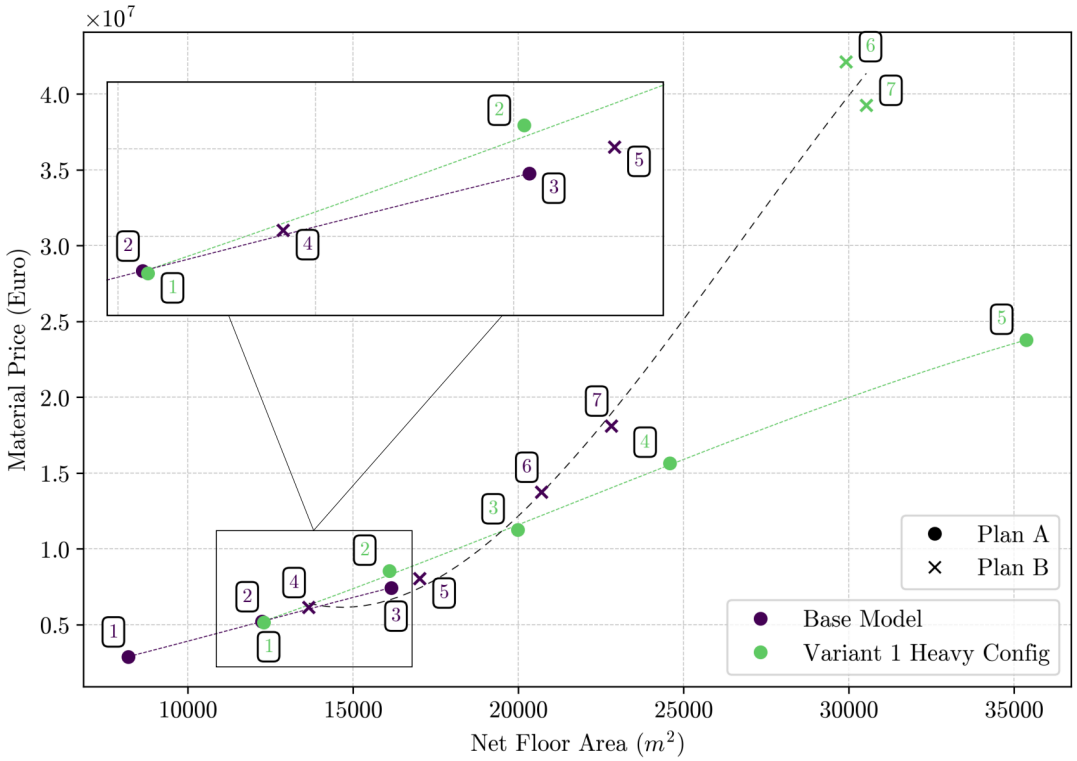

Figure 4.8: Variant 1: Heavy Configuration compared to Base Model for Net Floor Area vs Material Price

From Figure 4.8, the following observations can be made.

1. Data points of the new variant that follow Plan A maintain a linear trend, similar to what is observed in the base model. This implies that the material cost per unit of net floor area remains approximately constant across varying heights, which in turn suggests that the effect of increasing material dimensions is negligible compared to the net floor area gain per additional storey.
2. Plan B still exhibits a steeper and exponential trend. The underlying mechanism has already been described in Section 4.1.1. It can be observed that points 6 and 7, although shown to be irrelevant based on their net floor area, continue to follow the general trend of the Plan B data points, which is in line with expectations.
3. The graph includes a magnified view of the region where the trend lines of the base model and the Variant clearly move away from each other. In this magnified view, it becomes clear that the slope of the trend line for the Variant is greater than that of the base model. This results from the addition of the large amount of diagonal elements and their associated connections, which leads to significantly more material use and therefore higher costs. As a consequence, for lower building heights (up to approximately 25 storeys) it is less favorable to apply this variant when evaluating material cost. The (abstract) break-even point in this study lies around $20000\ m^2$, as indicated by the intersection of the trend lines of Plan A and Plan B.
4. However, beyond this point, the variant performs more effectively. For net floor areas exceeding $20000\ m^2$, the graph shows that the variant achieves considerably better results. The ability to maintain a smaller core results in significantly more net floor area being obtained with fewer storeys. This advantage is clearly reflected in the material cost when evaluated per unit of net floor area. For example, data point 5, with approximately 17% more net floor area, has a cost that is nearly half that of data points 6 and 7. It is important to note that this comparison does not concern total building height. As shown in Figure 4.7, data point 4 of the variant has the same number of storeys (and thus the same height) as data point 6 of the base model. Data point 4 here, with a material cost of approximately €16 million, is more expensive than data point 6 of the base model, which costs about €14 million. However, because it can incorporate Floor Plan A, the material price per net floor area is clearly increased.

After the material price has been evaluated relative to the net floor area, the same approach can be applied to the CO_2 sequestration. This is presented in Figure 4.9.

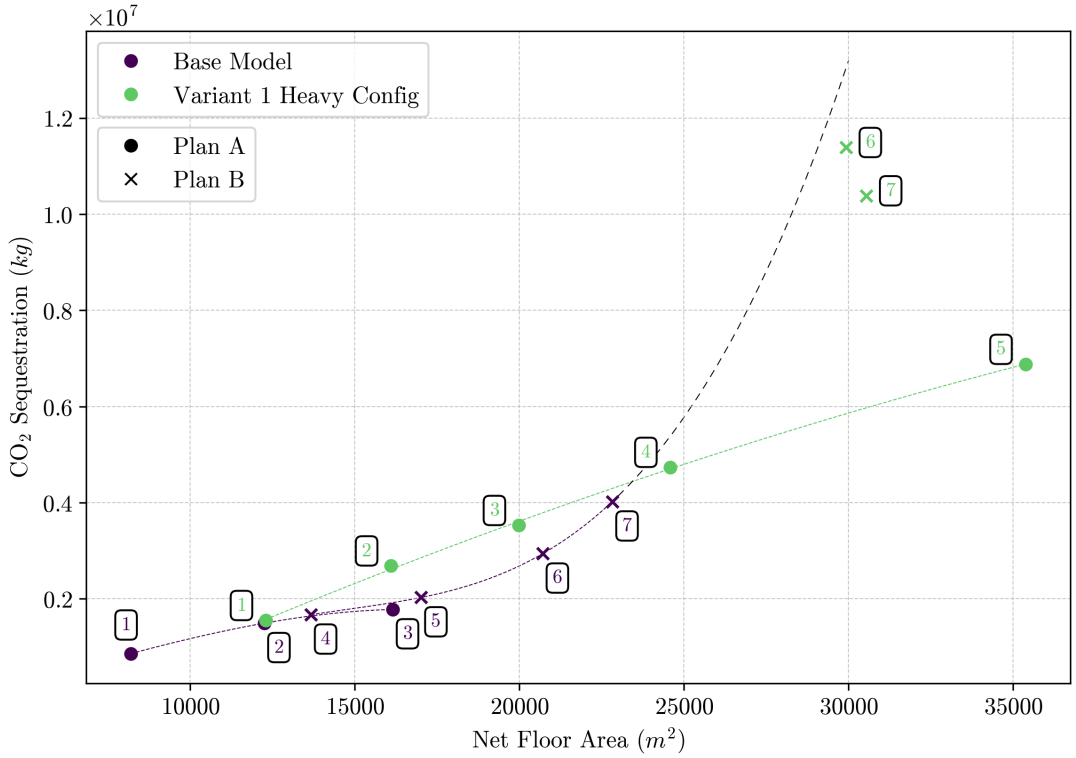

Figure 4.9: Variant 1: Heavy Configuration for Net Floor Area vs CO_2 Sequestration

From Figure 4.9, the following observations can be made.

1. The overall graph shows behavior similar to that of the material cost. The comparison again demonstrates that increased use of timber corresponds to higher costs, but also to greater CO_2 sequestration.
2. Data points 6 and 7 show lower CO_2 sequestration than would be expected if the general trend line of the base model were extrapolated. In the Variant, many timber diagonals have been added, so the expectation was that this would result in higher CO_2 sequestration in the graph. Why the data points nevertheless fall below the extrapolated trend line cannot be explained based solely on the current data. Additional data points would be necessary to more accurately determine the trend that new iterations of the Variant with Plan B would follow. However, since Figure 4.7 has shown that applying Plan B in the Variant provides no additional benefit in terms of net floor area compared to Plan A, this question becomes less relevant for the remainder of the analysis.

4.1.4 Variant 2: Outrigger System (Timber and Concrete Columns)

The final variant analyzed is the outrigger system. A description of the functioning of this system is provided in 2.5.2, while the specific implementation within this study is detailed in 3.2.3. Since only iterations that could potentially offer an improvement over the base model were documented, the two configurations (Timber and Concrete columns) are combined in this section. For this variant, Timber columns are used as the starting point (Variant 2T), and if no improvement could be achieved, the same iteration was also executed with concrete columns (Variant 2C). Table 4.5 presents all Model Runs for

both Timber and Concrete columns, including the number of storeys, the applicable Floor Plan, and the corresponding table of dimensions and Unity Checks from Appendix J.

Table 4.5: Overview of model runs Variant 2 (Timber and Concrete Columns)

Model Run	Number of Storeys	Floor Plan	Dimensions & UCs (Table)
Timber Columns			
1	20	A	J.24
2	31	B	J.25
3	35	B	J.26
4	40	B	J.27
Concrete Columns			
1	25	A	J.28
2	25	B	J.29
3	45	B	J.30

Figure 4.10 shows the net floor area per number of storeys for Variant 2. As with the other variants, the numbers indicated in the graph correspond to the Model Runs listed in Table 4.5. Particular attention should be paid in the graphs of this variant to the difference between the data points of the iterations of Variant 2T and Variant 2C.

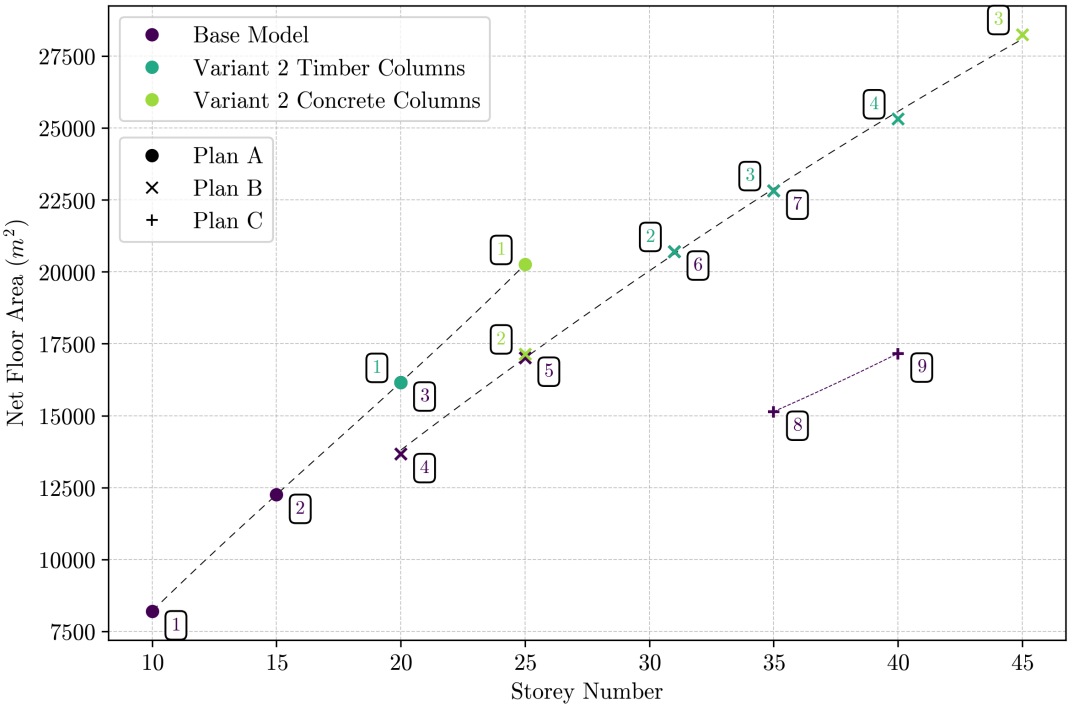

Figure 4.10: Variant 2 for Storey Number vs Net Floor Area

From Figure 4.11, the following observations can be made.

1. As well for this variant, the new data points follow the same trend line as the base model. Minor differences are visible in some cases, for example when comparing point 2 of Variant 2C with point 5 of the base model.
2. As with the previous variants and the base model, Floor Plan C does not result in any improvement in terms of net floor area and is therefore excluded from the following figures.
3. Variant 2T was able to provide an improvement over the base model in only one data point. Data point 4 of Variant 2T satisfied the requirements for 40 storeys using Plan B, while the base model could only meet these requirements up to 35 storeys. In general, Variant 2T did not yield significant improvements. This is related to a deeper underlying cause associated with the structural behaviour of this variant. More specifically, the Differential Vertical Shortening, discussed in Section 2.6 is handled in another matter. This both haves positive and negative effects for the structure. The underlying theory behind this principle is further discussed in Section 4.2.
4. In cases where Variant 2T did not result in improvement, the Timber columns were replaced with Concrete columns. This substitution led to improvements in certain instances. For example, Variant 2C was able to satisfy the requirements for 25 storeys using Floor Plan A, as indicated by data point 1 of Variant 2C in the graph. Additionally, for Plan B, Variant 2C succeeded in meeting the requirements for 45 storeys, which also contributed to an increase in the maximum net floor area that could be achieved by this variant.

Since Variant 2C is used in some iterations, where the Timber columns are replaced with concrete columns, this will affect both the material cost and CO_2 emissions. First, for Variant 2, the material cost is plotted against the net floor area, which is shown in Figure 4.11. Also here, a similar plot has been made for the material price per m^2 of Net Floor Area on the y-axis versus the Net Floor Area on the x-axis. It is displayed in Figure I.4 of Appendix I.

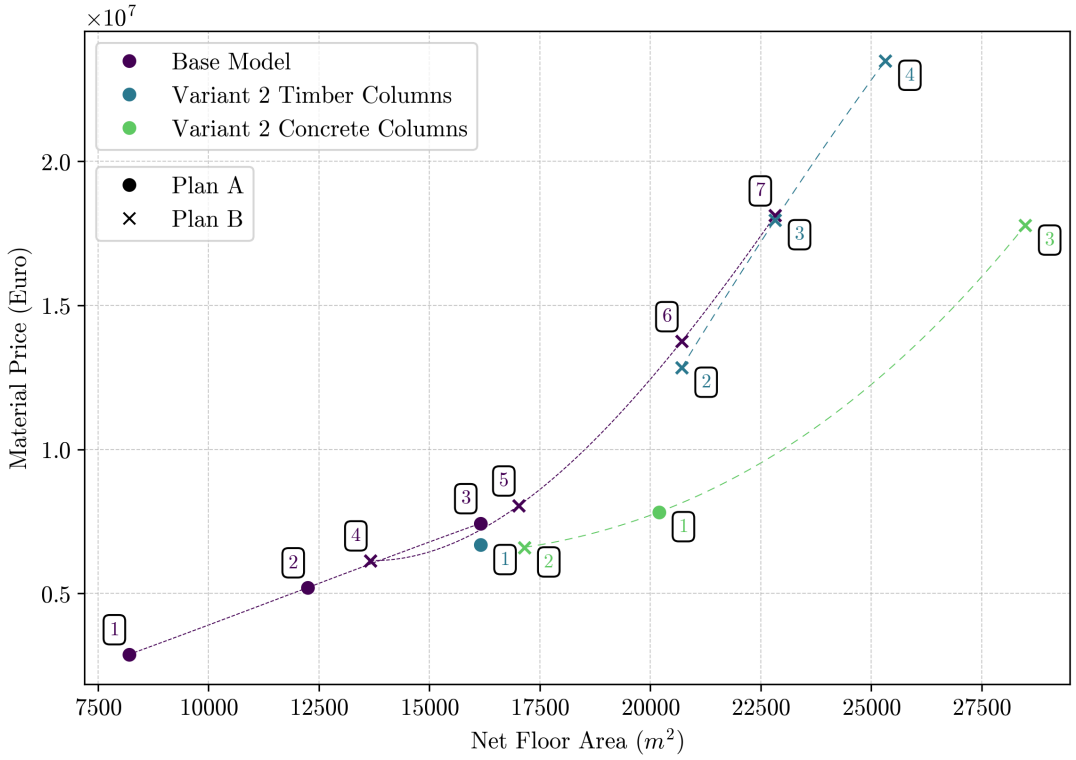

Figure 4.11: Variant 2 compared to Base Model for Net Floor Area vs Material Price

From Figure 4.11, the following observations can be made.

1. Variant 2T closely follows the trend of the Base Model. While the timber volume increases due to the addition of the two outriggers, the overall material usage decreases because of structural efficiency, which results in the data points remaining approximately at the same position.
2. The trend line of the data points of Variant 2C, similar to the other variants, shows an exponentially increasing curve, which aligns with expectations. However, it is clearly noticeable that this curve lies significantly lower compared to the base model and the other variants that apply Plan B, reflecting the price difference between timber and concrete, as the total costs drop substantially when the columns are switched to concrete.

After the material cost of Variant 2 has been determined, the CO_2 emissions can also be plotted against the net floor area. In Figure 4.12, the CO_2 sequestration is shown as a function of the net floor area. It should be noted in this figure that a negative value indicates CO_2 emissions rather than sequestration.

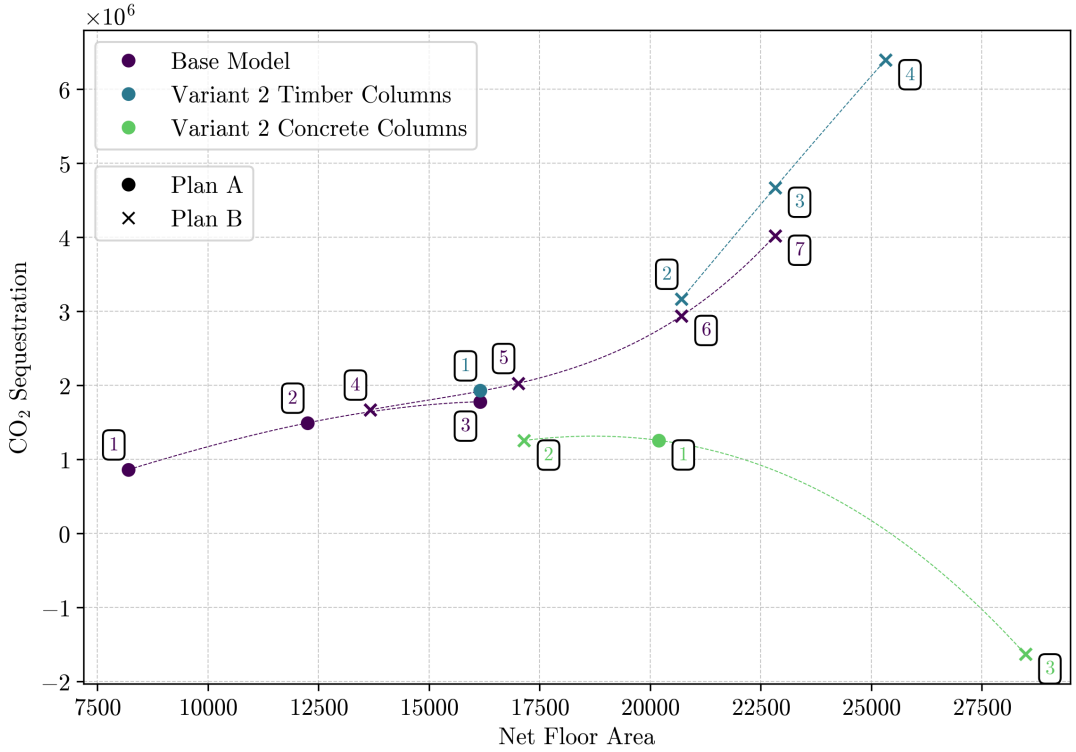

Figure 4.12: Variant 2 for Net Floor Area vs CO_2 Sequestration

From Figure 4.11, the following observations can be made.

1. Variant 2T closely follows the trend of the base model. However, in data points 2, 3, and 4 of Variant 2T, a steeper increase is visible compared to the base model. The reason for this is that a higher reinforcement ratio had to be applied in the base model than in the variant. This is a logical outcome, as the core principle of the outrigger system is to transfer loads from the core to the perimeter columns. As a result, the tensile forces in the core are reduced, leading to a lower reinforcement demand in the core. This translates into reduced steel use, lower emissions, and therefore higher CO_2 sequestration.

2. The data points of Variant 2C are the only ones in all CO_2 graphs that exhibit a downward trend. Data point 3 even falls below zero, indicating that more CO_2 is emitted than sequestered during material production (cradle-to-gate). This clearly illustrates the significant impact of the columns on the total material volume. Instead of timber, large quantities of concrete and reinforcement steel are used for the columns. Both materials emit CO_2 during their production. It should be noted, however, that the value of data point 3 (approximately 1.7 million kg of CO_2 emissions) is still lower than that of conventional construction composed entirely of concrete and steel. This is due to the fact that the beams and a substantial portion of the floor structure still consist of timber, which compensate the emissions. What this graph primarily highlights is the influence of the columns on the total material volume of a structure.

4.1.5 Top Floor Dynamic Accelerations

Section 2.4, in addition to the determination of the wind load, also explained how the dynamic accelerations of a building can be calculated based on the method described in the Eurocode. Figure 4.13 presents the calculated dynamic accelerations for the top floor of the variants relevant to this study. All variants that could provide an independent data point were included in this analysis. Diagonal elements were excluded from these calculations based on the assumption that their contribution to the overall weight of the structure is minimal. Since these diagonals only add extra weight, they have a favourable influence on the calculated accelerations, and therefore, the Eurocode-method based results can be considered conservative for the variants, since the base model iterations are applied. The base model lacked an iteration for 45 storeys. Therefore, the dimensions of Variant 1H (Diagonal Bracing System: Heavy Configuration) were used. The iterations for Variant 2C (Timber Outrigger with Concrete Columns) were also included separately, as replacing timber columns with concrete significantly increases the total building weight and thus affects the dynamic behavior. Lastly, the figure contains two reference lines: Line 1 applies to office or utility buildings, while Line 2 corresponds to residential buildings. After observation of the results, the obtained results and their implications will be further addressed in Section 4.2.3.

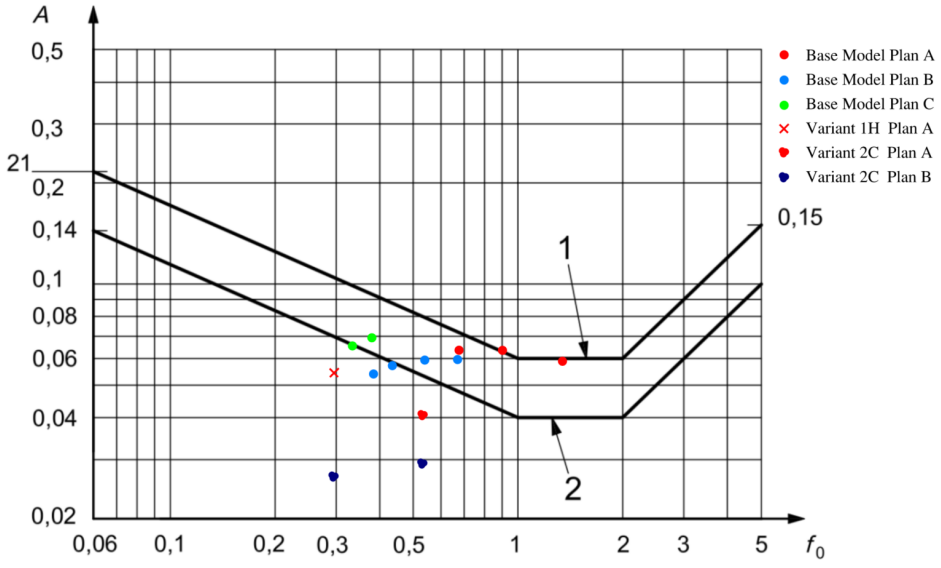

Figure 4.13: Dynamic Accelerations of the top level for relevant and distinct iterations

1. Since the natural frequency was calculated using the rule of thumb $\frac{46}{h}$, the building height is inversely proportional to this frequency. Consequently, the data points from left to right represent building heights from tall to short, respectively.
2. The applied Floor Plan has a clear effect on the acceleration magnitude. This is due to the fact that each Floor Plan has a different core size. In this model, the space inside the core is empty, so larger cores (i.e., Floor Plan C) contain more empty space and thus result in a lower total weight, which leads to higher accelerations as seen in the graph.
3. Given the selection of a residential function for the investigated building, several points are positioned above the line representing the comfort requirement for residential buildings, meaning they do not validate. However, all points fall below the line indicating the threshold for office buildings. This observation is further interpreted in Section 4.2.3.
4. Since higher accelerations are permitted for lower natural frequencies, the iterations with 31 storeys and higher do satisfy the requirement.
5. In all data points associated with Variant 2C, the comfort criterion is comfortably met. This is due to the significant increase in self-weight resulting from the implementation of concrete in the columns.

4.2 Discussion

4.2.1 Interpretation of Results and Comperative Analysis

After all results have been established, a discussion can be conducted based on the observed outcomes. While the results chapter focused on evaluating each variant in comparison to the Base Model, this section provides a further interpretation of those findings. To determine which configuration is most suitable under different design constraints, the variants are now assessed in relation to one another through a comparative analysis. The analysis first considers their performance based on the evaluation indicators presented in the results, namely net floor area efficiency, material price and CO_2 impact. Next, the variants are compared in terms of their individual structural characteristics and design-specific implications.

Net Floor Area Efficiency
As a starting point for the comparative analysis, a brief recap of the key results is provided. All variants demonstrated structural improvements compared to the base model. Significant reductions in net floor area occurred when switching the Floor Plan configuration, first from A to B and then from B to C. For the base model, these transitions took place at 20 and 35 storeys respectively, although Floor Plan C no longer provided additional benefits beyond that point. In the Light Configuration of the Diagonal Bracing System (Variant 1L), the switch from Plan A to B was delayed until 25 storeys. Within the Outrigger System, only the version with concrete columns (Variant 2C) achieved a similar delay. However, the Timber Columns variant (Variant 2T) maintained Plan B up to 40 storeys, compared to 30 storeys in the base model. Variant 2C validated with Plan B requirements up to 45 storeys.

The Heavy Configuration of the Diagonal Bracing System variant (Variant 1H) showed a distinctly different behavior compared to the other variants. The high density of diagonal GLT elements enabled the structure to reach 45 storeys while still complying with Floor Plan A. This is an increase of approximately 75% in comparison to the other variants. Floor Plan B validated up to 50 storeys, but, similar to Floor Plan C in the Base Model, it did not result in any improvement in net floor area.

It is important to consider what these results actually indicate in a broader sense. Variants 1L, 2T and 2C made it possible to maintain reduced core dimensions at slightly greater building heights, purely from a structural perspective. The significant increase in Net Floor Area that these variants provide in specific cases makes them relevant design options to consider in similar high-rise constructions. While the concrete core continues to function as the primary stabilizing element, the additional support provided by these variants is non-negligible.

This provides a strong indication that the application of this quantity of diagonal beams may not just support, but rather take over the stabilizing function of the concrete core. If the objective of the building is to maximize net floor area, Variant 1H offers an effective solution by achieving lateral stability around the perimeter of the structure, rather than in the center.

Material Cost-Effectiveness
The results indicate that the total material cost of the building is largely determined by the volume of timber used in the structure. Due to the relatively small volume share of steel and the low price of concrete, these two materials had a considerably smaller impact on overall cost. However, as shown in the previous subparagraph, the application of additional stabilizing timber elements results in a sufficient increase in net floor area to maintain material cost-effectiveness. First, a brief recap of the main findings of the variants is provided, followed by a discussion of their implications.

All variants displayed differing behaviour with respect to material costs. Variant 1L achieved a reduction in material cost per net floor area due to its ability to extend the use of Floor Plan A, after which it maintained approximately 10% lower material costs. Variant 1H initially showed an increase in material costs. In the range between 12,500 and 20,000 m^2 net floor area, the large number of diagonal elements in this variant resulted in a rise in material cost. Around 20,000 m^2, a break-even point was observed, after which the curve for the Variant clearly has a lower steepness, showing that the increase in net floor area leads to a significant reduction in material costs, and proving the effectiveness of Variant 1H. Variant 2T remained nearly equal to the base model in terms of material costs, while in Variant 2C, the use of concrete columns led to a clear reduction in timber volume, resulting in a cost decrease of approximately 50%.

Based on these findings, it becomes evident that the increase in net floor area resulting from the continued use of smaller core dimensions can indeed lead to a reduction in material costs. This is reflected in Variant 1L during the transition from Plan A to Plan B, and more prominently in the significant decrease in material costs observed in Variant 1H due to the prolonged applicability of Plan A. It can therefore be concluded that the application of these variants can indeed result in an increase in cost-effectiveness, provided that the core can be reduced in size based on structural behaviour. The notable reduction in material cost per net floor area in Variant 2C, resulting from the use of concrete columns, can be attributed to the well-established fact that the price of concrete is considerably lower than that of timber. The following subparagraph will address the implications of this on the CO_2 impact.

CO_2 Impact

The material cost per net floor area has shown that the timber volume largely dominates the cost indication. A similar observation can generally be made regarding the sequestration or emission of CO_2. Due to the high percentage of timber present in all variants, it was observed that CO_2 sequestration almost always exceeds emissions. Furthermore, the CO_2 sequestration closely corresponds with the material costs. This principle implies that aiming for better performance CO_2 sequestration is directly associated with higher material costs. As a result, structures that are less slender and less efficiently designed tend to perform better in this regard. For this reason, it remains essential to consider the trade-off between CO_2 impact and material costs.

In Variants 1L and 2T, the total CO_2 impact remains nearly equal to that of the Base Model. Variant 1H initially shows higher CO_2 sequestration at lower storey numbers, followed by lower sequestration at higher storey numbers. This behaviour aligns with with the material cost per net floor area and can be explained by the additional use of numerous diagonal beams, which initially increases timber volume. Later, when Variant 1H is still able to ulitize Plan A, the lower CO_2 sequestration can be explained by the higher net floor area efficiency, which results in a lower overall timber requirement.

Variant 2C showed deviating behaviour compared to the other variants. In this variant, the use of concrete columns resulted in a CO_2 impact that was initially positive and later negative, indicating that sequestration occurred at first, followed by emissions. At higher storey counts, the column dimensions increased, which led to a greater share of concrete in the overall structure. Additionally, the amount of reinforcement steel used in this variant also increased. These two factors ultimately resulted in net emissions.

Variant 2C illustrates the essence of the trade-off between material costs and CO_2 impact. Although some variants showed advantages or disadvantages under specific conditions with respect to one of these two evaluation criteria, the results do not reveal a clear optimum in this trade-off. There is no case in which substantial CO_2 benefits can be achieved without increasing material costs, nor one in which significant cost reductions occur while the CO_2 impact remains constant.

Comparative analysis for other technical considerations

In addition to comparing the variants based on the established evaluation criteria, the advantages and disadvantages of both configurations must also be examined across other relevant aspects. The selection of a specific design variant involves more implications than structural characteristics, material costs, and CO_2 impact alone. This subsection identifies several factors that may indicate differences in the structural behavior of the variants and highlights additional considerations on which a design decision may be based.

The first aspect concerns the impact of both variants on façade openness. While the base model results in a fully open façade, both variants negatively affect this openness to varying degrees. The light configuration of the diagonal bracing system introduces several diagonal elements within the façade, which impose some restrictions but with reduced visual and spatial impact. In contrast, the heavy configuration significantly limits façade openness due to the large number of diagonals, which considerably reduce daylight exposure. It could also be argued that the impact is relatively minor, as each side of the façade contains only 3, 4, or 5 diagonals per floor, corresponding to a spacing of approximately 10, 7.5, or 6 meters respectively, depending on the floor plan. Finally, the use of an outrigger structure has a more favourable outcome for this evaluation criterion, as the diagonal beams are only present at the outrigger levels, allowing the façade to remain unobstructed on all other floors.

In addition to façade openness, the variants also differ in terms of fire safety. The diagonal beams in Variant 1 have the disadvantage that, if ignited, they can facilitate vertical fire spread. As a result, a fire could potentially propagate more easily from one floor to another. To mitigate this risk, the diagonals must be covered with an additional fire-resistant layer, and other necessary measures must be taken. The outrigger variant, however, has the potential to offer a significant advantage over the other configurations in this respect. If the outrigger levels are made fully fireproof, these floors could function as refuge floors. This principle is described in Section 2.7.1. The implementation of a refuge floor could provide significant benefits, as it may allow for reduced fire safety requirements on the remaining storeys. Especially in combination with concrete columns, this could lead to a relaxation of fire protection demands for the timber elements on other floors. How exactly these relaxations can be realised remains an interesting follow-up question for future research.

The final principle that was not included in this study but could influence the implementation and the advantages and disadvantages of the different variants is the concept of robustness or redundancy. This principle is based on the idea that an alternative load path must be available in the event of the sudden failure of a load-bearing structural element. For a practical design, a secondary load path must be ensured for each column or diagonal, in compliance with the Eurocode and other applicable regulatory requirements. All loads carried by such a column are then transferred to adjacent columns through tensile forces in the floors and connection forces. The presence of diagonals in the various configurations positively affects this behaviour. If a façade column fails, the heavy configuration of the diagonal bracing system allows the forces to be relatively easily redistributed to adjacent columns via the diagonals. Due to the large number of diagonals, redundancy is significantly increased in this variant. The same principle applies to the light configuration, although it only holds for the columns to which diagonals are connected. The outrigger variant also enhances redundancy. The outrigger ensures that the vertical forces from the columns located both directly above the failed column and above the outrigger itself can be redirected to an adjacent column. The exact mechanism of this principle is also highly relevant for further investigation in future research.

4.2.2 Black Box Problem and Underlying Structural Principles

When developing a parametric model and working through multiple iterations, it is important to maintain a certain level of speed and efficiency. As discussed in Section 3.6, Unity Checks were obtained directly after running the model, and based on these Unity Checks, it was determined whether adjustments were necessary for that specific iteration. One issue that can arise from this process is the so-called 'black box' problem. This is a problem often encountered in Artificial Intelligence applications, where there is a clear input and output, but limited insight into the underlying processes. For structural design, this represents a significant pitfall that should be avoided as much as possible.

Moreover, due to the implementation of the connection size, which influenced the rotational stiffness of the joints (see Sections 3.4 and 2.3), a large number of variable parameters emerged. This principle, combined with the fact that each model iteration was relatively computationally expensive, made the model and the process highly prone to converging towards local minima.

To address these two issues as effectively as possible, the most relevant underlying structural mechanisms that occurred during the dimensioning and result collection process are discussed.

Wind Forces combined with DVS

Forces resulting from wind loading are transferred to the core through the diaphragmatic action of the floors. It is therefore important that both the floors and the beams parallel to the wind have pinned supports or, at the very least, very low rotational stiffness. If these connections and supports were moment-resistant, axial tension and compression would arise in the columns (see Section 2.5). This is not necessarily problematic, as Variant 2 is even based on this principle (see Section 3.2.3). However, additional moments and shear forces would also develop in the beams parallel to the wind, which are undesirable because they increase the required capacity of these beams. In Figure 4.14, the underlying mechanical principle is visualized. This figure schematically shows the moment distribution in the beams parallel to the wind direction.

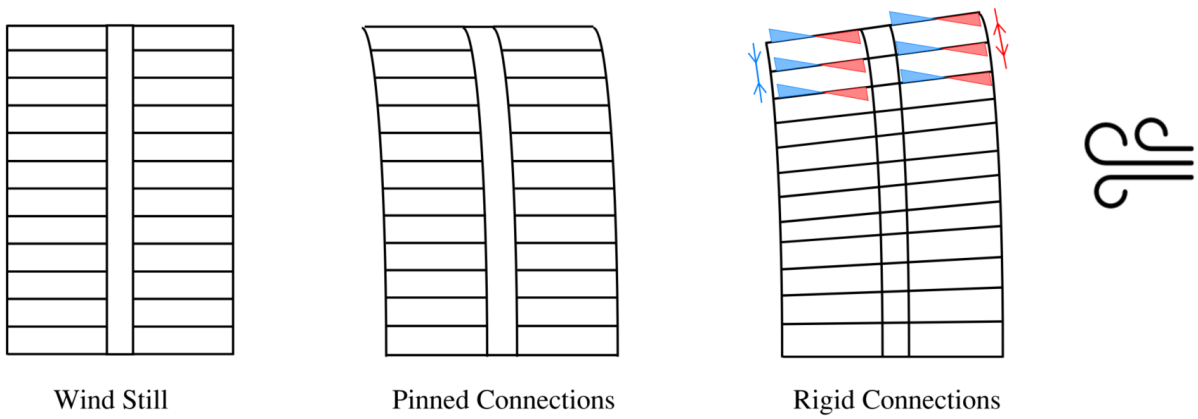

Figure 4.14: Reaction to wind forces for pinned and rigid connections

As described in Section 2.6, hybrid structures are not only subjected to wind loading but also to the effect of differential vertical shortening (DVS). To briefly recap, differential vertical shortening refers, as the name suggests, to the difference in shortening between the timber columns and the concrete core due to their differing material properties. This effect includes both elastic deformations and time-dependent deformations. Due to the self-weight of the structure, the differential shortage will occur. For this mechanism as well, it is important that the beams and floors act in a pinned manner. In the case of

moment-resistant connections, unwanted moments and shear forces develop in the beams, similar to the wind loading scenario. Here too, the underlying mechanical principle is visualized in Figure 4.15. This figure schematically shows the moment distribution in the beams that are connected to the core in case of a rigid connection.

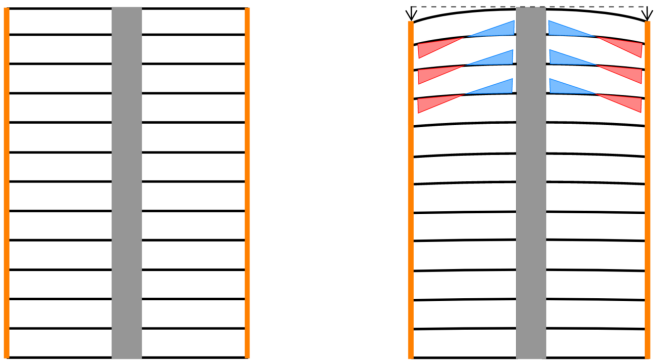

Figure 4.15: Reaction to DVS

In Figure 4.14, it can be observed that the moment distribution on the right side is identical to the moment distribution in that beam resulting from wind loading (assuming the wind originates from that direction). This implies that, in this beam, the effects amplify each other on the right side. On the left side, however, they cancel each other out.

Section 3.4 showed that slotted-in steel plate connections inherently acquire a certain rotational stiffness when designed for the desired capacity. However, the rotational stiffness values assigned to the model were very low. As an example, the Base Model with 15 storeys is used, where the dimension of the beams connected to the core (the Y-Beams) was 467×700 mm and the embedment depth of the steel plate in the connection was 400 mm (see Table J.2). When these values are inserted into Equation B.16, a value of $3.36 \cdot 10^3\ kNm$ is obtained. For a rotational stiffness of this magnitude, no significant stresses would be expected in the beams. However, such stresses were in fact observed in the results. Figure 4.16 presents the moment distributions for two different load cases and the governing combination of these two cases. The figure includes the load cases and combinations by their names as defined in Section 3.3.

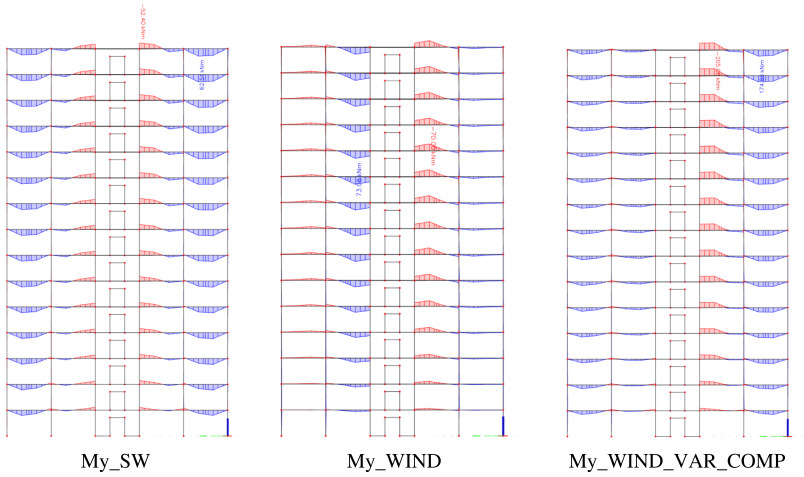

Figure 4.16: Effect of Self Weight and Wind Forces on the moment distribution of the Y-beams of the Structure (Base Model, Floor Plan A, 15 Storeys)

In Figure 4.16, it can be observed that, as previously described, the combination of both load cases results in amplified moments on the right side of the core, leading to large and undesired stresses. This suggests that a rigid or highly stiff connection force was still present in the model. Initially, it was assumed that these forces and moments were caused by the implemented rotational stiffness values. Notably, in the self-weight load case, the beams that are not directly connected to the core show behaviour that does resemble that of a pinned or flexible connection. This is also apparent in the wind load case, where the moments on the core side are significantly higher than on the opposite side, both on the left and right of the core. This indicates that the moment-resistant behaviour is only occuring in the connections at the core, which in turn implies that the cause is not the implemented rotational stiffness of the connections of the Y-beams.

When reviewing the implemented model in SCIA, it became clear that the issue is located at the interface between the floor and the core. The floors are connected to the Y-beams using line-hinges, but they should not be connected to the core at all and should instead move independently. In SCIA, connections are automatically modelled as moment-resistant unless specified otherwise. Figure 4.17 clearly shows that a moment-resistant connection was modelled at these locations as there is a line-hinge or other type of specification missing.

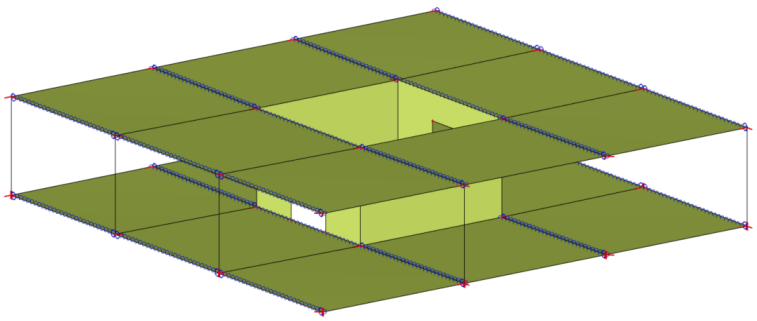

Figure 4.17: Cause of model issue by misplaced rigid connection between core and floors (missing line-hinge)

Due to the direct connection between the Y-beams and the floor elements, these forces were transferred into the beams, resulting in undesired stresses in these elements.

Since this issue was only identified at a later stage, and in order to quantify its effect, line-hinges were added at the previously missing locations in the base model with 20 storeys. The resulting moments in the Y-beams were then recalculated. Figure 4.18 presents the moment distributions of the top two storeys for the base model iteration with 20 storeys. On the left side of the figure, the original iteration is shown with a maximum moment of 89.18 kNm, while on the right side, the improved version with line-hinges added at the previously missing locations displays a reduced maximum moment of 62.68 kNm. This is a difference of around 40%. Therefore, the maximum allowable Unity Check for these beams was set to 1.4 during the dimensioning of the various iterations.

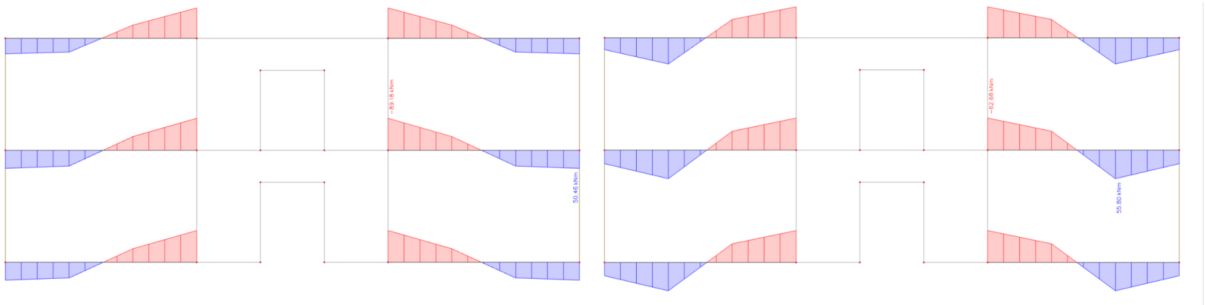

Figure 4.18: Maximum moment in the Y-beams of the two upper storeys of the model without the line-hingens (left) and with the added line-hinges (right)

As described in Section 2.6, the effects of DVS can be mitigated in practical design by placing shim plates located at the column to column connections. This prevents the occurrence of stresses currently observed in the Y-beams. With this approach, the timber columns initially extend slightly above the corresponding connection position of the core. Once they are loaded by the self-weight of the upper storeys, they align with the height of the core. The building sequence plays a significant role in this process. To properly account for its influence, the sequence must also be included in the structural analysis. This can be implemented in FEM software such as SCIA. However, in order to maintain model simplicity, this was not incorporated in the current study.

Flow of Forces in Outrigger

During the result collection process of the outrigger variant, specifically the outrigger combined with timber columns (Variant 2T), it was observed that less force was transferred from the core to the columns than initially expected. The underlying structural mechanism behind this, similar to the DVS mechanism, relates to the higher compressibility of timber compared to concrete. The purpose of the outrigger is to relieve part of the moment in the core caused by wind loading. It does so by transferring forces outward toward the outer columns. However, if these columns are more compressible, the forces cannot be effectively resisted by the columns, as they themselves deform under the load. As a result, the effectiveness of the system is reduced. This principle is schematically illustrated in Figure 4.19.

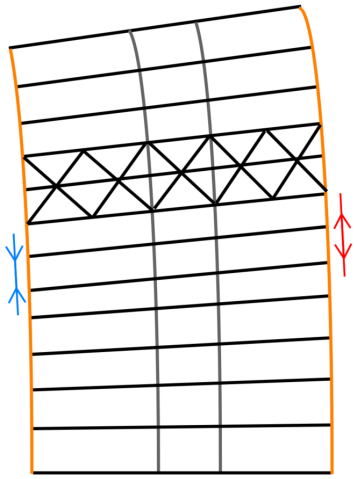

Figure 4.19: Shortening of timber columns due to wind load transfer through outrigger

By using concrete columns (Variant 2C), this issue was immediately resolved, as the difference in compressibility no longer occurred. This was the underlying reason why Variant 2C performed better in terms of net floor area. As a result, a higher number of storeys could also be achieved with this variant.

It was also found that the Unity Checks of the Y-beams in this variant were lower than in the other variants. This is again related to the occurring differential vertical shortening (DVS). In the Outrigger Variant, the differences in vertical displacement were smaller compared to the Base Model and the other variants. This is illustrated in Figure 4.20.

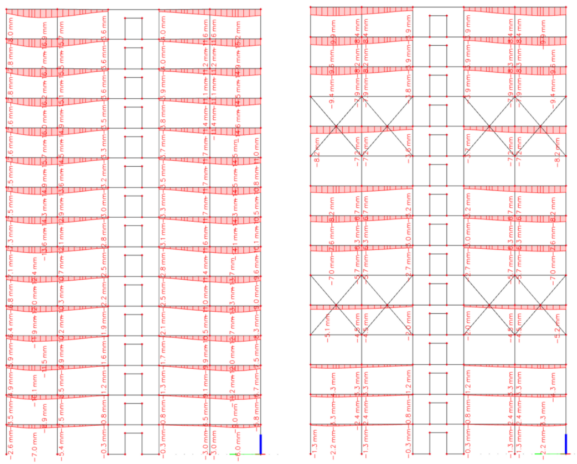

Figure 4.20: Vertical displacement of Y-beams for the Base Model on the left (maximum 16.9 mm) and the Outrigger Variant on the right (maximum 9.9 mm)

The reason for this behaviour lies in an underlying structural mechanism. The greater the number of columns stacked on top of each other, the larger the effect of differential vertical shortening (DVS) becomes. The stiffness of the outrigger, combined with its direct connection to the core, causes the columns to effectively bear on the outrigger, as a result of their self weight, such that forces are transferred from the outrigger back into the core. This has a favourable effect on the required reinforcement in the core, as the resulting tensile forces are reduced. However, for compressive forces, this is a disadvantage:

the additional load imposed by the outrigger on the core increases the compressive demand, requiring a thicker core. The resulting flow of forces associated with this mechanism is schematically illustrated in Figure 4.21.

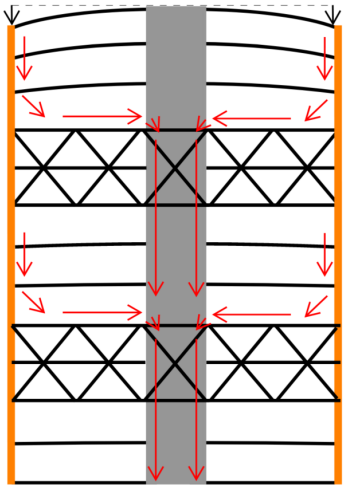

Figure 4.21: Flow of forces as a result of timber column shortening (DVS)

Gravity-induced spreading mechanism of diagonal bracings

In the light configuration of the diagonal braced system, an additional structural mechanism is observed. Due to gravitational forces, the diagonal members tend to spread outwards, which induces horizontal displacements at their points of attachment. This effect only occurs in the light configuration, as its zigzag pattern introduces geometric asymmetry. A potential consequence is a zigzag-shaped tilt of the entire building. Since a concrete core is included in the design, the effect will be largely countered. However, this resistance may result in stresses within the floor elements. Figure 4.22 illustrates this mechanism. On the left, a schematization shows how the effect potentially propagates through the structure. In the middle, the actual displacements of the diagonal elements in the y-direction under self-weight are displayed based on the parametric model. Lastly, on the right, the in-plane normal stresses in the y-direction in the floor elements directly surrounding the diagonals under the same load case are shown. As an example, the iteration with 20 storeys is presented.

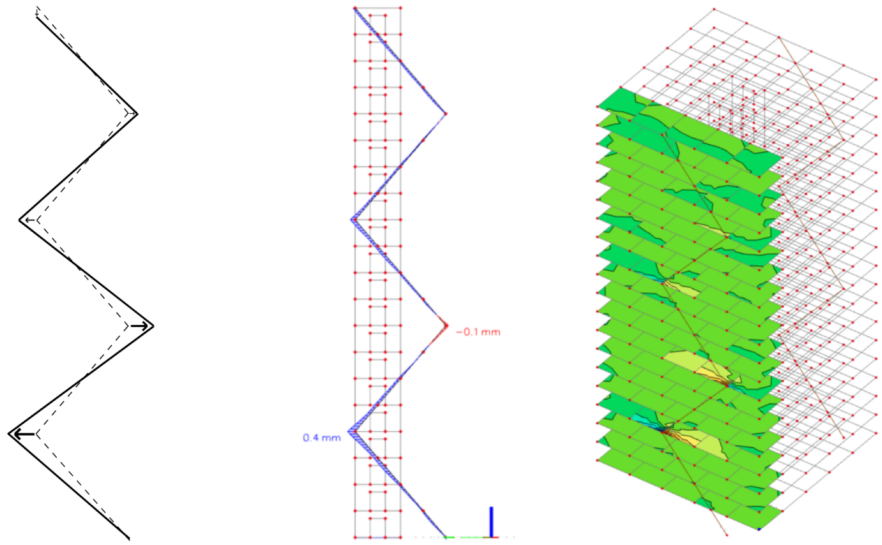

Figure 4.22: Gravity-induced spreading mechanism of the diagonal bracings of variant 1L with 20 storeys

As shown in the figure, the SCIA model does reveal horizontal displacements during the analysis as a result of this mechanism. These displacements reach maximum values of 0.1 mm and 0.4 mm, which appear to be low and are unlikely to significantly affect displacement-related design criteria. However, the display of normal forces in the y-direction of the two-dimensional floor elements (right side of the figure) shows that tensile and compressive forces do occur around the attachment points of the diagonals. In this example, these forces amount to a maximum of 76 kN/m in tension and 61 kN/m in compression, indicating stress magnitudes that are not negligible. However, it is also visible that the stresses are highly localised around the diagonal connections and decrease rapidly outside these areas. For this reason, such stresses must be taken into account, but they can be mitigated with local adjustments, such as additional reinforcement or strengthening around the affected locations.

4.2.3 Wind induced Dynamic Behaviour

Due to time constraints, dynamic accelerations were not included during the initial structural dimensioning process. These accelerations were calculated at a later stage and are therefore critically discussed, with the aim of formulating recommendations for future research. The equation from the Eurocode (Eq. 2.10), used to calculate dynamic accelerations, is highly complex. It is containing multiple parameters that are each defined by additional sub-equations. In the equation, parameter μ_{ref}, the reference mass, requires the calculation of the weight per square meter of floor area, while parameter m_e, the equivalent mass of the fundamental mode of vibration, demands the estimation of the total weight of the top one-third of the building. Accurately determining these values proved challenging, as the weight of the structural system itself had to be included. Given the level of abstraction in this research, the total structural weight may still vary significantly. Although actual cross-sectional dimensions of structural elements were used in the calculations, verifying the accuracy of the total weight remains difficult due to uncertainties related to finishing layers, live loads, mechanical systems, and other architectural or technical components. Verifying the correctness of the calculations was also challenging, as the large number of interdependent equations makes it difficult to trace possible inaccuracies.

As shown in Section 4.1.5, a significant number of data points do not meet the comfort requirement for buildings with a residential function. Increasing the building dimensions to raise the mass will not provide a sufficient solution in this context, as it would not be economically viable. Therefore, further research is necessary to determine the accelerations with greater accuracy.

In this follow-up research, determining the natural frequencies would be an appropriate first step. For the current study, the rule of thumb $n_{1,x} = \frac{46}{h}$ was used, which is derived from the Eurocode but represents a significant simplification. Moreover, this rule is not intended for buildings that incorporate timber in their structural system. The natural frequency could be calculated by simplifying the building geometry into a mass-spring system, although this would require determining the spring stiffness, which depends on the horizontal load and the horizontal displacement at the top. This approach still constitutes a simplified representation of reality. Alternatively, the natural frequency could be determined using FEM software.

The acceleration at the top floor of the building is also highly dependent on the damping of the structure. Accurately determining the damping of a timber high-rise construction remains complex, as it relies on empirical data from real-world projects. Given the limited number of timber high-rise buildings constructed to date, it is necessary to work with conservative damping values. Nevertheless, further investigation into this topic is justified, since it is known that higher damping coefficients can be applicable to timber structures, which could lead to a significant reduction in the calculated accelerations.

In addition to the natural frequency and damping, the assessment of cross-winds as well as displacements and accelerations due to torsion were not included in this study due to the limited scope. While cross-winds are generally not governing, the effect of vortex shedding at sharp corners of the building can lead to complications. Annex E of Eurocode 1-4 provides a method for addressing such effects. Torsion resulting from eccentric wind loads could also play a role, and accurately analysing this would require a dynamic model. The damping coefficients of timber will also influence these effects.

4.2.4 Practical and Technical Design Considerations

Due to the limited scope of this research, several topics have been excluded from further analysis. These topics were excluded because it was not assumed that they would have a significant influence on the outcomes of the research, nor that they would lead to substantial differences between the design variants within the defined evaluation criteria. However, when developing a real-world design, these aspects must be examined in more depth. This section outlines the main considerations that were not further addressed in this study.

Core Size Considerations
This study specifically focused on the structural behaviour and efficiency, material cost implications, and the CO_2 impact of the materials. Within this scope, reducing core dimensions while increasing the net floor area had a positive effect on performance based on these indicators. In practice, however, the core dimensions are not determined solely by structural aspects. They largely depend on architectural requirements, particularly the minimum number of elevators and stairwells that must be incorporated. Fire safety regulations also impose specific constraints on the core layout. Nevertheless, since the core contains a substantial amount of concrete, the relevance of this research remains, as it is still valuable to explore the structural limitations.

Concrete Reinforcement
The reinforcement ratio in the concrete elements is a key factor influencing both the structural behaviour and the material use of the building. For this study, several major assumptions were made in this area. As

described in Section 3.5, the reinforcement ratio was determined by placing a one-dimensional integration strip in the concrete core at the location where the highest tensile forces would occur. The tensile force at that location defines the required reinforcement ratio, which is then applied uniformly across the entire volume of the core. In practice, this approach could lead to highly conservative reinforcement ratios, as wind-induced loading typically decreases at higher elevations within the core. Additionally, in practice, the force distribution in the core is very uneven, with stress concentrations potentially forming around narrowings, such as openings, where more reinforcement is needed compared to other regions. The way in which reinforcement is placed within the core also partly determines the actual force path. This makes the calculations significantly more complex in reality than assumed in this study.

In this study, the dimensioning was focused on minimising the core thickness. However, if this results in a significantly higher amount of reinforcement, it may not lead to the optimal solution, given the higher material costs and CO_2 emissions of steel compared to concrete. A relevant follow-up study could investigate the optimal reinforcement configuration in the core and the effect of both reinforcement ratio and concrete thickness on the structural behaviour of the core.

Foundation Capacity and Settlements
For this study, it was assumed that the foundation behaves rigidly and that no asymmetric, irregular, or potentially unpredictable settlements would occur. In practical design, however, this is a critical factor for which sufficient care needs to be given. The integration of different structural variants can lead to significant differences in foundation loading, particularly in terms of uneven distribution. This is especially relevant in the Netherlands due to the relatively weak soil conditions and the necessity of deep foundation piles. Initially, it was hypothesised that tensile forces could develop in the columns due to the lower weight of timber compared to concrete, potentially resulting in uplift forces under wind loading. During the dimensioning process, this effect was observed only in a single case involving the heavy configuration of the diagonal bracing system. The tensile values were very small, and therefore this effect was not investigated further. However, for the development of a practical design, this aspect must be addressed in detail.

Durability of Timber and other aspects regarding Building Physics
Due to the organic nature of timber (see Section 2.2), the material is susceptible to faster degradation if appropriate mitigation strategies are not applied. Low durability of timber could have a considerable impact on the outcomes of this study. If timber elements need to be replaced more frequently, this would negatively affect the material cost outcomes of the design iterations. The durability of timber depends on several factors, including moisture content or absorption (which can lead to biological degradation), ventilation, as well as the timber type and its finishing or treatment. If these factors are carefully addressed and managed correctly, timber does not necessarily have to be less durable than concrete. The specific approach and measures required in terms of building physics to ensure the durability of the timber were not addressed in order to limit the scope of this research.

Finally, acoustics is an important aspect in the design of timber structures. The lower weight of timber makes the structure more sensitive to the propagation of sound waves. Additionally, the stiffness of the connections enables the transfer of sound through the structural system. In the design of the base model, TCC floors were applied. Besides their advantages in reducing dynamic accelerations, this system also offers significant benefits in terms of acoustics. The integration of TCC floors can reduce the propagation of sound waves between residential units (see Section 3.2.1). Although this aspect lies outside the scope of this study, it is essential that it needs to be taken into account for a practical design.

Chapter 5

Conclusions & Recommendations

5.1 Conclusions

This section discusses the main findings by addressing each sub-question, which together form the basis for answering the main research question. The sub-questions provided the primary structure and guiding framework for how this research was conducted. Below, each sub-question is addressed briefly and concisely, starting with the first. This sub-question was answered in Chapter 2.

What are the current construction approaches, effective techniques, and key challenges in timber high-rise building design?

Current construction approaches and effective techniques:

1. A concrete core is used in Brock Commons, HAUT, and Ascent, and was identified in the literature review as the most effective lateral stability system.
2. Diagonal bracing systems are well-supported in the literature for high-rise applications and have been implemented in buildings such as Mjøstårnet and Treet.
3. Timber outriggers have shown promising results in theoretical research, but have not yet been applied in real-life structures.
4. Slotted-in steel plate connections were used in Mjøstårnet.
5. HAUT and HoHo Wien use TCC floors to increase mass, eliminate punching shear effects, and improve acoustic performance.
6. Brock Commons employs steel shim plates to mitigate differential vertical shortening.

Key challenges in timber high-rise building design:

1. Timber is orthotropic and shows low strength in the perpendicular-to-grain direction.
2. Slotted-in steel plate connections introduce undesirable but unavoidable rotational stiffness.
3. The low mass of timber increases its susceptibility to wind-induced dynamic vibrations.
4. While CLT cores have been extensively studied, they generally fail to provide sufficient lateral stiffness for high-rise buildings due to low internal cohesion and a high reliance on steel connections, resulting in excessive steel use.
5. Differential vertical deformations between timber and concrete lead to unwanted stresses and distortions, particularly as building height increases.
6. Full burnout or self-extinguishment of timber elements cannot yet be guaranteed according to current research. Therefore, timber must be protected by gypsum boards to prevent charring from initiating.

The second sub-question to be addressed is the following. This sub-question was covered in Chapter 3.

In what way can a representative base model be designed for variable building heights, and how can meaningful structural variants be derived from it?

Base model design:

1. To keep the designs both parametric and generic, a fixed footprint of 30 by 30 meters was used.
2. Three floor plans were developed with varying core and grid sizes, allowing larger cores to be assigned to higher storey counts.
3. The structural system consists of GLT beams and columns, TCC floors, and a concrete core with variable wall thickness.

Structural variants:

1. All design variants are based on the same base model, with only diagonal GLT beams added to introduce additional lateral stability. The specific design strategies for each variant were derived from insights obtained in the literature review.
2. Two main variants were developed, each with two subtypes. Variant 1 features diagonal bracing along the building perimeter, with a light configuration containing fewer braces (Variant 1L) and a heavy configuration with denser bracing (Variant 1H).
3. Variant 2 incorporates timber outrigger structures positioned at one-third and two-thirds of the building height. Two subtypes exist: Variant 2T with timber columns, and Variant 2C in which the columns are replaced by concrete.

The third sub-question is addressed next. This sub-question was also examined in Chapter 3.

How can the design variants with varying storey numbers be efficiently and parametrically modelled, analysed, and dimensioned?

Process of modelling, analysing and dimensioning:

1. A parametric geometry was created in Grasshopper, incorporating all relevant design parameters. Using the KOALA plugin, this geometry was converted into a structural model with defined loads, supports, and connection properties.
2. The structural model was exported via KOALA as an XML file and sent to SCIA Engineer, where the structural analysis was executed in the background. Each iteration took approximately 5 to 20 minutes to compute.
3. SCIA automatically placed the results of each iteration into a predefined Engineering Report, which was exported as an Excel file. This file was then re-imported into Grasshopper for post-processing.
4. In Grasshopper, internal forces and moments from the Excel file were used to perform Unity Checks according to Eurocode. Based on these checks, cross-sections were manually adjusted until an acceptable optimum was reached. This process was repeated for every variant and storey number.

The fourth sub-question is addressed thereafter. This sub-question was partially examined in the final part of Chapter 3, and partially in Chapter 4.

How are the model iterations evaluated, structured, and visualised based on defined criteria, and how do the variants perform relative to the base model with respect to these criteria?

Evaluation, structuring and visualisation:

1. For each model iteration, the *net floor area* is calculated, as it is more relevant than the total building height and strongly influenced by the core dimensions.
2. Based on literature, estimates are made for material cost and CO_2 impact per m^3 of timber, concrete, and steel. These values are combined with the calculated net floor area to generate plots of material cost and CO_2 sequestration (with net emissions shown as negative values).
3. Chapter 4 first presents the results of the base model, followed by overlays of the variants. Each section includes three comparative plots (for net floor area, material price, and CO_2 sequestration), and where relevant, polynomial trend lines are added between data points with the same floor plan.

Performance of variants relative to the base model:

1. Variants 1L and 1H, both with perimeter diagonal bracing, showed improved lateral performance compared to the base model. Variant 1L maintained Floor Plan A up to 25 storeys (vs. 20 in the base model), with approximately 10% lower material cost and slightly higher CO_2 sequestration. Variant 1H extended the use of Floor Plan A even further; although material cost was initially higher (up to 20,000 m^2), it dropped significantly at greater heights. CO_2 sequestration followed a similar trend.
2. Outrigger variants 2T and 2C showed mixed results. Variant 2T allowed Plan B to remain valid up to 40 storeys (vs. 35 in the base model), with nearly identical material cost and slightly improved CO_2 sequestration due to reduced steel reinforcement. Variant 2C achieved more net floor area with smaller cores and significantly lower material cost due to the lower price of concrete compared to timber, but was the only case resulting in net emissions rather than sequestration, a clear deviation from all other cases.

Lastly, the fifth sub-question is addressed, as discussed in Chapter 4. An overview of the main limitations of the model is provided below.

How can the results of the design variants be interpreted and compared, and what are the limitations of the model?

Interpretation, Comparison, Limitations:

1. A comparison is made between the design variants, discussing their advantages and disadvantages. This is done first based on the defined evaluation criteria, and subsequently on additional technical implications where the variants differ, namely façade openness, fire safety implications, and structural robustness.
2. A major limitation of the model is the black box issue. To mitigate this as much as possible, the most relevant underlying structural principles are researched and explained as clearly and precisely as possible.

3. Another important limitation of the model lies in the simplification of natural frequency and damping estimations. This has resulted in values that, in some cases, do not yet meet the required performance criteria.
4. Assumptions and simplifications made in this study compared to a real-world design concern: core size and reinforcement, foundation capacity and settlements, timber durability, and other aspects related to building physics.

The sixth and last sub-question is addressed in this chapter and is divided into two parts. First, the key findings of this research are presented. Subsequently, the main research question is answered, and in the final section, the recommendations are discussed

What are the key findings of the research, and what recommendations can be made for use-cases within the model framework, general structural design, and future studies?

Key findings of this research:

1. When designing a timber high-rise construction, adopting a hybrid structural system with a concrete core is a highly viable option.
2. Additional stability can indeed be gained from complementary stabilising elements made of timber, meaning the material possesses sufficient stiffness to effectively assist the concrete core.
3. Measuring the (maximum achievable) net floor area is a more effective way to evaluate the performance of a system than measuring building height. The core size has a major influence on this; if the core becomes too large and no gain in net floor area can be achieved, opting for a lower number of storeys is more favourable.
4. As demonstrated by both the literature review and the parametric model, implementing a diagonal bracing system with a high bracing configuration (Variant 1H in this study) is a highly effective method for providing lateral stability in timber high-rise structures. The effects of this system nearly take over the role of the concrete core, and this benefit is reinforced by the possibility of reducing core size, which positively affects the net floor area.
5. Implementing diagonal bracings in a light configuration (Variant 1L in this study) also has potential benefits, especially in the cases when it enables a reduction in core dimensions, core thickness, or reinforcement ratio.
6. The use of a timber outrigger has shown to be effective, but it comes with important considerations. The columns must not experience greater compression deformation than the rotation of the core due to wind loading, as this would reduce the outrigger's effectiveness.
7. Differential vertical shortening can also cause the columns to bear on the outriggers, and thereby also bear on the core, further reducing the effectiveness of this variant. However, particularly when concrete columns are used, considerable gains in the maximum achievable net floor area can be realised.
8. Reducing the core size based on the integration of one of these variants is only valid if it is architecturally and regulatorily accepted; the results therefore specifically address a purely structural question.
9. Based on the findings of this study, the occurrence of tension in the columns due to wind loading is a less significant complication than initially assumed.
10. The workflow proved effective for comparing the variants. However, the introduction of rotational stiffnesses to all timber connections added a potentially excessive number of parameters to the model, making it vulnerable to the Black Box problem and to converging on local minima.

Now that all sub-questions have been answered, the main research question can be addressed.

What is the influence of different complementary timber lateral stability systems on the material costs and CO_2 impact of timber high-rise structures with a concrete core?

This sub-question is divided into the following parts: impact on material costs, impact on the CO_2 balance, and other key takeaways and trade-offs identified in the study.

Material Costs
Material cost evaluation is based solely on literature-derived estimates of material prices per m^3, excluding construction, labour, and transport costs. The study showed that the primary reason for higher costs is the material price of timber compared to concrete. This leads to the general conclusion that, in broad terms, the following statement holds: "the greater the required timber volume, the higher the cost." It was observed that in each model, the material cost per net floor area increased more rapidly for configurations with a larger core size, as the net floor area increased more slowly when increasing storey number. In certain cases, more efficient material use, such as reductions in column or beam dimensions, or steel savings resulting from a lower required reinforcement ratio, led to lower costs per net floor area. This was seen in the light configuration of the diagonal bracing system, where a material cost reduction of approximately 10% was observed. However, the most significant effects identified in this study were the cases where complementary stabilising elements allowed for a reduction in core size. As stated in the last sub-question, this had a major impact on the achievable net floor area. Since the number of storeys remains constant, this effect strongly translates to material cost per net floor area. Because the core size was constant with the core size of the base model at lower building heights, the application of stability systems had a negative impact on material cost. The variants proved more effective at higher heights, when enabling smaller core sizes This is reflected in their cost efficiency. In particular, the diagonal bracing system, after initially generating higher costs, showed a much lower rate of material cost increase per net floor area from 25 storeys onwards, resulting in significantly lower material costs at greater heights. This effect amounts to approximately 22% compared to the base model at 23,000 m^2 net floor area, and up to 50% when compared to selecting a larger core at 30,000 m^2 net floor area.

CO_2 Impact
The first key finding of this study is that, with one exception, all variants and the base model sequester more CO_2 than they emit. The results also suggest that the timber volume in the structure, plays a dominant role in the CO_2 impact. In other words, contrary to prior assumptions, the variation in CO_2 impact between iterations appears to be more strongly driven by the amount of timber used than by the share of concrete or steel. To directly address this part of the main research question: the influence of the complementary stabilising systems on the CO_2 impact of a timber high-rise structure with a concrete core is positive, but this effect is primarily the result of the increased timber volume. For this reason, it is ultimately more relevant to consider the trade-off between CO_2 impact and material cost, as the positive effect on CO_2 observed in this study consistently corresponded with an increase in material costs, and vice versa. The CO_2 impact and material cost were, as shown, strongly correlated. Additionally, this study also found that replacing timber with concrete columns in the outrigger variant leads to a significant decline of the CO_2 impact, as the sequestering effect is entirely lost and net emissions occur.

5.2 Recommendations

This section addresses the final part of the sixth sub-question. The recommendations are divided into three categories: use-case recommendations within the model framework, recommendations for general structural design and recommendations for future study.

What are the key findings of the research, and what recommendations can be made for use-cases within the model framework, general structural design, and future studies?

Recommendations for use-cases within the model framework

1. Between 20 and 25 storeys, it is advisable to apply the light configuration of the diagonal braced system (Variant 1L), as it leads to an increase in net floor area and a corresponding reduction in material cost. By adding a small number of diagonals, the material cost per m^2 of net floor area can be reduced by approximately 16%. This cost benefit remains present even beyond 25 storeys. However, this variant does not enable an increase in maximum building height. Additionally, attention must be paid to the potential risk of fire spread between storeys via the diagonals. Finally, asymmetric alignment of the diagonals may induce stresses in the floor panels due to outward rotation caused by self-weight. these stresses remain localised near the connection points of the diagonals. This effect can be appropriately mitigated by applying local reinforcements.
2. It is not recommended to apply the heavy configuration of the diagonal braced system (Variant 1H) in buildings with less than approximately 20,000 m^2 of net floor area, due to the additional costs associated with the large number of diagonals. Above this threshold, for net floor areas between 20,000 and approximately 35,000 m^2, the application of this variant becomes beneficial, with significantly lower costs per m^2 of net floor area compared to the base model. Its application is conditional on the architectural feasibility of accommodating sufficient space for stairs and elevators within the core. Moreover, this variant enables an increase of approximately 55% in maximum achievable net floor area compared to the base model under the design constraints applied in this study. Similar to Variant 1L, there is a potential risk of fire spread between storeys via the diagonals. In addition, the use of this variant reduces façade openness, which may be considered architecturally disadvantageous.
3. Between 35 and 40 storeys, corresponding to approximately 23,000 to 25,500 m^2 of net floor area, the outrigger variant with timber columns (Variant 2T) shows an improvement compared to the base model, and can therefore be applied in this range. The maximum achievable net floor area of the base model was approximately 23,000 m^2. However, the material cost of Variant 2T shows virtually no improvement over the base model, meaning that this variant is not recommended if cost reduction is the primary objective. An additional benefit of this variant is that it allows for greater freedom in maintaining façade openness. Variant 2T also shows interaction with the differential vertical shortening (DVS) mechanism, resulting in increased compressive loading on the core. The exact behaviour and implications of this interaction require further investigation.
4. By implementing concrete columns (Variant 2C), a building height of 45 storeys can be achieved. This variant also showed significantly lower material costs, making its application favourable for cost reduction. At a net floor area of 17,500 m^2, the cost reduction was approximately 20%, increasing to nearly 50% at 23,000 m^2 of net floor area. However, this comes at the expense of a substantial negative influence on the CO_2 impact. Variant 2C was the only variant to display a difference between material cost and CO_2 impact. From around 25,000 m^2 net floor area onwards, net emissions occurred, making this variant less recommendable from an environmental perspective. Nevertheless, it does offer potential improvements in fire safety, due to the possibility

of integrating refuge floors at the outrigger levels. This, however, requires further investigation. Façade openness can also be preserved with this variant.

Recommendations for general structural design:

1. In a practical design for a high-rise structure in which a timber variant with a concrete core is being considered, it is certainly worthwhile to explore whether additional gains in material efficiency or net floor area by reducing core size can be achieved for that specific scenario.
2. Based on the findings of this study, for timber high-rise structures exceeding 30 storeys, it is strongly recommended, to implement a diagonal bracing system with high bracing density in addition to a concrete core, but only when it is architecturally feasible.
3. The effect of adding additional rotational stiffness to the connections is minimal, while material costs increase relatively quickly as a result; for practical design, it is therefore recommended to aim for implementation of pinned connections wherever possible.
4. Based on the literature review conducted in this study, it is discouraged to use a CLT core as the primary lateral stability system in high-rise construction, due to the high stiffness requirements for connections and the accompanied steel usage.
5. The use of the KOALA plugin to connect Grasshopper with SCIA is highly recommended for rapid structural analyses involving complex parameters. This setup not only enables the direct modelling of numerous variants, but, despite not being a determining factor in this study, also allows for the efficient analysis and optimisation of geometrically complex structures due to the computational power of Grasshopper.

Recommendations for future studies:

1. Investigation of combined failure mechanisms for the capacity of slotted-in steel plate connections with multiple parallel steel plates.
2. Assessment of fire spread risks via diagonals and the potential relaxation of fire protection measures on adjacent floors when a refuge floor is created using a timber outrigger supported by concrete columns.
3. Further investigation of robustness and the availability of secondary load paths for the different variants.
4. Analysis of the interaction between differential vertical shortening and outrigger behaviour, including the resulting force distribution.
5. In-depth investigation of the dynamic structural behaviour under wind loading, including natural frequency of timber buildings, more precise application of damping coefficients, and the effects of cross-winds and eccentric wind loads on the torsional response of timber structures, with particular focus on ensuring compliance with comfort criteria for wind-induced vibrations.
6. Detailed study of the durability of timber to determine whether the intended design lifetime of high-rise structures can be achieved, or if timber elements require earlier replacement.

Bibliography

[1] Rune Abrahamsen. "Mjøstårnet – Construction of an 81 m Tall Timber Building". In: *23. Internationales Holzbau-Forum IHF 2017*. Moelven Limtre AS. Garmisch-Partenkirchen, Germany, 2017.

[2] Rune B. Abrahamsen and Kjell Arne Malo. "Structural Design and Assembly of "Treet" – A 14-Storey Timber Residential Building in Norway". In: *Proceedings of the World Conference on Timber Engineering (WCTE 2014)*. Quebec City, Canada: WCTE Organising Committee, 2014, pp. 1–10.

[3] Acton Ostry Architects Inc. *Design and Pre-Construction Overview Brock Commons Tallwood House*. Tech. rep. Retrieved from University of British Columbia. Vancouver, Canada: University of British Columbia, 2017.

[4] Shafayet Ahmed and Ingrid Arocho. "Analysis of Cost Comparison and Effects of Change Orders During Construction: Study of a Mass Timber and a Concrete Building Project". In: *Journal of Building Engineering* 33 (2021), p. 101856. DOI: 10.1016/j.jobe.2020.101856. URL: https://doi.org/10.1016/j.jobe.2020.101856.

[5] A. Bengtsson. "Sustainability of Timber and Wood Products". In: *Sustainability of Construction Materials*. Ed. by Jamal Khatib. 2nd ed. Woodhead Publishing, 2016. Chap. 21, pp. 609–641. DOI: 10.1016/B978-0-08-100411-1.00021-2.

[6] Carolien Boot-Dijkhuis et al. *Bouwbesluit 2014: Voorschriften omtrent brandveiligheid*. Delft, Netherlands: Nederlands Normalisatie-Instituut, 2014.

[7] Bouwkosten. *Welkom op Bouwkosten*. Accessed: 2025-06-27. 2025. URL: https://www.bouwkosten.nl/welkom#_=_.

[8] Bouwwereld redactie. *Knoop wand-vloer ter reductie geluidsoverdracht*. Accessed: 2025-05-18. 2023. URL: https://www.bouwwereld.nl/bouwtechniek/houtbouw/knoop-wand-vloer-ter-reductie-geluidsoverdracht/.

[9] Reinhard Brandner et al. "Cross Laminated Timber (CLT): Overview and Development". In: *European Journal of Wood and Wood Products* 74.3 (2016), pp. 331–351. DOI: 10.1007/s00107-015-0999-5.

[10] Andrew Buchanan, Birgit Östman, and Andrea Frangi. *Fire Resistance of Timber Structures*. White Paper. Draft report. New Zealand; Sweden; Switzerland: National Institute of Standards and Technology (NIST), Mar. 2014.

[11] José Manuel Cabrero, B. Iraola Sáenz, and Miguel Yurrita. "Failure of Timber Constructions". In: *Materials Failure Analysis With Case Studies From the Construction Industries*. Ed. by A. S. H. Makhlouf and M. Aliofkhazraei. Butterworth-Heinemann, 2018, pp. 123–152.

[12] Hi Sun Choi et al. *Outrigger Design for High-Rise Buildings, 2nd Edition*. Council on Tall Buildings and Urban Habitat (CTBUH). 2017.

[13] Galina Churkina et al. "Buildings as a Global Carbon Sink". In: *Nature Sustainability* 3.4 (2020), pp. 269–276. DOI: 10.1038/s41893-019-0462-4.

[14] Cobouw. *Advies aan nieuw kabinet: Nederland heeft 2 miljoen nieuwbouwwoningen nodig*. Accessed: October 21, 2024. 2023. URL: https://www.cobouw.nl/293981/advies-aan-nieuw-kabinet-nederland-heeft-2-miljoen-nieuwbouwwoningen-nodig?login=true.

[15] Roy Crielaard et al. "Self-Extinguishment of Cross-Laminated Timber". In: *Fire Safety Journal* 105 (2019), pp. 244–260. DOI: 10.1016/j.firesaf.2019.01.008. URL: https://doi.org/10.1016/j.firesaf.2019.01.008.

[16] Roberto Crocetti. "Timber Structures for Large-Span Structures". In: *Proceedings of the World Congress on Civil, Structural, and Environmental Engineering (CSEE'16)*. Prague, Czech Republic, Mar. 2016, ICSENM 124-1–124-23. DOI: 10.11159/icsenm16.124. URL: https://www.researchgate.net/publication/309293735_Timber_Structures_for_Large-Span_Structures.

[17] Delft University of Technology. *IDEMAT 2025 Materials Database (Excel Spreadsheet)*. Downloaded from EcocostsValue.com. Life Cycle Inventory dataset including eco-costs and carbon footprint indicators; spreadsheet format. 2025. URL: https://www.ecocostsvalue.com/data-tools-books/.

[18] Frédéric Dubois et al. "Long-Term Creep Behavior of Timber Columns: Experimental and Numerical Protocols". In: *Engineering Structures* 275 (2023), p. 115283. DOI: 10.1016/j.engstruct.2022.115283. URL: https://doi.org/10.1016/j.engstruct.2022.115283.

[19] C. Eckholm. *Exploration #1: How to Design a Timber Building That Can Reach 35 Stories*. Mar. 2021. URL: https://medium.com/sidewalk-talk/exploration-1-how-to-design-a-timber-building-that-can-reach-35-stories-1c68de983390.

[20] European Committee for Standardization (CEN). *EN 14080: Timber Structures – Glued Laminated Timber and Glued Solid Timber – Requirements*. NEN-EN 14080:2013. Dutch version of EN 14080:2013. Specifies requirements for glued laminated timber and glued solid timber. Nederlands Normalisatie-instituut. Brussels, Belgium: Nederlands Normalisatie-instituut, 2013. URL: https://www.nen.nl.

[21] European Committee for Standardization (CEN). *EN 1990: Eurocode - Basis of Structural and Geotechnical Design*. EN 1990:2025. Published by NEN as Dutch implementation of the European standard. CEN. Brussels, Belgium: Netherlands Standardization Institute (NEN), 2025. URL: https://www.nen.nl/en/nen-en-1990-2025-287162.

[22] European Committee for Standardization (CEN). *EN 338: Structural Timber – Strength Classes*. EN 338:2016. Supersedes EN 338:2009. CEN. Brussels, Belgium: European Committee for Standardization, 2016. URL: https://www.nen.nl/nen-en-338-2016-nl-189753.

[23] Paul Fast. "Case Study: An 18-Storey Tall Mass Timber Hybrid Student Residence at the University of British Columbia". In: *22. Internationales Holzbau-Forum IHF 2016*. Vancouver, Canada: Fast+Epp, 2016, pp. 1–10.

[24] M. Felicita. "Parametric Study of the Influence of Preliminary Design Parameters on the Wind-Induced Dynamic Response of Timber High-Rise Buildings". Master's thesis. Delft, Netherlands: Delft University of Technology, Mar. 2021. URL: http://repository.tudelft.nl/.

[25] Alejandro Fernandez, Jordan Komp, and John Peronto. "Ascent – Challenges and Advances of Tall Mass Timber Construction". In: *International Journal of High-Rise Buildings* 9.3 (2020), pp. 235–244.

[26] Robert M. Foster, Michael H. Ramage, and Thomas P. Reynolds. "Rethinking CTBUH Height Criteria in the Context of Tall Timber". In: *CTBUH Journal* 2017.Issue IV (2017), pp. 28–33.

[27] J.F. de Gaaij. "Multidisciplinary Design Optimization of Timber High-Rise: Research and Development of a Multidisciplinary Design Optimization Tool". Master's thesis. Delft, Netherlands: Delft University of Technology, June 2021. URL: http://repository.tudelft.nl/.

[28] Gelamineerdhoutopmaat.nl. *Vuren kolommen & liggers*. Accessed: 2025-07-04. 2025. URL: https://gelamineerdhoutopmaat.nl/product/vuren-kolommen-liggers/.

[29] GHL Consultants Ltd. *Fire Protection Report: Brock Commons Tall Wood Building*. Tech. rep. Vancouver, Canada: GHL Consultants Ltd., 2016.

[30] Laura E. Hasburgh et al. "Fire Performance of Mass-Timber Encapsulation Methods and the Effect of Encapsulation on Char Rate of Cross-Laminated Timber". In: *CD-ROM Proceedings of the World Conference on Timber Engineering (WCTE 2016)*. Ed. by J. Eberhardsteiner et al. Vienna, Austria: Vienna University of Technology, 2016, –. ISBN: 978-3-903039-00-1. DOI: 10.3301/wcte2016-CHAR. URL: https://www.researchgate.net/publication/311654224_Fire_Performance_of_Mass-Timber_Encapsulation_Methods_and_the_Effect_of_Encapsulation_on_Char_Rate_of_Cross-Laminated_Timber.

[31] J.C. Hoogeweg, R.J.M. van Mierlo, and A.D. Lemaire. *Sprinklerinstallaties en brandwerendheid op bezwijken van staalconstructies*. Definitief Rapport F.2015.0122.00.R001. Arnhem and Bleiswijk, Netherlands: DGMR Bouw B.V. and Efectis Nederland BV, June 28, 2017.

[32] Housing Evolutions. *HoHo Wien - The World's Tallest Wooden High-Rise*. 2024. URL: https://www.housingevolutions.eu/project/hoho-wien-the-worlds-tallest-wooden-high-rise/.

[33] International Organization for Standardization (ISO). *ISO 10137:2007 – Bases for Design of Structures – Serviceability of Buildings and Pedestrian Works of Art*. ISO 10137:2007. Accessed: 2025-05-09. ISO. Geneva, Switzerland: International Organization for Standardization, 2007. URL: https://www.iso.org/standard/40729.html.

[34] Leif Tore Isaksen and Martin Hagen. "Fire Safety Engineering of Buildings with Visible Timber Constructions: Mjøstårnet Case Study". In: *Proceedings of the International Conference on Fire Science and Engineering*. Case study of the tallest timber building in the world. Oslo, Norway, 2019, pp. 223–230. DOI: 10.52202/069179-0223.

[35] F.F. Janssens. "Influence of a Timber Outrigger System on Cross Laminated Timber Core Buildings". Master's thesis. Delft, Netherlands: Delft University of Technology, Mar. 2023. URL: http://repository.tudelft.nl/.

[36] R. van Lierop. "The Opportunities of Supplementary Damping Systems in Dutch High-Rise Buildings". Master's thesis. Delft, Netherlands: Delft University of Technology, Aug. 2021. URL: http://repository.tudelft.nl/.

[37] K. A. Malo, R. B. Abrahamsen, and M. A. Bjertnæs. "Some Structural Design Issues of the 14-Storey Timber Framed Building "Treet" in Norway". In: *European Journal of Wood and Wood Products* 74.3 (2016), pp. 407–424. DOI: 10.1007/s00107-016-1034-7.

[38] Sami S. Matar and William J. Faschan. "A Structural Engineer's Approach to Differential Vertical Shortening in Tall Buildings". In: *International Journal of High-Rise Buildings* 6.1 (2017), pp. 73–82. URL: https://doi.org/10.21022/IJHRB.2017.6.1.73.

[39] H. Meleki et al. "Differential Movements in a Timber Multi-Storey Hybrid Building". In: *Procedia Engineering*. Vol. 14. Presented at the Twelfth East Asia-Pacific Conference on Structural Engineering and Construction. Elsevier, 2011, pp. 1613–1620. DOI: 10.1016/j.proeng.2011.07.203. URL: https://doi.org/10.1016/j.proeng.2011.07.203.

[40] Yoshikazu Minegishi, Ken Matsuyama, et al. "Fire Safety Design of Super Tall Building: Case Study by Team Japan". In: *Proceedings of the 9th International Conference on Performance-Based Codes and Fire Safety Design Methods*. Presented 20–22 June 2012 in Hong Kong. Society of Fire Protection Engineers (SFPE). Hong Kong, China: Curran Associates, Inc., 2012, –.

[41] M. Mohammad et al. "Fire Safety Challenges of Tall Wood Buildings". In: *Case Studies in Fire Safety* 8 (2017), pp. 19–24. DOI: 10.1016/j.csfs.2017.05.001. URL: https://doi.org/10.1016/j.csfs.2017.05.001.

[42] Nederlands Normalisatie-instituut (NEN). *Nationale Bijlage bij NEN-EN 1990:2002+A1:2005+C2:2010 – Eurocode: Grondslagen van het Constructief Ontwerp*. Dutch. NEN-EN 1990+A1+A1/C2/NB:2019. Nationale bijlage bij de Eurocode 1990. Nederlands Normalisatie-instituut. Delft, Netherlands, 2019. URL: https://www.nen.nl.

[43] Government of the Netherlands. *Klimaatakkoord*. Published June 28, 2019. The Hague: Government of the Netherlands, June 2019. URL: https://www.klimaatakkoord.nl.

[44] Netherlands Standardization Institute (NEN). *Eurocode 1: Actions on Structures – Part 1-1: General Actions – Densities, Self-weight, Imposed Loads for Buildings*. NEN-EN 1991-1-1+C1+C11:2019. Dutch version including corrigendum C1 and national annex C11. Nederlands Normalisatie-instituut. Delft, Netherlands, 2019. URL: https://www.nen.nl.

[45] Netherlands Standardization Institute (NEN). *Eurocode 1: Belastingen op Constructies – Deel 1-4: Algemene Belastingen – Windbelastingen*. NEN-EN 1991-1-4+A1+C2:2011. Nederlandse versie inclusief wijziging A1 en correctieblad C2. Nederlands Normalisatie-instituut. Delft, Netherlands, 2011. URL: https://www.nen.nl.

[46] Netherlands Standardization Institute (NEN). *Eurocode 2: Design of Concrete Structures – Part 1-1: General Rules and Rules for Buildings*. NEN-EN 1992-1-1+C2:2011+A1:2015. Supersedes NEN-EN 1992-1-1:2005/A1:2015 and NEN-EN 1992-1-1+C2:2011. Nederlands Normalisatie-instituut. Delft, Netherlands, 2015.

[47] Netherlands Standardization Institute (NEN). *Eurocode 5: Design of Timber Structures – Part 1-1: General – Common Rules and Rules for Buildings*. NEN-EN 1995-1-1+C1+A1. Includes corrigendum C1:2006 and amendment A1:2008. Nederlands Normalisatie-instituut. Delft, Netherlands, 2011.

[48] Netherlands Standardization Institute (NEN). *Eurocode 5: Design of Timber Structures – Part 1-2: Structural Fire Design*. NEN-EN 1995-1-2:2023. Draft publication submitted for comment. Supersedes NEN-EN 1995-1-2:2005 and amendments. Nederlands Normalisatie-instituut. Delft, Netherlands, 2023.

[49] Netherlands Standardization Institute (NEN). *Nationale Bijlage bij NEN-EN 1991-1-4:2011+A1+C2:2011 – Eurocode 1: Windbelastingen voor de Toepassing in Nederland*. Dutch. NEN-EN 1991-1-4:2011+A1+C2:2011/NB:2019+C2:2023. Contains national provisions and additions to the Eurocode for wind actions. Nederlands Normalisatie-instituut. Delft, Netherlands, 2023. URL: https://www.nen.nl.

[50] Birgit Östman, Daniel Brandon, and Håkan Frantzich. "Fire Safety Engineering in Timber Buildings". In: *Fire Safety Journal* 91 (2017), pp. 11–20. DOI: 10.1016/j.firesaf.2017.03.001.

[51] Michael Ramage et al. "Super Tall Timber: Design Research for the Next Generation of Natural Structure". In: *The Journal of Architecture* 22.3 (2017), pp. 386–407. DOI: 10.1080/13602365.2017.1329829.

[52] A. van Rhijn. "Possibilities of Timber High-Rise: A Parametric Study on the Possibilities of Timber High-Rise in the Netherlands". Master's thesis. Delft, Netherlands: Delft University of Technology, Mar. 2020. URL: http://repository.tudelft.nl/.

[53] Royal Netherlands Meteorological Institute (KNMI). *Vochtigheid*. Accessed: 2025-05-02. 2025. URL: https://www.knmi.nl/kennis-en-datacentrum/uitleg/vochtigheid.

[54] Daniel Safarik, Jake Elbrecht, and Will Miranda. "State of Tall Timber 2022". In: *CTBUH Journal* 2022.Issue I (2022), pp. 12–19.

[55] Jeff Sanner et al. "River Beech Tower: A Tall Timber Experiment". In: *CTBUH Journal* 2017.Issue II (2017), pp. 40–46.

[56] E.C. Slooten. "Feasibility Study of a Wood-Concrete Hybrid Super Tall Building and Optimization of Its Wind-Induced Behaviour". Master's thesis. Delft, Netherlands: Delft University of Technology, Sept. 2018. URL: http://repository.tudelft.nl/.

[57] Pascal Steenbakkers et al. "Reaching New Heights in Timber-Hybrid Design: Designing the Netherlands' Tallest Timber-Hybrid Residential Building". In: *International Journal of High-Rise Buildings* 13.2 (2024), pp. 195–204.

[58] Studiengemeinschaft Holzleimbau. *Umweltdeklaration BS-Holz*. Tech. rep. Accessed: 2025-06-18. Studiengemeinschaft Holzleimbau, 2018. URL: https://www.studiengemeinschaft-holzleimbau.de/publish/binarydata/pdfs/2018/stghb_umweltdeklaration_bs-holz_2018_ihb_e_print_181109.pdf.

[59] Team V Architecture. *Haut Amsterdam Residential Building*. 2022. URL: https://www.archdaily.com/989552/haut-amsterdam-residential-building-team-v-architecture.

[60] The Skyscraper Center. *Ascent*. 2022. URL: https://www.skyscrapercenter.com/building/ascent/34292.

[61] The Skyscraper Center. *Mjøstårnet*. 2019. URL: https://www.skyscrapercenter.com/building/mjostarnet/26866.

[62] ThinkWood. *Ascent: Tallest Mass Timber Construction Project*. n.d. URL: https://www.thinkwood.com/construction-projects/ascent.

[63] United Nations Environment Programme. *2022 Global Status Report for Buildings and Construction: Towards a Zero emission, Efficient and Resilient Buildings and Construction Sector*. Retrieved from www.globalabc.org. Nairobi: United Nations Environment Programme, 2022.

[64] Rob Verhaegh, Mathew Vola, and Jorn de Jong. "Haut – A 21-Storey Tall Timber Residential Building". In: *International Journal of High-Rise Buildings* 9.3 (2020), pp. 213–220.

[65] Voll Arkitekter. *Mjøstårnet: The Tower of Lake Mjøsa*. 2020. URL: https://www.archdaily.com/934374/mjostarnet-the-tower-of-lake-mjosa-voll-arkitekter.

[66] O. Willebrands. "Differential Vertical Shortening in Timber-Concrete High-Rise Structures". Master's thesis. Delft, Netherlands: Delft University of Technology, Nov. 2017. URL: http://repository.tudelft.nl/.

[67] Henk Wind. *HAUT: De uitdagingen van hoogbouw in hout*. 2025. URL: https://www.jpvaneesteren.nl/nieuws/haut-de-uitdagingen-van-hoogbouw-hout.

[68] Antony Wood et al. "HoHo Wien: Construction of the Tallest Timber Structure in Austria". In: *International Journal of High-Rise Buildings* 13.2 (2024), pp. 177–186.

[69] Wood Solutions. *HoHo Wien: The World's Tallest Timber Building*. 2024. URL: https://www.youtube.com/watch?v=rGOlr37uhbw&t=965s&ab_channel=WoodSolutions.

[70] Richard Woschitz. "Holzhochhaus HoHo Wien: The Technical Solution". In: *21. Internationales Holzbau-Forum IHF 2015*. Garmisch-Partenkirchen, Germany, 2015.

[71] T. Znabei. "A Post-tensioned Cross-Laminated Timber Core for Buildings". Master's thesis. Delft, Netherlands: Delft University of Technology, Sept. 2020. URL: http://repository.tudelft.nl/.

Appendices

Appendix A

Wind Loads

A.1 Extreme Wind Pressure Table

Table A.1: Extreme wind pressure in kN/m^2 as a function of height for Zone II [49]

Height [m]	Coastal	Rural	Urban
1	0.78	0.60	0.58
2	0.93	0.60	0.58
3	1.02	0.60	0.58
4	1.09	0.60	0.58
5	1.14	0.66	0.58
6	1.19	0.71	0.58
7	1.23	0.75	0.58
8	1.26	0.79	0.62
9	1.29	0.82	0.65
10	1.32	0.85	0.68
15	1.43	0.98	0.80
20	1.51	1.07	0.90
25	1.57	1.14	0.97
30	1.63	1.20	1.03
35	1.67	1.25	1.09
40	1.71	1.30	1.13
45	1.75	1.34	1.17
50	1.78	1.38	1.21
60	1.81	1.42	1.25
70	1.83	1.45	1.28
80	1.86	1.48	1.31
90	1.88	1.50	1.34
100	1.90	1.53	1.37
110	1.92	1.55	1.39
120	1.94	1.58	1.42
130	1.96	1.60	1.44
140	1.98	1.62	1.46
150	1.99	1.64	1.48
160	2.03	1.68	1.52
170	2.05	1.71	1.55
180	2.08	1.74	1.59
190	2.10	1.77	1.62
200	2.13	1.80	1.65
225	2.15	1.83	1.67
250	2.17	1.85	1.70
275	2.19	1.88	1.72
300	2.20	1.90	1.75

A.2 Structural Factor

The Structural Factor $c_s c_d$ can be determined according to equation A.1

$$c_s c_d = \frac{1 + 2 \cdot k_p \cdot I_v(z_s) \cdot \sqrt{B^2 + R^2}}{1 + 7 \cdot I_v(z_s)} \tag{A.1}$$

Where:

- z_s is the reference height for determining the structural factor ($= 0.6 \cdot h$ for vertical structures such as buildings)
- k_p is the peak factor defined as the ratio of the maximum value of the fluctuating part of the response to its standard deviation, as found in A.2.
- B^2 is the background response factor, allowing for the lack of full correlation of the pressure on the structure surface, as found in A.4.
- R^2 is the resonance response factor, allowing for turbulence in resonance with the vibration mode as found in A.5.

Annexes B and C of the Eurocode provide two different methods for determining the parameters B^2 and R^2. According to the Dutch National Annex [49], Annex C is to be considered normative.

$$k_p = \sqrt{2 \cdot \ln(\nu \cdot T)} + \frac{0.6}{\sqrt{2 \cdot \ln(\nu \cdot T)}} \geq 3 \tag{A.2}$$

Where:

- ν is the frequency in a gust as given, as found in A.3.
- T is the averaging time of the reference wind speed, with $T = 600$ seconds.

$$\nu = n_{1,x} \sqrt{\frac{R^2}{B^2 + R^2}} \geq 0.08\, Hz \tag{A.3}$$

The value for $n_{1,x}$ is stated in section 2.4. Subsequently, the background response factor B^2 and the resonance response factor R^2 are presented in Equations A.4 and A.5, respectively.

$$B^2 = \frac{1}{1 + \frac{3}{2} \cdot \left(\left(\frac{b}{L(z_s)} \right)^2 + \left(\frac{h}{L(z_s)} \right)^2 + \left(\frac{b}{L(z_s)} \cdot \frac{h}{L(z_s)} \right)^2 \right)} \tag{A.4}$$

$$R^2 = \frac{\pi^2}{2 \cdot \delta} \cdot S_L(z_s, n_{1,x}) \cdot K_s(n_{1,x}) \tag{A.5}$$

Where:

- b, h are the width and height of the structure.
- $L(z_s)$ is the turbulence length scale defined A.6 at height z_s.
- S_L is the distribution of wind speed over frequencies, stated as a dimensionless spectral density function, defined in A.7.
- K_s is the size reduction function, defined in Equation A.9.
- δ is the logarithmic decrement of total damping, given in A.12.

$$L(z) = \begin{cases} L_t \cdot \left(\frac{z}{z_t}\right)^{\alpha} & \text{for } z \geq z_{\min} \\ L(z_{\min}) & \text{for } z < z_{\min} \end{cases} \tag{A.6}$$

Where:

- L_t is the reference length scale, with $L_t = 300$ meters.
- z_t is the reference height, with $z_t = 200$ meters.
- α is an empirical exponent that describes the vertical variation of the turbulence length, given as $0.67 + 0.05 \cdot \ln(z_0)$.

$$S_L(z, n) = \frac{6.8 \cdot f_L(z, n)}{(1 + 10.2 \cdot f_L(z, n))^{5/3}} \tag{A.7}$$

$$f_L(z, n) = \frac{n_{1,x} \cdot L(z)}{v_m(z)} \tag{A.8}$$

Where:

- $f_L(z, n)$ is the dimensionless frequency

$$K_s(n) = \frac{1}{\sqrt{1 + (G_y \cdot \phi_y)^2 + (G_z \cdot \phi_z)^2 + \left(\frac{2}{\pi} \cdot G_y \cdot \phi_y \cdot G_z \cdot \phi_z\right)^2}} \tag{A.9}$$

$$\phi_y = \frac{c_y \cdot b \cdot n}{v_m(z_s)} \tag{A.10}$$

$$\phi_z = \frac{c_z \cdot h \cdot n}{v_m(z_s)} \tag{A.11}$$

Where:

- G_y and G_z are constants that depend on the variation of the mode shape along the horizontal y-axis and the vertical z-axis, respectively, for high-rise buildings, $G_y = 1/2$ (Uniform) and $G_z = 3/8$ (Linear).
- c_y and c_z are decay constants, both equal to 11.5.

$$\delta = \delta_s + \delta_a + \delta_d \tag{A.12}$$

Where:

- δ_s is the logarithmic decrement of structural damping ($= 0.1125$ [1] [24])
- δ_a is the logarithmic decrement of aerodynamic damping for the fundamental mode of vibration, as found in Equation A.13.
- δ_d is the logarithmic decrement of damping due to special devices, such as tuned mass dampers, water tanks ($= 1.0$ for structures with no special devices).

$$\delta_a = \frac{c_f \cdot \rho \cdot b \cdot v_m(z_s)}{2 \cdot n_1 \cdot m_e} \tag{A.13}$$

Where:

- m_e is the equivalent mass of the fundamental mode of vibration, which can be approximated by the average value of m of the upper third part of the construction.

Appendix B

Connections

B.1 Connection Design in the Eurocode

The method for calculating the capacity of timber connections is defined in Eurocode 5 [47]. This capacity depends on the following factors:

- the method used to design the connection
- the type of fasteners (bolts, screws, dowels)
- the material of the fasteners (wood or steel)
- the thickness of the plates and their material

Figure B.1 shows the design of the connection to be calculated, as it is relevant to this research. Thin steel plates (located between the timber element) and steel bolts are used in the connection.

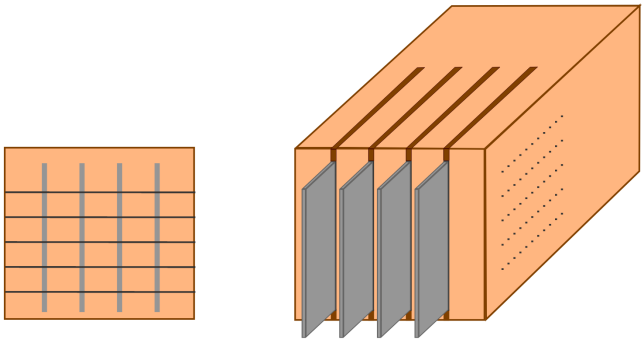

Figure B.1: Connection design choices that are relevant to this research

B.1.1 Failure Mechanisms and Rotational Stiffness

First, the characteristic strength per bolt per shear plane is calculated based on various failure mechanisms. The weakest failure mechanism will be the governing one, which depends on the size of the different parameters. Figure B.2 shows the failure mechanisms that are relevant to this research.

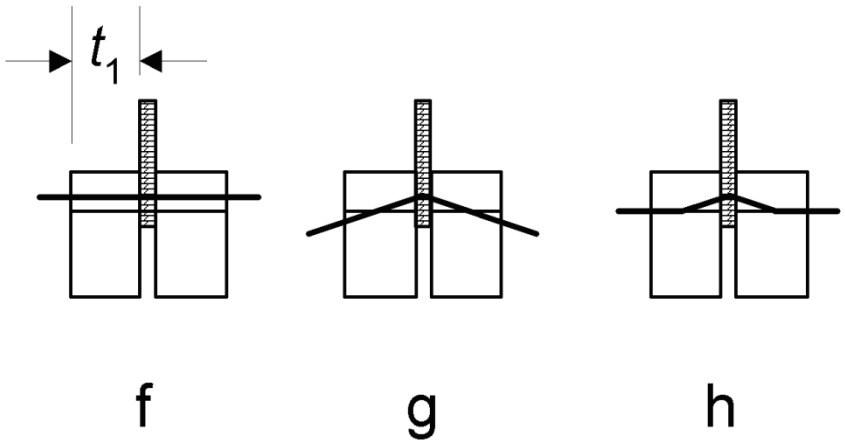

Figure B.2: Relevant Failure mechanisms for slotted-in steel plate connections

The characteristic strength per bolt per shear plane can then be calculated using Equation B.1.

$$F_{v,Rk} = \min \begin{cases} f_{h,1,k} t_1 d & \text{(f)} \\ f_{h,1,k} t_1 d \left[\sqrt{2 + \dfrac{4 M_{y,Rk}}{f_{h,1,k} d t_1^2}} - 1 \right] + \dfrac{F_{ax,Rk}}{4} & \text{(g)} \\ 2.3 \sqrt{M_{y,Rk} f_{h,1,k} d} + \dfrac{F_{ax,Rk}}{4} & \text{(h)} \end{cases} \tag{B.1}$$

Where:

- $F_{v,Rk}$ is the characteristic strength per shear plane per bolt
- $f_{h,k}$ is the characteristic shear strength in the timber element
- t_1 is the smallest value of the timber thickness of the element at the edge or the bonding length
- d is the diameter of the bolt
- $M_{y,Rk}$ is the characteristic yielding moment of the connecting medium

$M_{y,Rk}$ can be determined with Equation B.2.

$$M_{y,Rk} = 0.3 f_u d^{2.6} \tag{B.2}$$

$$f_{h,k} = 0.082(1 - 0.1d)\rho_k \tag{B.3}$$

Where:

- f_u is the tension strength of the steel bolts
- ρ_k is the characteristic density of the timber (in kg/m)

In addition to the characteristic strength, the corresponding rotational stiffness can also be calculated for the same connection. When a moment is applied to the connection, the geometric center of the bolts will act as the central rotation point. The bolts in the connection provide moment capacity, and this capacity depends, in addition to the properties of the bolts themselves, on the distance between the central rotation point and the bolts. The rotational stiffness, $K_{r,ser}$ is determined by the slip modulus, K_{ser}, of an individual bolt per shear plane and the sum of squared distances of the bolts to the central rotation point. Figure B.3 illustrates how the sum of the squared distances to the rotation point can be determined.

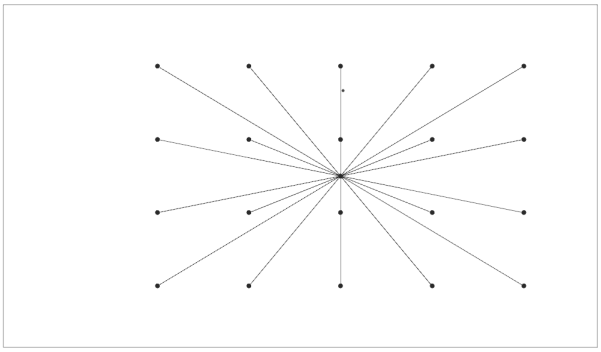

Figure B.3: Sum of squared distanced between bolts and rotation center

$$Kser = \rho_m^{1.5} \cdot \frac{d}{23} \tag{B.4}$$

$$K_{r,ser} = K_{ser} \cdot \sum r^2 \tag{B.5}$$

Where:

- K_{ser} is the slip modulus, (in N/mm)
- $K_{r,ser}$ is the rotational stiffness per shear plane (in Nmm/rad)
- ρ_m is the mean density of the timber (in kg/m^3)
- d is the dimension of the connection (in mm)
- $\sum r^2$ is the sum of the squared distances between bolts and rotation center (in mm)

The rotational stiffness per shear plane is determined from equation B.5. This value must first be multiplied by 2 (since there are two shear planes per steel plate) and then by the number of steel plates in the connection (this number depends on the dimensions of the element to be connected). Since a steel-to-timber connection will be used, the K_{ser} in Equation B.4 can be multiplied by 2.

B.1.2 Block Shear Capacity

In addition to the translational capacity, the connection should also be checked for block shear. Block shear is a failure mechanism where the bolts form a block, and the surrounding timber element fails under tension or shear. This failure mechanism occurs only in elements with a tensile force component parallel to the grain direction and is calculated according to Annex A of Eurocode 5 [47]. The element can fail in two ways: either under tension in the direction perpendicular to the grain or under shear in the sections parallel to the grain direction. Figure B.4 illustrates how this failure mechanism manifests and shows the corresponding net lengths over which the failure occurs.

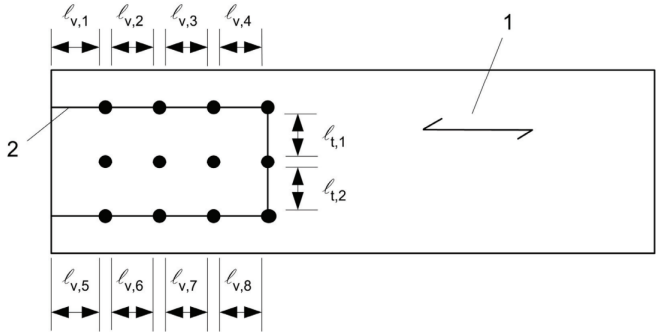

Figure B.4: Schematization of the block shear failure mode with netto failure lengths, as found in Annex A of Eurocode 5 [47]

The block shear capacity can then be calculated as follows.

$$F_{\text{bs,Rk}} = \max \begin{cases} 1.5 A_{\text{net},f} f_{t,0,k} \\ 0.7 A_{\text{net},v} f_{v,k} \end{cases} \tag{B.6}$$

$$A_{\text{net},t} = L_{\text{net},t} t_1 \tag{B.7}$$

$$A_{\text{net},v} = \begin{cases} L_{\text{net},v} t_1 & \text{for failure mechanisms (c, f, j/l, k, m)} \\ \dfrac{L_{\text{net},v}}{2} \left(L_{\text{net},t} + 2 t_{\text{ef}} \right) & \text{for all other failure mechanisms} \end{cases} \tag{B.8}$$

$$L_{\text{net},v} = \sum_i \ell_{v,i} \tag{B.9}$$

$$L_{\text{net},t} = \sum_i \ell_{t,i} \tag{B.10}$$

Where:

- $A_{net,t}$ is the net cross-sectional area perpendicular to the grain direction
- $A_{net,v}$ is the net shear surface parallel to the grain direction
- $L_{net,t}$ is the net width of the cross-section perpendicular to the grain direction
- $L_{net,v}$ is the total net length of the shear surface at failure

Since thin steel plates are used for this study, the only failure mechanism that can occur specifically for block shear is failure mechanism (f).

B.1.3 Minimum Bolt Distances

The number of bolts that can be placed in a connection depends on the minimum distance that bolts must have from each other. These minimum distances are defined in the Eurocode. In this table, α represents the angle between the force and the grain direction, which generally equals $90°$ for beams and $0°$ for truss elements.

Table B.1: Spacing and end/edge distances

Spacing and end/edge distances	**Angle**	**Minimum spacing or distance**
a_1 (parallel to grain)	$0° \leq \alpha \leq 360°$	$(4 + \lvert\cos\alpha\rvert)d$
a_2 (perpendicular to grain)	$0° \leq \alpha \leq 360°$	$4d$
$a_{3,t}$ (loaded end)	$-90° \leq \alpha \leq 90°$	$\max(7d, 80mm)$
$a_{3,c}$ (unloaded end)	$90° \leq \alpha \leq 150°$	$(1 + 6\sin\alpha)d$
	$150° \leq \alpha \leq 210°$	$4d$
	$210° \leq \alpha \leq 270°$	$(1 + 6\lvert\sin\alpha\rvert)d$
$a_{4,t}$ (loaded edge)	$0° \leq \alpha \leq 180°$	$\max([(2 + \sin\alpha)d, 3d])$
$a_{4,c}$ (unloaded edge)	$180° \leq \alpha \leq 360°$	$3d$

In addition to the minimum bolt distances, the reduction of the effective number of bolts working in a row parallel to the grain direction must also be considered. The number of effective working bolts is denoted as n_{ef} and is given by Equation B.11.

$$n_{\text{ef}} = \min \begin{cases} n \\ n^{0.9}\sqrt[4]{\frac{a_1}{13d}} \end{cases} \tag{B.11}$$

B.1.4 Conversion from Characteristic to Design Values

Based on the design principles, the capacity of a slotted-in steel plate timber connection can be calculated. However, this represents the characteristic value, which must subsequently be transformed into a design value. This procedure is described in Eurocode 5 [47] and is carried out in the following manner.

$$X_d = k_{\text{mod}} \frac{X_k}{\gamma_M} \tag{B.12}$$

Where:

- X_k is the characteristic value of the strength property
- γ_M is the partial factor for a material property ($= 1.25$ for laminated timber)
- k_{mod} is a modification factor that accounts for the effect of load duration and moisture content ($= 0.6$ see Table F.2 of Appendix F).

To determine the rotational stiffness, the slip modulus K_{ser} must be reduced in two ways. First, for the ULS calculation, the value of K_{ser} must be multiplied by a factor of $2/3$. Second, for permanent loads, the factor k_{def}, which accounts for time-dependent deformations, must be incorporated to obtain the design stiffness. This principle is elaborated in Section C.2, from which Equation B.13 can be derived. In this equation, $\psi_2 = 1$ if the quasi-permanent value of the load that accounts for the highest stress is a permanent load. For this research, to reduce the complexity of the model, the conservative assumption is used that this is always the case.

$$K_{\text{ser,fin}} = \frac{K_{\text{ser}}}{(1 + \psi_2 \, k_{\text{def}})} = \frac{K_{\text{ser}}}{(1 + 1 \cdot (2 \cdot 0.8))} \approx K_{\text{ser}} \cdot 0.384 \tag{B.13}$$

B.2 Optimization of Slotted-in Steel Plate Connection Parameters

B.2.1 Glulam Type

As a first step, the effect of the timber type on the strength and stiffness of slotted-in steel plate connections is analyzed. This influence is assessed by plotting the element size on the x-axis against the corresponding connection strength and rotational stiffness on the y-axis. All other parameters that are held constant are arbitrarily realistically chosen values to isolate the effect of the timber type. The resulting plot is generated for various Glulam types, allowing visual comparison of differences in capacity between them.

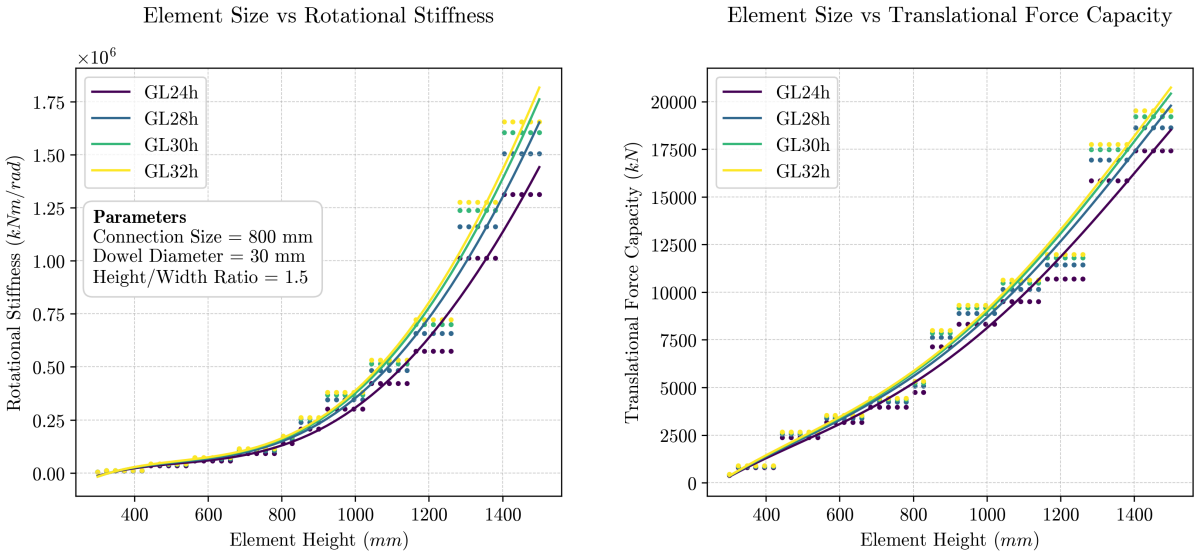

Figure B.5: The influence of the Glulam Type on the capacity of a timber connection with set parameters

For the generation of this plot, the connection size was set to 800 mm, the dowel diameter to 30 mm, and the height-to-width ratio to 1.5. From Figure B.5, it can be observed that the type of Glulam used does affect the connection capacity, although this influence remains limited. This implies that no significant differences in capacity are expected between different Glulam types under otherwise identical conditions. For the investigation of the influence of the other variables, type GL28h is applied.

B.2.2 Height/Width Ratio

The next variable that is analyzed is the influence of the height-to-width ratio on the strength and stiffness of the connection. Naturally, when the elements height is kept constant, higher capacities can be expected at lower height-to-width ratios. This is due to the increased available width, resulting in a larger cross-sectional area that can accommodate more steel plates. To account for this effect in the analysis, the x-axis displays the total cross-sectional area of the element. This area can be calculated usingEquation B.14. When this area is plotted against the strength and stiffness on the y-axis, the influence of the height-to-width ratio can be directly observed. This plot is displayed in Figure B.6.

$$\text{Area} = \frac{\text{Element Height}^2}{\text{Height/Width Ratio}} \tag{B.14}$$

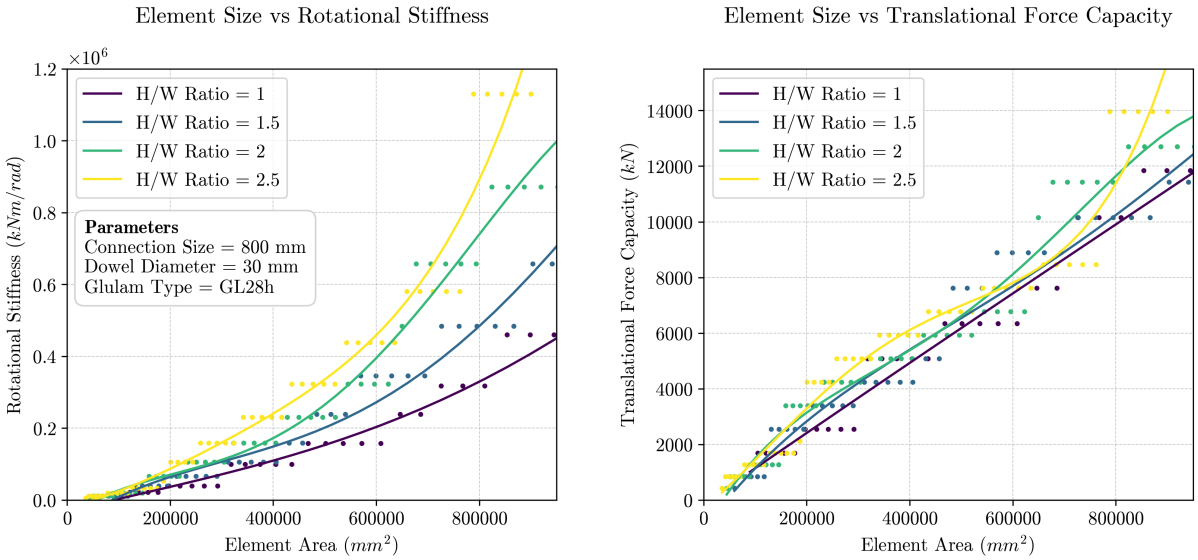

Figure B.6: The influence of the Height to Width Ratio on the capacity of a timber connection with set parameters

First, the figure on the right shows that the translational capacity remains approximately constant across the different height-to-width ratios. This suggests that this parameter does not have a significant influence on the capacity of a connection. The second observation is the influence of the height-to-width ratio on the rotational stiffness. A logical explanation is that elements with a higher height-to-width ratio need a greater height to have the same cross-sectional area. This means that the steel plates in the element will also be larger, and therefore the distances between the dowels and the central rotation point will be greater. Since the increased rotational stiffness is directly related to a greater element height, the choice of height-to-width ratio in the design will depend more on architectural and other requirements than on the efficiency of the connection. For the investigation of the influence of the remainder variables, a height-to-width ratio of 1.5 is applied.

B.2.3 Dowel Diameter

The next parameter being investigated is the dowel diameter. This parameter appears in the calculation for both the translational capacity and the rotational stiffness. Additionally, the dowel diameter is an important parameter in determining the minimum distance between the dowels. These minimum distances can be found in section 2.3. The minimum steel plate distance is not specifically defined in the Eurocode, but for this research, a plate distance of $7d$ is used, and the distance between a plate and the edge of the element is set to $0.125 \cdot$ Width. As mentioned earlier, these distances are highly relevant for the number of dowels that can be placed in the element, while the both the strength and stiffness of the connection are calculated per dowel per shear plane. This number is then summed or multiplied for the number of dowels and shear planes. This parameter will thereby have a significant influence on the strength and stiffness of the connection. This influence is shown in Figure B.7. In this plot, the element size is plotted on the x-axis for different dowel diameters, with the strength and stiffness of the connection shown on the y-axis.

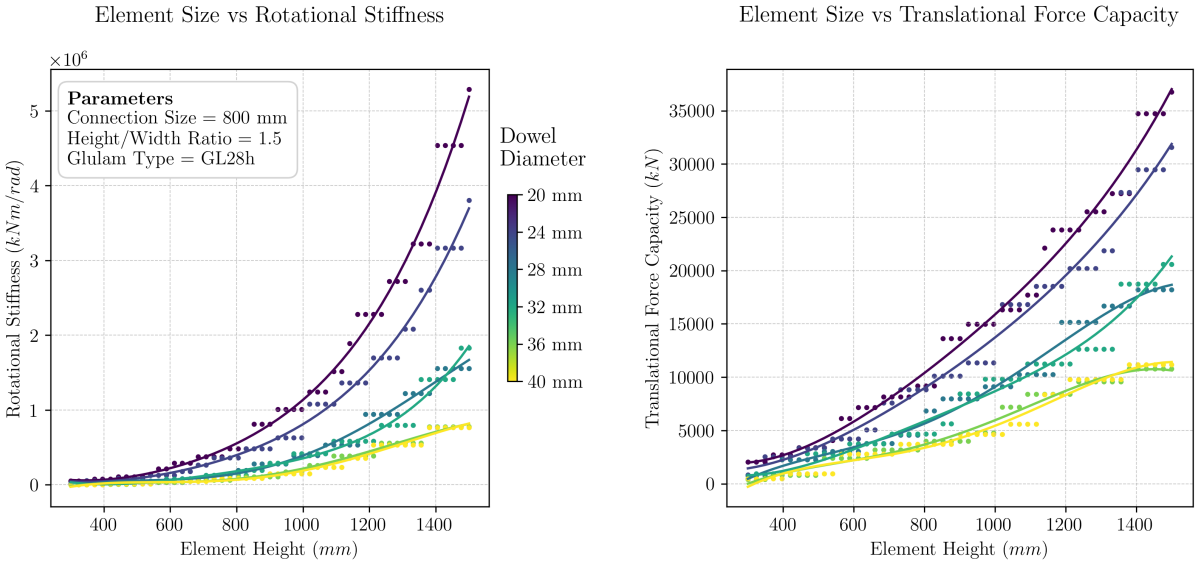

Figure B.7: The influence of the dowel diameter on the capacity of a timber connection with set parameters

From the figure, it can be concluded that, as previously assumed, the dowel diameter has a significant influence on both the strength and stiffness of the connection. The graph shows that smaller dowels result in higher stiffness and capacity. This is due to the fact that many more dowels can be placed in an element with the same dimensions. It can also be observed from the figure that, with smaller diameters, the increase in capacity is greater. For example, the differences in connection stiffness between diameters in the range of 28 to 40 mm are smaller than those of 20 or 24 mm. However, there are some disadvantages to using smaller dowel diameters. These mainly include the increased complexity of the connection. As a result of this complexity, both the assembly time and cost of the connection will increase. Additionally, the weight of the connection will increase due to the increased use of more steel plates and dowels. This results in higher loads on the structure, which brings additional disadvantages. For these reasons, a dowel diameter of 24 mm is assumed for this research.

B.2.4 Multivariate Polynomial Regression Curves

$$K_{r,ser,fitted}(c,h) = \sum_{i=0}^{4} \sum_{j=0}^{4-i} k_{ij}\, c^i\, h^j, \quad \{(c,h) \mid c \in (400, 2000),\ h \in (300, 1500)\} \tag{B.15}$$

Table B.2: Coefficients k_{ij} in Equation B.15

$j \backslash i$	0	1	2	3	4
0	$7.095 \cdot 10^{5}$	$-3.302 \cdot 10^{1}$	-1.302	$1.225 \cdot 10^{-3}$	$-3.264 \cdot 10^{-7}$
1	$-4.612 \cdot 10^{3}$	5.090	$-3.181 \cdot 10^{-3}$	$8.413 \cdot 10^{-7}$	
2	7.015	$-3.811 \cdot 10^{-3}$	$9.781 \cdot 10^{-7}$		
3	$-4.933 \cdot 10^{-3}$	$1.385 \cdot 10^{-6}$			
4	$1.258 \cdot 10^{-6}$				

$$F_{v,Rk,fitted}(c,h) = \sum_{i=0}^{4} \sum_{j=0}^{4-i} f_{ij}\, c^i\, h^j, \quad \{(c,h) \mid c \in (400, 2000),\ h \in (300, 1500)\} \tag{B.16}$$

Table B.3: Coefficients f_{ij} in Equation B.16

$j \backslash i$	0	1	2	3	4
0	$6.719 \cdot 10^{2}$	$1.522 \cdot 10^{1}$	$-2.764 \cdot 10^{-2}$	$1.811 \cdot 10^{-5}$	$-4.017 \cdot 10^{-9}$
1	$-2.499 \cdot 10^{1}$	$1.779 \cdot 10^{-2}$	$-1.110 \cdot 10^{-5}$	$3.090 \cdot 10^{-9}$	
2	$3.926 \cdot 10^{-2}$	$2.292 \cdot 10^{-6}$	$-3.100 \cdot 10^{-10}$		
3	$-3.209 \cdot 10^{-5}$	$3.221 \cdot 10^{-9}$			
4	$8.763 \cdot 10^{-9}$				

$$V_{fitted}(c,h) = \sum_{i=0}^{4} \sum_{j=0}^{4-i} v_{ij}\, c^i\, h^j, \quad \{(c,h) \mid c \in (400, 2000),\ h \in (300, 1500)\} \tag{B.17}$$

Table B.4: Coefficients v_{ij} in Equation B.17

$j \backslash i$	0	1	2	3	4
0	$5.134 \cdot 10^{-3}$	$5.110 \cdot 10^{-5}$	$-9.257 \cdot 10^{-8}$	$5.935 \cdot 10^{-11}$	$-1.295 \cdot 10^{-14}$
1	$-9.903 \cdot 10^{-5}$	$4.443 \cdot 10^{-8}$	$-2.525 \cdot 10^{-11}$	$6.975 \cdot 10^{-15}$	
2	$1.691 \cdot 10^{-7}$	$3.193 \cdot 10^{-11}$	$1.405 \cdot 10^{-15}$		
3	$-1.384 \cdot 10^{-10}$	$1.225 \cdot 10^{-14}$			
4	$3.808 \cdot 10^{-14}$				

In which:

- c is the connection size (length of connection in mm)
- h is the element height (given a height/width ratio of 1.5, in mm)

Appendix C

Time-Dependent Deformations

C.1 Time-Dependent Strains For Concrete Elements

For concrete, two time-dependent types of deformation must be considered separately: creep and shrinkage. Creep is a time-dependent strain that occurs when a particular element is subjected to a sustained load. According to Eurocode 2 (for concrete), creep is influenced by the degree of hardening of the concrete at the time the load is first applied and depends on the duration and magnitude of this load [46]. This can be calculated according to section 3.1.4 of Eurocode 2. It states that the additional strain resulting from creep under a compressive stress smaller than $0.45 f_{ck}$ is given by equation C.1.

$$\varepsilon_{\mathrm{cc}}(\infty, t_0) = \varphi(\infty, t_0) \cdot \left(\frac{\sigma_c}{E_c} \right) \tag{C.1}$$

Here, σ_c represents the applied stress and E_c denotes the relevant Young's modulus, which can be found in Figure F.1 of Appendix F. $\varphi(\infty, t_0)$ indicates the creep coefficient based on a duration approaching infinity. The coefficient is multiplied by the elastic strain $\varepsilon = (\frac{\sigma_c}{E_c})$, thereby increasing it. The value of $\varphi(\infty, t_0)$ lies between 1 to 7 and depends on the following parameters:

- the relative humidity (RH)
- the hardening rate class of the cement type used ($R,\ N$ or S)
- the strength class of the concrete
- the age in days of the concrete at the time of loading (t_0)
- the notional size A_c/u, where A_c is the concrete cross-section and u is the perimeter where the concrete is exposed to drying

Based on these variables, the creep factor can be derived from the graphs in Figure C.1.

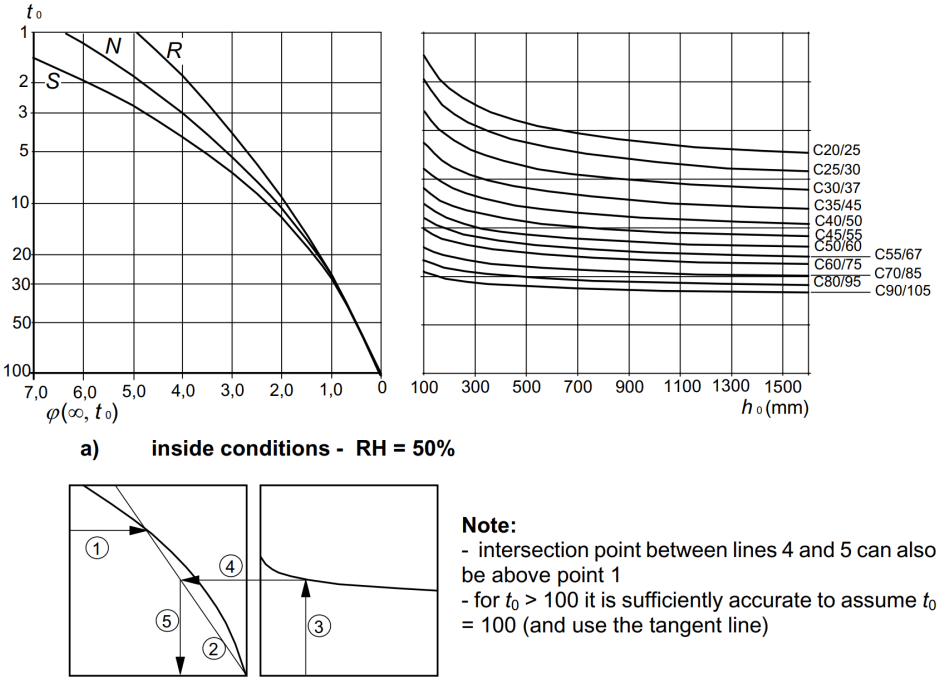

Figure C.1: Determination of creep factor $\varphi(\infty, t_0)$ with a RH of 50% [46]

It can be inferred from the graph that t_0 is plotted on a logarithmic scale. This means that the influence of t_0 on the creep factor $\varphi(\infty, t_0)$ indicates a decreasing positive exponential relation. Additionally, it is evident that the concrete strength class also has a significant influence on the creep factor.

For higher stresses, closer to the capacity of the concrete, a nonlinear creep factor must be taken into account, denoted as $\varphi_k(\infty, t_0)$, which is given by equation C.2.

$$\varphi_k(\infty, t_0) = \varphi(\infty, t_0) \cdot e^{1.5(k_\sigma - 0.45)} \tag{C.2}$$

In this equation, k_σ represents the stress-strength ratio $\sigma_c / f_{cm}(t_0)$, where σ_c is the compressive stress and $f_{cm}(t_0)$ is the mean concrete compressive strength at the time of loading. This latter factor is crucial, as the age of the concrete at the time of the first load application has a significant influence on its strength and time-dependent deformation.

In addition to creep, the displacement due to shrinkage must also be calculated. Shrinkage consists of two components: the first is drying shrinkage strain, which is a function of the migration of water through the hardened concrete and therefore develops slowly. The second component is autogenous shrinkage strain, which is a linear function of the concrete strength. This component develops during the hardening of the concrete, with the most significant part occurring in the first days after pouring [46]. The total strain due to shrinkage is determined according to equation C.3.

$$\varepsilon_{\text{cs}} = \varepsilon_{\text{cd}} + \varepsilon_{\text{ca}} \tag{C.3}$$

Where:

- ε_{cs} is the total shrinkage strain
- ε_{cd} is the drying shrinkage strain
- ε_{ca} is the autogenous shrinkage strain

The exact method of calculating ε_{cs} is extensively outlined in section 3.1.4 of EN-1992.

C.2 Time-Dependent Strains For Timber Elements

Due to the organic and thus orthotropic nature of timber (see section 2.2), the development of calculation methods has become more complicated. As a result, Eurocode 5 uses a specific factor that accounts for the effects of both creep and shrinkage [47]. This factor is based on rheological models combined with empirical research [18]. The total displacement of timber elements, including time-dependent factors, is referred to as u_{fin} in Eurocode 5 and is determined in the following manner.

$$u_{\text{fin}} = u_{\text{fin},G} + u_{\text{fin},Q} + u_{\text{fin},Q} \tag{C.4}$$

Where:

For a permanent action, G:

$$u_{\text{fin},G} = u_{\text{inst},G}\,(1 + k_{\text{def}}) \tag{C.5}$$

For the leading variable action, Q_1:

$$u_{\text{fin},Q_1} = u_{\text{inst},Q_1}\,(1 + \psi_{2,1} k_{\text{def}}) \tag{C.6}$$

For accompanying variable actions, Q_i $(i > 1)$:

$$u_{\text{fin},Q_i} = u_{\text{inst},Q_i}\,(\psi_{0,i} + \psi_{2,i} k_{\text{def}}) \tag{C.7}$$

And:

- $u_{\text{inst},G}$, u_{inst,Q_1}, and u_{inst,Q_i} are the instantaneous deformations for action G, Q_1, and Q_i, respectively;
- $\psi_{2,1}$, $\psi_{2,i}$ are the factors for the quasi-permanent value of variable actions (EN-1990 [21]);
- $\psi_{0,i}$ are the factors for the combination value of variable actions (EN-1990 [21]);
- k_{def} is displayed in Table C.1

Table C.1: Service classes and corresponding k_{def} values for glued laminated timber

Service Class	**RH** (exceeded only a few weeks per year)	$\boldsymbol{k}_{\text{def}}$
Class 1	$< 65\%$	0.60
Class 2	$< 85\%$	0.80
Class 3	$> 85\%$	2.00

For buildings in an indoor climate in the Netherlands, it can be assumed that the relative humidity averages between 60% and 70% [53]. Therefore, service class 2 can be used. For connections between two timber elements with the same time-dependent properties, the k_{def} value for determining the stiffness of the connection must be doubled.

The applied shear, slip, and elasticity moduli are also influenced by the k_{def} factor. This is done according to Table C.2.

Table C.2: Adjusted Modulus of Elasticity, Shear Modulus, and Slip Modulus for SLS and ULS (EN-1995 2.3.2.2, [47])

Symbol	**SLS**	**ULS**
$E_{\text{mean,fin}}$	$\frac{E_{\text{mean}}}{(1+k_{\text{def}})}$	$\frac{E_{\text{mean}}}{(1+\psi_2 k_{\text{def}})}$
$G_{\text{mean,fin}}$	$\frac{G_{\text{mean}}}{(1+k_{\text{def}})}$	$\frac{G_{\text{mean}}}{(1+\psi_2 k_{\text{def}})}$
$K_{\text{ser,fin}}$	$\frac{K_{\text{ser}}}{(1+k_{\text{def}})}$	$\frac{K_{\text{ser}}}{(1+\psi_2 k_{\text{def}})}$

The ψ factors can be found in EN-1990, they are displayed in Table C.3 for buildings with either office or residential function.

Table C.3: $\boldsymbol{\psi}$ for buildings with residential or office function

Action	$\boldsymbol{\psi_0}$	$\boldsymbol{\psi_1}$	$\boldsymbol{\psi_2}$
Category A: domestic, residential areas	0.7	0.5	0.3
Category B: office areas	0.7	0.5	0.3

Appendix D

Fire Safety

D.1 Fire Engineering in the Eurocode

When exposed to fire, the temperature of structural timber rises, leading to the formation of a *char layer*. This char layer no longer has load-bearing capacity, which reduces the strength of a timber structural element due to the loss of cross-sectional area. However, the char layer serves to limit the temperature rise in the inner core of the structural element. As such, the char layer can be considered a protective barrier that helps maintain the structural integrity of the element.

The method for determining the structural strength of timber beams will be described in this section. The calculations are done according to Eurocode 5, NEN-EN-1995-1-1 [47] and NEN-EN-1995-1-2 [48]. First, the approach to calculating the design strength of timber differs under fire conditions. Equation (D.1) describes the determination of the design strength of structural timber elements under *normal* conditions.

$$f_d = k_{\text{mod}} \frac{f_k}{\gamma_M} \tag{D.1}$$

Where:

- f_k is the characteristic value of the strength property;
- γ_M is the partial factor for a material property;
- k_{mod} is a modification factor that accounts for the influence of load duration and moisture content.

In this equation, the k_{mod} for laminated timber under permanent load in the relevant service class, which is governing in this study, is equal to 0.6 (see Section F.2 of Appendix F). The material factor γ_M for laminated timber is 1.25. Under normal conditions, these factors result in a reduction of the characteristic strength of the timber by a factor of $0.6/1.25 =$ **0.48**. Subsequently, under *fire* conditions, different factors are applied to determine the design strength. These are described by equations (2.1) and (D.2).

$$f_{d,fi} = k_{mod,fi} \frac{f_{20}}{\gamma_{M,fi}} \tag{2.1}$$

$$f_{20} = k_{fi} f_k \tag{D.2}$$

Where:

- $f_{d,fi}$ is the design value of strength under fire conditions;
- f_{20} is the 20%-fractile value of strength at room temperature;
- $k_{mod,fi}$ is the modification factor for fire conditions;
- $\gamma_{M,fi}$ is the partial safety factor for timber under fire conditions;
- k_{fi} is a factor for conversion from the 5% to the 20% fractile.

As shown, in this case, the 20% fractile is used as the characteristic strength instead of the usual 5% fractile. To obtain this factor, the conversion factor k_{fi} is applied, which is 1.15 for laminated timber. Additionally, the material factor $\gamma_{M,fi}$ under fire conditions differs from normal conditions and is now equal to 1. Finally, the $k_{\text{mod,fi}}$ factor has also changed during fire conditions. Its value is determined using the equations (4.2), (4.3) and (4.4).

For elements in bending:

$$k_{mod,fi} = 1.0 - \frac{1}{200} \cdot \frac{p}{A_t} \tag{4.2}$$

For elements in compression:

$$k_{mod,fi} = 1.0 - \frac{1}{125} \cdot \frac{p}{A_t} \tag{4.3}$$

For elements in tension:

$$k_{mod,fi} = 1.0 - \frac{1}{330} \cdot \frac{p}{A_t} \tag{4.4}$$

Where:

- p is the perimeter of the fire-exposed reduced cross-section, in m;
- A_t is the area of the residual cross-section, in m^2.

As can be inferred from the equations above, the $k_{mod,fi}$ factor now depends on the dimensions of the element. From Figure D.1, it can be observed that for elements with large cross-sections, the corresponding $k_{mod,fi}$ factor approaches 1. A reasonable assumption is made that columns relevant to this study will be larger than $0.5m$ (high-rise structures), ensuring that the $k_{mod,fi}$ factor is at least greater than 0.935.

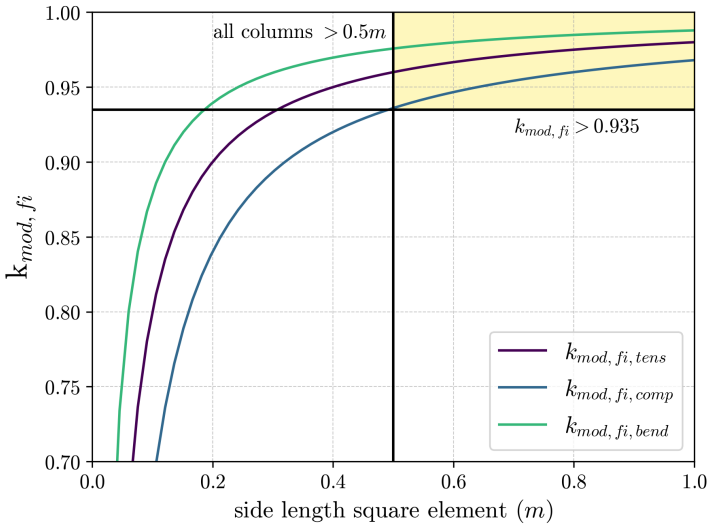

Figure D.1: $k_{mod,fi}$ vs. side length of an arbitrary squared timber element

To determine the design strength of laminated timber columns under fire conditions from the characteristic strength, the factor $0.935 \cdot 1.15/1 = 1.07$ is applied. This shift from 0.48 to 1.07 allows for less conservative calculations, meaning the reduction in cross-sectional area due to charring is less likely to result in structural failure according to the Eurocode.

Subsequently, the reduction in functional cross-sectional area of timber elements due to charring can be determined by calculating the charring depth in accordance with NEN-EN-1995-1-2. The charring depth can be determined using equations (D.3) and (D.4).

$$d_{ef} = d_{char,(0,n)} + k_0\, d_0 \tag{D.3}$$

$$d_{char,(0,n)} = \beta_{(0,n)}\, t \tag{D.4}$$

Where:

- d_{ef} is the effective charring depth;
- $k_0\, d_0$ is the charring layer thickness;
- $d_{char,(0,n)}$ is the design value of the apparent charring depth for one-dimensional (0) or notional (n) charring;
- $\beta_{(0,n)}$ is the one-dimensional or notional charring rate under exposure to the standard fire;
- t is the duration of fire exposure.

As can be deduced from the equations above, charring is modelled as a linear process. The remaining functional cross-sectional area is therefore directly proportional to time. In equation (D.3), $k_0\, d_0$, equals 1 for fire durations longer than 20 minutes, and d_0 equals 7 mm. For laminated timber, the charring rates β_0 and β_n are 0.65 min/mm and 0.7 min/mm, respectively.

To observe the effect of fire on the effective cross-sectional area, a small calculation experiment is performed. Square glulam columns with varying side lengths are exposed to a standard fire for 120 minutes. The unity check (UC) of the element under *fire conditions* is evaluated when the UC of the element in *normal conditions* is set to 1. This means that, for this experiment, the applied load will depend on this assumption. In this way, the UC of the element under fire conditions is compared to its UC under normal conditions.

The analysis assumes square columns located in an open compartment, meaning that notional charring is considered, and this charring occurs simultaneously on all four sides. The columns are assumed to be under compression and made of GL28c, a strength class with a characteristic compressive strength of 28 N/mm^2

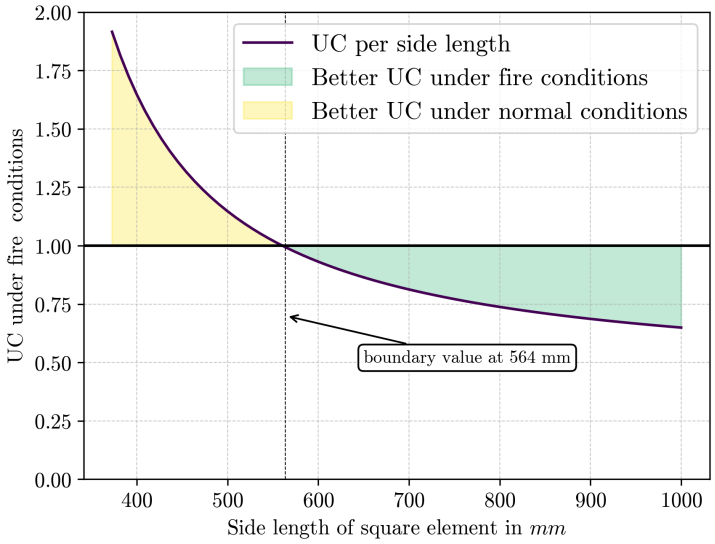

Figure D.2: UC for fire conditions when the UC under normal conditions is equal to 1

From Figure D.2, it can be deduced that the UC under fire conditions is even more conservative when the side length of the columns exceeds 564 mm. This is related to the fact that less conservative assumptions can be made under fire conditions. For large cross-sections, these factors have a significant impact on the UC.

Appendix E

Design Verifications

E.1 Verification According to Eurocode

This section presents the relevant verifications based on the Eurocode. The material capacity values are listed in Table F.3 for timber and in Table F.1 for concrete.

Axial Stress Parallel to the Grain
For tension and compression, the stresses in an arbitrary element are determined using equations E.2 and E.1, respectively. These equations apply to timber, concrete, and steel, each with their own specific material capacities.

$$\sigma_{c,0,d} \leq f_{c,0,d} \tag{E.1}$$

$$\sigma_{t,0,d} \leq f_{t,0,d} \tag{E.2}$$

Bending Stress
Elements must be verified for bending around two different axes. The capacity of the axis with the lowest bending utilization may be reduced by a factor k_m. This factor accounts for the redistribution of stresses and the heterogeneity of the material within the cross-section. For rectangular elements made of sawn timber, LVL, or GLT, this factor is equal to 0.7. The corresponding Unity Check is therefore defined as Equation E.3.

$$\max\left(\frac{\sigma_{m,y,d}}{f_{m,y,d}} + k_m \cdot \frac{\sigma_{m,z,d}}{f_{m,z,d}},\ k_m \cdot \frac{\sigma_{m,y,d}}{f_{m,y,d}} + \frac{\sigma_{m,z,d}}{f_{m,z,d}}\right) \leq 1 \tag{E.3}$$

Shear Stress
Shear with a stress component oriented either parallel or perpendicular to the grain can be determined using equation E.4. For the verification of shear in timber elements, the effective width must be reduced by a factor k_{cr}. For GLT, this factor is generally equal to 0.67.

$$\tau_d \leq f_{v,d} \tag{E.4}$$

Combined Axial and Bending Stresses
Elements subjected to a combination of bending and axial loading must be verified using equation E.5 for tension and equation E.6 for compression, respectively.

$$\frac{\sigma_{t,0,d}}{f_{t,0,d}} + \max\left(k_m \cdot \frac{\sigma_{m,y,d}}{f_{m,y,d}} + \frac{\sigma_{m,z,d}}{f_{m,z,d}},\ \frac{\sigma_{m,y,d}}{f_{m,y,d}} + k_m \cdot \frac{\sigma_{m,z,d}}{f_{m,z,d}}\right) \leq 1 \tag{E.5}$$

$$\left(\frac{\sigma_{c,0,d}}{f_{c,0,d}}\right)^2 + \max\left(\frac{\sigma_{m,y,d}}{f_{m,y,d}} + k_m \cdot \frac{\sigma_{m,z,d}}{f_{m,z,d}},\ k_m \cdot \frac{\sigma_{m,y,d}}{f_{m,y,d}} + \frac{\sigma_{m,z,d}}{f_{m,z,d}}\right) \leq 1 \tag{E.6}$$

Buckling Resistance
Columns that are significantly subjected to compression and that may additionally experience a certain degree of bending must be verified for buckling stability. The relative slenderness must first be calculated, as defined in equation E.7. $i \in \{z, y\}$ for all corresponding equations.

$$\lambda_{\text{rel},i} = \frac{\lambda_i}{\pi}\sqrt{\frac{f_{c,0,k}}{E_{0,05}}} \tag{E.7}$$

$$\lambda_i = \frac{l_{\text{eff},i}}{i_i} \tag{E.8}$$

$$i_i = \sqrt{\frac{I_i}{A}} \tag{E.9}$$

Where:

- λ_i is the slenderness
- i_i is the radius of gyration
- $l_{eff,i}$ is the effective length, in this research equal to 3.5 (storey height)

If the slenderness for bending in both the y and z directions exceeds 0.3, the compressive capacity $f_{c,0,d}$ in equation E.6 is modified by a reduction factor k_i.

$$\frac{\sigma_{c,0,d}}{k_{c,i} f_{c,0,d}} + \max\left(\frac{\sigma_{m,y,d}}{f_{m,y,d}} + k_m \cdot \frac{\sigma_{m,z,d}}{f_{m,z,d}},\ k_m \cdot \frac{\sigma_{m,y,d}}{f_{m,y,d}} + \frac{\sigma_{m,z,d}}{f_{m,z,d}}\right) \leq 1 \tag{E.10}$$

$$k_{c,i} = \frac{1}{k_i + \sqrt{k_i^2 - \lambda_{\text{rel},i}^2}} \tag{E.11}$$

$$k_i = 0{,}5\left(1 + \beta_c(\lambda_{\text{rel},i} - 0{,}3) + \lambda_{\text{rel},i}^2\right) \tag{E.12}$$

In equation E.12, β_c is a factor for elements within the straightness limits and is equal to 0.1 for GLT.

Appendix F

Material Properties

F.1 Properties of concrete according to NEN-EN-1992-1-1

Table F.1: Strength- and deformation properties for concrete according to NEN-EN-1992-1-1 [46]

Strength classes for light weight concrete														Analytical relation/Explanation
f_{lck} (MPa)	12	16	20	25	30	35	40	45	50	55	60	70	80	
$f_{lck,cube}$ (MPa)	13	18	22	28	33	38	44	50	55	60	66	77	88	
f_{lcm} (MPa)	17	22	28	33	38	43	48	53	58	63	68	78	88	For $f_{lck} \geq 20$ MPa $f_{lcm} = f_{lck} + 8$ (MPa)
f_{lctm} (MPa)	$f_{lctm} = f_{ctm} \cdot \eta_1$													η_1=0,40+0,60ρ/2200
$f_{lctk,0,05}$ (MPa)	$f_{lctk,0,05} = f_{ctk,0,05} \cdot \eta_1$													5% - fractile
$f_{lctk,0,95}$ (MPa)	$f_{lctk,0,95} = f_{ctk,0,95} \cdot \eta_1$													95% - fractile
E_{lcm} (GPa)	$E_{lcm} = E_{cm} \cdot \eta_E$													$\eta_E = (\rho/2200)^2$
ε_{lc1} (‰)	$kf_{lcm}/(E_{lci} \cdot \eta_E)$ { k = 1,1 for sanded lightweight aggregate concrete; k = 1,0 for all lightweight aggregate concrete													see Figure 3.2
ε_{lcu1}(‰)	ε_{lc1}													see Figure 3.2
ε_{lc2} (‰)	2,0									2,2	2,3	2,4	2,5	see Figure 3.3
ε_{lcu2} (‰)	3,5 η_1									3,1η_1	2,9η_1	2,7η_1	2,6η_1	see Figure 3.3 $\lvert\varepsilon_{lcu2u}\rvert \geq \lvert\varepsilon_{lc2}\rvert$
n	2,0									1,75	1,6	1,45	1,4	
ε_{lc3}(‰)	1,75									1,8	1,9	2,0	2,2	see Figure 3.4
ε_{lcu3}(‰)	3,5 η_1									3,1η_1	2.9η_1	2.7η_1	2,6η_1	see Figure 3.4 $\lvert\varepsilon_{lcu3}\rvert \geq \lvert\varepsilon_{lc3}\rvert$

F.2 Modification k_{mod} for timber

Table F.2: Modification factor k_{mod} depending on material, service class and load-duration class [47]

Material	Standard	Service class	Load-duration class				
			Permanent action	Long term action	Medium term action	Short term action	Instantaneous action
Solid timber	EN 14081-1	1	0,60	0,70	0,80	0,90	1,10
		2	0,60	0,70	0,80	0,90	1,10
		3	0,50	0,55	0,65	0,70	0,90
Glued laminated timber	EN 14080	1	0,60	0,70	0,80	0,90	1,10
		2	0,60	0,70	0,80	0,90	1,10
		3	0,50	0,55	0,65	0,70	0,90
LVL	EN 14374, EN 14279	1	0,60	0,70	0,80	0,90	1,10
		2	0,60	0,70	0,80	0,90	1,10
		3	0,50	0,55	0,65	0,70	0,90
Plywood	EN 636						
	Part 1, Part 2, Part 3	1	0,60	0,70	0,80	0,90	1,10
	Part 2, Part 3	2	0,60	0,70	0,80	0,90	1,10
	Part 3	3	0,50	0,55	0,65	0,70	0,90
OSB	EN 300						
	OSB/2	1	0,30	0,45	0,65	0,85	1,10
	OSB/3, OSB/4	1	0,40	0,50	0,70	0,90	1,10
	OSB/3, OSB/4	2	0,30	0,40	0,55	0,70	0,90
Particle-board	EN 312						
	Part 4, Part 5	1	0,30	0,45	0,65	0,85	1,10
	Part 5	2	0,20	0,30	0,45	0,60	0,80
	Part 6, Part 7	1	0,40	0,50	0,70	0,90	1,10
	Part 7	2	0,30	0,40	0,55	0,70	0,90
Fibreboard, hard	EN 622-2						
	HB.LA, HB.HLA 1 or 2	1	0,30	0,45	0,65	0,85	1,10
	HB.HLA1 or 2	2	0,20	0,30	0,45	0,60	0,80
Fibreboard, medium	EN 622-3						
	MBH.LA1 or 2	1	0,20	0,40	0,60	0,80	1,10
	MBH.HLS1 or 2	1	0,20	0,40	0,60	0,80	1,10
	MBH.HLS1 or 2	2	–	–	–	0,45	0,80
Fibreboard, MDF	EN 622-5						
	MDF.LA, MDF.HLS	1	0,20	0,40	0,60	0,80	1,10
	MDF.HLS	2	–	–	–	0,45	0,80

F.3 Properties of timber according to EN 14080

Table F.3: Strength- and deformation properties for timber according to EN 14080 [20]

		Glulam strength class						
Property	**Symbol**	**GL 20h**	**GL 22h**	**GL 24h**	**GL 26h**	**GL 28h**	**GL 30h**	**GL 32h**
Bending strength	$f_{m,g,k}$	20	22	24	26	28	30	32
Tensile strength	$f_{t,0,g,k}$	16	17,6	19,2	20,8	22,3	24	25,6
	$f_{t,90,g,k}$	0,5						
Compression strength	$f_{c,0,g,k}$	20	22	24	26	28	30	32
	$f_{c,90,g,k}$	2,5						
Shear strength (shear and torsion)	$f_{v,g,k}$	3,5						
Rolling shear strength	$f_{r,g,k}$	1,2						
Modulus of elasticity	$E_{0,g,mean}$	8 400	10 500	11 500	12 100	12 600	13 600	14 200
	$E_{0,g,05}$	7 000	8 800	9 600	10 100	10 500	11 300	11 800
	$E_{90,g,mean}$	300						
	$E_{90,g,05}$	250						
Shear modulus	$G_{g,mean}$	650						
	$G_{g,05}$	540						
Rolling shear modulus	$G_{r,g,mean}$	65						
	$G_{r,g,05}$	54						
Density	$\rho_{g,k}$	340	370	385	405	425	430	440
	$\rho_{g,mean}$	370	410	420	445	460	480	490

F.4 Properties of GL 28h as implemented in SCIA

Table F.4: Material properties of GL 28h (EN 14080) as implemented in SCIA

Material: GL 28h (EN 14080)		**Value**
Norm-independent properties		
Material type		Timber
Thermal expansion coefficient	$[\mathrm{m/mK}]$	$5.00 \cdot 10^{-6}$
Mass density	$[\mathrm{kg/m^3}]$	460.00
Young's modulus E	$[\mathrm{MPa}]$	12600
Poisson's ratio	$[-]$	0.00
Shear modulus G (independent)	$[\mathrm{MPa}]$	650
Log. decrement (non-uniform damping)	$[-]$	0.15
Specific heat capacity	$[\mathrm{J/gK}]$	0.6
Thermal conductivity	$[\mathrm{W/mK}]$	0.045
EC5 Strength and Stiffness Properties		
Timber type		Glued laminated timber
Bending strength $f_{m,k}$	$[\mathrm{MPa}]$	28.0
Tension strength parallel to grain $f_{t,0,k}$	$[\mathrm{MPa}]$	22.3
Tension strength perpendicular to grain $f_{t,90,k}$	$[\mathrm{MPa}]$	0.5
Compression strength parallel to grain $f_{c,0,k}$	$[\mathrm{MPa}]$	28.0
Compression strength perpendicular to grain $f_{c,90,k}$	$[\mathrm{MPa}]$	2.5
Shear strength $f_{v,k}$	$[\mathrm{MPa}]$	3.5
Stiffness modulus $E_{0.05}$	$[\mathrm{MPa}]$	10500
Modulus E_{90} (mean)	$[\mathrm{MPa}]$	300

F.5 Properties of C30/37 as implemented in SCIA

Table F.5: Material properties of concrete C30/37 according to EN 1992-1-1 as implemented in SCIA

Material: C30/37 Concrete		**Value**
Norm-independent properties		
Material type		Concrete
Thermal expansion coefficient	$[\mathrm{m/mK}]$	$1.0 \cdot 10^{-5}$
Mass density	$[\mathrm{kg/m^3}]$	2500
Density in wet state	$[\mathrm{kg/m^3}]$	2600
Young's modulus E	$[\mathrm{MPa}]$	32800
Poisson's ratio	$[-]$	0.2
Shear modulus G	$[\mathrm{MPa}]$	13667
Log. decrement (non-uniform damping)	$[-]$	0.2
Specific heat capacity	$[\mathrm{J/gK}]$	0.6
Thermal conductivity	$[\mathrm{W/mK}]$	0.045
EN 1992-1-1 properties		
Characteristic compressive strength $f_{ck}(28)$	$[\mathrm{MPa}]$	30.00
Mean compressive strength $f_{cm}(28)$	$[\mathrm{MPa}]$	38.00
$f_{cm}(28) - f_{ck}(28)$	$[\mathrm{MPa}]$	8.00
Mean tensile strength $f_{ctm}(28)$	$[\mathrm{MPa}]$	2.90
5% fractile tensile strength $f_{ctk,0.05}(28)$	$[\mathrm{MPa}]$	2.00
95% fractile tensile strength $f_{ctk,0.95}(28)$	$[\mathrm{MPa}]$	3.80
Design compressive strength (long-term)	$[\mathrm{MPa}]$	20.00
Design compressive strength (short-term)	$[\mathrm{MPa}]$	25.00
Strain at 50% of peak strength ε_{c2}	$[\cdot 10^{-4}]$	12.4
Ultimate strain ε_{cu2}	$[\cdot 10^{-4}]$	35.0
Strain at peak strength ε_{c3}	$[\cdot 10^{-4}]$	17.5
Ultimate strain ε_{cu3}	$[\cdot 10^{-4}]$	35.0
Maximum aggregate size	$[\mathrm{mm}]$	16.00
Aggregate type		Quartzite

Appendix G

Cross Sections

Table G.1: Cross-section catalogue – GLT and Concrete Columns

Code	Material	Dimension	Type
GL1RECT	TIMB	RECT200x300	GL 28h
GL2RECT	TIMB	RECT233x350	GL 28h
GL3RECT	TIMB	RECT267x400	GL 28h
GL4RECT	TIMB	RECT300x450	GL 28h
GL5RECT	TIMB	RECT333x500	GL 28h
GL6RECT	TIMB	RECT367x550	GL 28h
GL7RECT	TIMB	RECT400x600	GL 28h
GL8RECT	TIMB	RECT433x650	GL 28h
GL9RECT	TIMB	RECT467x700	GL 28h
GL10RECT	TIMB	RECT500x750	GL 28h
GL11RECT	TIMB	RECT533x800	GL 28h
GL12RECT	TIMB	RECT567x850	GL 28h
GL13RECT	TIMB	RECT600x900	GL 28h
GL14RECT	TIMB	RECT633x950	GL 28h
GL15RECT	TIMB	RECT667x1000	GL 28h
GL16RECT	TIMB	RECT700x1050	GL 28h
GL17RECT	TIMB	RECT733x1100	GL 28h
GL18RECT	TIMB	RECT767x1150	GL 28h
GL19RECT	TIMB	RECT800x1200	GL 28h
GL20RECT	TIMB	RECT833x1250	GL 28h
GL21RECT	TIMB	RECT867x1300	GL 28h
GL22RECT	TIMB	RECT900x1350	GL 28h
GL23RECT	TIMB	RECT933x1400	GL 28h
GL24RECT	TIMB	RECT967x1450	GL 28h
GL25RECT	TIMB	RECT1000x1500	GL 28h
GL1SQ	TIMB	RECT300x300	GL 28h
GL2SQ	TIMB	RECT350x350	GL 28h
GL3SQ	TIMB	RECT400x400	GL 28h
GL4SQ	TIMB	RECT450x450	GL 28h
GL5SQ	TIMB	RECT500x500	GL 28h
GL6SQ	TIMB	RECT550x550	GL 28h
GL7SQ	TIMB	RECT600x600	GL 28h
GL8SQ	TIMB	RECT650x650	GL 28h
GL9SQ	TIMB	RECT700x700	GL 28h
GL10SQ	TIMB	RECT750x750	GL 28h

Continued on next page

Code	Material	Dimension	Type
GL11SQ	TIMB	RECT800x800	GL 28h
GL12SQ	TIMB	RECT850x850	GL 28h
GL13SQ	TIMB	RECT900x900	GL 28h
GL14SQ	TIMB	RECT950x950	GL 28h
GL15SQ	TIMB	RECT1000x1000	GL 28h
GL16SQ	TIMB	RECT1050x1050	GL 28h
GL17SQ	TIMB	RECT1100x1100	GL 28h
GL18SQ	TIMB	RECT1150x1150	GL 28h
GL19SQ	TIMB	RECT1200x1200	GL 28h
GL20SQ	TIMB	RECT1250x1250	GL 28h
GL21SQ	TIMB	RECT1300x1300	GL 28h
GL22SQ	TIMB	RECT1350x1350	GL 28h
GL23SQ	TIMB	RECT1400x1400	GL 28h
GL24SQ	TIMB	RECT1450x1450	GL 28h
GL25SQ	TIMB	RECT1500x1500	GL 28h
CONC1SQ	CONC	RECT300x300	C30/37
CONC2SQ	CONC	RECT350x350	C30/37
CONC3SQ	CONC	RECT400x400	C30/37
CONC4SQ	CONC	RECT450x450	C30/37
CONC5SQ	CONC	RECT500x500	C30/37
CONC6SQ	CONC	RECT550x550	C30/37
CONC7SQ	CONC	RECT600x600	C30/37
CONC8SQ	CONC	RECT650x650	C30/37
CONC9SQ	CONC	RECT700x700	C30/37
CONC10SQ	CONC	RECT750x750	C30/37
CONC11SQ	CONC	RECT800x800	C30/37
CONC12SQ	CONC	RECT850x850	C30/37
CONC13SQ	CONC	RECT900x900	C30/37
CONC14SQ	CONC	RECT950x950	C30/37
CONC15SQ	CONC	RECT1000x1000	C30/37
CONC16SQ	CONC	RECT1050x1050	C30/37
CONC17SQ	CONC	RECT1100x1100	C30/37
CONC18SQ	CONC	RECT1150x1150	C30/37
CONC19SQ	CONC	RECT1200x1200	C30/37
CONC20SQ	CONC	RECT1250x1250	C30/37
CONC21SQ	CONC	RECT1300x1300	C30/37
CONC22SQ	CONC	RECT1350x1350	C30/37
CONC23SQ	CONC	RECT1400x1400	C30/37
CONC24SQ	CONC	RECT1450x1450	C30/37
CONC25SQ	CONC	RECT1500x1500	C30/37

Appendix H

Load Combinations

Table H.1: Load combinations and corresponding coefficients

Name	Load Cases	Coeff. [-]
SELF_WEIGHT	LC_SW	1.500
	LC_PERM	1.500
	LC_IMPOSED	0.660
FLOOR_VAR	LC_SW	1.300
	LC_PERM	1.300
	LC_IMPOSED	1.650
WIND_VAR_COMP	LC_SW	1.300
	LC_PERM	1.300
	LC_WIND	1.650
	LC_IMPOSED	0.660
WIND_VAR_TENS	LC_SW	0.900
	LC_PERM	0.900
	LC_WIND	1.650
HOR_DEFLECT1	LC_SW	1.000
	LC_PERM	1.000
	LC_WIND	1.000
HOR_DEFLECT2	LC_SW	1.000
	LC_PERM	1.000
	LC_WIND	1.000
	LC_IMPOSED	0.400
VERT_DEFLECT	LC_SW	1.000
	LC_PERM	1.000
	LC_IMPOSED	1.000

Appendix I

Material price per m^2 of Net Floor Area

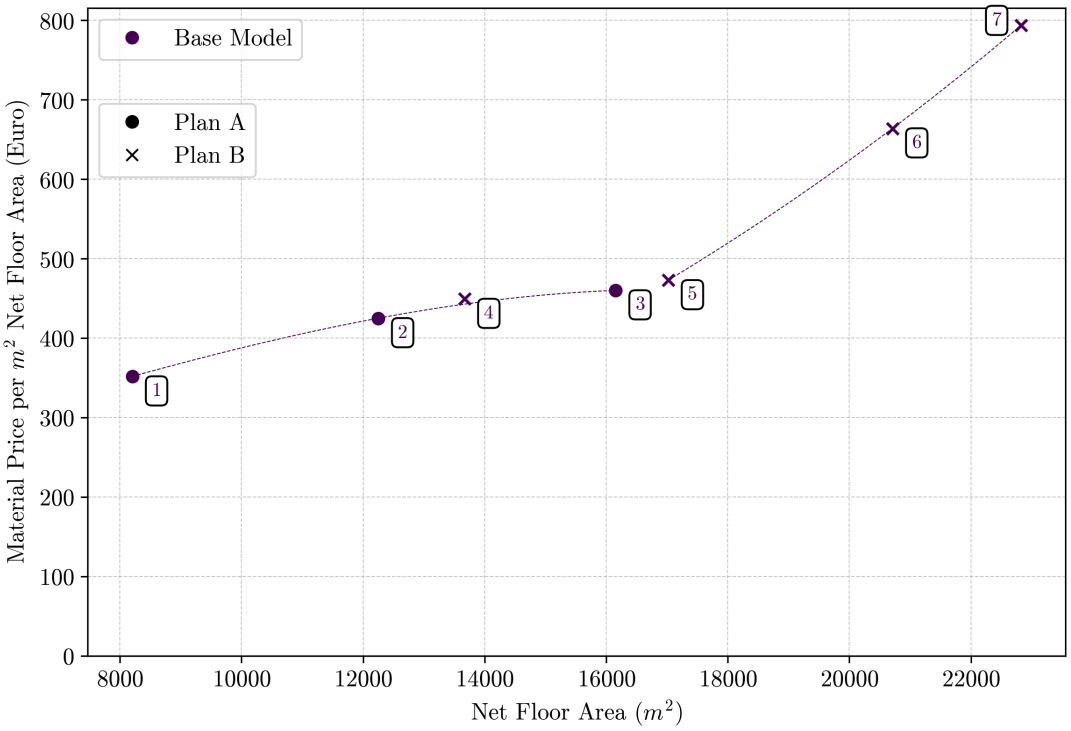

Figure I.1: Base Model for Material Price per m^2 of Net Floor Area vs Net Floor Area

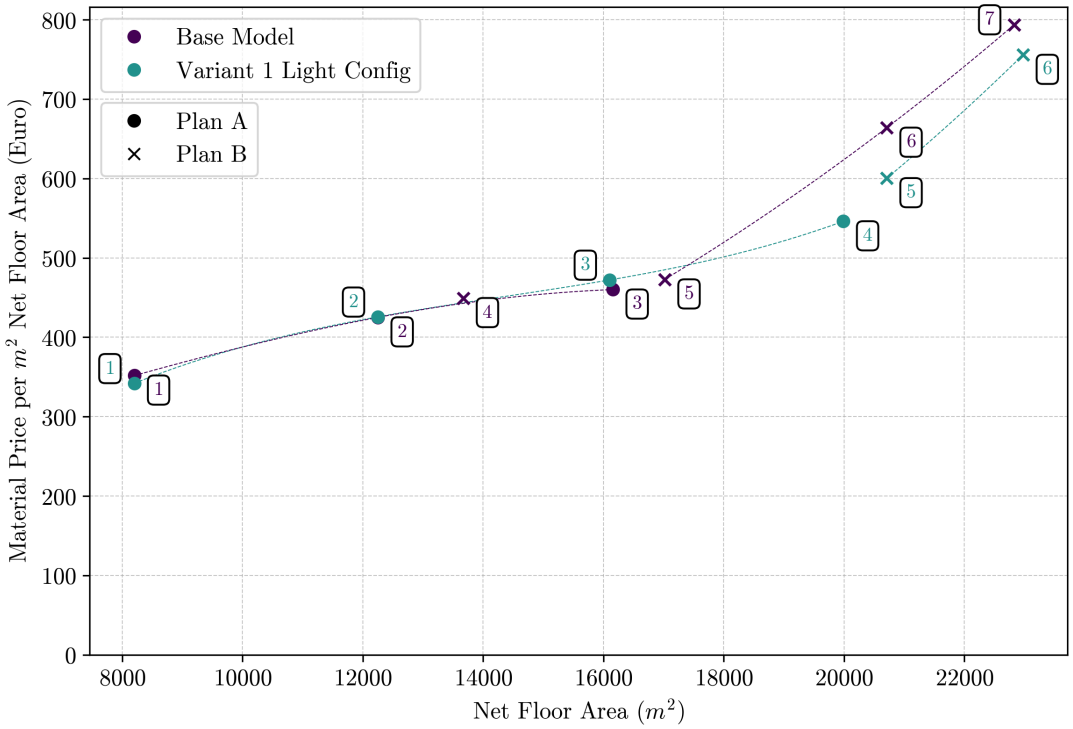

Figure I.2: Variant 1: Light Configuration for Material Price per m^2 of Net Floor Area vs Net Floor Area

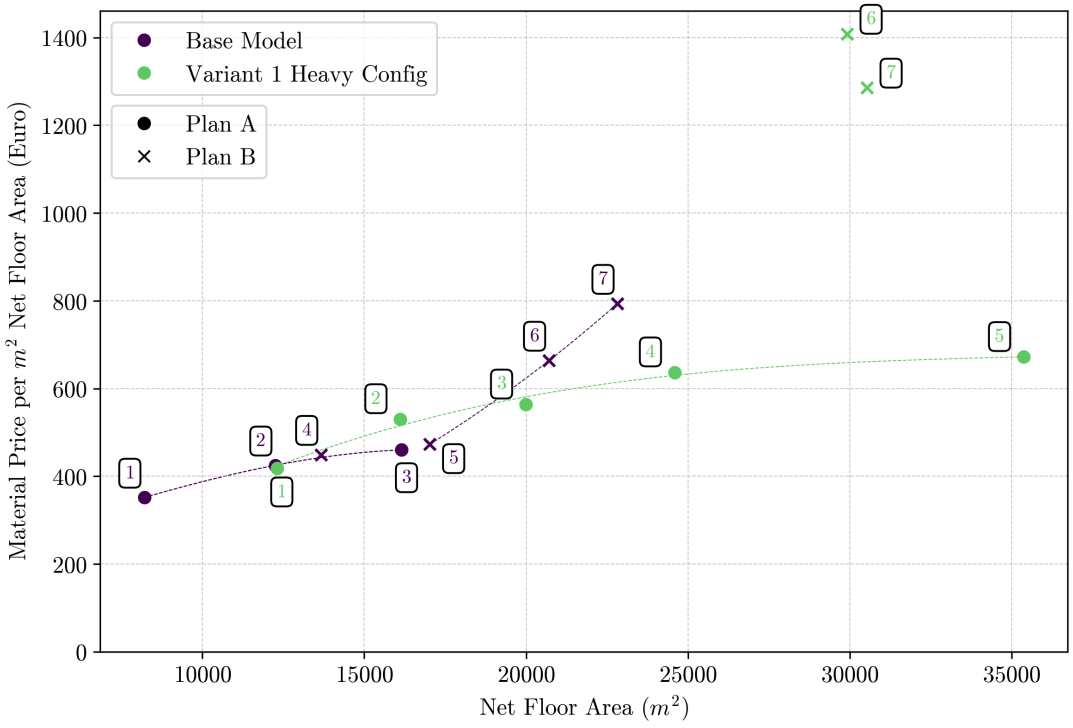

Figure I.3: Variant 1: Heavy Configuration for Material Price per m^2 of Net Floor Area vs Net Floor Area

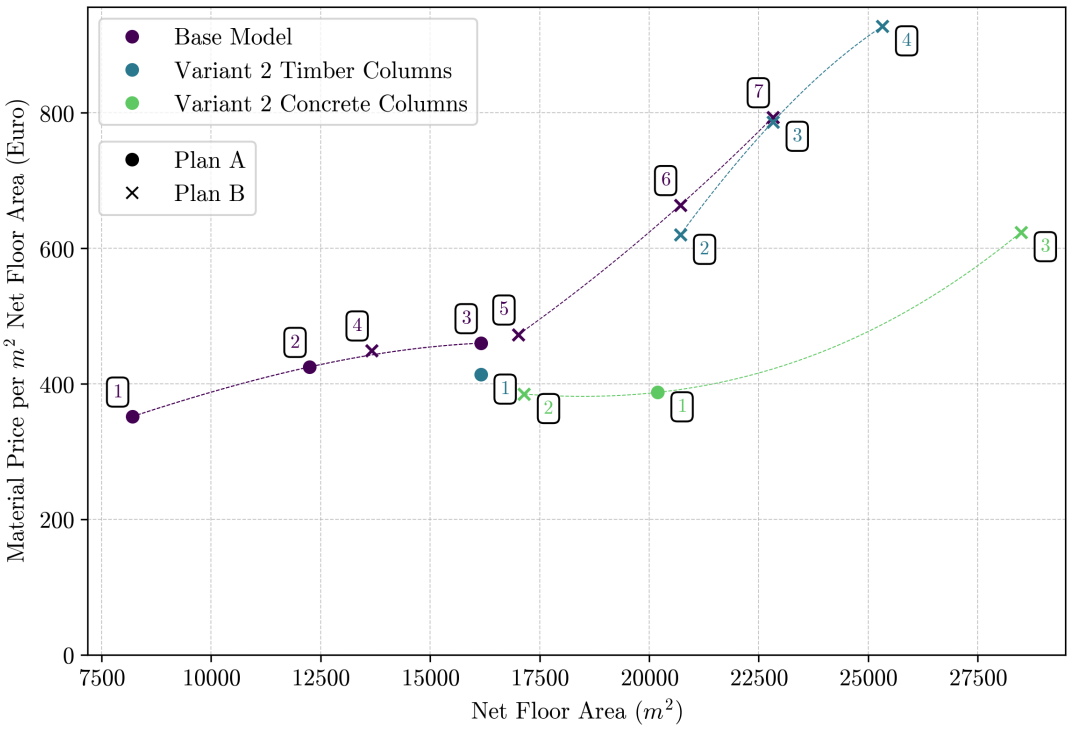

Figure I.4: Variant 2 for Material Price per m^2 of Net Floor Area vs Net Floor Area

Appendix J

UC Iterations

J.1 Base Model

Table J.1: Overview of dimensions and Unity Checks, Base Model, 10 storeys, Iteration 3

BASE MODEL		**UCs (Iteration 3)**				
		WIND_VAR TENS	WIND_VAR COMP	FLOOR VAR	SELF WEIGHT	VERT DEFLECT
DIMENSIONS						
CS X-Beams	GL5RECT	0.41 (shear)	0.67 (shear)	0.79 (shear)	0.76 (shear)	0.44
CS Y-Beams	GL6RECT	0.72 (shear)	0.96 (shear)	0.90 (shear)	0.83 (shear)	0.56
CS Columns	GL3SQ	0.00	0.87 (comb)	0.62 (comb)	0.60 (comb)	
X - Con Size	400	0.11	0.17	0.21	0.20	
Y - Con Size	400	0.18	0.24	0.22	0.20	
Col - Con Size	400	0.00				
Core Thickness	100	1.75%	0.98	0.36	0.38	
HOR_DEFLECT1		0.39				
HOR_DEFLECT2		0.39				
Storey Number		10				
Floor Plan		A				

Table J.2: Overview of dimensions and Unity Checks, Base Model, 15 storeys, Iteration 2

BASE MODEL		**UCs (Iteration 2)**				
		WIND_VAR TENS	WIND_VAR COMP	FLOOR VAR	SELF WEIGHT	VERT DEFLECT
DIMENSIONS						
CS X-Beams	GL5RECT	0.45 (shear)	0.73 (shear)	0.87 (shear)	0.83 (shear)	0.39
CS Y-Beams	GL9RECT	1.03 (shear)	1.23 (shear)	0.68 (shear)	0.68 (shear)	0.41
CS Columns	GL4SQ	1.10	0.92 (comb)	0.45 (comb)	0.46 (comb)	
X - Con Size	400	0.12	0.19	0.23	0.22	
Y - Con Size	400	0.21	0.26	0.14	0.14	
Col - Con Size	400	1.10				
Core Thickness	250	1.78%	0.82	0.26	0.27	
HOR_DEFLECT1		0.56				
HOR_DEFLECT2		0.56				
Storey Number		15				
Floor Plan		A				

Table J.3: Overview of dimensions and Unity Checks, Base Model, 20 storeys, Iteration 7

BASE MODEL		**UCs (Iteration 7)**				
		WIND_VAR TENS	WIND_VAR COMP	FLOOR VAR	SELF WEIGHT	VERT DEFLECT
DIMENSIONS						
CS X-Beams	GL5RECT	0.42 (shear)	0.70 (shear)	0.82 (shear)	0.79 (shear)	0.25
CS Y-Beams	GL8RECT	0.87 (shear)	1.08 (comb)	0.87 (shear)	0.81 (shear)	0.12
CS Columns	GL9SQ	No Tension	0.93 (comb)	0.95 (comb)	0.97 (comb)	
X - Con Size	400	0.11	0.18	0.21	0.21	
Y - Con Size	700	0.06	0.07	0.06	0.05	
Col - Con Size	400	0.00				
Core Thickness	400	1.79%	0.89	0.28	0.30	
HOR_DEFLECT1		1.04				
HOR_DEFLECT2		1.04				
Storey Number		20				
Floor Plan		A				

Table J.4: Overview of dimensions and Unity Checks, Base Model, 20 storeys, Iteration 6

BASE MODEL		**UCs (Iteration 6)**				
		WIND_VAR TENS	WIND_VAR COMP	FLOOR VAR	SELF WEIGHT	VERT DEFLECT
DIMENSIONS						
CS X-Beams	GL5RECT	0.33 (shear)	0.54 (shear)	0.63 (shear)	0.61 (shear)	0.14
CS Y-Beams	GL5RECT	1.02 (comb)	1.33 (comb)	0.99 (comb)	1.00 (comb)	0.15
CS Columns	GL5SQ	No Tension	0.74 (comb)	0.51 (comb)	0.51 (comb)	
X - Con Size	400	0.09	0.14	0.16	0.16	
Y - Con Size	400	0.14	0.21	0.21	0.20	
Col - Con Size	400	0.00				
Core Thickness	200	1.28%	0.77	0.29	0.31	
HOR_DEFLECT1		0.38				
HOR_DEFLECT2		0.38				
Storey Number		20				
Floor Plan		B				

Table J.5: Overview of dimensions and Unity Checks, Base Model, 25 storeys, Iteration 1

BASE MODEL		**UCs (Iteration 1)**				
		WIND_VAR TENS	WIND_VAR COMP	FLOOR VAR	SELF WEIGHT	VERT DEFLECT
DIMENSIONS						
CS X-Beams	GL5RECT	0.34 (shear)	0.56 (shear)	0.65 (shear)	0.63 (shear)	0.14
CS Y-Beams	GL5RECT	1.32 (comb)	1.38 (comb)	1.16 (comb)	1.18 (comb)	0.24
CS Columns	GL7SQ	No Tension	0.81 (comb)	0.50 (comb)	0.51 (comb)	
X - Con Size	400	0.09	0.15	0.17	0.16	
Y - Con Size	400	0.18	0.25	0.23	0.21	
Col - Con Size	400	0.00				
Core Thickness	250	1.75%	1.00	0.36	0.39	
HOR_DEFLECT1		0.98				
HOR_DEFLECT2		0.98				
Storey Number		25				
Floor Plan		B				

Table J.6: Overview of dimensions and Unity Checks, Base Model, 31 storeys, Iteration 4

BASE MODEL		**UCs (Iteration 4)**				
		WIND_VAR TENS	WIND_VAR COMP	FLOOR VAR	SELF WEIGHT	VERT DEFLECT
DIMENSIONS						
CS X-Beams	GL5RECT	0.35 (shear)	0.56 (shear)	0.65 (shear)	0.63 (shear)	0.14
CS Y-Beams	GL9RECT	1.05 (comb)	1.29 (comb)	0.83 (comb)	0.84 (comb)	0.08
CS Columns	GL11SQ	No Tension	0.71 (comb)	0.74 (comb)	0.80 (comb)	
X - Con Size	400	0.10	0.15	0.17	0.16	
Y - Con Size	700	0.05	0.06	0.05	0.05	
Col - Con Size	400	0.00				
Core Thickness	400	1.25%	0.90	0.37	0.41	
HOR_DEFLECT1		0.48				
HOR_DEFLECT2		0.48				
Storey Number		31				
Floor Plan		B				

Table J.7: Overview of dimensions and Unity Checks, Base Model, 35 storeys, Iteration 1

BASE MODEL		**UCs (Iteration 1)**				
		WIND_VAR TENS	WIND_VAR COMP	FLOOR VAR	SELF WEIGHT	VERT DEFLECT
DIMENSIONS						
CS X-Beams	GL5RECT	0.34 (shear)	0.54 (shear)	0.63 (shear)	0.54 (shear)	0.14
CS Y-Beams	GL10RECT	1.08 (comb)	1.22 (comb)	0.61 (shear)	0.59 (shear)	0.06
CS Columns	GL15SQ	No Tension	0.46 (comb)	0.43 (comb)	0.47 (comb)	
X - Con Size	400	0.11	0.14	0.16	0.16	
Y - Con Size	900	0.04	0.05	0.03	0.03	
Col - Con Size	400	0.00				
Core Thickness	400	1.28%	0.96	0.41	0.44	
HOR_DEFLECT1		1.00				
HOR_DEFLECT2		1.00				
Storey Number		35				
Floor Plan		B				

Table J.8: Overview of dimensions and Unity Checks, Base Model, 35 storeys, Iteration 10

BASE MODEL		**UCs (Iteration 10)**				
		WIND_VAR TENS	WIND_VAR COMP	FLOOR VAR	SELF WEIGHT	VERT DEFLECT
DIMENSIONS						
CS X-Beams	GL7RECT	0.43 (shear)	0.71 (shear)	0.83 (shear)	0.79 (shear)	0.35
CS Y-Beams	GL9RECT	0.77 (comb)	1.02 (comb)	0.78 (comb)	0.77 (comb)	0.12
CS Columns	GL14SQ	No Tension	0.77 (comb)	0.86 (comb)	0.96 (comb)	
X - Con Size	400	0.14	0.16	0.19	0.18	
Y - Con Size	900	0.04	0.05	0.04	0.04	
Col - Con Size	400	0				
Core Thickness	300	0.94%	0.97	0.47	0.51	
HOR_DEFLECT1		0.88				
HOR_DEFLECT2		0.88				
Storey number		35				
Floor Plan		C				

Table J.9: Overview of dimensions and Unity Checks, Base Model, 40 storeys, Iteration 4

BASE MODEL		**UCs (Iteration 4)**				
		WIND_VAR TENS	WIND_VAR COMP	FLOOR VAR	SELF WEIGHT	VERT DEFLECT
DIMENSIONS						
CS X-Beams	GL7RECT	0.43 (shear)	0.71 (shear)	0.82 (shear)	0.78 (shear)	0.35
CS Y-Beams	GL10RECT	0.73 (comb)	0.95 (comb)	0.70 (shear)	0.69 (shear)	0.11
CS Columns	GL16SQ	No Tension	0.71 (comb)	0.78 (comb)	0.87 (comb)	
X - Con Size	400	0.15	0.18	0.19	0.18	
Y - Con Size	700	0.05	0.06	0.05	0.05	
Col - Con Size	400	0.00				
Core Thickness	400	0.94%	0.97	0.46	0.50	
HOR_DEFLECT1		0.98				
HOR_DEFLECT2		0.98				
Storey Number		40				
Floor Plan		C				

J.2 Variant 1: Light Configuration

Table J.10: Overview of dimensions and Unity Checks, Variant 1L, 10 storeys, Iteration 2

VARIANT 1L		**UCs (Iteration 2)**				
		WIND_VAR TENS	WIND_VAR COMP	FLOOR VAR	SELF WEIGHT	VERT DEFLECT
DIMENSIONS						
CS X-Beams	GL5RECT	0.41 (shear)	0.67 (shear)	0.79 (shear)	0.76 (shear)	0.26
CS Y-Beams	GL8RECT	0.81 (shear)	1.11 (shear)	0.99 (shear)	0.97 (shear)	0.19
CS Columns	GL3SQ	No Tension	0.79 (comb)	0.62 (comb)	0.61 (comb)	
CS Diagonals	GL2RECT	0.09	0.11 (comb)	0.13 (comb)	0.13 (comb)	
X - Con Size	400	0.11	0.17	0.21	0.20	
Y - Con Size	400	0.18	0.24	0.21	0.21	
Col - Con Size	400	0.00				
Diag - Con Size	600	0.33	0.78			
Core Thickness	100	1.20%	0.87	0.40	0.41	
HOR_DEFLECT1		0.50				
HOR_DEFLECT2		0.50				
Storey Number		10				
Floor Plan		A				

Table J.11: Overview of dimensions and Unity Checks, Variant 1L, 15 storeys, Iteration 1

VARIANT 1L		**UCs (Iteration 1)**				
		WIND_VAR TENS	WIND_VAR COMP	FLOOR VAR	SELF WEIGHT	VERT DEFLECT
DIMENSIONS						
CS X-Beams	GL5RECT	0.43 (shear)	0.71 (shear)	0.83 (shear)	0.80 (shear)	0.26
CS Y-Beams	GL9RECT	1.36 (shear)	1.85 (shear)	1.52 (shear)	1.52 (shear)	0.17
CS Columns	GL5SQ	No Tension	1.13 (comb)	0.79 (comb)	0.79 (comb)	
CS Diagonals	GL3RECT	0.24	0.15 (comb)	0.14 (comb)	0.15 (comb)	
X - Con Size	400	0.11	0.19	0.22	0.21	
Y - Con Size	400	0.28	0.39	0.32	0.32	
Col - Con Size	400	0.00				
Diag - Con Size	600	0.60	0.80			
Core Thickness	200	1.79%	0.98	0.37	0.39	
HOR_DEFLECT1		0.89				
HOR_DEFLECT2		0.89				
Storey Number		15				
Floor Plan		A				

Table J.12: Overview of dimensions and Unity Checks, Variant 1L, 20 storeys, Iteration 3

VARIANT 1L		**UCs (Iteration 3)**				
		WIND_VAR TENS	WIND_VAR COMP	FLOOR VAR	SELF WEIGHT	VERT DEFLECT
DIMENSIONS						
CS X-Beams	GL5RECT	0.42 (shear)	0.69 (shear)	0.81 (shear)	0.78 (shear)	0.25
CS Y-Beams	GL8RECT	1.30 (shear)	1.39 (shear)	1.06 (shear)	1.06 (shear)	0.15
CS Columns	GL10SQ	0.13	0.80 (comb)	0.88 (comb)	0.93 (comb)	
CS Diagonals	GL7RECT	0.28	0.13 (comb)	0.08 (comb)	0.08 (comb)	
X - Con Size	400	0.11	0.18	0.21	0.22	
Y - Con Size	400	0.29	0.39	0.30	0.32	
Col - Con Size	400	0.57				
Diag - Con Size	900	0.32	0.29			
Core Thickness	350	1.79%	0.92	0.31	0.33	
HOR_DEFLECT1		1.05				
HOR_DEFLECT2		1.05				
Storey Number		20				
Floor Plan		A				

Table J.13: Overview of dimensions and Unity Checks, Variant 1L, 25 storeys, Iteration 1

VARIANT 1L		**UCs (Iteration 1)**				
		WIND_VAR TENS	WIND_VAR COMP	FLOOR VAR	SELF WEIGHT	VERT DEFLECT
DIMENSIONS						
CS X-Beams	GL5RECT	0.45 (shear)	0.72 (shear)	0.83 (shear)	0.79 (shear)	0.25
CS Y-Beams	GL10RECT	0.89 (comb)	1.08 (comb)	0.75 (shear)	0.72 (shear)	0.14
CS Columns	GL12SQ	0.10	0.79 (comb)	0.80 (comb)	0.86 (comb)	
CS Diagonals	GL7RECT	0.35	0.17 (comb)	0.08 (comb)	0.09 (comb)	
X - Con Size	400	0.12	0.19	0.22	0.21	
Y - Con Size	700	0.08	0.11	0.08	0.09	
Col - Con Size	400	0.42				
Diag - Con Size	900	0.42	0.36			
Core Thickness	400	1.76%	1.01	0.38	0.41	
HOR_DEFLECT1		1.06				
HOR_DEFLECT2		1.06				
Storey number		25				
Floor Plan		A				

Table J.14: Overview of dimensions and Unity Checks, Variant 1L, 31 storeys, Iteration 2

VARIANT 1L		**UCs (Iteration 2)**				
		WIND_VAR TENS	WIND_VAR COMP	FLOOR VAR	SELF WEIGHT	VERT DEFLECT
DIMENSIONS						
CS X-Beams	GL5RECT	0.34 (shear)	0.55 (shear)	0.64 (shear)	0.62 (shear)	0.14
CS Y-Beams	GL7RECT	1.14 (comb)	1.04 (comb)	0.89 (comb)	0.91 (comb)	0.14
CS Columns	GL11SQ	No Tension	0.77 (comb)	0.76 (comb)	0.82 (comb)	
CS Diagonals	GL2RECT	0.35	0.23 (comb)	0.09 (comb)	0.10 (comb)	
X - Con Size	400	0.09	0.14	0.17	0.16	
Y - Con Size	400	0.17	0.22	0.17	0.18	
Col - Con Size	400	0.00				
Diag - Con Size	500	0.89	0.74			
Core Thickness	400	1.46%	0.93	0.35	0.39	
HOR_DEFLECT1		1.07				
HOR_DEFLECT2		1.07				
Storey number		31				
Floor Plan		B				

Table J.15: Overview of dimensions and Unity Checks, Variant 1L, 35 storeys, Iteration 1

VARIANT 1L		**UCs (Iteration 1)**				
		WIND_VAR TENS	WIND_VAR COMP	FLOOR VAR	SELF WEIGHT	VERT DEFLECT
DIMENSIONS						
CS X-Beams	GL5RECT	0.34 (shear)	0.54 (shear)	0.64 (shear)	0.61 (shear)	0.14
CS Y-Beams	GL10RECT	1.04 (comb)	1.20 (comb)	0.63 (comb)	0.64 (comb)	0.07
CS Columns	GL14SQ	No Tension	0.54 (comb)	0.51 (comb)	0.56 (comb)	
CS Diagonals	GL3RECT	0.37	0.21 (comb)	0.08 (comb)	0.09 (comb)	
X - Con Size	400	0.10	0.14	0.17	0.16	
Y - Con Size	900	0.04	0.05	0.03	0.04	
Col - Con Size	400	0.00				
Diag - Con Size	600	0.55	0.49			
Core Thickness	400	1.21%	0.95	0.41	0.45	
HOR_DEFLECT1		0.97				
HOR_DEFLECT2		0.97				
Storey number		35				
Floor Plan		B				

Table J.16: Overview of dimensions and Unity Checks, Variant 1L, 40 storeys, Iteration 1

VARIANT 1L		**UCs (Iteration 1)**				
		WIND_VAR TENS	WIND_VAR COMP	FLOOR VAR	SELF WEIGHT	VERT DEFLECT
DIMENSIONS						
CS X-Beams	GL7RECT	0.42 (shear)	0.70 (shear)	0.82 (shear)	0.78 (shear)	0.35
CS Y-Beams	GL10RECT	0.85 (comb)	1.10 (comb)	0.82 (comb)	0.82 (comb)	0.10
CS Columns	GL17SQ	0.00	0.87 (comb)	0.74 (comb)	0.65 (comb)	
CS Diagonals	GL5RECT	0.22	0.16 (comb)	0.12 (comb)	0.13 (comb)	
X - Con Size	400	0.14	0.17	0.19	0.18	
Y - Con Size	900	0.08	0.11	0.09	0.09	
Col - Con Size	400	0.01				
Diag - Con Size	600	0.38	0.35			
Core Thickness	350	0.93%	0.98	0.51	0.55	
HOR_DEFLECT1		0.98				
HOR_DEFLECT2		0.98				
Storey number		40				
Floor Plan		C				

J.3 Variant 1: Heavy Configuration

Table J.17: Overview of dimensions and Unity Checks, Variant 1H, 15 storeys, Iteration 1

VARIANT 1H		**UCs (Iteration 1)**				
		WIND_VAR TENS	WIND_VAR COMP	FLOOR VAR	SELF WEIGHT	VERT DEFLECT
DIMENSIONS						
CS X-Beams	GL5RECT	0.40 (shear)	0.65 (shear)	0.76 (shear)	0.73 (shear)	0.26
CS Y-Beams	GL9RECT	0.99 (shear)	1.36 (shear)	1.34 (shear)	1.34 (shear)	0.19
CS Columns	GL3SQ	No Tension	0.73 (comb)	0.66 (comb)	0.66 (comb)	
CS Diagonals	GL3RECT	0.18	0.18 (comb)	0.13 (comb)	0.14 (comb)	
X - Con Size	400	0.53	0.76	0.71	0.74	
Y - Con Size	400	0.32	0.43	0.34	0.36	
Col - Con Size	400	0.00				
Diag - Con Size	400	0.89	0.86			
Core Thickness	150	0.71%	0.83	0.43	0.46	
HOR_DEFLECT1		0.45				
HOR_DEFLECT2		0.45				
Storey number		15				
Floor Plan		A				

Table J.18: Overview of dimensions and Unity Checks, Variant 1H, 20 storeys, Iteration 5

VARIANT 1H		**UCs (Iteration 5)**				
		WIND_VAR TENS	WIND_VAR COMP	FLOOR VAR	SELF WEIGHT	VERT DEFLECT
DIMENSIONS						
CS X-Beams	GL5RECT	0.48 (comb)	0.71 (comb)	0.76 (shear)	0.73 (shear)	0.24
CS Y-Beams	GL8RECT	0.53 (comb)	0.74 (shear)	0.86 (shear)	0.81 (shear)	0.14
CS Columns	GL10SQ	0.03	0.70 (comb)	0.83 (comb)	0.88 (comb)	
CS Diagonals	GL11RECT	0.13	0.21 (comb)	0.06 (comb)	0.07 (comb)	
X - Con Size	600	0.30	0.40	0.32	0.33	
Y - Con Size	500	0.34	0.44	0.32	0.34	
Col - Con Size	400	0.15				
Diag - Con Size	400	0.54	0.33			
Core Thickness	100	0.26%	1.02	0.73	0.76	
HOR_DEFLECT1		0.31				
HOR_DEFLECT2		0.31				
Storey number		20				
Floor Plan		A				

Table J.19: Overview of dimensions and Unity Checks, Variant 1H, 25 storeys, Iteration 2

VARIANT 1H		**UCs (Iteration 2)**				
		WIND_VAR TENS	WIND_VAR COMP	FLOOR VAR	SELF WEIGHT	VERT DEFLECT
DIMENSIONS						
CS X-Beams	GL5RECT	0.63 (comb)	0.91 (comb)	0.86 (comb)	0.86 (comb)	0.28
CS Y-Beams	GL8RECT	0.77 (comb)	1.06 (comb)	0.95 (shear)	0.94 (comb)	0.22
CS Columns	GL12SQ	0.07	0.65 (comb)	0.77 (comb)	0.82 (comb)	
CS Diagonals	GL11RECT	0.16	0.31 (comb)	0.09 (comb)	0.10 (comb)	
X - Con Size	500	0.59	0.77	0.56	0.59	
Y - Con Size	500	0.49	0.62	0.41	0.44	
Col - Con Size	400	0.32				
Diag - Con Size	400	0.67	0.43			
Core Thickness	200	0.26%	0.92	0.56	0.59	
HOR_DEFLECT1		0.62				
HOR_DEFLECT2		0.62				
Storey number		25				
Floor Plan		A				

Table J.20: Overview of dimensions and Unity Checks, Variant 1H, 31 storeys, Iteration 1

VARIANT 1H		**UCs (Iteration 1)**				
		WIND_VAR TENS	WIND_VAR COMP	FLOOR VAR	SELF WEIGHT	VERT DEFLECT
DIMENSIONS						
CS X-Beams	GL5RECT	0.63 (comb)	0.89 (comb)	0.81 (comb)	0.81 (comb)	0.28
CS Y-Beams	GL9RECT	0.74 (comb)	0.95 (comb)	0.88 (shear)	0.83 (shear)	0.14
CS Columns	GL14SQ	0.18	0.87 (comb)	0.78 (comb)	0.84 (comb)	
CS Diagonals	GL11RECT	0.24	0.34 (comb)	0.08 (comb)	0.08 (comb)	
X - Con Size	500	0.58	0.74	0.49	0.53	
Y - Con Size	500	0.45	0.55	0.33	0.35	
Col - Con Size	600	0.33				
Diag - Con Size	400	1.05	0.80			
Core Thickness	250	0.42%	1.02	0.59	0.63	
HOR_DEFLECT1		0.64				
HOR_DEFLECT2		0.64				
Storey number		31				
Floor Plan		A				

Table J.21: Overview of dimensions and Unity Checks, Variant 1H, 45 storeys, Iteration 1

VARIANT 1H		**UCs (Iteration 1)**				
		WIND_VAR TENS	WIND_VAR COMP	FLOOR VAR	SELF WEIGHT	VERT DEFLECT
DIMENSIONS						
CS X-Beams	GL5RECT	0.63 (comb)	0.89 (comb)	0.81 (comb)	0.81 (comb)	0.28
CS Y-Beams	GL10RECT	0.62 (comb)	0.79 (comb)	0.76 (shear)	0.72 (shear)	0.14
CS Columns	GL16SQ	0.15	0.59 (comb)	0.53 (comb)	0.57 (comb)	
CS Diagonals	GL11RECT	0.24	0.34 (comb)	0.08 (comb)	0.08 (comb)	
X - Con Size	500	0.58	0.74	0.49	0.53	
Y - Con Size	500	0.39	0.48	0.29	0.31	
Col - Con Size	600	0.28				
Diag - Con Size	700	0.36	0.27			
Core Thickness	400	0.27%	0.64	0.37	0.39	
HOR_DEFLECT1		0.44				
HOR_DEFLECT2		0.44				
Storey number		45				
Floor Plan		A				

Table J.22: Overview of dimensions and Unity Checks, Variant 1H, 50 storeys, Iteration 4

VARIANT 1H		**UCs (Iteration 4)**				
		WIND_VAR TENS	WIND_VAR COMP	FLOOR VAR	SELF WEIGHT	VERT DEFLECT
DIMENSIONS						
CS X-Beams	GL8RECT	0.86 (comb)	0.94 (comb)	0.37 (comb)	0.42 (comb)	0.09
CS Y-Beams	GL10RECT	0.99 (comb)	1.08 (comb)	0.63 (shear)	0.60 (shear)	0.08
CS Columns	GL25SQ	0.27	0.58 (comb)	0.22 (comb)	0.24 (comb)	
CS Diagonals	GL17RECT	0.32	0.33 (comb)	0.05 (comb)	0.06 (comb)	
X - Con Size	500	0.53	0.65	0.37	0.40	
Y - Con Size	500	0.46	0.55	0.27	0.29	
Col - Con Size	1000	0.28				
Diag - Con Size	700	0.50	0.45			
Core Thickness	350	0.63%	1.03	0.55	0.61	
HOR_DEFLECT1		0.89				
HOR_DEFLECT2		0.89				
Storey number		50				
Floor Plan		B				

Table J.23: Overview of dimensions and Unity Checks, Variant 1H, 50 storeys, Iteration 5

VARIANT 1H		**UCs (Iteration 5)**				
		WIND_VAR TENS	WIND_VAR COMP	FLOOR VAR	SELF WEIGHT	VERT DEFLECT
DIMENSIONS						
CS X-Beams	GL7RECT	0.62 (comb)	0.81 (comb)	0.60 (comb)	0.62 (comb)	0.15
CS Y-Beams	GL10RECT	0.83 (comb)	0.99 (comb)	0.81 (shear)	0.77 (shear)	0.11
CS Columns	GL23SQ	0.33	0.88 (comb)	0.39 (comb)	0.43 (comb)	
CS Diagonals	GL17RECT	0.32	0.39 (comb)	0.06 (comb)	0.07 (comb)	
X - Con Size	500	0.72	0.87	0.47	0.51	
Y - Con Size	500	0.61	0.73	0.37	0.40	
Col - Con Size	1000	0.24				
Diag - Con Size	700	0.50	0.42			
Core Thickness	400	0.63%	1.03	0.55	0.61	
HOR_DEFLECT1		0.95				
HOR_DEFLECT2		0.95				
Storey number		50				
Floor Plan		B				

J.4 Variant 2: Timber Columns

Table J.24: Overview of dimensions and Unity Checks, Variant 2T, 20 storeys, Iteration 3

VARIANT 2T		**UCs (Iteration 3)**				
		WIND_VAR TENS	WIND_VAR COMP	FLOOR VAR	SELF WEIGHT	VERT DEFLECT
DIMENSIONS						
CS X-Beams	GL5RECT	0.40 (shear)	0.66 (shear)	0.77 (shear)	0.74 (shear)	0.25
CS Y-Beams	GL6RECT	0.61 (shear)	0.82 (shear)	0.91 (shear)	0.85 (shear)	0.20
CS Columns	GL9SQ	No Tension	0.83 (comb)	0.93 (comb)	0.98 (comb)	
CS Diagonals	GL2RECT	0.81	0.91 (comb)	0.95 (comb)	0.98 (comb)	
X - Con Size	400	0.10	0.17	0.20	0.19	
Y - Con Size	400	0.18	0.25	0.22	0.24	
Col - Con Size	400	0.00				
Diag - Con Size	700	0.94	0.98			
Core Thickness	300	1.25%	1.00	0.45	0.48	
HOR_DEFLECT1		0.76				
HOR_DEFLECT2		0.76				
Storey number		20				
Floor Plan		A				

Table J.25: Overview of dimensions and Unity Checks, Variant 2T, 31 storeys, Iteration 1

VARIANT 2T		**UCs (Iteration 1)**				
		WIND_VAR TENS	WIND_VAR COMP	FLOOR VAR	SELF WEIGHT	VERT DEFLECT
DIMENSIONS						
CS X-Beams	GL5RECT	0.31 (shear)	0.50 (shear)	0.57 (shear)	0.55 (shear)	0.14
CS Y-Beams	GL9RECT	0.48 (comb)	0.59 (comb)	0.56 (shear)	0.55 (shear)	0.07
CS Columns	GL11SQ	0.05	0.50 (comb)	0.41 (comb)	0.45 (comb)	
CS Diagonals	GL7RECT	0.66	0.64 (comb)	0.51 (comb)	0.58 (comb)	
X - Con Size	400	0.08	0.13	0.15	0.14	
Y - Con Size	700	0.07	0.08	0.04	0.04	
Col - Con Size	400	0.20				
Diag - Con Size	500	0.78	1.03			
Core Thickness	350	0.48%	0.94	0.53	0.57	
HOR_DEFLECT1		0.65				
HOR_DEFLECT2		0.65				
Storey number		31				
Floor Plan		B				

Table J.26: Overview of dimensions and Unity Checks, Variant 2T, 35 storeys, Iteration 1

VARIANT 2T		**UCs (Iteration 1)**				
		WIND_VAR TENS	WIND_VAR COMP	FLOOR VAR	SELF WEIGHT	VERT DEFLECT
DIMENSIONS						
CS X-Beams	GL5RECT	0.30 (shear)	0.49 (shear)	0.57 (shear)	0.55 (shear)	0.14
CS Y-Beams	GL9RECT	0.65 (comb)	0.69 (comb)	0.43 (shear)	0.55 (shear)	0.05
CS Columns	GL13SQ	0.12	0.59 (comb)	0.54 (comb)	0.58 (comb)	
CS Diagonals	GL9RECT	0.35	0.30 (comb)	0.28 (shear)	0.29 (shear)	
X - Con Size	400	0.08	0.13	0.15	0.14	
Y - Con Size	700	0.07	0.08	0.04	0.04	
Col - Con Size	400	0.18				
Diag - Con Size	500	0.83	0.93			
Core Thickness	350	0.70%	1.00	0.53	0.57	
HOR_DEFLECT1		0.73				
HOR_DEFLECT2		0.73				
Storey number		35				
Floor Plan		B				

Table J.27: Overview of dimensions and Unity Checks, Variant 2T, 40 storeys, Iteration 1

VARIANT 2T		**UCs (Iteration 1)**				
		WIND_VAR TENS	WIND_VAR COMP	FLOOR VAR	SELF WEIGHT	VERT DEFLECT
DIMENSIONS						
CS X-Beams	GL5RECT	0.30 (shear)	0.49 (shear)	0.57 (shear)	0.55 (shear)	0.14
CS Y-Beams	GL10RECT	0.75 (comb)	0.79 (comb)	0.49 (shear)	0.47 (shear)	0.05
CS Columns	GL19SQ	0.05	0.32 (comb)	0.21 (comb)	0.23 (comb)	
CS Diagonals	GL9RECT	0.42	0.36 (comb)	0.28 (shear)	0.29 (shear)	
X - Con Size	400	0.14	0.16	0.15	0.14	
Y - Con Size	900	0.10	0.11	0.04	0.04	
Col - Con Size	400	0.22	3.29	2.63	2.80	
Diag - Con Size	600	0.72	0.72	0.35	0.35	
Core Thickness	400	0.96%	0.96	0.51	0.56	
HOR_DEFLECT1		0.85				
HOR_DEFLECT2		0.85				
Storey number		40				
Floor Plan		B				

J.5 Variant 2: Concrete Columns

Table J.28: Overview of dimensions and Unity Checks, Variant 2C, 25 storeys, Iteration 8

VARIANT 2C		**UCs (Iteration 8)**				
		WIND_VAR TENS	WIND_VAR COMP	FLOOR VAR	SELF WEIGHT	VERT DEFLECT
DIMENSIONS						
CS X-Beams	GL5RECT	0.40 (shear)	0.65 (shear)	0.76 (shear)	0.73 (shear)	0.25
CS Y-Beams	GL8RECT	0.77 (shear)	0.88 (shear)	0.63 (shear)	0.59 (shear)	0.14
CS Columns	CONC9SQ	No Tension	0.90 (comb)	0.41 (comb)	0.42 (comb)	
CS Diagonals	GL5RECT	0.65	0.59 (shear)	0.61 (shear)	0.63 (shear)	
X - Con Size	400	0.15	0.17	0.20	0.19	
Y - Con Size	400	0.26	0.28	0.16	0.16	
Diag - Con Size	1100	0.72	0.75			
Core Thickness	400	1.34%	1.03	0.45	0.48	
HOR_DEFLECT1		0.81				
HOR_DEFLECT2		0.81				
Storey number		25				
Floor Plan		A				

Table J.29: Overview of dimensions and Unity Checks, Variant 2C, 25 storeys, Iteration 6

VARIANT 2C		**UCs (Iteration 6)**				
		WIND_VAR TENS	WIND_VAR COMP	FLOOR VAR	SELF WEIGHT	VERT DEFLECT
DIMENSIONS						
CS X-Beams	GL5RECT	0.30 (shear)	0.49 (shear)	0.57 (shear)	0.55 (shear)	0.14
CS Y-Beams	GL5RECT	0.56 (comb)	0.66 (shear)	0.69 (shear)	0.65 (shear)	0.13
CS Columns	CONC5SQ	No Tension	0.98 (comb)	0.44 (comb)	0.46 (comb)	
CS Diagonals	GL3RECT	0.57	0.51 (comb)	0.55 (comb)	0.57 (comb)	
X - Con Size	400	0.08	0.13	0.15	0.14	
Y - Con Size	400	0.16	0.18	0.18	0.17	
Diag - Con Size	900	0.69	0.81			
Core Thickness	200	0.78%	0.98	0.51	0.54	
HOR_DEFLECT1		0.63				
HOR_DEFLECT2		0.63				
Storey number		25				
Floor Plan		B				

Table J.30: Overview of dimensions and Unity Checks, Variant 2C, 45 storeys, Iteration 2

VARIANT 2C		**UCs (Iteration 2)**				
		WIND_VAR TENS	WIND_VAR COMP	FLOOR VAR	SELF WEIGHT	VERT DEFLECT
DIMENSIONS						
CS X-Beams	GL5RECT	0.31 (shear)	0.49 (shear)	0.57 (shear)	0.55 (shear)	0.14
CS Y-Beams	GL11RECT	0.93 (comb)	0.43 (shear)	0.41 (shear)	0.41 (shear)	0.04
CS Columns	CONC20SQ	No Tension	0.62 (comb)	0.80 (comb)	0.96 (comb)	
CS Diagonals	GL8RECT	0.51	0.47 (comb)	0.31 (shear)	0.32 (shear)	
X - Con Size	400	0.16	0.18	0.15	0.14	
Y - Con Size	1000	0.09	0.09	0.02	0.03	
Diag - Con Size	1200	0.46	0.44			
Core Thickness	400	0.96%	1.02	0.49	0.54	
HOR_DEFLECT1		0.73				
HOR_DEFLECT2		0.73				
Storey number		45				
Floor Plan		B				

Appendix K

SCIA Engineering Report Example

K.1 Base Model - Plan A - 15 storeys

1. Belastingsgevallen

Naam	Omschrijving	Actie type	Lastgroep	Richting	Duur	'Master' belastingsgeval
	Spec	Type last				
LC_SW		Permanent	LG3	-Z		
		Eigen gewicht				
LC_PERM		Permanent	LG3			
		Standaard				
LC_WIND		Variabel	LG2		Kort	Geen
	Standaard	Statisch				
LC_IMPOSED		Variabel	LG2		Lang	Geen
	Standaard	Statisch				

2. Combinaties

Naam	Omschrijving	Type	Belastingsgevallen	Coëff. [-]
SELF_WEIGHT		Lineair - UGT	LC_SW	1.500
			LC_PERM	1.500
			LC_IMPOSED	0.660
FLOOR_VAR		Lineair - UGT	LC_SW	1.300
			LC_PERM	1.300
			LC_IMPOSED	1.650
WIND_VAR_COMP		Lineair - UGT	LC_SW	1.300
			LC_PERM	1.300
			LC_WIND	1.650
			LC_IMPOSED	0.660
WIND_VAR_TENS		Lineair - UGT	LC_SW	0.900
			LC_PERM	0.900
			LC_WIND	1.650
HOR_DEFLECT1		Lineair - BGT	LC_SW	1.000
			LC_PERM	1.000
			LC_WIND	1.000
HOR_DEFLECT2		Lineair - BGT	LC_SW	1.000
			LC_PERM	1.000
			LC_WIND	1.000
			LC_IMPOSED	0.400
VERT_DEFLECT		Lineair - BGT	LC_SW	1.000
			LC_PERM	1.000
			LC_IMPOSED	1.000

3. Columns

3.1. Columns ULS SELF_WEIGHT

Lineaire berekening
Combinatie: SELF_WEIGHT
Coördinatenstelsel: Hoofd
Extreme 1D: Globaal
Selectie: Alle
Filter: Laag = Columns
Resultaten over 1D-elementen:

Naam	dx [m]	Belasting	N [kN]	V_y [kN]	V_z [kN]	M_x [kNm]	M_y [kNm]	M_z [kNm]
COL285	52.553	SELF_WEIGHT/1	**-4123.03**	-0.06	1.14	0.00	0.00	0.00
COL45	0.000	SELF_WEIGHT/1	**251.09**	-3.22	-1.77	0.00	3.24	5.82
COL14	0.000	SELF_WEIGHT/1	-55.45	**11.53**	-1.50	**-0.01**	3.21	-25.04
COL119	0.000	SELF_WEIGHT/1	-153.43	-0.04	**-15.71**	0.00	**25.80**	0.18
COL120	0.000	SELF_WEIGHT/1	-148.63	-0.04	**15.71**	0.00	**-29.24**	-0.06
COL466	3.504+	SELF_WEIGHT/1	-110.67	-6.56	0.90	**0.01**	-1.51	10.09
COL90	35.035	SELF_WEIGHT/1	-112.03	**-13.50**	2.82	0.00	6.26	**-30.27**
COL13	3.504	SELF_WEIGHT/1	-55.41	11.53	0.45	-0.01	0.51	**25.03**

Naam	Combinatiesleutel
SELF_WEIGHT/1	1.50*LC_SW + 1.50*LC_PERM + 0.66*LC_IMPOSED

3.2. Columns ULS FLOOR_VAR

Lineaire berekening
Combinatie: FLOOR_VAR
Coördinatenstelsel: Hoofd
Extreme 1D: Globaal
Selectie: Alle
Filter: Laag = Columns

Naam	dx [m]	Belasting	N [kN]	V_y [kN]	V_z [kN]	M_x [kNm]	M_y [kNm]	M_z [kNm]
COL285	52.553	FLOOR_VAR/1	**-4020.66**	-0.05	1.11	0.00	0.00	0.00
COL45	0.000	FLOOR_VAR/1	**224.00**	-3.10	-1.83	0.00	3.40	5.60
COL14	0.000	FLOOR_VAR/1	-56.00	**11.74**	-1.56	**-0.01**	3.34	-25.42
COL119	0.000	FLOOR_VAR/1	-166.77	-0.04	**-15.41**	0.00	**25.34**	0.20
COL120	0.000	FLOOR_VAR/1	-162.60	-0.04	**15.41**	0.00	**-28.65**	-0.05
COL466	3.504+	FLOOR_VAR/1	-112.67	-6.12	0.86	**0.01**	-1.43	9.29
COL90	35.035	FLOOR_VAR/1	-113.11	**-14.14**	2.85	0.00	6.32	**-31.66**
COL13	3.504	FLOOR_VAR/1	-55.97	11.74	0.46	-0.01	0.53	**25.42**

Naam	Combinatiesleutel
FLOOR_VAR/1	1.30*LC_SW + 1.30*LC_PERM + 1.65*LC_IMPOSED

3.3. Columns ULS WIND_VAR_COMP

Lineaire berekening
Combinatie: WIND_VAR_COMP
Coördinatenstelsel: Hoofd
Extreme 1D: Globaal
Selectie: Alle
Filter: Laag = Columns

Naam	dx [m]	Belasting	N [kN]	V_y [kN]	V_z [kN]	M_x [kNm]	M_y [kNm]	M_z [kNm]
COL331	0.000	WIND_VAR_COMP/1	**-3939.57**	0.17	2.46	0.00	0.00	0.00
COL45	0.000	WIND_VAR_COMP/1	**220.47**	-1.98	-0.18	0.02	-0.11	3.37
COL14	0.000	WIND_VAR_COMP/1	-44.46	**9.77**	0.54	-0.01	-2.88	-21.69
COL196	35.035+	WIND_VAR_COMP/1	187.14	0.16	**-41.13**	0.03	73.60	-0.28
COL155	3.503+	WIND_VAR_COMP/1	-2905.18	-0.33	-1.28	**-0.04**	1.34	0.88
COL1	3.503+	WIND_VAR_COMP/1	-618.96	5.72	-0.35	**0.07**	4.45	-11.17
COL205	0.000	WIND_VAR_COMP/1	-149.30	-0.07	**46.93**	0.01	**-90.80**	0.00
COL206	3.504-	WIND_VAR_COMP/1	-489.53	0.15	44.21	0.02	**81.02**	0.15
COL90	35.035	WIND_VAR_COMP/1	-92.04	**-11.83**	0.04	0.02	-0.72	**-26.50**
COL470	0.000	WIND_VAR_COMP/1	-43.59	-10.76	3.00	0.01	-6.68	**22.12**

Naam	Combinatiesleutel
WIND_VAR_COMP/1	1.30*LC_SW + 1.30*LC_PERM + 1.65*LC_WIND + 0.66*LC_IMPOSED

3.4. Columns ULS WIND_VAR_TENS

Lineaire berekening
Combinatie: WIND_VAR_TENS
Coördinatenstelsel: Hoofd
Extreme 1D: Globaal
Selectie: Alle
Filter: Laag = Columns

Naam	dx [m]	Belasting	N [kN]	V_y [kN]	V_z [kN]	M_x [kNm]	M_y [kNm]	M_z [kNm]
COL331	0.000	WIND_VAR_TENS/1	**-2695.73**	0.17	2.35	0.00	0.00	0.00
COL45	0.000	WIND_VAR_TENS/1	**150.64**	-0.98	0.42	0.02	-1.24	1.57
COL14	0.000	WIND_VAR_TENS/1	-26.11	**5.92**	1.05	0.00	-3.99	-13.34
COL196	35.035+	WIND_VAR_TENS/1	123.53	0.15	**-37.55**	0.03	67.30	-0.25
COL155	3.503+	WIND_VAR_TENS/1	-1806.14	-0.31	-1.32	**-0.04**	1.52	0.82
COL1	3.503+	WIND_VAR_TENS/1	-382.27	3.95	-0.50	**0.07**	4.79	-7.73
COL205	0.000	WIND_VAR_TENS/1	-88.33	-0.06	**42.27**	0.01	**-81.74**	0.00
COL206	3.504-	WIND_VAR_TENS/1	-291.08	0.12	40.02	0.02	**73.30**	0.12
COL90	35.035	WIND_VAR_TENS/1	-54.97	**-7.14**	-0.90	0.02	-2.79	**-15.99**
COL470	0.000	WIND_VAR_TENS/1	-28.25	-6.68	2.47	0.01	-5.60	**13.78**

Naam	Combinatiesleutel
WIND_VAR_TENS/1	0.90*LC_SW + 0.90*LC_PERM + 1.65*LC_WIND

4. Core

4.1. Core ULS SELF_WEIGHT

Lineaire berekening
Combinatie: SELF_WEIGHT
Coördinatenstelsel: Hoofd
Extreme 1D: Globaal
Selectie: CM1, CM2
Resultaten over integratiestroken:

Naam	dx [m]	Belasting	N [kN]	V_y [kN]	V_z [kN]	M_x [kNm]	M_y [kNm]	M_z [kNm]
CM1	0.643	SELF_WEIGHT/1	-1349.60	0.86	**23.67**	1.37	-8.81	-0.81
CM1	3.500	SELF_WEIGHT/1	**-1285.36**	**1.13**	23.67	**-2.36**	13.91	**-0.76**
CM1	0.000	SELF_WEIGHT/1	-1364.06	0.80	23.67	**2.21**	-13.92	-0.82
CM2	3.500	SELF_WEIGHT/1	-1392.49	0.13	**-24.58**	1.62	**-14.19**	-0.82
CM2	0.000	SELF_WEIGHT/1	**-1477.34**	**-0.48**	-24.58	-1.66	**13.96**	**-0.88**

Naam	Combinatiesleutel
SELF_WEIGHT/1	1.50*LC_SW + 1.50*LC_PERM + 0.66*LC_IMPOSED

4.2. Core ULS FLOOR_VAR

Lineaire berekening
Combinatie: FLOOR_VAR
Coördinatenstelsel: Hoofd
Extreme 1D: Globaal
Selectie: CM1, CM2
Resultaten over integratiestroken:

Naam	dx [m]	Belasting	N [kN]	V_y [kN]	V_z [kN]	M_x [kNm]	M_y [kNm]	M_z [kNm]
CM1	0.643	FLOOR_VAR/1	-1262.59	0.82	**22.36**	1.29	-8.55	-0.81
CM1	3.500	FLOOR_VAR/1	**-1202.41**	**1.10**	22.36	**-2.22**	**13.55**	**-0.76**
CM1	0.000	FLOOR_VAR/1	-1276.13	0.76	22.36	**2.08**	-13.53	-0.82
CM2	3.500	FLOOR_VAR/1	-1306.09	0.15	**-23.24**	1.67	**-13.71**	-0.82
CM2	0.000	FLOOR_VAR/1	**-1385.76**	**-0.46**	-23.24	-1.69	13.46	**-0.88**

Naam	Combinatiesleutel
FLOOR_VAR/1	1.30*LC_SW + 1.30*LC_PERM + 1.65*LC_IMPOSED

4.3. Core ULS WIND_VAR_COMP

Lineaire berekening
Combinatie: WIND_VAR_COMP
Coördinatenstelsel: Hoofd
Extreme 1D: Globaal
Selectie: CM1, CM2
Resultaten over integratiestroken:

Naam	dx [m]	Belasting	N [kN]	V_y [kN]	V_z [kN]	M_x [kNm]	M_y [kNm]	M_z [kNm]
CM1	0.000	WIND_VAR_COMP/1	**-4575.81**	-172.26	116.88	-3.22	50.93	**2.12**
CM1	3.500	WIND_VAR_COMP/1	-4305.99	**-181.80**	116.88	-1.52	-6.34	1.64
CM2	0.071	WIND_VAR_COMP/1	2096.50	172.71	**74.40**	-6.48	74.86	-3.40
CM1	0.643	WIND_VAR_COMP/1	-4526.25	-174.02	**116.88**	-2.91	40.41	2.03
CM2	3.500	WIND_VAR_COMP/1	1972.43	**182.66**	74.40	**1.90**	**-33.13**	-2.83
CM2	0.000	WIND_VAR_COMP/1	**2099.09**	172.50	74.40	**-6.65**	**77.11**	**-3.41**

Naam	Combinatiesleutel
WIND_VAR_COMP/1	1.30*LC_SW + 1.30*LC_PERM + 1.65*LC_WIND + 0.66*LC_IMPOSED

4.4. Core ULS WIND_VAR_TENS

Lineaire berekening
Combinatie: WIND_VAR_TENS
Coördinatenstelsel: Hoofd
Extreme 1D: Globaal
Selectie: CM1, CM2
Resultaten over integratiestroken:

Naam	dx [m]	Belasting	N [kN]	V_y [kN]	V_z [kN]	M_x [kNm]	M_y [kNm]	M_z [kNm]
CM1	0.000	WIND_VAR_TENS/1	**-4169.88**	-172.51	109.74	-3.88	55.30	**2.39**
CM1	3.500	WIND_VAR_TENS/1	-3923.52	**-182.15**	109.74	-0.81	-10.72	1.89
CM2	0.071	WIND_VAR_TENS/1	2537.26	172.85	**81.83**	-5.94	70.70	-3.11
CM1	0.643	WIND_VAR_TENS/1	-4124.63	-174.28	**109.74**	-3.32	43.17	2.30
CM2	3.500	WIND_VAR_TENS/1	2388.33	**182.61**	81.83	**1.35**	**-28.71**	-2.57
CM2	0.000	WIND_VAR_TENS/1	**2540.37**	172.65	81.83	**-6.09**	**72.78**	**-3.12**

Naam	Combinatiesleutel
WIND_VAR_TENS/1	0.90*LC_SW + 0.90*LC_PERM + 1.65*LC_WIND

5. Y-Beams

5.1. ULS Y_Beams SELF_WEIGHT

Lineaire berekening
Combinatie: SELF_WEIGHT
Coördinatenstelsel: Hoofd
Extreme 1D: Globaal

Selectie: Alle
Filter: Laag = Y-Beams

Naam	dx [m]	Belasting	N [kN]	V_y [kN]	V_z [kN]	M_x [kNm]	M_y [kNm]	M_z [kNm]
BY376	6.000	SELF_WEIGHT/1	**-222.57**	**2.54**	179.22	0.01	-145.41	**6.88**
BY408	0.000	SELF_WEIGHT/1	**155.81**	0.47	-15.27	0.10	-27.97	2.21
BY377	0.000	SELF_WEIGHT/1	-213.39	**-2.30**	-134.99	0.00	-116.01	6.55
BY405	0.000	SELF_WEIGHT/1	-194.31	-2.20	**-136.91**	0.09	-117.31	5.20
BY416	0.000	SELF_WEIGHT/1	1.14	0.18	77.24	**-1.06**	-6.35	-0.26
BY393	0.000	SELF_WEIGHT/1	3.89	-0.35	67.96	**0.87**	-0.86	0.31
BY404	6.000	SELF_WEIGHT/1	-196.01	1.80	**180.24**	-0.07	**-146.28**	5.21
BY403	4.000-	SELF_WEIGHT/1	49.86	-0.43	-44.23	-0.40	**171.94**	-0.02
BY381	0.000	SELF_WEIGHT/1	-213.96	2.41	-133.91	0.00	-117.59	**-6.77**

Naam	Combinatiesleutel
SELF_WEIGHT/1	1.50*LC_SW + 1.50*LC_PERM + 0.66*LC_IMPOSED

5.2. ULS Y_Beams FLOOR_VAR

Lineaire berekening
Combinatie: FLOOR_VAR
Coördinatenstelsel: Hoofd
Extreme 1D: Globaal
Selectie: Alle
Filter: Laag = Y-Beams

Naam	dx [m]	Belasting	N [kN]	V_y [kN]	V_z [kN]	M_x [kNm]	M_y [kNm]	M_z [kNm]
BY376	6.000	FLOOR_VAR/1	**-238.22**	**2.78**	179.03	0.01	-148.18	**7.38**
BY408	0.000	FLOOR_VAR/1	**170.11**	0.50	-17.41	0.10	-32.11	2.39
BY377	0.000	FLOOR_VAR/1	-229.24	**-2.55**	-134.95	0.00	-118.83	7.06
BY405	0.000	FLOOR_VAR/1	-206.80	-2.36	**-137.15**	0.09	-120.31	5.55
BY416	0.000	FLOOR_VAR/1	1.23	0.19	79.64	**-1.10**	-6.27	-0.28
BY393	0.000	FLOOR_VAR/1	3.91	-0.35	70.73	**0.88**	-0.99	0.33
BY404	6.000	FLOOR_VAR/1	-208.78	1.97	**180.33**	-0.07	**-149.23**	5.56
BY403	4.000-	FLOOR_VAR/1	56.28	-0.44	-44.30	-0.38	**176.83**	-0.03
BY381	0.000	FLOOR_VAR/1	-229.79	2.65	-134.02	0.00	-120.42	**-7.28**

Naam	Combinatiesleutel
FLOOR_VAR/1	1.30*LC_SW + 1.30*LC_PERM + 1.65*LC_IMPOSED

5.3. ULS Y_Beams WIND_VAR_COMP

Lineaire berekening
Combinatie: WIND_VAR_COMP
Coördinatenstelsel: Hoofd
Extreme 1D: Globaal
Selectie: Alle
Filter: Laag = Y-Beams

Naam	dx [m]	Belasting	N [kN]	V_y [kN]	V_z [kN]	M_x [kNm]	M_y [kNm]	M_z [kNm]
BY376	6.000	WIND_VAR_COMP/1	**-286.71**	4.03	**285.71**	-0.03	-197.68	**8.46**
BY381	6.000	WIND_VAR_COMP/1	**124.82**	-0.28	-30.30	-0.04	-28.22	1.51
BY45	0.000	WIND_VAR_COMP/1	-100.21	**-8.62**	-13.02	-0.05	-38.78	-2.34
BY41	0.000	WIND_VAR_COMP/1	-124.49	**9.71**	-5.90	-0.33	-33.34	2.51
BY403	6.000	WIND_VAR_COMP/1	85.67	-0.45	**-148.83**	-0.29	5.11	-0.20
BY416	0.000	WIND_VAR_COMP/1	-16.06	0.19	59.50	**-0.97**	3.21	-0.24
BY393	0.000	WIND_VAR_COMP/1	-73.22	-0.19	48.86	**0.75**	9.15	0.50
BY348	4.000-	WIND_VAR_COMP/1	-118.68	-0.49	90.98	-0.06	**-205.06**	0.21
BY403	4.000-	WIND_VAR_COMP/1	24.19	-0.42	-49.60	-0.29	**174.86**	-0.03
BY380	6.000	WIND_VAR_COMP/1	-257.46	-2.45	206.32	-0.04	-145.33	**-7.46**

Naam	Combinatiesleutel
WIND_VAR_COMP/1	1.30*LC_SW + 1.30*LC_PERM + 1.65*LC_WIND + 0.66*LC_IMPOSED

5.4. ULS Y_Beams WIND_VAR_TENS

Lineaire berekening
Combinatie: WIND_VAR_TENS
Coördinatenstelsel: Hoofd
Extreme 1D: Globaal
Selectie: Alle
Filter: Laag = Y-Beams

Naam	dx [m]	Belasting	N [kN]	V_y [kN]	V_z [kN]	M_x [kNm]	M_y [kNm]	M_z [kNm]
BY376	6.000	WIND_VAR_TENS/1	**-207.00**	3.09	227.27	-0.03	-148.95	**5.99**
BY381	6.000	WIND_VAR_TENS/1	**76.76**	-0.16	-18.25	-0.04	-30.06	0.74
BY45	0.000	WIND_VAR_TENS/1	-76.07	**-8.18**	11.34	-0.05	-14.09	-1.68
BY41	0.000	WIND_VAR_TENS/1	-99.60	**9.26**	16.62	-0.32	-10.15	1.83
BY375	6.000	WIND_VAR_TENS/1	28.74	-0.27	**-106.24**	-0.10	5.71	-0.14
BY320	6.000	WIND_VAR_TENS/1	-181.71	2.50	**228.19**	-0.09	-149.08	5.16
BY416	0.000	WIND_VAR_TENS/1	-16.47	0.13	33.20	**-0.60**	5.24	-0.15
BY393	0.000	WIND_VAR_TENS/1	-74.50	-0.07	25.42	**0.46**	9.49	0.39
BY320	4.000-	WIND_VAR_TENS/1	-99.73	0.27	72.96	-0.09	**-170.84**	0.12
BY403	4.000-	WIND_VAR_TENS/1	5.03	-0.27	-35.13	-0.17	**116.53**	-0.02
BY380	6.000	WIND_VAR_TENS/1	-182.13	-1.64	182.57	-0.04	-119.57	**-5.14**

Naam	Combinatiesleutel
WIND_VAR_TENS/1	0.90*LC_SW + 0.90*LC_PERM + 1.65*LC_WIND

5.5. SLS Y-Beams Local U_z

Lineaire berekening
Combinatie: VERT_DEFLECT
Coördinatenstelsel: Staaf
Extreme 1D: Globaal
Selectie: Alle
Filter: Laag = Y-Beams
Vervormingen

Naam	dx [m]	Belasting	u_x [mm]	u_y [mm]	u_z [mm]	φ_x [mrad]	φ_y [mrad]	φ_z [mrad]	U_{total} [mm]
BY405	4.000-	VERT_DEFLECT/1	**-1.8**	0.8	-8.9	0.0	1.7	0.0	9.1
BY13	0.000	VERT_DEFLECT/1	**0.0**	0.0	-0.2	0.0	0.6	0.0	0.2
BY16	6.000	VERT_DEFLECT/1	0.0	**0.0**	-0.2	0.0	-0.3	0.0	0.2
BY397	6.000	VERT_DEFLECT/1	-1.7	**0.8**	-5.7	0.2	-0.9	0.0	6.0
BY398	3.000	VERT_DEFLECT/1	-1.8	0.8	**-19.3**	0.0	0.0	0.0	**19.4**
BY17	0.000	VERT_DEFLECT/1	0.0	0.0	**-0.2**	0.0	0.6	0.0	0.2
BY416	0.000	VERT_DEFLECT/1	-1.7	0.7	-9.4	**-0.6**	1.4	0.0	9.6
BY393	0.000	VERT_DEFLECT/1	-1.7	0.8	-7.5	**0.4**	0.8	0.0	7.7
BY403	0.000	VERT_DEFLECT/1	-1.7	0.8	-10.7	-0.2	**2.3**	0.0	10.8
BY404	4.000-	VERT_DEFLECT/1	-1.5	0.7	-6.3	0.0	**-2.9**	**0.0**	6.5
BY405	2.000-	VERT_DEFLECT/1	-1.8	0.8	-5.0	0.0	2.1	**0.0**	5.4

Naam	Combinatiesleutel
VERT_DEFLECT/1	LC_SW + LC_PERM + LC_IMPOSED

6. X-Beams

6.1. ULS X_Beams SELF_WEIGHT

Lineaire berekening
Combinatie: SELF_WEIGHT
Coördinatenstelsel: Hoofd
Extreme 1D: Globaal
Selectie: Alle
Filter: Laag = X-Beams

Naam	dx [m]	Belasting	N [kN]	V_y [kN]	V_z [kN]	M_x [kNm]	M_y [kNm]	M_z [kNm]
BX141	0.000	SELF_WEIGHT/1	**-14.30**	0.10	83.65	0.01	-53.92	-0.02
BX132	0.000	SELF_WEIGHT/1	**17.73**	0.00	67.38	0.02	-19.50	-0.01
BX146	4.000-	SELF_WEIGHT/1	4.06	**-0.13**	-25.02	-0.03	65.61	-0.02
BX132	6.000	SELF_WEIGHT/1	14.15	0.06	**-81.20**	0.02	-49.04	-0.11
BX143	0.000	SELF_WEIGHT/1	14.94	-0.01	72.45	**-0.06**	-32.32	-0.16
BX142	0.000	SELF_WEIGHT/1	12.98	0.06	67.32	**0.04**	-18.88	0.00
BX131	0.000	SELF_WEIGHT/1	4.02	-0.01	**85.08**	0.00	**-57.83**	0.08
BX141	4.000-	SELF_WEIGHT/1	3.48	**0.14**	-20.96	0.01	**69.62**	0.02
BX144	0.000	SELF_WEIGHT/1	0.82	-0.01	77.13	0.01	-41.18	**-0.20**
BX148	6.000	SELF_WEIGHT/1	11.37	0.04	-77.88	-0.01	-43.02	**0.18**

Naam	Combinatiesleutel
SELF_WEIGHT/1	1.50*LC_SW + 1.50*LC_PERM + 0.66*LC_IMPOSED

6.2. ULS X_Beams FLOOR_VAR

Lineaire berekening
Combinatie: FLOOR_VAR
Coördinatenstelsel: Hoofd
Extreme 1D: Globaal
Selectie: Alle
Filter: Laag = X-Beams

Naam	dx [m]	Belasting	N [kN]	V_y [kN]	V_z [kN]	M_x [kNm]	M_y [kNm]	M_z [kNm]
BX141	0.000	FLOOR_VAR/1	**-14.61**	0.10	86.82	0.02	-54.61	-0.02
BX132	0.000	FLOOR_VAR/1	**19.12**	0.00	71.06	0.02	-21.32	0.00
BX146	4.000-	FLOOR_VAR/1	4.53	**-0.14**	-26.16	-0.04	68.89	-0.02
BX132	6.000	FLOOR_VAR/1	13.95	0.06	**-84.49**	0.02	-50.04	-0.13
BX143	0.000	FLOOR_VAR/1	14.80	0.00	76.00	**-0.06**	-33.91	-0.18
BX142	0.000	FLOOR_VAR/1	14.23	0.06	71.00	**0.04**	-20.72	0.00
BX131	0.000	FLOOR_VAR/1	4.29	-0.01	**88.25**	0.00	**-58.54**	0.09
BX141	4.000-	FLOOR_VAR/1	4.00	**0.15**	-22.23	0.02	**72.78**	0.02
BX144	0.000	FLOOR_VAR/1	0.67	-0.01	80.54	0.01	-42.42	**-0.22**
BX149	0.000	FLOOR_VAR/1	9.75	0.03	80.72	0.01	-42.50	**0.20**

Naam	Combinatiesleutel
FLOOR_VAR/1	1.30*LC_SW + 1.30*LC_PERM + 1.65*LC_IMPOSED

6.3. ULS X_Beams WIND_VAR_COMP

Lineaire berekening
Combinatie: WIND_VAR_COMP
Coördinatenstelsel: Hoofd
Extreme 1D: Globaal
Selectie: Alle
Filter: Laag = X-Beams

Naam	dx [m]	Belasting	N [kN]	V_y [kN]	V_z [kN]	M_x [kNm]	M_y [kNm]	M_z [kNm]
BX9	0.000	WIND_VAR_COMP/1	**-10.24**	-0.07	60.39	-0.02	-28.36	0.00
BX133	0.000	WIND_VAR_COMP/1	**28.32**	0.58	63.69	-0.03	-27.57	-0.43
BX143	6.000	WIND_VAR_COMP/1	-2.83	**-0.70**	-66.53	-0.03	-33.82	-0.42
BX141	0.000	WIND_VAR_COMP/1	3.09	**0.76**	73.18	0.01	-46.64	-0.14
BX142	6.000	WIND_VAR_COMP/1	5.22	-0.66	**-70.10**	0.04	-39.77	-0.36
BX3	0.000	WIND_VAR_COMP/1	15.17	0.52	60.96	**-0.06**	-29.97	-0.23
BX147	0.000	WIND_VAR_COMP/1	13.23	-0.07	68.19	**0.06**	-36.25	-0.02
BX131	0.000	WIND_VAR_COMP/1	17.72	0.69	**74.59**	0.00	**-50.40**	-0.04
BX141	4.000-	WIND_VAR_COMP/1	10.73	-0.10	-18.57	0.01	**61.02**	0.26
BX133	6.000	WIND_VAR_COMP/1	19.49	-0.62	-66.80	-0.03	-34.15	**-0.45**
BX121	2.000-	WIND_VAR_COMP/1	14.56	0.33	23.50	-0.01	50.60	**0.31**

Naam	Combinatiesleutel
WIND_VAR_COMP/1	1.30*LC_SW + 1.30*LC_PERM + 1.65*LC_WIND + 0.66*LC_IMPOSED

6.4. ULS X_Beams WIND_VAR_TENS

Lineaire berekening
Combinatie: WIND_VAR_TENS
Coördinatenstelsel: Hoofd
Extreme 1D: Globaal
Selectie: Alle
Filter: Laag = X-Beams

Naam	dx [m]	Belasting	N [kN]	V_y [kN]	V_z [kN]	M_x [kNm]	M_y [kNm]	M_z [kNm]
BX9	0.000	WIND_VAR_TENS/1	**-11.17**	-0.07	39.21	-0.02	-17.92	0.00
BX132	6.000	WIND_VAR_TENS/1	**23.78**	-0.53	-41.97	0.00	-23.50	-0.33
BX143	6.000	WIND_VAR_TENS/1	-3.72	**-0.67**	-40.33	-0.01	-20.56	-0.35
BX141	0.000	WIND_VAR_TENS/1	7.89	**0.73**	44.45	0.01	-28.72	-0.13
BX110	6.000	WIND_VAR_TENS/1	1.61	0.02	**-43.17**	-0.01	-25.92	0.00
BX3	0.000	WIND_VAR_TENS/1	13.91	0.53	40.29	**-0.06**	-20.45	-0.22
BX147	0.000	WIND_VAR_TENS/1	8.75	-0.04	41.20	**0.04**	-21.86	-0.01
BX111	0.000	WIND_VAR_TENS/1	13.53	0.69	**45.43**	-0.01	**-31.32**	-0.08
BX141	4.000-	WIND_VAR_TENS/1	9.37	-0.15	-11.16	0.01	**36.87**	0.25
BX133	6.000	WIND_VAR_TENS/1	17.89	-0.62	-40.47	-0.02	-20.73	**-0.39**
BX121	2.000-	WIND_VAR_TENS/1	13.92	0.31	15.31	-0.01	33.06	**0.31**

Naam	Combinatiesleutel
WIND_VAR_TENS/1	0.90*LC_SW + 0.90*LC_PERM + 1.65*LC_WIND

6.5. SLS X_Beams Local U_z

Lineaire berekening
Combinatie: VERT_DEFLECT
Coördinatenstelsel: Staaf
Extreme 1D: Globaal
Selectie: Alle
Filter: Laag = X-Beams
Vervormingen

Naam	dx [m]	Belasting	u_x [mm]	u_y [mm]	u_z [mm]	φ_x [mrad]	φ_y [mrad]	φ_z [mrad]	U_{total} [mm]
BX146	2.000-	VERT_DEFLECT/1	**-0.8**	-1.7	-10.2	0.1	1.2	0.0	10.4
BX5	6.000	VERT_DEFLECT/1	**0.0**	0.0	-1.6	0.0	-1.6	0.0	1.6
BX10	5.333	VERT_DEFLECT/1	0.0	**0.0**	-2.5	0.0	-2.0	0.0	2.5
BX142	2.000-	VERT_DEFLECT/1	-0.8	**-1.7**	**-19.0**	0.0	0.2	0.0	**19.1**
BX6	0.000	VERT_DEFLECT/1	0.0	0.0	**-0.8**	0.0	1.7	0.0	0.8
BX142	6.000	VERT_DEFLECT/1	-0.8	-1.7	-10.7	**-0.1**	-2.6	0.0	10.8
BX146	6.000	VERT_DEFLECT/1	-0.8	-1.6	-5.9	**0.2**	-1.8	0.0	6.2
BX142	5.333	VERT_DEFLECT/1	-0.8	-1.7	-12.8	-0.1	**-2.9**	0.0	12.9
BX141	0.667	VERT_DEFLECT/1	-0.8	-1.7	-9.9	0.0	**3.4**	0.0	10.1
BX134	2.000-	VERT_DEFLECT/1	-0.7	-1.5	-13.9	0.0	1.6	**0.0**	14.0
BX142	4.000-	VERT_DEFLECT/1	-0.8	-1.7	-17.0	-0.1	-2.2	**0.0**	17.1

Naam	Combinatiesleutel
VERT_DEFLECT/1	LC_SW + LC_PERM + LC_IMPOSED

7. Global Horizontal Deflection

7.1. HOR_DEFLECT1

Lineaire berekening
Combinatie: HOR_DEFLECT1
Extreme: Globaal
Selectie: Alle

Naam	Belasting	U_x [mm]	U_y [mm]	U_z [mm]	Φ_x [mrad]	Φ_y [mrad]	Φ_z [mrad]	U_{total} [mm]
NCOL14	HOR_DEFLECT1/1	**-5.6**	**56.4**	-6.1	-1.0	**0.3**	-0.3	**57.0**
NCOL501	HOR_DEFLECT1/1	**4.5**	46.4	-3.4	-1.0	-0.3	-0.3	46.7
NCORE2	HOR_DEFLECT1/1	0.0	**0.0**	0.0	0.0	0.0	0.0	0.0
NCOL127	HOR_DEFLECT1/1	-3.6	54.4	**-14.3**	-0.1	0.0	-0.3	56.3
NBY237	HOR_DEFLECT1/1	-0.8	18.0	**1.4**	-1.1	0.0	-0.2	18.0
NCOL8	HOR_DEFLECT1/1	-4.2	30.8	-5.2	**-1.3**	0.1	-0.3	31.6
NCOL218	HOR_DEFLECT1/1	-1.6	54.4	-9.6	**0.1**	0.0	-0.3	55.3
NCOL96	HOR_DEFLECT1/1	-5.5	46.4	-7.8	-1.1	**-0.5**	-0.3	47.4
NBY489	HOR_DEFLECT1/1	-1.5	46.6	1.0	-1.1	0.0	**-0.4**	46.6
NBY22	HOR_DEFLECT1/1	0.2	0.8	-0.8	-0.3	0.1	**0.0**	1.1

Naam	Combinatiesleutel
HOR_DEFLECT1/1	LC_SW + LC_PERM + LC_WIND

7.2. HOR_DEFLECT2

Lineaire berekening
Combinatie: HOR_DEFLECT2
Extreme: Globaal
Selectie: Alle

Naam	Belasting	U_x [mm]	U_y [mm]	U_z [mm]	Φ_x [mrad]	Φ_y [mrad]	Φ_z [mrad]	U_{total} [mm]
NCOL14	HOR_DEFLECT2/1	**-5.6**	**56.3**	-6.4	-1.1	**0.4**	-0.3	**57.0**
NCOL501	HOR_DEFLECT2/1	**4.4**	46.3	-3.5	-1.0	-0.4	-0.3	46.7
NCORE2	HOR_DEFLECT2/1	0.0	**0.0**	0.0	0.0	0.0	0.0	0.0
NCOL127	HOR_DEFLECT2/1	-3.6	54.3	**-15.4**	-0.1	0.0	-0.3	56.5
NBY237	HOR_DEFLECT2/1	-0.8	18.0	**1.3**	-1.1	0.0	-0.2	18.0
NCOL8	HOR_DEFLECT2/1	-4.2	30.8	-5.4	**-1.3**	0.1	-0.3	31.6
NCOL218	HOR_DEFLECT2/1	-1.6	54.3	-10.3	**0.1**	0.0	-0.3	55.3
NCOL96	HOR_DEFLECT2/1	-5.6	46.3	-8.2	-1.1	**-0.5**	-0.3	47.4
NBY489	HOR_DEFLECT2/1	-1.5	46.5	0.9	-1.1	0.0	**-0.4**	46.5
NBY22	HOR_DEFLECT2/1	0.2	0.8	-0.8	-0.3	0.1	**0.0**	1.1

Naam	Combinatiesleutel
HOR_DEFLECT2/1	LC_SW + LC_PERM + LC_WIND + 0.40*LC_IMPOSED